JULY-SEPTEMBER 2021 VOL. 13 № 3 (50)

ISSN 2075-8251

ActaNaturae

Molecular Tools for Targeted Control of Nerve Cell Electrical Activity

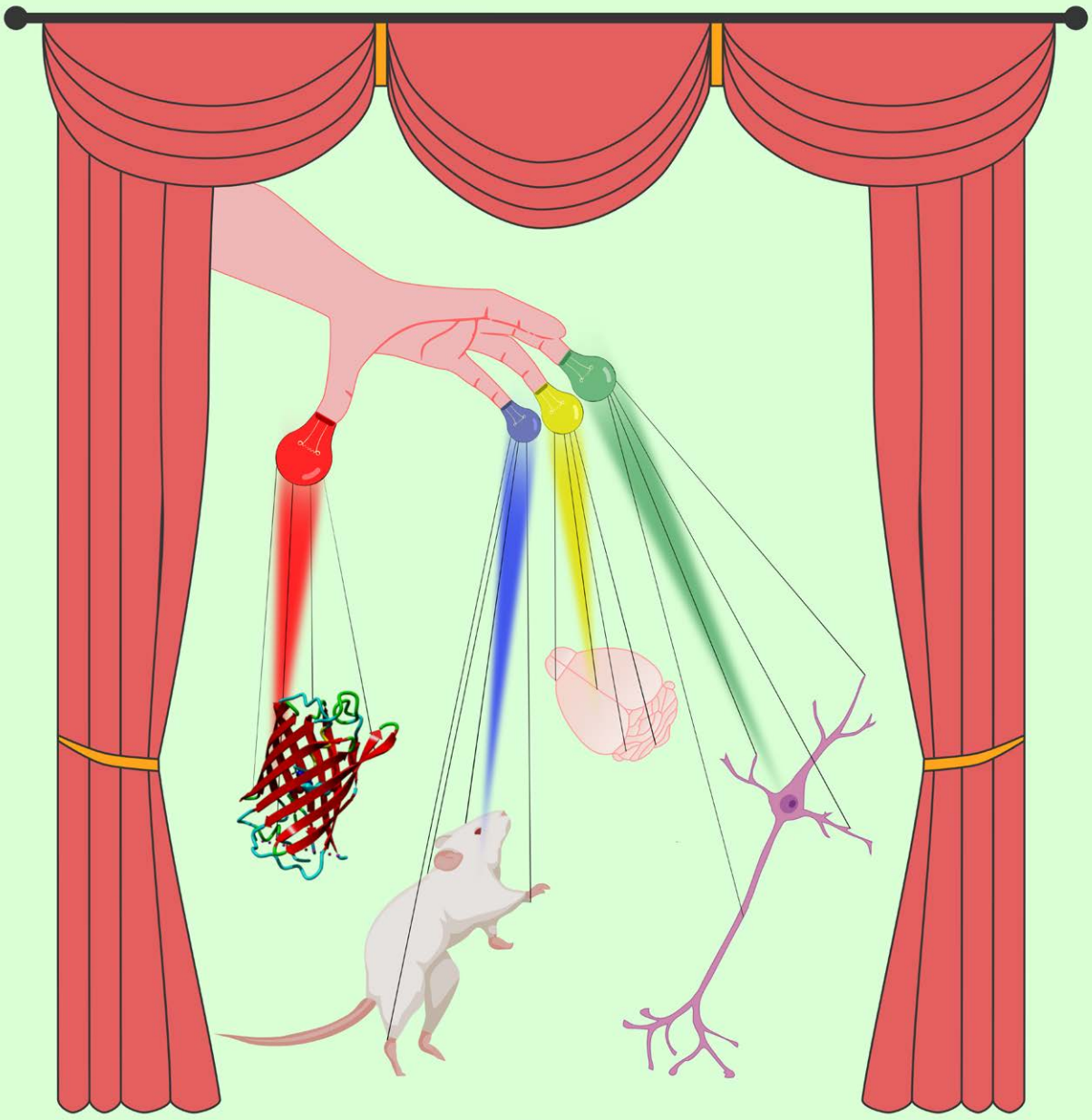

The Role of Non-coding RNAs in the Pathogenesis of Glial Tumors

T. F. Kovalenko, T. D. Larionova, N. V. Antipova, M. I. Shakhparonov, M. S. Pavlyukov

Among the many malignant neoplasms, glioblastoma (GBM) leads to one of the worst prognosis for patients and has an almost 100% recurrence rate. In this review, authors summarize the functions of long noncoding RNAs, circular RNAs, as well as microRNAs, PIWI-interacting RNAs, small nuclear and small nucleolar RNAs. They provide a classification of these transcripts and describe their role in various signaling pathways and physiological processes. Authors also provide examples of oncogenic and tumor suppressor ncRNAs belonging to each of these classes in the context of their involvement in the pathogenesis of gliomas and glioblastomas. In conclusion, authors considered the potential use of ncRNAs as diagnostic markers and therapeutic targets for the treatment of glioblastoma.

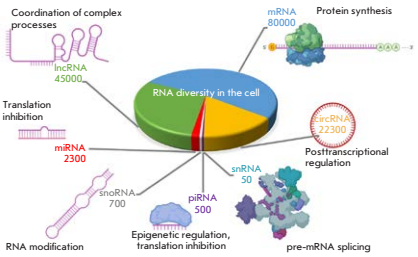

Functions of different types of ncRNAs in the cell

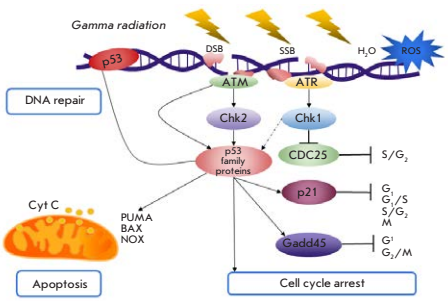

The response mechanisms to ionizing radiation involving p53-family proteins

The p53 Protein Family in the Response of Tumor Cells to Ionizing Radiation: Problem Development

O. A. Kuchur, D. O. Kuzmina, M. S. Dukhinova, A. A. Shtil

Survival mechanisms are activated in tumor cells in response to therapeutic ionizing radiation. This reduces a treatment's effectiveness. The p53, p63, and p73 proteins belonging to the family of proteins that regulate the numerous pathways of intracellular signal transduction play a key role in the development of radioresistance. This review analyzes the p53-dependent and p53-independent mechanisms involved in overcoming the resistance of tumor cells to radiation exposure.

Neutrophil Extracellular Traps (NETs): Opportunities for Targeted Therapy

D. V. Volkov, G. V. Tetz, Y. P. Rubtsov, A. V. Stepanov, A. G. Gabibov

Antitumor therapy, including adoptive immunotherapy, inevitably faces powerful counteraction from advanced cancer. Recent studies show that the development of the tumor and its ability to metastasize directly affect the extracellular traps of neutrophils (neutrophil extracellular traps, NETs) formed as a result of the response to tumor stimuli. In addition, the nuclear DNA of neutrophils – the main component of NETs – erects a spatial barrier to the interaction of CAR-T with tumor cells. Previous studies have demonstrated the promising potential of deoxyribonuclease I (DNase I) in the destruction of NETs. In this regard, the use of eukaryotic deoxyribonuclease I (DNase I) is promising in the quest to increase the efficiency of CAR-T by reducing the NETs influence in TME. Authors will examine the role of NETs in TME and the various approaches in the effort to reduce the effect of NETs on a tumor.

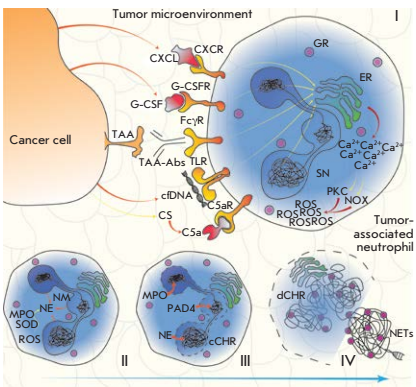

The signaling pathway of NOX-dependent NETosis

Genetic Diversity and Evolution of the Biological Features of the Pandemic SARS-CoV-2

A. A. Nikonova, E. B. Faizuloev, A. V. Gracheva, I. Yu. Isakov, V. V. Zverev

In this review, authors have focused on the general characteristics of SARS-CoV-2 and COVID-19. Also, authors have analyzed available publications on the genetic diversity of the virus and the relationship between the diversity and the biological properties of SARS-CoV-2, such as virulence and contagiousness.

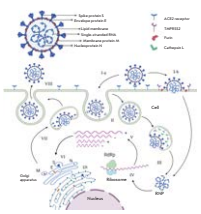

The SARS-CoV-2 virion and life cycle

ActaNaturae
JULY–SEPTEMBER 2021 VOL. 13 № 3 (50)
since april 2009, 4 times a year

Founders
Acta Naturae, Ltd,
National Research University
Higher School of Economics

Adress: 101000, Moscow, Myasnitskaya Ulitsa, 13, str. 4
Phone/Fax: +7 (495) 727 38 60
E-mail: actanaturae@gmail.com

Номер подписан в печать 30 сентября 2021 г.
Тираж 25 экз. Цена свободная.
Отпечатано в типографии: НИУ ВШЭ,
г. Москва, Измайловское шоссе, 44, стр. 2

Indexed in Pubmed, Web of Science, Scopus, and RISC

Impact Factor: 1.845

CONTENTS

REVIEWS

RESEARCH ARTICLES

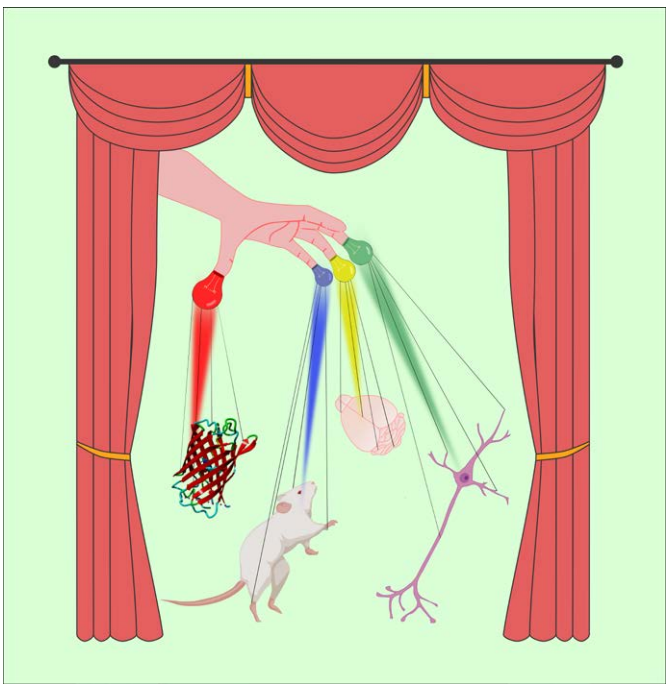

IMAGE ON THE COVER PAGE
(see the article by D. V. Kolesov et al.)

Cardiovascular Effects of Snake Toxins: Cardiotoxicity and Cardioprotection

A. S. Averin[1*], Yu. N. Utkin[2]
[1]Institute of Cell Biophysics of the Russian Academy of Sciences PSCBR RAS, Pushchino, Moscow region, 142290 Russia
[2]Shemyakin-Ovchinnikov Institute of Bioorganic Chemistry, Russian Academy of Sciences, Moscow, 117997 Russia
*E-mail: averinas82@gmail.com
Received March 09, 2021; in final form, April 13, 2021
DOI: 10.32607/actanaturae.11375

ABSTRACT **Snake venoms, as complex mixtures of peptides and proteins, affect various vital systems of the organism. One of the main targets of the toxic components from snake venoms is the cardiovascular system. Venom proteins and peptides can act in different ways, exhibiting either cardiotoxic or cardioprotective effects. The principal classes of these compounds are cobra cardiotoxins, phospholipases A2, and natriuretic, as well as bradykinin-potentiating peptides. There is another group of proteins capable of enhancing angiogenesis, which include, e.g., vascular endothelial growth factors possessing hypotensive and cardioprotective activities. Venom proteins and peptides exhibiting cardiotropic and vasoactive effects are promising candidates for the design of new drugs capable of preventing or constricting the development of pathological processes in cardiovascular diseases, which are currently the leading cause of death worldwide. For example, a bradykinin-potentiating peptide from *Bothrops jararaca* snake venom was the first snake venom compound used to create the widely used antihypertensive drugs captopril and enalapril. In this paper, we review the current state of research on snake venom components affecting the cardiovascular system and analyse the mechanisms of physiological action of these toxins and the prospects for their medical application.**
KEYWORDS **bradykinin-potentiating peptides, snake venom, cardioprotector, cardiotoxin, natriuretic peptide, cardiovascular system.**
ABBREVIATIONS **ACE – angiotensin-converting enzyme; AR – adrenergic receptor; BPP – bradykinin-potentiating peptide; CT – cardiotoxin; NP – natriuretic peptide; NPR – NP receptor; CVD – cardiovascular disease; CVS – cardiovascular system; TFT – three-finger toxin; PLA2 – phospholipase A2; VEGF – vascular endothelial growth factor; ANP – atrial NP; BNP – brain NP; CNP – C-type NP; SRTX – sarafotoxin; VEGFR – vascular endothelial growth factor receptor.**

INTRODUCTION

Cardiovascular diseases (CVDs) are a vast group of heart and blood vessel diseases of various etiologies. They lead to impairment of the normal functions of various organs and, in severe cases, death. They put a huge burden on health care systems and the economy around the world. According to WHO estimates, more than 17 million people die from heart diseases every year. By 2030, this number is estimated to exceed 23 million. The leading causes of death are strokes and coronary heart diseases, which account for 31% of all deaths. In Russia, this indicator stands at 57%. Currently, a large number of drugs with various mechanisms of action exist, and they are used for the treatment of CVDs. Naturally, all possess certain side effects. For example, antiplatelet agents and anticoagulants can cause gastrointestinal tract complications and intracranial bleeding. The most common side effects of angiotensin-converting enzyme inhibitors are arterial hypotension, paroxysmal unproductive dry cough, angioedema of the upper respiratory tract, cholestasis, hyperkalemia, proteinuria, and impaired renal function. The use of β-blockers can be accompanied by a number of side effects, both cardiac (weakening of the pumping function of the heart, bradycardia, etc.) and extracardiac (drowsiness, depression, bronchospasm, etc.). In addition, a significant problem is associated with the insufficient efficacy of drug therapy for a number of CVDs, something that is especially pronounced in patients with concomitant pathologies. For

Snake venom toxins that affect the CVS

Toxin	Molecular weight, kDa	Main biological target	Effect on CVS
Bradykinin-potentiating peptides	1.5–2.0	Angiotensin-converting enzyme	Lowering of blood pressure through a decrease in the concentration of angiotensin II and an increase in the concentration of bradykinin [3]
Natriuretic peptides	2.5–5.5	Natriuretic peptide receptors A, B, and C	Lowering of blood pressure through a reduction in vascular resistance (due to a decrease in the influx of calcium ions into muscle cells) and a decrease in the volume of circulating blood (due to an increase in the volume of excreted urine) [4–6]
Sarafotoxins	2.3–2.7	Endothelin type A (ET_A) and B (ET_B) receptors	Increased vasoconstriction followed by narrowing of the bronchi and increased airway resistance as well as an increase in hydrostatic pressure of microvessels in the lungs, which leads to their edema. Failure of various parts of the heart, mainly the left ventricle [7, 8]
Three-finger toxins	6.2–8.0	Cell membranes, adrenergic receptors, cholinergic receptors	Suppression of contractility and irreversible contracture of the myocardium; lowering blood pressure; cardioprotection [9–11]
Cysteine-rich secretory proteins (CRISPs)	23–25	Voltage-gated ion channels	Inhibition or activation of aortic smooth muscle contraction [12, 13]
Alternagin-C	21.7	Integrin α2β1 and VEGFR-2	Enhancement of cardiac activity; protection against hypoxia/reoxygenation-induced cardiomyocyte negative inotropism [14, 15]
Endothelial vascular growth factors	24–26	Receptor tyrosine kinases VEGFR-1, VEGFR-2, and VEGFR-3	Cardioprotective effect; reduction in reperfusion injury to the heart and infarct size [16, 17]
Phospholipases A2	13–14	Cell membrane, secretory PLA2 receptors	Cardiotoxicity; myocardial contracture, vascular relaxation [18–21]

example, a serious challenge in modern medicine is the chronic heart failure that is increasingly common in many cases and is difficult to correct. All these obstacles speak to the need for more effective drugs, with a fundamentally new mechanism of action: drugs that are free of the limitations typical of existing medicines.

SNAKE VENOMS: COMPOSITION AND PROPERTIES

Snake venoms are complex mixtures of compounds with high biological activity and a high selectivity of action. These compounds are capable of affecting various systems of the organism, but their main targets are the nervous and cardiovascular systems (CVS). Depending on the most affected system, snake venoms are classified as neurotoxic and hemotoxic. Neurotoxic venoms are typical of snakes from the Elapidae family (cobras, kraits, mambas, coral snakes, and some other snakes) and contain mainly non-enzymatic toxins that block nerve impulse conduction. Hemotoxic venoms are typical of snakes from the Viperidae family (vipers, moccasins, rattlesnakes and some other snakes). Hemotoxic venoms consist mainly of enzymes that cause coagulopathy. Both types of venoms can contain toxins that affect the CVS, with the venom of one individual comprising up to several hundred different peptides and proteins. Snake venom proteins and peptides affecting the CVS can act in different ways, causing both cardiotoxic and cardioprotective effects. These compounds belong to different toxin families and interact with various biological targets in the organism. Snake venom poisoning is associated with a number of cardiovascular effects, including hypotension, myocardial infarction, cardiac arrest, hypertension, brady- or tachycardia, and atrial fibrillation [1]. Given the multiplicity of the effects, it may be stated that snake venom is a rich source of compounds that affect the CVS. These compounds, with various biological activities, could be of significant pharmacological value and represent a promising basis for the development of new drugs.

It should be noted that snake venoms contain a large number of peptides and proteins that affect blood cells and enzyme systems. However, in this review, we will limit ourselves to the consideration of toxins that directly affect the CVS.

Snake toxins affecting the CVS

As has already been noted, snake venoms contain a number of compounds that affect the CVS. By their

BPP-9a, Тепротид [*Bothrops jararaca*]	ZWPRPQIPP
BPP-12b [*Bothrops jararaca*]	ZWGRPPGPPIPP
BPP-10c [*Bothrops jararaca*]	ZNWPHPQIPP
R-BPP [*Azemiops feae*]	ZRPPGVYYPP
Y-BPP [*Azemiops feae*]	ZYLPPHPHYPP
BPPB [*Agkistrodon blomhofii*]	ZGLPPRPKIPP
BPPC [*Agkistrodon blomhofii*]	ZGLPPGPPIPP
BPP-XIe [*Bothrops jajaracussu*]	ZARPPHPPIPP

A

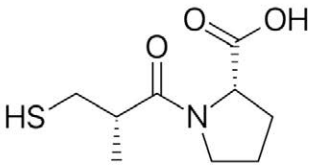

B

Fig. 1. Amino acid sequences of BPPs (A) and the structure of captopril (B). Z is a pyroglutamic acid residue

chemical nature, these can be low-molecular-weight organic compounds (e.g., adenosine), peptides, and proteins. These snake venom components include, in particular, bradykinin-potentiating peptides (BPPs), natriuretic peptides (NPs), sarafotoxins (SRTXs), and three-finger toxins (TFTs), including cobra cardiotoxins (CTs), phospholipases A2 (PLA2s), and vascular endothelial growth factors (VEGFs) [2] (*Table*). These toxins affect the heart muscle, vascular smooth muscles, and the capillary vascular bed.

Peptide toxins

Bradykinin-potentiating peptides (BPPs). BPPs consist of 5–14 amino acid residues and contain a proline-rich region [2, 22] (*Fig. 1A*). In the organism, BPPs inhibit the angiotensin-converting enzyme (ACE) that breaks down angiotensin I, converting it into angiotensin II, a potent vasoconstrictive and hypertensive agent. BPPs lower blood pressure by blocking the formation of angiotensin II. In addition, ACE is also capable of cleaving bradykinin that possesses hypotensive activity and inhibition of the enzyme enhances the effect of bradykinin and leads to vasodilation and decreased cardiac output [3]. The first antihypertensive drug of its class, the ACE inhibitor captopril (*Fig. 1B*), was derived from a BPP (teprotide) from the venom of the snake *Bothrops jararaca.*

It should be noted that ACE is a two-domain enzyme. The generation of a potent vasoconstrictor, angiotensin II, occurs primarily through the action of the ACE C-domain. Both homologous domains hydrolyze bradykinin, with the C-domain being somewhat more efficient [23]. The ACE inhibitors including captopril commonly used in clinic are not domain-selective. However, they can lead to life-threatening angioedema associated with the systemic accumulation of bradykinin upon the inhibition of both ACE domains. Therefore, the development of a domain-specific inhibitor is urgently needed. Selectivity of action on a certain domain was found for some BPPs. For example, the decapeptide Bj-BPP-10c (*Fig. 1*) is 400-fold more selective for the active site in the C domain (Ki = 0.5 nM) than for the N domain (Ki = 200 nM) [24]. The opposite was discovered for Bj-BPP-12b (*Fig. 1*), which is more selective for the N domain (Ki = 5 nM) and 30-fold less effective for the C domain [25]. The BPPs R-BPP and Y-BPP, which we uncovered in the venom of the viper *Azemiops feae* (*Fig. 1*) [26], are more similar to peptides exhibiting specificity for the ACE C domain and may be considered as a basis for the development of C domain-selective drugs, which would differ structurally from captopril.

In addition to inhibiting ACE, some BPPs kinetically modulate the activity of argininosuccinate synthase *in vitro* and *in vivo*, which ultimately leads to the production of nitric oxide (NO) in endothelial cells and a decrease in blood pressure [27]. Modulation of argininosuccinate synthase not only stimulates the production of nitric oxide, but also enhances the synthesis of protective molecules, such as polyamines (spermine, spermidine, and putrescine) and agmatine, which, as was shown in one of our studies, can lead to a positive inotropic effect even upon reduced activity of Ca^{2+}-ATPase of the sarcoplasmic reticulum [28], a characteristic of heart failure [29]. Recently, one of the mentioned BPPs was shown to protect SH-SY5Y neuroblastoma cells from the oxidative stress caused by hydrogen peroxide [30]. It should be noted that post-heart-attack reperfusion induces oxidative stress, leading to severe cardiac dysfunction. Therefore, biologically active compounds that reduce oxidative stress can be considered a promising therapeutic strategy for heart diseases. Potentially, BPPs could be such compounds. In addition, BPPs have a direct effect on the components of the cardiovascular system. For example, in some cases there is no correlation between ACE inhibition and the hypotensive effect [31], and a BPP from the venom of the cobra *Naja haje haje* dose-dependently reduces the contractility of the rat atria [32]. The BPP Bj-PRO-5a was also found to cause vasodilation by interacting with the muscarinic cholinergic receptors M1 and bradykinin receptors BK_{B2} and

Fig. 2. Amino acid sequences of NPs. Identical amino acid residues are underlined. The disulfide bond is shown as a line connecting cysteine residues. hANP and hBNP are human atrial and brain NPs, respectively. hCNP is the human C-type NP. DNP is an NP from *Dendroaspis angusticeps* mamba venom (UniProtKB -P28374), CA-CNP is a C-type NP from *Crotalus atrox* venom (P0CV87), COA-NP2 is an NP from *C. oreganus abyssus* venom (B3EWY2), and PNP is an NP from *Pseudocerastes persicus* venom (P82972)

triggering NO synthesis by the endothelium [33]. There is evidence that BPPs can enhance the effect of bradykinin by increasing the sensitivity of its receptors. But the mechanism of this action has not been elucidated [34]. Therefore, many physiological mechanisms, both central and peripheral, underlie the general hypotensive effect of BPPs.

Natriuretic peptides. A number of snake venom peptides mimic the actions of endogenous peptides. These compounds include, in particular, natriuretic peptides (NPs). NPs contain about 20 to 50 amino acid residues and are based on a conserved 17-aa sequence confined by a disulfide bond (*Fig. 2*). There are three isoforms of mammalian NPs: namely atrial NP (ANP), brain NP (BNP), and C-type NP (CNP). NPs also include urodilatin, which is an extended ANP derived from a precursor using an alternative processing system. In addition, a D-type NP (DNP) and ventricular NPs (VNPs) are sometimes distinguished. The DNP is a unique NP isolated only from the venom of the eastern green mamba *Dendroaspis angusticeps*. To date, VNP expression has been confirmed only in the heart of primitive bony fish [35]. Atrial NPs are the key hormones in the regulation of pressure–volume homeostasis. These peptides interact with membrane-bound NP receptors (NPRs) in the heart, vasculature, and kidneys, reducing blood pressure and circulation volume. The effects of NPs can be quite diverse: in mice, endogenous BNPs and CNPs increase the heart rate [36], while in the rat myocardium, CNP causes a decrease in contractility [37]. A common property of NPs is the ability to induce an increase in NO production and activate protein kinase G, which mediates their vasorelaxant effect [4, 38] in most cases; however, some NPs can also induce relaxation on endothelium-denuded aortic preparations [38, 39]. Therefore, NPs cause a whole spectrum of physiological effects that can potentially be used to correct CVD. For example, intravenous infusion of NPs improves the hemodynamic status in patients with heart failure, but sometimes it is accompanied by severe hypotension, which requires the development of NP analogs lacking these side effects.

NPs are found in the venoms of various snake species, including the eastern green mamba *D. angusticeps* [40], rattlesnakes *C. atrox* and *C. oreganus abyssus* [4], and others [41, 42] (*Fig. 2*). Their action leads to vascular relaxation and a decrease in myocardial contractility [4, 6]. Venom NPs are of interest as a basis for the creation of NPs with a longer half-life and improved selectivity for vessels and kidneys [43]. In this regard, snake venom NPs are considered a good basis for the design of NPs with therapeutic potential. To date, venom NPs have been used to develop several analogs with the prospect of clinical application; of these, the most successful agent is cenderitide [5]. Cenderitide is a chimeric peptide consisting of a human C-type NP fused to the C-terminal fragment of an NP from the venom of the eastern green mamba *D. angusticeps* (*Fig. 2*). Cenderitide was developed to co-activate two NP receptors, in particular the guanylyl cyclases pGC-A and pGC-B, for improving renal function, but without clinically significant hypotension. Cenderitide was shown to be well tolerated by healthy volunteers, without side effects and to activate cGMP, which corresponded to the activation of the NP receptor. Cenderitide induced a minimal decrease in blood pressure, along with natriuresis and diuresis. Preliminary experiments in patients with heart failure demonstrated good tolerance and no side effects. Cenderitide is a promising agent for the treatment of heart failure.

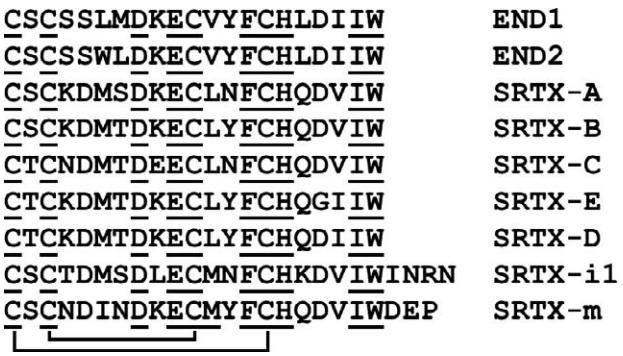

Fig. 3. Amino acid sequences of endothelins and sarafotoxins. Disulfide bonds are shown as lines connecting cysteine residues. END1 (UniProtKB – P05305) and END2 (P20800) are human endothelin 1 and 2, respectively. SRTX-A (UniProtKB – P13208), SRTX-B (P13208), SRTX-C (P13208), SRTX-E (P13208), and SRTX-D (P13211) are sarafotoxins A, B, C, E, and D from *A. engaddensis* venom, respectively. SRTX-i1 (P0DJK0) is sarafotoxin i1 from *A. irregularis* venom; SRTX-m (Q6RY98) is sarafotoxin m from the venom of *A. microlepidota microlepidota*

Sarafotoxins. Sarafotoxins (SRTXs), which possess strong vasoconstrictive properties, are short peptide toxins found in the venom of snakes of the genus *Atractaspis*. These peptides, which have a high degree of identity with endothelins, recognize and bind endothelin receptors. SRTXs from the venom of *Atractaspis engaddensis* contain 21 amino acid residues and two disulfide bonds (*Fig. 3*); the toxins of other snake species have an extended C-terminal fragment. They stimulate endothelin receptors and increase vasoconstriction, followed by left ventricular dysfunction, bronchospasm, and increased airway resistance. SRTX-B binds to endothelin receptors with high affinity and causes cardiac arrest and death in mice within minutes of intravenous administration.

The contractile response of vessels to sarafotoxins is mainly associated with the input of extracellular calcium through L-type calcium channels, while intracellular calcium stores released through ryanodine and IP-3 channels play a relatively small role [8].

The effect of SRTX-C can be multidirectional. For example, a small negative inotropic effect is observed in the intact right papillary muscles of a rabbit, while a strong increase in contractility occurs upon removal of the endothelium and inhibition of nitric oxide or prostaglandin signaling [44]. In the human myocardium, SRTX-C causes an increase in contractility associated with arrhythmia, which is most pronounced in the right atrium compared with other myocardial tissues [45]. Intracoronary administration of SRTX-C is known to lead to a decrease in cardiac output and an increase in the time parameters of cardiac contraction in pigs [46]. In this case, the classic short SRTXs from *A. engaddensis* cause disturbances in the left ventricle, while SRTX-m from the venom of *A. microlepidota microlepidota* [47] leads to a dysfunction of the right ventricle [7].

In scientific research, SRTXs are used to label endothelin receptors and develop vasospasm models [48].

Non-enzymatic protein toxins

Three-finger toxins. Three-finger toxins (TFTs) constitute one of the most abundant families of snake venom toxins. TFTs consist of 57–82 amino acid residues; structurally, TFT molecules are represented by three β-structural loops extending from a compact hydrophobic core that is stabilized by four conserved disulfide bonds. The biological properties of TFTs are very diverse; a number of TFTs affect the CVS [11].

Cytotoxins, also called cardiotoxins (CTs), are TFTs that consist of about 60 amino acid residues and contain four disulfide bonds (*Fig. 4*). A common property of cytotoxins is their direct interaction with the membrane to form an ionic pore, which causes depolarization of a cell and its death. This is most clearly seen in the heart, which imparts to this group the alternative name cardiotoxins. Despite the fact that the amino acid sequences of CTs are very similar [49], their biological activity can differ significantly [50, 51]. Most studies have shown that CTs begin to act even at a concentration of less than 1 μM, initially causing an increase in contraction, followed by a decrease and a concomitant rise in the resting tension [9, 52, 53]. Comparison of various myocardial tissues showed that the effect of CTs on the ventricular tissue is more pronounced than that on the atria [54, 55]. Usually, contracture caused by the CT effect is irreversible and leads to cell death [10, 53, 56–58]. Initial cell depolarization results in an increase in the intracellular calcium concentration from intra- and extracellular sources [53]. The role of individual calcium-transporting mechanisms in the development of CT effects can vary depending on myocardial characteristics. For example, the L-type Ca^{2+} current in neonatal rat cardiomyocytes is the leading mechanism for increasing the level of intracellular calcium [57], while the blocking of this mechanism in adult cardiomyocytes [53] and guinea pig myocardium [10] does not prevent the development of contracture. It should be noted that the CT effect depends on the concen-

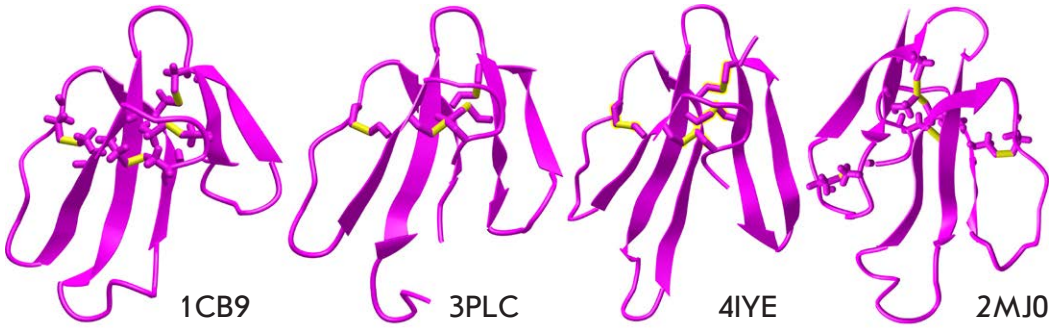

Fig. 4. Spatial structures of some three-finger toxins. Cardiotoxin II from *Naja oxiana* (PDB code – 1CB9), β-cardiotoxin from *Ophiophagus hannah* (3PLC), toxin ρ-Da1a from *Dendroaspis angusticeps* (4IYE), and weak toxin WTX from *Naja kaouthia* (2MJ0). The structures of cardiotoxin II and WTX were established by NMR, the structures of β-cardiotoxin and toxin ρ-Da1a were determined by X-ray analysis. Disulfide bonds are highlighted in yellow

tration of extracellular calcium, high concentrations of which (about 10 mM) block CT effects [10, 53, 57]. CTs induce a long-term increase in the intracellular calcium concentration, accompanied by the activation of peptidases inside the cell and disintegration of the cardiomyocyte structure [53, 57], which results in a chain of pathological processes leading to cell death [53] through the necrotic mechanism [58].

In blood vessels, as in other muscle tissue types, CTs cause contracture; in this case, a transient relaxation effect caused by the activation of endothelial cells is observed in phenylephrine-precontracted aortic rings [59]. The contractile response involves both the input of extracellular calcium [59] and its release from intracellular stores [60]. The effects of CT on both the smooth muscle and endothelial cells are curbed by high calcium concentrations [61, 62].

Despite the fact that CTs are very toxic compounds highly unlikely to exert a positive effect on the heart and blood vessels, CTs (fraction 1 from *N. naja siamensis*) have been reported to induce a positive inotropic response with no contractures at a dose of up to 100 μg/mL [10], which may be useful in myocardial pathology, accompanied by a decrease in the pumping function of the heart. Currently, only cardiac glycosides are used as drugs with a positive inotropic effect, which, according to the DIG study, is particularly good on patients with chronic heart failure with a reduced left ventricular ejection function [63]. Therefore, searching for new compounds possessing a cardiotonic effect remains a priority. However, there is nary information about studies of CTs with such a profile of action in pathological myocardium models; e.g., in SHR rats with reduced cardiac contractility. CTs may also be useful in exploring the mechanisms of dystrophic vascular calcification [64]. In this case, CTs are used as a methodological approach for triggering a cascade of pathological events that may be used to investigate vasoprotective mechanisms.

The TFT group also includes venomous cardiotoxin-like proteins [65] that interact with the different adrenergic receptors (ARs) abundant in the cardiovascular system. For example, a number of toxins have been isolated from the venom of the eastern green mamba *D. angusticeps*. These specifically interact with different subtypes of adrenergic receptors: ρ-Da1a (*Fig. 4*) selectively blocks the α1A-AR subtype [66, 67], and ρ-Da1b blocks all three α2-AR subtypes [68, 69]. The so-called muscarinic toxins MT1 and MT2 reversibly bind to α1-ARs [70]. The toxins MTβ and CM-3, similar to ρ-Da1a, were isolated from the venom of the black mamba *D. polylepis*; however, they interact with higher affinity with the α1B- and α1D-AR subtypes [71].

β-Cardiotoxin was isolated from the venom of the king cobra *Ophiophagus hannah* (*Fig. 4*). It is capable of blocking β1 and β2 ARs [72]. This leads to a decrease in the heart rate *in vivo* and *in vitro* without noticeable cytotoxicity, which may be associated with the inability of β-cardiotoxin to directly interact with the membrane, due to some of its structural features [73]. Later, a cytotoxic effect on cultured smooth muscle cells and no effect on skeletal cells and cardiac myocytes were shown in [74]. Interestingly, the study revealed direct negative inotropic and lusitropic effects, with the intracellular calcium concentration in systole remaining unchanged. These data may indicate the existence of direct mechanisms of β-cardiotoxin action which are

not associated with AR activation, and the ability of ARs to alter the sensitivity of myofilaments to calcium ions. The presence of compounds in the TFT group which interact highly specifically with individual AR subtypes may be of great utility in pharmacological studies, because each of the three subtypes plays an important role in CVS pathologies and their correction. For example, blocking β-ARs is one of the main directions in the therapy of various forms of hypertension and chronic heart failure [75, 76]; activation of α1-ARs may be considered as a compensatory pathway in the desensitization of the β-AR pathway [77–79]; and α2 activation may be considered as a cardioprotective pathway preventing adrenergic overload of the heart [80, 81] and, as shown in our publications, blocking the development of arrhythmias and Ca-overload in cardiomyocytes [82, 83].

One of the TFT groups is composed of the so-called non-conventional toxins that contain an additional disulfide bond in the N-terminal fragment and are usually characterized by low toxicity. Interestingly, one of the representatives of this group, toxin WTX, when administered intravenously, reduced blood pressure in rats [84] by affecting cholinergic transmission.

Another TFT group is represented by toxins affecting the activity of various ion channels and the receptors present in the CVS. However, since there are no data on the effect of these toxins on the CVS, they are not discussed in this review.

Other types of toxins. There are a number of other toxins that affect the CVS and lack enzymatic activity. These include toxins of the CRISP (Cysteine-RIch Secretory Protein) family, which are 23–25 kDa proteins containing eight disulfide bonds. For example, ablomin from the venom of *A. blomhoffi* and some similar toxins blocked the contraction of rat arterial smooth muscles caused by a high concentration of potassium ions. Ablomin is supposed to inhibit the voltage-gated influx of extracellular calcium, which causes vascular contraction [13]. Natrin of *N. atra* venom induces a contractile response in the endothelium-denuded thoracic aorta of mice [85]. Further experiments showed that natrin is able to block the high-conductance calcium-activated potassium channels (BK_{Ca}) that play a significant role in the regulation of the vascular tone. In addition, natrin can block the skeletal isoform of the ryanodine receptor [86] and voltage-gated potassium channels $K_V1.3$ [87].

The protein alternagin-C, isolated from *Bothrops alternatus* snake venom, has a very interesting effect on the CVS [88]. This protein can induce the expression of the vascular endothelial growth factor, proliferation and migration of endothelial cells, enhance angiogenesis, and increase the viability of myoblasts. Therefore, this peptide can play a crucial role in the mechanisms of tissue regeneration. A study of the alternagin-C effect on the cardiac function *in vitro* in freshwater fish showed that the protein enhances cardiac activity, promoting a significant increase in the contraction force and the rate of contraction and relaxation with a concomitant decrease in time to peak tension and improving the cardiac pumping capacity [14]. Alternagin-C improves the cardiac function by increasing the efficiency of calcium ion transport, which leads to positive inotropism and chronotropism [14]. Therefore, this protein can improve the regulation of the cardiac output, which indicates the possibility of its use in the treatment of cardiac contractile dysfunction. Also, the effect of alternagin-C on hypoxia/reoxygenation in isolated ventricular strips of fish and on morphological changes and the density of blood vessels was studied [15]. Treatment with alternagin-C provided protection of cardiomyocytes from the negative inotropism caused by hypoxia/reoxygenation. This protein also stimulated angiogenesis and improved excitation–contraction coupling during hypoxic conditions. These results indicate a new therapeutic strategy for the treatment of diseases associated with ischemia.

A number of snake venom proteins mimic the effects of the endogenous factors that regulate the physiological functions of the body. Regarding the CVS, of interest is a group of proteins, such as vascular endothelial growth factors (VEGFs), that can enhance angiogenesis and increase vascular permeability. VEGFs exhibit hypotensive [17] and cardioprotective effects [16]. Three receptor tyrosine kinases, known as VEGFR-1, VEGFR-2, and VEGFR-3, act as VEGF receptors. VEGFR-1 and VEGFR-2 are present primarily on vascular endothelial cells and mediate several major angiogenic activities: for example, endothelial cell proliferation. Reperfusion injury of the heart includes, among various mechanisms, coronary endothelial dysfunction. VEGF activates endothelial cells and has a cardioprotective effect. Snake venoms contain proteins that induce VEGF-like effects in endothelial cells. A number of the proteins that interact with VEGF receptors have been isolated and characterized [16]. In this case, some snake proteins selectively interacted with VEGFR-2, e.g., vammin from *V. ammodytes*, while others exhibited selectivity for VEGFR-1, e.g., VEGF from *T. flavoviridis* [89]. It was found that a protein from *V. lebetina*, like VEGF, significantly reduces reperfusion injury and infarct size thanks to a stimulation of VEGFR-2 receptors [16]. However, its activity proved somewhat less impactful than that of VEGF. Probably, snake venoms contain proteins with

the same cardioprotective activity as in VEGFs, but without their inherent side effects.

Enzymatic protein toxins

Of the many enzymes present in snake venoms, so far only phospholipases A2 (PLA2s) have exhibited direct action on the CVS. Snake venom PLA2s belong to the class of secreted lipolytic enzymes that hydrolyze the ester bond of glycerophospholipids at the Sn2 position to form lysophospholipids and free fatty acids [90], which serve as a source for the synthesis of the secondary mediators involved in the physiological processes taking place in cells. However, the effect of lipolysis products is not decisive for cardiotoxicity [91]; rather, damage to the cell membrane plays a leading role here [92]. In addition, some of the physiological effects are mediated through interaction with secretory PLA2 receptors [93]. Snake venom PLA2s can lower blood pressure through the production of arachidonic acid, a precursor of cyclooxygenase metabolites (prostaglandins or prostacyclins). It should be noted that systemic administration of high PLA2 doses can cause disruptions in the structure of myocardial tissue [21, 94] and its functioning, such as bradycardia and atrioventricular block [95, 96]. Interestingly, some of the cardiotoxic effects observed in *in vivo* animal studies are due to disruptions in the composition of the internal medium of the organism [97, 98]. PLA2s derived from the venoms of different snakes can differ significantly in their cardiotoxicity; e.g., PLA2s from *O. hannah* and *N. nigricollis* cause intracellular structural changes and contracture [94, 96, 99], in contrast to the PLA2 from the venom of *N. naja atra* that lacks cardiotoxicity [99]. The inotropic effect can be multidirectional; usually, contractility decreases after short growth, accompanied by an increase in the resting tension that can be transformed into contracture [20, 21, 99]. Acting on blood vessels, PLA2s usually exert a vasorelaxant effect that is independent of the endothelium and is partially mediated by an increase in cGMP in smooth muscle cells [18, 19]. The PLA2 effects can be significantly weakened by suramin [100] and a phospholipase A2 inhibitor: *p*-bromophenacyl bromide [21, 97]. As in the case of CTs, the PLA2 effects can be blocked by a high concentration of calcium ions, while calcium channel blockers are ineffective [19, 96]. PLA2s and CTs induce myocardial contracture, whereas PLA2 induces vascular relaxation.

PROSPECTS OF SNAKE VENOMS IN DRUG DEVELOPMENT AND POSSIBLE ROADBLOCKS

Snake venom toxins highly efficiently and selectively affect the various systems in living organisms, including the CVS, which makes them very attractive as a basis for drug design. The main disadvantages of toxins are their high toxicity and irreversibility of action; i.e., the inability of an affected system to return to its original state. Given the abovementioned data, there are many highly active cardiotropic or vasoactive snake toxins which may be used in the future as a basis for the development of new drugs. Some of these proteins and peptides have demonstrated that they can be highly selective tools in research into physiological processes. Others have been used as probes for potential therapeutic targets or a basis for the development of therapeutic agents.

We have already considered the antihypertensive drug captopril (*Fig. 1*) derived from a bradykinin-potentiating peptide of the South American jararaca. Another drug based on this peptide is enalapril, (S)-1-[N-[1-(ethoxycarbonyl)-3-phenylpropyl] -L-alanyl]-L-proline, that is currently widely used in hypertension.

A promising drug is cenderitide, produced by the addition of a 15 aa C-terminal fragment of a natriuretic peptide isolated from *D. angusticeps* venom to the full-length human C-type natriuretic peptide. It may be used in heart failure. Cenderitide has already passed the first and second phases of clinical trials, albeit with a small number of participants, and has shown promise in maintaining left-ventricular function in myocardial infarction.

There are good prospects for alternagin-C, its analogs, and endothelial vascular growth factor analogs from snake venoms for the development of drugs that prevent reperfusion injuries. However, it remains necessary to evaluate the *in vivo* activity of these proteins and their stability in the organism. To date, there are still no data on clinical studies of these proteins.

In conclusion, it should be noted that, despite their existing drawbacks, a number of snake venom peptides and proteins that affect the CVS have good prospects as a basis for the development of new drugs. ●

The reported study was funded by RFBR, project number 20-14-50134.

REFERENCES

1. Kakumanu R., Kemp-Harper B.K., Silva A., Kuruppu S., Isbister G.K., Hodgson W.C. // Sci. Repts. 2019. V. 9. № 1. P. 20231.
2. Péterfi O., Boda F., Szabó Z., Ferencz E., Bába L. // Molecules. 2019. V. 24. № 15. P. 2778.
3. Morais K.L.P., Ianzer D., Miranda J.R.R., Melo R.L., Guerreiro J.R., Santos R.A.S., Ulrich H., Lameu C. // Peptides.

2013. V. 48. P. 124–133.
4. Da Silva S.L., Dias-Junior C.A., Baldasso P.A., Damico D.C.S., Carvalho B.M.A., Garanto A., Acosta G., Oliveira E., Albericio F., Soares A.M., et al. // Peptides. 2012. V. 36. № 2. P. 206–212.
5. Ichiki T., Dzhoyashvili N., Burnett J.C. // Internat. J. Cardiol. 2019. V. 281. P. 166–171.
6. Park S.-A., Kim T.-G., Han M.-K., Ha K.-C., Kim S.-Z., Kwak Y.-G. // Exp. Mol. Med. 2012. V. 44. № 6. P. 363–368.
7. Mahjoub Y., Malaquin S., Mourier G., Lorne E., Abou Arab O., Massy Z.A., Dupont H., Ducancel F. // PLoS One. 2015. V. 10. № 7. P. e0132864.
8. Watanabe C., Hirano K., Kanaide H. // British J. Pharmacol. 1993. V. 108. № 1. P. 30–37.
9. Averin A.S., Astashev M.E., Andreeva T.V., Tsetlin V.I., Utkin Y.N. // Doklady. Biochem. Biophys. 2019. V. 487. № 1. P. 282–286.
10. Harvey A.L., Marshall R.J., Karlsson E. // Toxicon: Official J. Internat. Soc. Toxinol. 1982. V. 20. № 2. P. 379–396.
11. Kini R.M., Koh C.Y. // Biochem. Pharmacol. 2020. V. 181. P. 114105.
12. Wang C.-H., Wu W.-G. // FEBS Lett. 2005. V. 579. № 14. P. 3169–3174.
13. Yamazaki Y., Koike H., Sugiyama Y., Motoyoshi K., Wada T., Hishinuma S., Mita M., Morita T. // Eur. J. Biochem. 2002. V. 269. № 11. P. 2708–2715.
14. Monteiro D.A., Kalinin A.L., Selistre-de-Araujo H.S., Vasconcelos E.S., Rantin F.T. // Toxicon: Official J. Internat. Soc. Toxinol. 2016. V. 110. P. 1–11.
15. Monteiro D.A., Kalinin A.L., Selistre-de-Araújo H.S., Nogueira L.A.N., Beletti M.E., Fernandes M.N., Rantin F.T. // Comp. Biochem. Physiol. Toxicol. Pharmacol.: CBP. 2019. V. 215. P. 67–75.
16. Messadi E., Aloui Z., Belaidi E., Vincent M.-P., Couture-Lepetit E., Waeckel L., Decorps J., Bouby N., Gasmi A., Karoui H., et al. // J. Cardiovasc. Pharmacol. 2014. V. 63. № 3. P. 274–281.
17. Takahashi H., Hattori S., Iwamatsu A., Takizawa H., Shibuya M. // J. Biol. Chem. 2004. V. 279. № 44. P. 46304–46314.
18. Bing R.J., Saeed M. // Mol. Cell. Biochem. 1987. V. 78. № 1. P. 81–88.
19. Huang H.-C., Lee C.Y. // Eur. J. Pharmacol. 1985. V. 118. № 1–2. P. 139–146.
20. Karabuva S., Lukšić B., Brizić I., Latinović Z., Leonardi A., Križaj I. // Toxicon: Official J. Internat. Soc. Toxinol. 2017. V. 139. P. 94–100.
21. Rodrigues M.A.P., Dias L., Rennó A.L., Sousa N.C., Smaal A., da Silva D.A., Hyslop S. // Toxicology. 2014. V. 323. P. 109–124.
22. Sciani J.M., Pimenta D.C. // J. Venom. Anim. Toxins Including Trop. Dis. 2017. V. 23. P. 45.
23. Sturrock E.D., Lubbe L., Cozier G.E., Schwager S.L.U., Arowolo A.T., Arendse L.B., Belcher E., Acharya K.R. // Biochem. J. 2019. V. 476. № 10. P. 1553–1570.
24. Cotton J., Hayashi M.A.F., Cuniasse P., Vazeux G., Ianzer D., de Camargo A.C.M., Dive V. // Biochemistry. 2002. V. 41. № 19. P. 6065–6071.
25. Hayashi M.A.F., Murbach A.F., Ianzer D., Portaro F.C.V., Prezoto B.C., Fernandes B.L., Silveira P.F., Silva C.A., Pires R.S., Britto L.R.G., et al. // J. Neurochem. 2003. V. 85. № 4. P. 969–977.
26. Babenko V.V., Ziganshin R.H., Weise C., Dyachenko I., Shaykhutdinova E., Murashev AN., Zhmak M., Starkov V., Hoang A.N., Tsetlin V., et al. // Biomedicines. 2020. V. 8. № 8. P. 249.
27. Camargo A.C.M., Ianzer D., Guerreiro J.R., Serrano S.M.T. // Toxicon: Official J. Internat. Soc. Toxinol. 2012. V. 59. № 4. P. 516–523.
28. Nakipova O.V., Averin A.S., Tarlachkov S.V., Kokoz Y.M. // Doklady Biological Sciences: Proc. Acad. Sci. USSR, Biol. Sci. Sect. 2013. V. 451. P. 203–208.
29. Zhihao L., Jingyu N., Lan L., Michael S., Rui G., Xiyun B., Xiaozhi L., Guanwei F. // Heart Failure Rev. 2020. V. 25. № 3. P. 523–535.
30. Querobino S.M., Ribeiro C.A.J., Alberto-Silva C. // Peptides. 2018. V. 103. P. 90–97.
31. Ianzer D., Santos R.A.S., Etelvino G.M., Xavier C.H., de Almeida Santos J., Mendes E.P., Machado L.T., Prezoto B.C., Dive V., de Camargo A.C.M. // J. Pharmacol. Exp. Therapeutics. 2007. V. 322. № 2. P. 795–805.
32. El-Saadani M.A.M., El-Sayed M.F. // Comp. Biochem. Physiol. Toxicol. Pharmacol.: CBP. 2003. V. 136. № 4. P. 387–395.
33. Morais K.L.P., Hayashi M.A.F., Bruni F.M., Lopes-Ferreira M., Camargo A.C.M., Ulrich H., Lameu C. // Biochem. Pharmacol. 2011. V. 81. № 6. P. 736–742.
34. Mueller S., Paegelow I., Reissmann S. // Signal Transduction. 2006. V. 6. № 1. P. 5–18.
35. Meems L.M.G., Burnett J.C. // JACC. Basic Translat. Sci. 2016. V. 1. № 7. P. 557–567.
36. Springer J., Azer J., Hua R., Robbins C., Adamczyk A., McBoyle S., Bissell M.B., Rose R.A. // J. Mol. Cell. Cardiol. 2012. V. 52. № 5. P. 1122–1134.
37. Brusq J.M., Mayoux E., Guigui L., Kirilovsky J. // Brit. J. Pharmacol. 1999. V. 128. № 1. P. 206–212.
38. Fry B.G., Wickramaratana J.C., Lemme S., Beuve A., Garbers D., Hodgson W.C., Alewood P. // Biochem. Biophys. Res. Commun. 2005. V. 327. № 4. P. 1011–1015.
39. Chen B.-Y., Chen J.-K., Zhu M.-Z., Zhang D.-L., Sun J.-S., Pei J.-M., Feng H.-S., Zhu X.-X., Jin J., Yu J. // PLoS One. 2011. V. 6. № 5. P. e20477.
40. Schweitz H., Vigne P., Moinier D., Frelin C., Lazdunski M. // J. Biol. Chem. 1992. V. 267. № 20. P. 13928–13932.
41. Soares M.R., Oliveira-Carvalho A.L., Wermelinger L.S., Zingali R.B., Ho P.L., Junqueira-de-Azevedo I.L.M., Diniz M.R.V. // Toxicon: Official J. Internat. Soc. Toxinol. 2005. V. 46. № 1. P. 31–38.
42. Aminasab M., Elmi M.M., Endlich N., Endlich K., Parekh N., Naderi-Manesh H., Schaller J., Mostafavi H., Sattler M., Sarbolouki M.N., et al. // FEBS Lett. 2004. V. 557. V. 1–3. P. 104–108.
43. Sridharan S., Kini R.M., Richards A.M. // Pharmacol. Res. 2020. V. 155. P. 104687.
44. Leite-Moreira A.F., Brás-Silva C. // Am. J. Physiol. Heart Circulatory Physiol. 2004. V. 287. № 3. P. H1194–H1199.
45. Burrell K.M., Molenaar P., Dawson P.J., Kaumann A.J. // J. Pharmacol. Exp. Therapeutics. 2000. V. 292. № 1. P. 449–459.
46. Konrad D., Oldner A., Wanecek M., Rudehill A., Weitzberg E., Biber B., Johansson G., Häggmark S., Haney M. // Am. J. Physiol. Heart Circulatory Physiol. 2005. V. 289. № 4. H1702–H1709.
47. Hayashi M.A.F., Ligny-Lemaire C., Wollberg Z., Wery M., Galat A., Ogawa T., Muller B.H., Lamthanh H., Doljansky Y., Bdolah A., et al. // Peptides. 2004. V. 25. № 8. P. 1243–1251.
48. Skovsted G.F., Kruse L.S., Berchtold L.A., Grell A.-S., Warfvinge K., Edvinsson L. // PLoS One. 2017. V. 12. № 3. P. e0174119.

49. Dufton M.J., Hider R.C. // Pharmacol. Therapeutics. 1988. V. 36. № 1. P. 1–40.
50. Jang J.Y., Krishnaswamy T., Kumar S., Jayaraman G., Yang P.W., Yu C. // Biochemistry. 1997. V. 36. № 48. P. 14635–14641.
51. Jayaraman G., Kumar T.K., Tsai C.C., Srisailam S., Chou S.H., Ho C.L., Yu C. // Protein Sci.: Publ. Protein Soc. 2000. V. 9. № 4. P. 637–646.
52. Huang S.J., Wu C.K., Sun J.J. // Zhongguo Yao Li Xue Bao = Acta Pharmacologica Sinica. 1991. V. 12. № 2. P. 125–131.
53. Wang H.X., Lau S.Y., Huang S.J., Kwan C.Y., Wong T.M. // J. Mol. Cell. Cardiol. 1997. V. 29. № 10. P. 2759–2770.
54. Loots J.M., Meij H.S., Meyer B.J. // British J. Pharmacol. 1973. V. 47. № 3. P. 576–585.
55. Sun J.J., Walker M.J. // Toxicon: Official J. Internat. Soc. Toxinol. 1986. V. 24. № 3. P. 233–245.
56. Debnath A., Saha A., Gomes A., Biswas S., Chakrabarti P., Giri B., Biswas A.K., Gupta S.D., Gomes A. // Toxicon: Official J. Internat. Soc. Toxinol. 2010. V. 56. № 4. P. 569–579.
57. Tzeng W.F., Chen Y.H. // Biochem. J. 1988. V. 256. № 1. P. 89–95.
58. Wang C.-H., Monette R., Lee S.-C., Morley P., Wu W.-G. // Toxicon: Official J. Internat. Soc. Toxinol. 2005. V. 46. № 4. P. 430–440.
59. Ho K.H., Kwan C.Y., Huang S.J., Bourreau J.P. // Zhongguo Yao Li Xue Bao = Acta Pharmacologica Sinica. 1998. V. 19. № 3. P. 197–202.
60. Chen K.M., Guan Y.Y., Sun J.J. // Zhongguo Yao Li Xue Bao = Acta Pharmacologica Sinica. 1993. V. 14. № 6. P. 500–504.
61. Kwan C.Y., Kwan T.K., Huang S.J. // Clin. Exp. Pharmacol. Physiol. 2002. V. 29. № 9. P. 823–828.
62. Ou Y.J., Leung Y.M., Huang S.J., Kwan C.Y. // Biochim. Biophys. Acta. 1997. V. 1330. № 1. P. 29–38.
63. Perry G., Brown E., Thornton R., Shiva T., Hubbard J., Reddy K.R., Doherty J.E., Cardello F.P., Fast A., Radford M.J. // N. Engl. J. Med. 1997. V. 336. № 8. P. 525–533.
64. Zhao Y., Urganus A.L., Spevak L., Shrestha S., Doty S.B., Boskey A.L., Pachman L.M. // Calcified Tissue Internat. 2009. V. 85. № 3. P. 267–275.
65. Blanchet G., Collet G., Mourier G., Gilles N., Fruchart-Gaillard C., Marcon E., Servent D. // Biochimie. 2014. V. 103. P. 109–117.
66. Palea S., Maiga A., Guilloteau V., Rekik M., Guérard M., Rouget C., Rischmann P., Botto H., Camparo P., Lluel P., et al. // British J. Pharmacol. 2013. V. 168. № 3. P. 618–631.
67. Quinton L., Girard E., Maiga A., Rekik M., Lluel P., Masuyer G., Larregola M., Marquer C., Ciolek J., Magnin T., et al. // British J. Pharmacol. 2010. V. 159. № 2. P. 316–325.
68. Maïga A., Mourier G., Quinton L., Rouget C., Gales C., Denis C., Lluel P., Sénard J.-M., Palea S., Servent D., et al. // Toxicon: Official J. Internat. Soc. Toxinol. 2012. V. 59. № 4. P. 487–496.
69. Rouget C., Quinton L., Maïga A., Gales C., Masuyer G., Malosse C., Chamot-Rooke J., Thai R., Mourier G., de Pauw E., et al. // British J. Pharmacol. 2010. V. 161. № 6. P. 1361–1374.
70. Harvey A.L., Kornisiuk E., Bradley K.N., Cerveñansky C., Durán R., Adrover M., Sánchez G., Jerusalinsky D. // Neurochem. Res. 2002. V. 27. № 11. P. 1543–1554.
71. Blanchet G., Upert G., Mourier G., Gilquin B., Gilles N., Servent D. // Toxicon: Official J. Internat. Soc. Toxinol. 2013. V. 75. P. 160–167.
72. Rajagopalan N., Pung Y.F., Zhu Y.Z., Wong P.T.H., Kumar P.P., Kini R.M. // FASEB J.: Official Publ. Fed. Am. Sci. Exp. Biol. 2007. V. 21. № 13. P. 3685–3695.
73. Roy A., Qingxiang S., Alex C., Rajagopalan N., Jobichen C., Sivaraman J., Kini R. M. // Protein Sci.: Publ. Protein Soc. 2019. V. 28. № 5. P. 952–963.
74. Lertwanakarn T., Suntravat M., Sanchez E.E., Boonhoh W., Solaro R.J., Wolska B.M., Martin J.L., de Tombe P.P., Tachampa K. // J. Venom. Anim. Toxins Incl. Trop. Dis. 2020. V. 26. P. e20200005.
75. Perros F., de Man F.S., Bogaard H.J., Antigny F., Simonneau G., Bonnet S., Provencher S., Galiè N., Humbert M. // Circulation. Heart Failure. 2017. V. 10. № 4. P. e003703.
76. Wiysonge C.S., Bradley H.A., Volmink J., Mayosi B.M., Opie L.H. // Cochrane Database Systematic Rev. 2017. V. 1. № 1. P. CD002003.
77. Nozdrachyov A.D., Tsirkin V.I., Korotaeva Y.V. // Ros. Fiziol. Zh. im. I.M. Sechenova. 2016. V. 102. № 2. P. 130–145.
78. Nozdrachyov A.D., Tsirkin V.I., Korotaeva Y.V. // Ros. Fiziol. Zh. im. I.M. Sechenova. 2016. V. 102. № 3. P. 262–275.
79. O'Connell T.D., Jensen B.C., Baker A.J., Simpson P.C. // Pharmacol. Rev. 2014. V. 66. № 1. P. 308–333.
80. Alekseev A.E., Park S., Pimenov O.Y., Reyes S., Terzic A. // Pharmacol. Therapeutics. 2019. V. 197. P. 179–190.
81. Bao N., Tang B. // Mediators Inflamm. 2020. P. 6136105.
82. Averin A.S., Nakipova O.V., Kosarsky L.S., Pimenov O.Y., Galimova M.H., Nenov M.N., Berejnov A.V., Alekseev A.E. // Biophysics. 2019. V. 64. № 5. P. 793–798.
83. Kokoz Y.M., Evdokimovskii E.V., Maltsev A.V., Nenov M.N., Nakipova O.V., Averin A.S., Pimenov O.Y., Teplov I.Y., Berezhnov A.V., Reyes S., et al. // J. Mol. Cell. Cardiol. 2016. V. 100. P. 9–20.
84. Ogay A.Y., Rzhevsky D.I., Murashev A.N., Tsetlin V.I., Utkin Y.N. // Toxicon: Official J. Internat. Soc. Toxinol. 2005. V. 45. № 1. P. 93–99.
85. Wang J., Shen B., Guo M., Lou X., Duan Y., Cheng X. P., Teng M., Niu L., Liu Q., Huang Q., et al. // Biochemistry. 2005. V. 44. № 30. P. 10145–10152.
86. Zhou Q., Wang Q.-L., Meng X., Shu Y., Jiang T., Wagenknecht T., Yin C.-C., Sui S.-F., Liu Z. // Biophys. J. 2008. V. 95. № 9. P. 4289–4299.
87. Wang F., Li H., Liu M.-N., Song H., Han H.-M., Wang Q.-L., Yin C.-C., Zhou Y.-C., Qi Z., Shu Y.-Y., et al. // Biochem. Biophys. Res. Commun. 2006. V. 351. № 2. P. 443–448.
88. Souza D.H., Iemma M.R., Ferreira L.L., Faria J.P., Oliva M.L., Zingali R.B., Niewiarowski S., Selistre-de-Araujo H.S. // Arch. Biochem. Biophys. 2000. V. 384. № 2. P. 341–350.
89. Yamazaki Y., Matsunaga Y., Tokunaga Y., Obayashi S., Saito M., Morita T. // J. Biol. Chem. 2009. V. 284. № 15. P. 9885–9891.
90. Arni R.K., Ward R.J. // Toxicon: Official J. Internat. Soc. Toxinol. 1996. V. 34. № 8. P. 827–841.
91. Barrington P.L., Yang C.C., Rosenberg P. // Life Sci. 1984. V. 35. № 9. P. 987–995.
92. Gutiérrez J.M., Ownby C.L. // Toxicon: Official J. Internat. Soc. Toxinol. 2003. V. 42. № 8. P. 915–931.
93. Gasanov S.E., Dagda R.K., Rael E.D. // J. Clin. Toxicol. 2014. V. 4. № 1. P. 1000181.
94. Huang M.Z., Gopalakrishnakone P. // Toxicon: Official J. Internat. Soc. Toxinol. 1996. V. 34. № 2. P. 201–211.
95. Evangelista I.L., Martins A.M.C., Nascimento N.R.F., Havt A., Evangelista J.S.A.M., de Norões T.B.S., Toyama M.H., Diz-Filho E.B., de Oliveira Toyama D., Fonteles M.C., et al. // Toxicon: Official J. Internat. Soc. Toxinol. 2010. V. 55. № 6. P. 1061–1070.
96. Huang M.Z., Wang Q.C., Liu G.F. // Toxicon: Official J.

Internat. Soc. Toxinol. 1993. V. 31. № 5. P. 627–635.
97. Dias L., Rodrigues M.A.P., Rennó A.L., Stroka A., Inoue B.R., Panunto P.C., Melgarejo A.R., Hyslop S. // Toxicon: Official J. Internat. Soc. Toxinol. 2016. V. 123. P. 1–14.
98. Lee C.Y., Lin W.W., Chen Y.M., Lee S.Y. // Acta Physiol. Pharmacol. Latinoamericana: Organo de la Asociacion Latinoamericana de Ciencias Fisiologicas y de la Asociacion Latinoamericana de Farmacologia. 1989. V. 39. № 4. P. 383–391.
99. Fletcher J.E., Yang C.C., Rosenberg P. // Toxicol. Appl. Pharmacol. 1982. V. 66. № 1. P. 39–54.
100. Sifuentes D.N., El-Kik C.Z., Ricardo H.D., Tomaz M.A., Strauch M.A., Calil-Elias S., Arruda E.Z., Schwartz E.F., Melo P.A. // Toxicon: Official J. Internat. Soc. Toxinol. 2008. V. 51. № 1. P. 28–36.

Neutrophil Extracellular Traps (NETs): Opportunities for Targeted Therapy

D. V. Volkov[1], G. V. Tetz[2], Y. P. Rubtsov[1], A. V. Stepanov[1*], A. G. Gabibov[1]
[1]Shemyakin-Ovchinnikov Institute of Bioorganic Chemistry RAS, Moscow, 117997 Russia
[2]Pavlov First State Medical University of St. Petersburg, St Petersburg, 197022 Russia
*E-mail: stepanov.aleksei.v@gmail.com
Received June 29, 2021; in final form, September 06, 2021
DOI: 10.32607/actanaturae.11503

ABSTRACT **Antitumor therapy, including adoptive immunotherapy, inevitably faces powerful counteraction from advanced cancer. If hematological malignancies are currently amenable to therapy with CAR-T lymphocytes (T-cells modified by the chimeric antigen receptor), solid tumors, unfortunately, show a significantly higher degree of resistance to this type of therapy. As recent studies show, the leading role in the escape of solid tumors from the cytotoxic activity of immune cells belongs to the tumor microenvironment (TME). TME consists of several types of cells, including neutrophils, the most numerous cells of the immune system. Recent studies show that the development of the tumor and its ability to metastasize directly affect the extracellular traps of neutrophils (neutrophil extracellular traps, NETs) formed as a result of the response to tumor stimuli. In addition, the nuclear DNA of neutrophils – the main component of NETs – erects a spatial barrier to the interaction of CAR-T with tumor cells. Previous studies have demonstrated the promising potential of deoxyribonuclease I (DNase I) in the destruction of NETs. In this regard, the use of eukaryotic deoxyribonuclease I (DNase I) is promising in the effort to increase the efficiency of CAR-T by reducing the NETs influence in TME. We will examine the role of NETs in TME and the various approaches in the effort to reduce the effect of NETs on a tumor.**
KEYWORDS **cancer, tumor microenvironment, neutrophils, NETosis.**

INTRODUCTION

Unlike hematologic cancers, malignant solid tumors form a closed structure consisting of several layers. Cancer cells residing in the tumor center and carrying adhesion receptors on their surface are linked by tunneling nanotubes and communicate with each other through autocrine and paracrine signals transmitted via soluble factors and the extracellular matrix. A layer forming another niche (involving vessels, cancer-associated fibroblasts and stromal cells receiving signals via adhesion receptors and soluble factors) lies closer to the periphery. Farther away from the tumor's center lies a confined layer that is reached by stimulation or inhibition signals from tumor cells and includes the neovasculature, intratumoral lymph nodes, immune cells, cancer-associated fibroblasts, the extracellular matrix, and nerve endings. The proximal (with respect to the normal tissue) layer that involves the nearest lymphatic and blood vessels, immune cells, and proximal lymphoid elements is considered to be the outermost layer. The additional levels of tumor cell architecture that influence cancer development refer to metastatic foci. The so-called confined layer is considered a boundary of the tumor microenvironment. The neoplasm's complex structural morphology requires the engineering of targeted therapy based on a significant mechanistic understanding of therapeutic agents' penetration directly to transforming cells [1–5].

The major portion of TME consists of the host's immune cells, with neutrophils being the most numerous group. Inflammation develops within the tumor growth region, and the signals released by malignant and tumor-associated cells recruit neutrophils, which are converted to tumor-associated neutrophils (TANs). They belong to the group of myeloid-derived suppressor cells (MDSCs). MDSCs can also manifest in non-cancer cases; however, these cells inhibit the protective antitumor immune response in cancer patients. TANs also receive cell death (cellular suicide) signals, which induces a specific type of cell death accompanied by the release of a large quantity of genomic DNA, as well as the proteins and enzymes associated with it, which eventually form NETs. The composition of NETs varies depending on the type of the initial stimulus/a combination of stimuli. The chromosomal DNA network is an invariable part of NETs. This has led researchers to suggest that deoxyribonucleases can be used to efficiently degrade NETs. Indeed, recent studies

have demonstrated that DNase I administered to experimental mice slows the progression of a primary tumor, inhibits the metastatic potential of tumor cells, and increases animals' lifespan. The hopeful results of research focusing on the administration of purified DNase I to mice have driven the elaboration of novel methods for the delivery of DNase I into the body.

FORMATION OF NETS AND THEIR COMPOSITION

Neutrophil extracellular traps were discovered as one of the defense mechanisms of neutrophils in response to bacterial infection [6]. Released NETs impede the transmission of pathogens in the blood flow and kill pathogenic microorganisms [6, 7]. Later, NETs were also found in tumor biopsy specimens from patients with different types of cancer. Their presence correlated with poor prognosis in patients [8–11]. This discovery has spurred active research into the role played by NETs in oncogenesis.

In the best-studied pathway leading to the expulsion of NETs (*Fig. 1*), signal transduction by extracellular signal-regulated kinase (EPK) results in the activation of NADPH oxidase (NOX) (*Fig. 1*, I) and production of superoxide radicals, which are converted to hydrogen peroxide by superoxide dismutase (*Fig. 1*, II) [12]. Myeloperoxidase (MPO) converts hydrogen peroxide to hypochlorous acid, and activates neutrophil elastase (NE) (*Fig. 1*, II). Neutrophil elastase is responsible for the disassembly of the cytoskeleton and nuclear membrane; it allows the nuclear content to mix with the cytoplasm (*Fig. 1*, II) [13]. The conversion of the arginine residues within histones to citrulline (citrullination) by activated protein arginine deiminase (PAD) and proteolytic cleavage of MPO and NE cause chromatin decondensation (*Fig. 1*, III) [14]. Chromatin fibers bind to granules and cytoplasmic proteins, to be eventually expelled from the cell (*Fig. 1*, IV).

Production of reactive oxygen species (ROS) is the key event in NETosis (*Fig. 1*, I). The mitochondrial respiratory chain and NOX contribute independently to the formation of oxygen species. Many different receptors trigger the formation of NETs by activating NOX in the classical suicidal NETosis [15] (*Fig. 1*, I). Identically, phorbol 12-myristate 13-acetate (PMA) mimics diacylglycerol and activates protein kinase C (PKC) [16] and ERK signal transduction, which is similar to the induction of NETs by pathogenic bacteria and fungi. Interestingly, the pathways of PMA-mediated induction of NETosis in cultivated neutrophils can differ significantly [17].

The NOX-independent NETosis pathway is based on the production of mitochondrial ROS promoted by alkaline pH, which increases the inflow of Ca^{2+} [18]. In turn, Ca^{2+} activates SK3, one of the types of small conductance calcium-activated potassium channels (SK), a crucial step in NOX-independent NETosis [19]. PAD4 activation and histone citrullination are clearly visible in NOX-independent NETosis. Calcium ionophores such as ionomycin and A23187 (calcimycin) activate PKC-ζ and, then, PAD4 [16], thus triggering

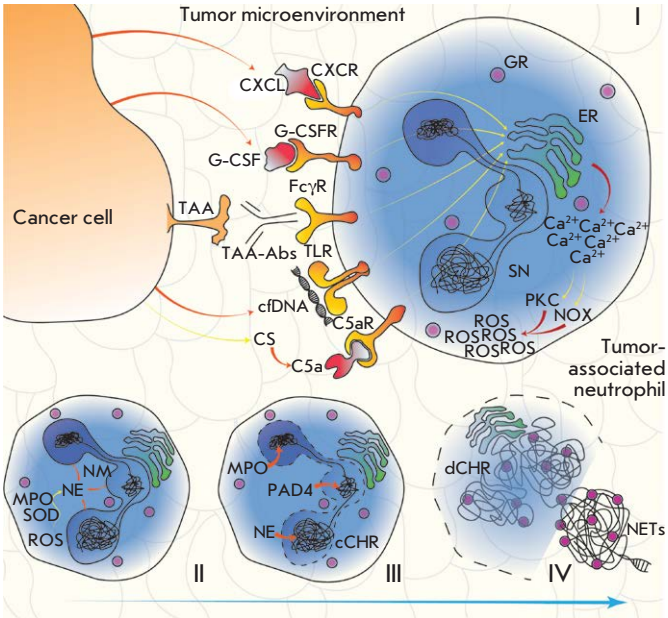

Fig. 1. The signaling pathway of NOX-dependent NETosis. Various cancer-associated stimuli increase the cytoplasmic Ca^{2+} concentration in TANs, which results in the activation of PKC and NOX and, therefore, leads to intracellular production of ROS (I). As SOD and MPO interact, ROS are converted into HClO, leading to the activation of NE (II). NE promotes NM degradation, and then PAD4, MPO, and NE ensure chromatin decondensation and its mixing with cytoplasmic granules (III); the resulting mixture (in the form of NETs) is released into the extracellular space during NETosis (IV). Abbreviations: TAA – tumor-associated antigen; cfDNA – cell-free DNA; TAA-Abs – anti-TAA antibodies; FcγR – receptor for the fragment crystallizable region of IgG; TLR – toll-like receptor; CXCL – cytokine belonging to the CXC family; CXCR – CXCL receptor; ER – endoplasmic reticulum; GR – granule; G-CSF – granulocyte colony-stimulating factor; G-CSFR – G-CSF receptor; CS – complement system; C5a – complement component 5a; C5aR – C5a receptor; SN – segmented nucleus; NM – nuclear membrane; NE – neutrophil elastase; MPO – myeloperoxidase; SOD – superoxide dismutase; ROS – reactive oxygen species; PKC – protein kinase C; NOX – NADPH oxidase; cCHR – condensed chromatin; PAD4 – protein arginine deiminase 4; dCHR – decondensed chromatin; NETs – extracellular neutrophil traps

NOX-independent NETosis. Under certain conditions, nuclear and mitochondrial DNA is released via the NOX-independent pathway from live neutrophils. It was shown that ribonucleoprotein immune complexes act upon normal neutrophils or low-density immunosuppressive neutrophils, thus inducing the production of mitochondrial ROS and release of NETs containing mitochondrial DNA from living cells [20]. In patients with sepsis, activated platelets adhere to neutrophils and cause the extrusion of NETs from living cells [21].

Although production of ROS and enzyme activities play different roles in NETosis induction, the different activation pathways result in the formation of NETs exhibiting similar bactericidal capabilities [22].

Along with ionophores and PMA, there are more than a dozen substances capable of inducing NETosis, which can be used *in vitro* to analyze this process [10]. A proteomic analysis of NETs induced by various stimuli has revealed 330 proteins within these NETs; 74 of these proteins were present regardless of the method used for NETosis induction, comprising a pool of key elements that characterizes any type of the known NETs [23, 24].

THE ROLE OF NETS IN TUMOR PROCESSES

The data on the link between NETs and cancer progression have driven intense research into the functions of NETs in different tumor types. It was reported soon after that NETs have a direct impact on the proliferation of tumor cells through proteases or activating signaling [25–28].

Cancer cells are one of the reasons for NETosis

Cancer cells were shown to be able to induce NETosis both *in vivo* and *in vitro* [11], and the link between TANs and NET formation was also demonstrated [11, 29–31]. Thus, it has been found *in vitro* that the human pancreatic tumor cell line (AsPC-1) induces NET formation [32]; the extracellular proteins expressed in this cell line are considered to play a crucial role in NETosis. The study has also demonstrated that NETs enhance the endogenous thrombin potential of normal plasma and induce the migration, invasion, and angiogenesis of cancer cells [32]. As shown in another *in vitro* study, extracellular RNAs from Lewis lung carcinoma cells cause NET formation [33].

Neutrophils in mice with chronic myeloid leukemia, breast or lung cancer are more susceptible to NETosis than those in healthy animals. The high susceptibility of neutrophils to NET formation in these pathologies correlates with the systemic effect tumors have on the organism [34, 35].

Neutrophil recruitment by a conditioned medium from hypoxic cancer cells was observed *in vitro*. Cell migration was mediated by high levels of chemokines and HMGB1, which can also generate NETs in the TME [31]. Tohme *et al*. [31] have recently shown that NETs promote tumor cell growth by enhancing their mitochondrial function. Furthermore, tumors implanted subcutaneously grew faster in control mice than in PAD4 knockout (PAD4-KO) ones in these researchers' experiments. PAD4-deficient mice had fewer hepatic metastases compared to the control group. Recombinant DNase I injected intraperitoneally also reduced the number of metastases in PAD4 wild-type mice. Immunofluorescence staining of tumor tissue slices in PAD4-KO mice showed a very low level of neutrophil infiltration compared to the control. Overall, these data emphasize the pivotal role played by neutrophil recruitment and NET formation in tumor growth and progression [31]. Park *et al*. also revealed a close relationship between metastatic cancer cells, neutrophil recruitment, and NET formation [11]. They showed that metastatic breast cancer cells induce NETosis that maintains metastases due to NETs. Cytokine CXCL1 mediated neutrophil recruitment in tumor in mice with orthotypically transplanted breast cancer cells: 4T1 (metastatic) and 4T07 (non-metastatic). Primary 4T1 tumors were found to contain more neutrophils than 4T07 tumors do. The lower CXCL1 level in 4T1 cells reduced neutrophil infiltration in the tumor. It was shown by immunofluorescence staining of lung tissue slices that NETs form immediately after 4T1 has been injected into the tail vein. Furthermore, metastatic cells released a granulocyte colony-stimulating factor (G-CSF), which induced NETosis around these cells, while antibodies blocking G-CSF significantly reduced NET formation after injection of 4T1 cells [11].

NETs are involved in circulatory disturbance

Changes in blood vessels and increased neutrophil infiltration in the heart and kidney resembling the systemic lesions in cancer patients were revealed in RIP1-Tag2 (spontaneous insulinoma) and MMTV-PyMT (breast cancer) transgenic mice. Furthermore, platelet–neutrophil complexes were detected in the kidney of these animals, an indication of NET formation. It is noteworthy that this phenomenon was observed in none of the analyzed healthy mice [36]. It was shown earlier that platelets drive neutrophils to release NETs, thus promoting bacterial death [21]. Olsson *et al.* found that accumulation of NETs in the vasculature was related to the activation of the proinflammatory adhesion molecules ICAM-1, VCAM-1. and E-selectin, as well as the proinflammatory cytokines IL-1b, IL-6 and chemokine CXCL1. DNase I injected to ensure NET degradation normalized renal and cardiac perfusion and prevented vascular occlusion in these organs. The results of this

study strongly suggest that NETs mediate the detrimental harmful effects of tumors on distal organs by disrupting tumor vasculature and increasing the likelihood of inflammation in them [36].

In case of pancreatic adenocarcinoma (PA), NETs and platelets play a crucial role in blood hypercoagulation, which increases the risk of venous thromboembolism and cancer-associated thrombosis both in the orthotopic PA model in C57BL/6 mice and in patients [37]. Berger-Achituv *et al.* [8] showed that TANs are found in diagnostic biopsy specimens from children with Ewing sarcoma. In two specimens, NETs were produced due to TANs. These patients had metastases and early tumor recurrence after high-dose chemotherapy, thus indicating that NETs might play a role in the progression of Ewing sarcoma [8]. The association of NETs with altered coagulation in patients with tumors attests to the important role of NETs in cancer. NETs stimulate cancer-associated thrombosis, a symptom accompanying a very poor prognosis [26, 38]. The levels of circulating NETs were also measured in patients with hepatocellular carcinoma (HCC) by assessing the levels of the respective markers (DNA–histone complexes, double-stranded DNA, and NE). Markers of contact phase activation (factor XIIa and high-molecular-weight kininogen) were measured in the same way. The levels of NETs and markers of contact phase activation were higher in patients with HCC compared to those in healthy subjects in [39]. Jung *et al.* revealed a correlation between the high levels of NET markers and hypercoagulation observed in patients with malignant pancreatic neoplasms [32]. Furthermore, the plasma levels of citrullinated histone H3 (H3-cit) were higher in late-stage cancer patients compared to those in healthy subjects while an elevated H3-cit level was found in the neutrophils of cancer patients. In addition, the plasma level of H3-cit in cancer patients did correlate with the levels of NETosis activators: NE, MPO, interleukins-6 and -8 [40, 41].

An elevated level of NETs correlates with the presence of a tumor process

Spontaneous intestinal neoplasia in mice correlates with the accumulation of immunosuppressive pro-oncogenic low-density neutrophils with an N2 phenotype, activation of the complement receptor C3a, and NET formation [42].

A positive correlation between an elevated plasma level of NETs and various tumor processes was revealed in studies that compared cancer patients and healthy subjects. Li *et al.* detected NETs in the lung tissue, peripheral blood, and sputum in patients with lung cancer [33]. In patients with colorectal cancer, the levels of NETs produced by neutrophils after *in vitro* stimulation were significantly higher than those in the control group consisting of healthy subjects and came with an unfavorable clinical outcome [10]. Park *et al.* demonstrated the presence of NETs in patients with breast cancer. NETs were also detected in lung metastases in this case; the highest percentage was revealed in patients with triple-negative breast cancer [11]. Identically, Tohme *et al.* [41] found that the amount of TANs and NETs in the histopathology specimens of hepatic metastases from colorectal cancer patients was increased compared to that in healthy subjects. Furthermore, high levels of citrullinated histones were also detected in tumors, being indicative of NETosis. The preoperative serum levels of MPO–DNA, a reliable marker of systemic NETosis [41], were higher in patients compared to those in healthy controls and were associated with a poor prognosis. Therefore, the serum levels of MPO–DNA can potentially be a prognostic marker in these patients [31].

NETs and cancer cells adhere to each other

Along with exhibiting local tumor and systemic effects, NETs can promote metastasizing by entrapping circulating tumor cells (CTCs) (*Fig. 2,* IV) [43]. Adhesion of cancer cells to NETs and upregulated expression of integrin beta-1 both in cancer cells and in NETs, which seems to be a key factor of CTC adhesion to NETs, was demonstrated in mice with intraperitoneal sepsis mimicking postoperative inflammation. Treatment with DNase I inhibited this process [44]. In mouse models, NETosis and the entrapment of CTCs in lungs caused hepatic micrometastases [45]. Finally, NETs contributed to the development and progression of hepatic metastases after a surgical intervention [41]. Monti *et al.* [46] demonstrated that different cancer cell lines (HT1080, U-87MG, H1975, DU 145, PC-3, and A-431) can adhere *in vitro* to NETs formed from neutrophil-like cells through the integrins $\alpha_5\beta_1$, $\alpha_v\beta_3$ and $\alpha_v\beta_5$ that were present on the cell surface. An excess of cyclic peptide RGD inhibited the adhesion of cancer cells to NETs to a level similar to that observed during hydrolysis of NETs by DNase I.

NETs induce metastases

In addition to all the functions described earlier, NETs awaken dormant cancer cells (*Fig. 2,* I). The involvement of NET in tumor recurrence was recently established [47]. Chronic lung inflammation caused by tobacco smoke or nasal instillation of a NETosis-activating lipopolysaccharide was found to promote the activation of dormant cancer cells and metastasizing. NETs were found bound to the extracellular matrix and triggered laminin cleavage and remodeling to give rise to a new surface epitope, which initiated

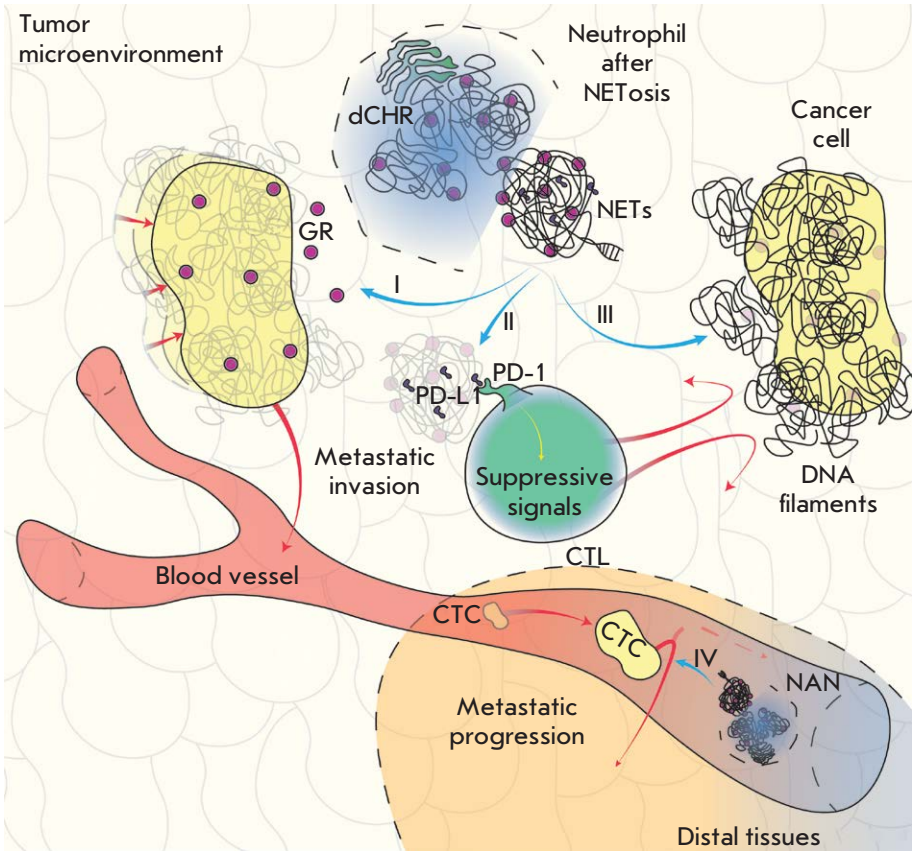

Fig. 2. The diverse effects of NETs. NET granules contain fragments that promote dormant cancer cell awakening and change their phenotype to a metastatic one (I); NETs also contain suppressor molecules (PD-L1), which interact with cytotoxic cells and suppress their activity (II); DNA filaments, the key component of NETs, ensnare tumor cells, thus acting as a steric hindrance to the interaction with cytotoxic cells (III); the awakened cancer cells leave the microenvironment and enter blood vessels; these circulating cells are entrapped in distal tissues via NETs, which promotes metastasizing (IV). Abbreviations: dCHR – decondensed chromatin; NETs – neutrophil extracellular traps; GR – granule; PD-L1 – programmed death ligand 1; PD-1 – PD-L1 receptor; CTL – cytotoxic T lymphocyte; CTC – circulating tumor cell; NAN – neutrophil after NETosis

the proliferation of dormant cells by activating integrin and transducing signals through the FAK/ERK/MLCK/YAP kinase pathway. The *in vitro* and *in vivo* NET degradation by DNase I suppressed metastasizing. Monteiro *et al.* [47] assessed the ability of isolated NETs to change the phenotype of human breast cancer cells to a pro-metastatic one. NETs change the typical morphology of MCF7 cells from the epithelial phenotype to a mesenchymal one, when the migratory properties of a tumor are enhanced and there are typical signs of epithelial–mesenchymal transition (EMT) such as elevated levels of N-cadherin and fibronectin. Meanwhile, the E-cadherin level was found to decrease. Interestingly, NETs positively regulate the expression of genes encoding several factors associated with proinflammatory and pro-metastatic properties. Comparison of the Cancer Genome Atlas and RNA sequencing data revealed that specimens taken from patients with breast cancer show a significant correlation between the expression of the protumor genes and the expression of the genes whose products are involved in the interaction with neutrophils. Therefore, NETs drive the pro-metastatic phenotype in human breast cancer cells by activating the EMT program.

NETs suppress the activity of cytotoxic cells

In addition to the functions already listed above, an important function of NETs is that they "hide" cancer cells from cytotoxic immune ones. In their recent study, Melero *et al.* [48] showed that CXCL chemokines released by tumor cells induce NETosis in TANs. The resulting NETs envelop the tumor using DNA filaments to form a physical hindrance to any interaction between T cells or NK cells and tumors (*Fig. 2*, III). Furthermore, as established recently, NETs can contain suppressor molecules (e.g., PD-L1) and have a negative effect on the activity of cytotoxic lymphocytes (*Fig. 2*, II) [49]. A specific role in the study of NETs should be assigned to work on the treatment of cancer pathologies with the help of re-programmed T cells with induced cytolytic activity. CAR-T therapy of hematological cancer, taking into account the approaches of personalized medicine, is increasingly becoming a reality [50, 51]. At the same time, the possibilities of CAR-T therapy for solid tumors remain very limited

[52]. It is likely that NETs, in this case, will become important in efforts to overcome the barriers to effective CAR-T therapy.

METHODS FOR DETECTING AND INFLUENCING NETS

According to recent findings, NETs could turn into a promising therapeutic target for cancer. Judging by the crucial role played by NETs in enhancing the metastatic potential of malignant cells, patients prognosis can be improved by inhibiting NET formation and activity [11].

Markers of NETs

To perform clinical screening of NETs, the reference levels of NETosis need to be identified using a standardized procedure. However, a fully reliable method has not been reported in the literature yet. The simplest techniques for detecting NETs *in vivo* include measuring of the blood levels of NET-bound substances such as circulating cell-free DNA, H3-cit, NE, and MPO. Thus, the amount of circulating free DNA was measured in the serum specimens of patients with colorectal and breast cancer using simple nucleic acid staining [53, 54]. Although the amount of circulating DNA is known to correlate with the size and grade of breast tumor [55], the direct DNA staining technique was not specific enough in order to measure NETosis. The increased serum level of cell-free DNA (cfDNA) in cancer patients can also be related to other factors such as apoptotic and necrotic cells or the microorganisms passing into the systemic blood flow when permeability of the intestinal wall increases [56]. Hence, measuring circulating MPO–DNA conjugates is more specific to NET formation than for assessing the cfDNA level only [57]. H3-cit results from PAD4-mediated citrullination during NETosis and is the most specific marker of circulating NETs [58]. Furthermore, H3-cit can have prognostic significance, since Thålin *et al.* [40] have revealed that a high plasma level of H3-cit is a significant prognostic factor of short-term mortality in patients with late-stage cancer. Despite this, there were no significant differences in other NET-related markers, including NE and MPO, in severely ill patients with or without malignant neoplasms. The reason is that these enzymes can be released independently during neutrophil degranulation, in the absence of NET formation. These findings indicate that H3-cit currently remains the most reliable indicator of NETosis.

NETs as a therapeutic target

According to the review by Jorch and Kubes [59], the vast majority of experimental and clinical studies focusing on NETs were conducted for noncancer pathologies such as autoimmune or lung diseases, or the complications associated with autoimmune disorders. Autoimmune pathologies characterized by a high level of antibodies to DNA are of particular interest in terms of studying the role of NETs [60–64]. Studies involving patients with systemic lupus erythematosus (SLE) have shown that serum DNase I is important for the hydrolysis of NET chromatin. Moreover, in some patients with SLE, DNase I dysfunction causes severe renal damage, which reinforces the fact that the balance between NET formation and degradation is extremely important [65]. Based on these findings, DNase I was tested using experimental cancer models. Thus, treatment with DNase I mitigated disease severity in mouse models of breast cancer [36]. Furthermore, in the mouse model of intraperitoneal sepsis mimicking a postoperative inflammatory environment, DNase I disrupted *in vivo* interaction between NETs and circulating tumor cells [44]. Systemic administration of DNase I also reduced the number of metastases in the mouse model of metastatic lung cancer [45], while DNase I-coated nanoparticles exhibited an even stronger effect due to enzyme stabilization. The DNase I nanoparticles hydrolyzed NETs *in vitro* and inhibited the spread of metastatic breast cancer to the lungs *in vivo*, although it had no effect on the growth of the primary tumor [11, 66]. In a recent study [67], a novel method for increasing plasma activity of DNase I was demonstrated. DNase I gene transfer to hepatocytes mediated by adeno-associated viruses after a single intravenous injection in a mouse model of colorectal cancer suppressed metastases and increased the number of $CD8^+$ T cells in the tumors [68, 69]. These encouraging results obtained using animal studies give grounds for performing clinical trials once DNase I can be used as an antitumor agent.

It would be reasonable to extend the application of the inhibitors of the molecules involved in NETosis and preventing NET formation currently employed for non-cancer pathologies so as to use these inhibitors on cancer patients after they have undergone clinical trials. These agents include NE inhibitors, which are used to treat the chronic obstructive pulmonary disease, and PAD4 inhibitors. These compounds can improve the clinical outcome for cancer patients [25] even though the commercially available PAD4 inhibitors (e.g., Cl-amidine) have a short half-life in blood serum [70]. Domingo-Gonzalez *et al.* proposed to use prostaglandin E_2 (PGE_2) as an alternative inhibitor of NET formation; through the prostaglandin receptors EP_2 or EP_4, prostaglandin negatively affects NETosis both in mice and in patients who have undergone hematopoieic stem cell transplantation [71]. Another study has shown either that PGE_2 inhibits the NET formation induced both by cancer cells and PMA (probably due to the increased

concentration of intracellular cAMP and reduced concentration of intracellular Ca^{2+} needed for NET formation) or that antithrombin significantly inhibits the NET formation induced by cancer cells [72]. Along with the NETosis inhibitors listed above, the NET inhibitor chloroquine was proved to reduce platelet aggregation, the level of circulating tissue factor (coagulation factor III), and hypercoagulation in mice with tumor. The same effects were uncovered in patients with cancer [37].

Unfortunately, clinical trials are far from being concluded, and the optimal method for affecting NETs is yet to be determined (NCT03781531, NCT04177576, NCT04294589, NCT01491230, and NCT01533779).

CONCLUSIONS

The unique role played by NETs in carcinogenesis, including their ability to initiate neoplastic transformation, accelerate tumor growth and metastatic spread, not to mention enhance resistance to anticancer therapy, makes NETs a relevant therapeutic target. There is an increasing number of promising studies that focus on using various approaches to NETs degradation in oncology, including the use of DNase I. The application of DNase I implies that both NETs and cfDNA will undergo degradation, which is expected to ensure a more efficient inhibitory effect on cancer. The optimal approach to combatting NETs is yet to be identified; future research does need to focus on NETosis regulation and the balance between NET formation and degradation, so that NETs could be affected without disturbing the immune system functions. Furthermore, there is additional value in considering as cancer therapy disrupters tight junctions. They maintain the integrity of solid epithelial tumors and prevent the penetration of bulky agents, including T cells and NK cells, into the tumor's depth. In the areas of the intercellular junction of epithelial cells protein desmoglein 2 is in action. It provides structural adhesion of neighboring cells [73]. Recombinant proteins called "junction openers" bind desmoglein 2. They cause a temporary and specific opening of tight junctions that allows various therapeutic agents to penetrate tumors [74, 75]. It seems possible that the combined use of DNase I and "junction openers" could increase the effectiveness of anticancer therapy, since it would facilitate the effective penetration of agents, including cytotoxic cells, into the depths of a malignant neoplasm. ●

This work was supported by the Ministry Education and Science of the Russian Federation (grant No. 075-15-2020-773).

REFERENCES

1. Stepanov A.V., Belogurov A.A.J., Ponomarenko N.A., Stremovskiy O.A., Kozlov L.V., Bichucher A.M., Dmitriev S.E., Smirnov I.V., Shamborant O.G., Balabashin D.S., et al. // PLoS One. 2011. V. 6. № 6. P. e20991.
2. Ukrainskaya V.M., Rubtsov Y.P., Knorre V.D., Maschan M.A., Gabibov A.G., Stepanov A.V. // Acta Naturae. 2019. V. 11. № 4. P. 33–41.
3. Guryev E.L., Volodina N.O., Shilyagina N.Y., Gudkov S.V., Balalaeva I.V., Volovetskiy A.B., Lyubeshkin A.V., Sen' A.V., Ermilov S.A., Vodeneev V.A., et al. // Proc. Natl. Acad. Sci. USA. 2018. V. 115. № 39. P. 9690–9695.
4. Ukrainskaya V.M., Stepanov A.V., Glagoleva I.S., Knorre V.D., Belogurov A.A., Gabibov A.G. // Acta Naturae. 2017. V. 9. № 3. P. 55–63.
5. Sokolova E., Proshkina G., Kutova O., Shilova O., Ryabova A., Schulga A., Stremovskiy O., Zdobnova T., Balalaeva I., Deyev S. // J. Control. Release. 2016. V. 233. P. 48–56.
6. Brinkmann V., Reichard U., Goosmann C., Fauler B., Uhlemann Y., Weiss D.S., Weinrauch Y., Zychlinsky A. // Science (80-.). 2004. V. 303. № 5663. P. 1532–1535.
7. Branzk N., Lubojemska A., Hardison S.E., Wang Q., Gutierrez M.G., Brown G.D., Papayannopoulos V. // Nat. Immunol. 2014. V. 15. № 11. P. 1017–1025.
8. Berger-Achituv S., Brinkmann V., Abu-Abed U., Kühn L., Ben-Ezra J., Elhasid R., Zychlinsky A. // Front. Immunol. 2013. V. 4. P. 48.
9. Oklu R., Sheth R.A., Wong K.H.K., Jahromi A.H., Albadawi H. // Cardiovasc. Diagn. Ther. 2017. V. 7. Suppl. 3. P. S140–S149.
10. Richardson J.J.R., Hendrickse C., Gao-Smith F., Thickett D.R. // Int. J. Inflam. 2017. V. 2017. P. 4915062.
11. Park J., Wysocki R.W., Amoozgar Z., Maiorino L., Fein M.R., Jorns J., Schott A.F., Kinugasa-Katayama Y., Lee Y., Won N.H., et al. // Sci. Transl. Med. 2016. V. 8. № 361. P. 138.
12. Delgado-Rizo V., Martínez-Guzmán M., Iñiguez-Gutierrez L., García-Orozco A., Alvarado-Navarro A., Fafutis-Morris M. // Front. Immunol. 2017. V. 8. P. 81.
13. Papayannopoulos V., Metzler K.D., Hakkim A., Zychlinsky A. // J. Cell Biol. 2010. V. 191. № 3. P. 677–691.
14. Wang Y., Li M., Stadler S., Correll S., Li P., Wang D., Hayama R., Leonelli L., Han H., Grigoryev S.A., et al. // J. Cell Biol. 2009. V. 184. № 2. P. 205–213.
15. Yang H., Biermann M.H., Brauner J.M., Liu Y., Zhao Y., Herrmann M. // Front. Immunol. 2016. V. 7. P. 302.
16. Radic M., Neeli I. // Front. Immunol. 2013. V. 4. P. 38.
17. Hoppenbrouwers T., Autar A.S.A., Sultan A.R., Abraham T.E., van Cappellen W.A., Houtsmuller A.B., van Wamel W. J.B., van Beusekom H.M.M., van Neck J.W., de Maat M.P.M. // PLoS One. 2017. V. 12. № 5. P. e0176472.
18. Naffah de Souza C., Breda L.C.D., Khan M.A., Almeida S.R. de, Câmara N.O.S., Sweezey N., Palaniyar N. // Front. Immunol. 2018. V. 8. P. 1849.
19. Douda D.N., Khan M.A., Grasemann H., Palaniyar N. // Proc. Natl. Acad. Sci. USA. 2015. V. 112. № 9. P. 2817–2822.
20. Lood C., Blanco L.P., Purmalek M.M., Carmona-Rivera C., De Ravin S.S., Smith C.K., Malech H.L., Ledbetter J.A., Elkon K.B., Kaplan M.J. // Nat. Med. 2016. V. 22. № 2. P. 146–153.
21. Clark S.R., Ma A.C., Tavener S.A., McDonald B., Goodarzi

Z., Kelly M.M., Patel K.D., Chakrabarti S., McAvoy E., Sinclair G.D., et al. // Nat. Med. 2007. V. 13. № 4. P. 463–469.
22. Kenny E.F., Herzig A., Krüger R., Muth A., Mondal S., Thompson P.R., Brinkmann V., von Bernuth H., Zychlinsky A. // Elife. 2017. V. 6. P. e24437.
23. Urban C.F., Ermert D., Schmid M., Abu-Abed U., Goosmann C., Nacken W., Brinkmann V., Jungblut P.R., Zychlinsky A. // PLoS Pathog. 2009. V. 5. № 10. P. e1000639.
24. Fadini G.P., Menegazzo L., Rigato M., Scattolini V., Poncina N., Bruttocao A., Ciciliot S., Mammano F., Ciubotaru C.D., Brocco E., et al. // Diabetes. 2016. V. 65. № 4. P. 1061–1071.
25. Brinkmann V. // J. Innate Immun. 2018. V. 10. № 5–6. P. 414–421.
26. Cools-Lartigue J., Spicer J., Najmeh S., Ferri L. // Cell. Mol. Life Sci. 2014. V. 71. № 21. P. 4179–4194.
27. Sangaletti S., Tripodo C., Vitali C., Portararo P., Guarnotta C., Casalini P., Cappetti B., Miotti S., Pinciroli P., Fuligni F., et al. // Cancer Discov. 2014. V. 4. № 1. P. 110–129.
28. Homa-Mlak I., Majdan A., Mlak R., Małecka-Massalska T. // Postepy Hig. Med. Dosw. (Online). 2016. V. 70. P. 887–895.
29. Masucci M.T., Minopoli M., Carriero M.V. // Front. Oncol. 2019. V. 9. P. 1146.
30. Powell D.R., Huttenlocher A. // Trends Immunol. 2016. V. 37. № 1. P. 41–52.
31. Yazdani H.O., Roy E., Comerci A.J., van der Windt D.J., Zhang H., Huang H., Loughran P., Shiva S., Geller D.A., Bartlett D.L., et al. // Cancer Res. 2019. V. 79. № 21. P. 5626–5639.
32. Jung H.S., Gu J., Kim J.-E., Nam Y., Song J.W., Kim H.K. // PLoS One. 2019. V. 14. № 4. P. e0216055.
33. Li Y., Yang Y., Gan T., Zhou J., Hu F., Hao N., Yuan B., Chen Y., Zhang M. // Int. J. Oncol. 2019. V. 55. № 1. P. 69–80.
34. Demers M., Krause D.S., Schatzberg D., Martinod K., Voorhees J.R., Fuchs T.A., Scadden D.T., Wagner D.D. // Proc. Natl. Acad. Sci. USA. 2012. V. 109. № 32. P. 13076–13081.
35. Demers M., Wagner D.D. // Oncoimmunology. 2013. V. 2. № 2. P. e22946.
36. Cedervall J., Zhang Y., Huang H., Zhang L., Femel J., Dimberg A., Olsson A.-K. // Cancer Res. 2015. V. 75. № 13. P. 2653–2662.
37. Boone B.A., Murthy P., Miller-Ocuin J., Doerfler W.R., Ellis J.T., Liang X., Ross M.A., Wallace C.T., Sperry J.L., Lotze M.T., et al. // BMC Cancer. 2018. V. 18. № 1. P. 678.
38. Demers M., Wagner D.D. // Semin. Thromb. Hemost. 2014. V. 40. № 3. P. 277–283.
39. Seo J. Do, Gu J.-Y., Jung H.S., Kim Y.J., Kim H.K. // Clin. Appl. Thromb. 2019. V. 25. P. 1076029618825310.
40. Thålin C., Lundström S., Seignez C., Daleskog M., Lundström A., Henriksson P., Helleday T., Phillipson M., Wallén H., Demers M. // PLoS One. 2018. V. 13. № 1. P. e0191231.
41. Tohme S., Yazdani H.O., Al-Khafaji A.B., Chidi A.P., Loughran P., Mowen K., Wang Y., Simmons R.L., Huang H., Tsung A. // Cancer Res. 2016. V. 76. № 6. P. 1367–1380.
42. Guglietta S., Chiavelli A., Zagato E., Krieg C., Gandini S., Ravenda P.S., Bazolli B., Lu B., Penna G., Rescigno M. // Nat. Commun. 2016. V. 7. № 1. P. 11037.
43. Szczerba B.M., Castro-Giner F., Vetter M., Krol I., Gkountela S., Landin J., Scheidmann M.C., Donato C., Scherrer R., Singer J., et al. // Nature. 2019. V. 566. № 7745. P. 553–557.
44. Najmeh S., Cools-Lartigue J., Rayes R.F., Gowing S., Vourtzoumis P., Bourdeau F., Giannias B., Berube J., Rousseau S., Ferri L.E., et al. // Int. J. Cancer. 2017. V. 140. № 10. P. 2321–2330.
45. Cools-Lartigue J., Spicer J., McDonald B., Gowing S., Chow S., Giannias B., Bourdeau F., Kubes P., Ferri L. // J. Clin. Invest. 2013. V. 123. № 8. P. 3446–3458.
46. Monti M., De Rosa V., Iommelli F., Carriero M.V., Terlizzi C., Camerlingo R., Belli S., Fonti R., Di Minno G., Del Vecchio S. // Int. J. Mol. Sci. 2018. V. 19. № 8. P. 2350.
47. Martins-Cardoso K., Almeida V.H., Bagri K.M., Rossi M.I., Mermelstein C.S., König S., Monteiro R.Q. // Cancers (Basel). 2020. V. 12. № 6. P. 1542.
48. Teijeira Á., Garasa S., Gato M., Alfaro C., Migueliz I., Cirella A., de Andrea C., Ochoa M.C., Otano I., Etxeberria I., et al. // Immunity. 2020. V. 52. № 5. P. 856–871.
49. Zhang H., van der Windt D.J., Ren J., Tsung A., Huang H. // J. Immunol. 2019. V. 202. № 1. P. 135.
50. Stepanov A.V., Markov O.V., Chernikov I.V., Gladkikh D.V., Zhang H., Jones T., Sen'kova A.V., Chernolovskaya E.L., Zenkova M.A., Kalinin R.S., et al. // Sci. Adv. 2018. V. 4. № 11. P. 4580.
51. Huang J., Alexey S., Li J., Jones T., Grande G., Douthit L., Xie J., Chen D., Wu X., Michael M., et al. // Leukemia. 2019. V. 33. № 9. P. 2315–2319.
52. Kalinin R.S., Petukhov A.V., Knorre V.D., Maschan M.A., Stepanov A.V., Gabibov A.G. // Acta Naturae. 2018. V. 10. № 2. P. 16–23.
53. Agassi R., Czeiger D., Shaked G., Avriel A., Sheynin J., Lavrenkov K., Ariad S., Douvdevani A. // Am. J. Clin. Pathol. 2015. V. 143. № 1. P. 18–24.
54. Czeiger D., Shaked G., Eini H., Vered I., Belochitski O., Avriel A., Ariad S., Douvdevani A. // Am. J. Clin. Pathol. 2011. V. 135. № 2. P. 264–270.
55. Kohler C., Radpour R., Barekati Z., Asadollahi R., Bitzer J., Wight E., Bürki N., Diesch C., Holzgreve W., Zhong X.Y. // Mol. Cancer. 2009. V. 8. № 1. P. 105.
56. Bronkhorst A.J., Ungerer V., Diehl F., Anker P., Dor Y., Fleischhacker M., Gahan P.B., Hui L., Holdenrieder S., Thierry A.R. // Hum. Genet. 2021. V. 140. № 4. P. 565–578.
57. Yoo D., Floyd M., Winn M., Moskowitz S.M., Rada B. // Immunol. Lett. 2014. V. 160. № 2. P. 186–194.
58. Mauracher L.-M., Posch F., Martinod K., Grilz E., Däullary T., Hell L., Brostjan C., Zielinski C., Ay C., Wagner D.D., et al. // J. Thromb. Haemost. 2018. V. 16. № 3. P. 508–518.
59. Jorch S.K., Kubes P. // Nat. Med. 2017. V. 23. № 3. P. 279–287.
60. Gabibov A.G., Ponomarenko N.A., Tretyak E.B., Paltsev M.A., Suchkov S.V. // Autoimmun. Rev. 2006. V. 5. № 5. P. 324–330.
61. Belogurov A.J., Kozyr A., Ponomarenko N., Gabibov A. // Bioessays. 2009. V. 31. № 11. P. 1161–1171.
62. Durova O.M., Vorobiev I.I., Smirnov I.V., Reshetnyak A.V., Telegin G.B., Shamborant O.G., Orlova N.A., Genkin D.D., Bacon A., Ponomarenko N.A., et al. // Mol. Immunol. 2009. V. 47. № 1. P. 87–95.
63. Gololobov G.V., Mikhalap S.V., Starov A.V., Kolesnikov A.F., Gabibov A.G. // Appl. Biochem. Biotechnol. 1994. V. 47. № 2–3. P. 305.
64. Kozyr A.V., Kolesnikov A.V., Zelenova N.A., Sashchenko L.P., Mikhalap S.V., Bulina M.E., Ignatova A.N., Favorov P.V., Gabibov A.G. // Appl. Biochem. Biotechnol. 2000. V. 83. № 1–3. P. 255–268.
65. Hakkim A., Fürnrohr B.G., Amann K., Laube B., Abed U.A., Brinkmann V., Herrmann M., Voll R.E., Zychlinsky A. // Proc. Natl. Acad. Sci. USA. 2010. V. 107. № 21. P. 9813–9818.
66. Hollmén M., Karaman S., Schwager S., Lisibach A., Christiansen A.J., Maksimow M., Varga Z., Jalkanen S.,

Detmar M. // Oncoimmunology. 2016. V. 5. № 3. P. 1115177.
67. Xia Y., He J., Zhang H., Wang H., Tetz G., Maguire C.A., Wang Y., Onuma A., Genkin D., Tetz V., et al. // Mol. Oncol. 2020. V. 14. № 11. P. 2920–2935.
68. Alcazar-Leyva S., Ceron E., Masso F., Montano L.F., Gorocica P., Alvarado-Vasquez N. // Med. Sci. Monit. 2009. V. 15. № 2. P. 51–55.
69. Alekseeva L.A., Sen'kova A.V., Zenkova M.A., Mironova N.L. // Mol. Ther. – Nucl. Acids. 2020. V. 20. P. 50–61.
70. Knight J.S., Subramanian V., O'Dell A.A., Yalavarthi S., Zhao W., Smith C.K., Hodgin J.B., Thompson P.R., Kaplan M.J. // Ann. Rheum. Dis. 2015. V. 74. № 12. P. 2199–2206.
71. Domingo-Gonzalez R., Martínez-Colón G.J., Smith A.J., Smith C.K., Ballinger M.N., Xia M., Murray S., Kaplan M.J., Yanik G.A., Moore B.B. // Am. J. Respir. Crit. Care Med. 2015. V. 193. № 2. P. 186–197.
72. Shishikura K., Horiuchi T., Sakata N., Trinh D.-A., Shirakawa R., Kimura T., Asada Y., Horiuchi H. // Br. J. Pharmacol. 2016. V. 173. № 2. P. 319–331.
73. Shilova O., Shilov E., Lieber A., Deyev S. // J. Control. Release. 2018. V. 286. P. 125–136.
74. Pitner R., Kim J., Davis-Bergthold J., Turner C., Stermann E., Adams J., Carter L., Ahlgren J., Fender P., Lieber A., et al. // Sci. Rep. 2019. V. 9. № 1. P. 1–13.
75. Choi I.-K., Strauss R., Richter M., Yun C.-O., Lieber A. // Front. Oncol. 2013. V. 3. P. 193.

Hybrid Complexes of Photosensitizers with Luminescent Nanoparticles: Design of the Structure

D. A. Gvozdev*, E. G. Maksimov, M. G. Strakhovskaya, V. Z. Pashchenko, A. B. Rubin
M.V. Lomonosov Moscow State University, Department of Biology, Moscow, 119991 Russia
*E-mail: danil131054@mail.ru
Received March 23, 2021; in final form, May 14, 2021
DOI: 10.32607/actanaturae.11379

ABSTRACT **Increasing the efficiency of the photodynamic action of the dyes used in photodynamic therapy is crucial in the field of modern biomedicine. There are two main approaches used to increase the efficiency of photosensitizers. The first one is targeted delivery to the object of photodynamic action, while the second one is increasing the absorption capacity of the molecule. Both approaches can be implemented by producing dye–nanoparticle conjugates. In this review, we focus on the features of the latter approach, when nanoparticles act as a light-harvesting agent and nonradiatively transfer the electronic excitation energy to a photosensitizer molecule. We will consider the hybrid photosensitizer–quantum dot complexes with energy transfer occurring according to the inductive-resonance mechanism as an example. The principle consisting in optimizing the design of hybrid complexes is proposed after an analysis of the published data; the parameters affecting the efficiency of energy transfer and the generation of reactive oxygen species in such systems are described.**
KEYWORDS **FRET, photosensitizer, luminescent nanoparticle, photodynamic therapy.**
ABBREVIATIONS **HC – hybrid complex; LNP – luminescent nanoparticle; Pc – phthalocyanine; PDT – photodynamic therapy; PS – photosensitizer; QD – semiconductor quantum dot, ROS – reactive oxygen species.**

INTRODUCTION

Theranostics, which combines photodynamic therapy (PDT) and fluorescence diagnostics, is a promising field in modern medicine that uses light to detect and eliminate tumors, other unwanted structures, as well as the foci of microbial and fungal infections of the skin and mucous membrane [1, 2]. Photodynamic reactions are carried out by dye molecules capable of absorbing a quantum of light and passing into a long-lived triplet state. During its deactivation, a dye molecule produces reactive oxygen species (ROSs) and free radicals. ROSs possess high oxidative activity and can be used to disrupt the functionality of individual biomolecules and the vital activity of whole cells. Such dyes are called photosensitizers (PSs). These are typically complex heterocyclic compounds with a number of absorption bands in the visible spectral range. A substantive search for highly effective PSs that can be used within the phenomenon of photosensitization for the treatment of cancer and infectious diseases is currently underway. A number of synthetic PSs are already successfully being used in clinical practice to fight certain types of cancer, in dentistry, etc. [3].

One of the key criteria in choosing dyes for PDT is the significant absorption capacity of PS in the red and near-infrared spectral regions, since light penetration depth into biological tissues is considered to be the greatest in this range. Modifying the structure of a PS molecule might be an inefficient way to meet this criterion; therefore, it might be required to use additional light collectors. Having absorbed light of the required spectral range, the light collector will transfer energy to the PS and, thereby, enhance its photodynamic effect.

The main mechanism of energy transfer in such hybrid complexes (HCs) is considered to be the nonradiative one (Förster resonant energy transfer, FRET). Accordingly, a number of requirements also apply regarding the light collector. In particular, the resonance condition imposes certain restrictions on the spectral characteristics of an energy donor and an energy acceptor. Taking into account the fact that the spectral properties of HC components largely depend on their structural properties, which can change during the complex formation, we obtain a complicated multicomponent system whose design optimization is

among the most consequential issues in applied biophysics.

Luminescent nanoparticles (LNPs) are currently the most commonly used as light collectors for PS molecules [4]. Such nanoparticles can be applied simultaneously as an antenna, a diagnostic marker, and a platform for targeted drug delivery. A sufficient number of reviews have focused on the latter two aspects of nanoparticle use [5–7], whereas the fundamental problems of using nanoparticles as a light collector receive less attention [8–10].

Upconversion [11, 12], silicon [13], and carbon [14, 15] nanoparticles are the LNPs most widely used in photobiology. Furthermore, a large number of studies have been devoted to the application of semiconductor nanoparticles (quantum dots, QDs) as energy donors for PS, although their biocompatibility still remains disputable [16]. Nevertheless, the question regarding the relationship between the spectral and structural properties of QDs is the one that has been resolved most satisfactorily, making it possible to study the energy transfer in HCs in detail.

This review considers the features of the design of HCs based on QDs and PSs with allowance for the complex formation mechanism, the stoichiometry of the complex, the structure of HC components, as well as the influence of these parameters on the efficiency of energy transfer and ROS generation in the complexes. We found out that the photodynamic properties of PS decrease with a rising ratio of the components of the PS : LNP complex because of its high local concentration on the nanoparticle surface even through energy transfer efficiency is enhanced. Enhancement of the luminescent properties of QDs due to protective shells can reduce the efficiency of energy transfer in HC, as the distance between the energy donor and the acceptor increases. Based on the correlations obtained, a technique allowing one to synthesize highly efficient HCs has been proposed; the aim of this technique is to maximize the generation of reactive oxygen species by the photosensitizer within a HC. The conclusions drawn in this review largely apply to HCs based on all other types of LNPs.

1. COMPONENTS OF THE HYBRID COMPLEX

1.1. Second-generation tetrapyrrolic photosensitizers

A photosensitizer that is highly efficient in terms of ROS yield is supposed to boast the following characteristics. First, the energy of its triplet state must be sufficient to enable a photodynamic reaction with molecular oxygen; the selection is performed to increase the yield of the triplet state and its lifetime. Second, the PS is supposed to exist in a monomeric state, since PS aggregates do not generate ROS as efficiently. Third, the PS should have a high absorption capacity, preferably within the "optical window" of biological tissues.

It is obvious that the photodynamic properties depend on the structure of a PS molecule. We will consider the relationship between the structural and photophysical properties of PSs using tetrapyrrole dyes, the most common second-generation PSs, as an example.

Porphin is the simplest dye of the tetrapyrrole series. The absorption spectrum of porphin contains an intense Soret band at the boundary between the UV and visible regions, as well as four low-intensity narrow bands in the visible region (Q_I–Q_{IV}; numbering starts at longer wavelengths). There are several main ways to modify the structure of a porphin molecule, making it possible to obtain PS that exhibit high photodynamic activity (*Fig. 1A*):

(A) sequential hydrogenation of two double bonds, which are not formally included in the conjugated system, shifts the Q_I band to the long-wavelength spectral region (a bathochromic shift) and increases its intensity by more than an order of magnitude. Hydrogenation gives rise to the classes of dihydroporphyrins (chlorins) and tetrahydroporphyrins (bacteriochlorins);

(B) replacement of carbon in the methine CH groups with a nitrogen atom (tetrazaporphyrins) or incorporation of benzene rings in the macrocycle of a dye molecule (tetrabenzoporphyrins) increases the intensity of the Q_I and Q_{III} bands, as well as causes their bathochromic shift. The strongest effect is obtained when these two approaches are combined, i.e., in the classes of tetrazatetrabenzoporphyrins or phthalocyanines (Pcs); and

(C) coordination of various elements by the macrocycle of a porphin molecule due to the lone electron pairs of the central nitrogen atoms. For porphyrins, complexes with divalent metals are the most typical. Formation of a metal complex leads to the degeneration of four absorption bands in the visible spectral region to leave two bands whose intensity is significantly increased. This situation is typical of all porphyrin dyes containing no hydrogenated pyrrole rings. When a metal atom is incorporated into the Pc macrocycle, insignificant bathochromic shifts of the Q_I and Q_{II} bands are observed and the magnitude of the bathochromic shift increases as the atomic number of the metal increases [17].

Modification of the porphyrin structure also changes the characteristics of the excited triplet state. Thus, the yield of the excited triplet state slightly decreases as one proceeds from porphyrins to chlorins [18]. Heavy and paramagnetic metal atoms within the Pc increase the probability of a singlet–triplet transition; therefore, such Pcs are characterized by a high yield of the

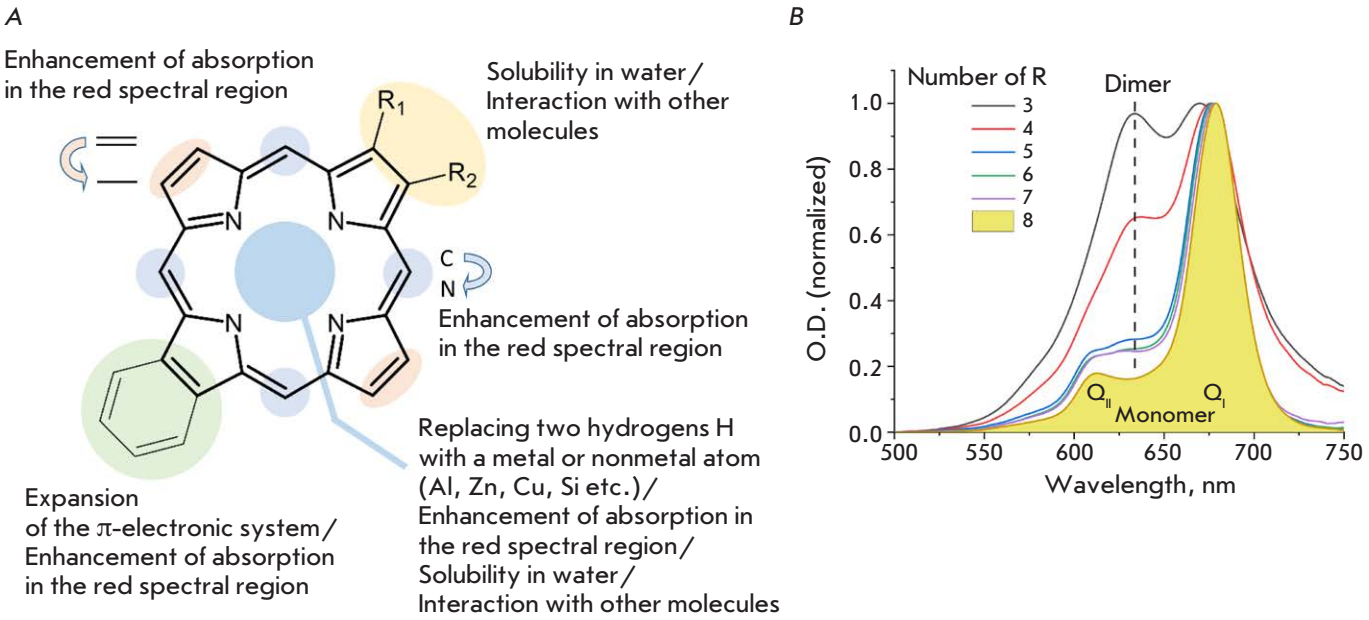

Fig. 1. (*A*) – The structure of a porphin molecule and possible ways for its modification. (*B*) – The absorption spectra of zinc phthalocyanines modified with different numbers of choline groups R

excited triplet state [19]. In addition, the probability of nonradiative deactivation to the ground state increases due to the involvement of the *d*-shells of the metal in the conjugation system [20]. The relationship between the constants of these processes depends on the nature of the metal and side substituents [21].

The solubility of a tetrapyrrolic PS in water is achieved by incorporating side substituents at the macrocycle periphery. These side substituents are usually low-molecular-weight ligands imparting polarity and/or charge to a molecule [22]. The maximum number of side substituents that can be inserted into a tetrapyrrole molecule is determined by the number of binding sites on pyrrole (or benzene in the case of benzoporphyrins) rings and is equal to eight for both the ortho- and meta-substitution [23]. For silicon PS (or PS complexes with trivalent metals), insertion of axial ligands is available [24]. Side substituents significantly affect the optical and photophysical properties of PS [17, 25, 26]. A wide range of substituents with specific properties, as well as the possibility of varying the degree of substitution, allow one to create substituted PSs for various fields of industry (catalysts, sensors, and solar cells) or medicine.

Although chemical modification of PS molecules makes them more water-soluble, the hydrophobic nature of the macrocycle determines the probability of aggregation of these molecules in aqueous solutions. Several types of tetrapyrrole aggregates have been proven to exist [27]. H-type (oligomeric) and D-type (dimeric) aggregates have a narrow absorption band in the visible region, which is shifted to the blue spectral region compared to the absorption band of monomeric form (*Fig. 1B*). Tetrapyrrole molecules in such aggregates form a "sandwich" structure; the aggregates do not fluoresce, since the excited state is nonradiatively deactivated due to intramolecular conversion. J-type (polymeric) aggregates have a wide absorption band shifted to the red spectral region, compared to the absorption band of the monomeric form; the aggregates are formed by PS molecules interacting with the edge parts. Porphyrin molecules can simultaneously exist in both forms (the monomer/aggregate equilibrium) of all types of aggregates; transitions between these states are also possible [28–30]. Aggregation can be caused by variation of a number of ambient parameters (pH and ionic strength of a solution) [31, 32] or an increase in PS concentration [33]. It can also be initiated by the formation of a complex between tetrapyrroles and molecules of a different nature [34]. The probability of aggregation also depends on the presence and nature of the central metal atom in the PS macrocycle.

1.2. Colloidal quantum dots

Quantum dots simultaneously have the physical and chemical properties of molecules and the optoelectronic

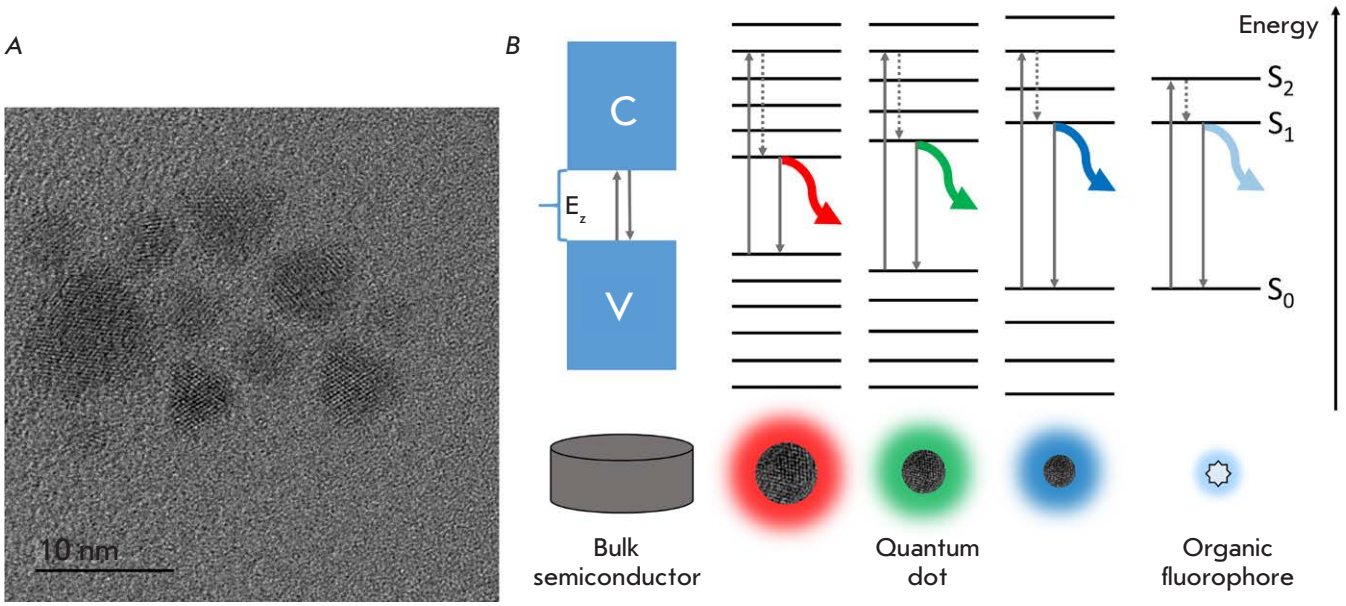

Fig. 2. (*A*) – An electron micrograph of CdSe/ZnS nanoparticles. (*B*) – The energy spectra of a bulk and nanosized semiconductor vs. the energy spectrum of an organic fluorophore. C – the conduction band; V – the valence band; E_z – the forbidden band; and S_0, S_1 and S_2 – the ground, first and second excited electronic levels, respectively. Vertical arrows indicate the electronic transitions; dashed arrows indicate the transitions to the lower excited levels accompanied by thermal energy dissipation

properties of semiconductors. A QD is a luminescent semiconductor nanocrystal whose characteristic dimensions lie in the range of 3–10 nm (*Fig. 2A*). It is known that the properties of nanomaterials qualitatively differ from those of a bulk analog [35] because of the quantum size effects. If the size of an object does not exceed the Bohr radius of the exciton, typical of a given material, the charge carrier inside the object appears in a three-dimensional potential well [36]. This leads to a modification of the energy spectrum (*Fig. 2B*). The classical spectrum of a semiconductor with a valence band, a forbidden band, and a conduction band is transformed into a set of discrete energy levels with a characteristic gap $h^2/8\pi^2mr^2$, where h is the Planck constant, m is the effective mass of the charge carrier, and r is the QD radius. Electron transitions are possible between these levels, accompanied by absorption or emission of a quantum of light in the visible wavelength range.

Due to the absorbed energy, the electron is transferred to a high-energy level, so that an exciton (an electron–"hole" pair) is formed in the QD crystal. Deactivation of the excited state is performed by exciton recombination accompanied by the emission of excess energy as a light quantum.

Since the gap between the energy levels of QDs depends on particle size, the luminescence spectrum of QDs undergoes a bathochromic shift when the crystal radius is increased. Thus, by varying the crystal size, one can choose QDs with the required spectral properties for specific research problems.

Quantum dots absorb light in a wide wavelength range with molar extinction coefficients of ~10^5–10^6 L/mol·cm. This fact has spurred a keen interest in QDs as promising luminescent labels for biological research. However, for a successful application of QD in biology, two significant disadvantages of QDs (the low luminescence quantum yield (φ) and hydrophobicity of semiconductor material) need to be overcome.

The main reason for the low φ values is the crystal lattice defects on the nanocrystal surface, which act as trap states for the charge carrier [36]. The charge carrier localized in such a trap prevents radiative recombination of the exciton. A QD is said to have passed into the so-called "off" state, which can be up to 100 s for an individual crystal [37].

The number of the defects on the QD surface was reduced for the first time in 1990 by coating a CdSe nanocrystal with a protective ZnS shell [38]. We will further refer to the luminescent central part of a multilayer QD as its core. Zinc sulfide is also a semiconductor, but with a wider gap, which creates a potential barrier for the charge carrier and pushes exciton to localize in the QD core. In addition, the protective shell is a physical barrier between the QD core and the en-

vironment, making the optical properties of the QD less sensitive to chemical reactions on its surface. By 1996, the development of methods for coating the QD core with a protective shell had given rise to samples of relatively monodisperse nanocrystals with φ ~ 50% [39]. The modern methods used to synthesize QDs yield nanocrystal samples with a φ ~ 80–90% [40]. It should be noted that the φ value depends nonlinearly on the thickness of the protective shell of the QD: the protective shell consisting of more than three ZnS layers was shown to quench the luminescence of the QD with a CdSe core [41]. It is believed that the probability of formation of intrinsic defects increases with the number of atomic layers in the shell [42].

Furthermore, the use of QDs in biological research involves the transfer of hydrophobic nanocrystals to the aqueous phase. Substitution chemistry methods are usually used for this purpose: the precursor molecules covering QDs during their synthesis are replaced with amphiphilic ligands with the target properties.

Any molecules containing nucleophilic groups can be adsorbed on the nanocrystal surface. The organic shell can be multilayered: an amphiphilic polymer is additionally adsorbed onto a layer of low-molecular-weight hydrophobic ligands, which is responsible for the surface properties of QDs. In addition to water solubility, the organic shell largely ensures passivation of crystal lattice defects [43]. However, organic ligands cannot cover the entire surface of QDs; therefore, some crystal lattice defects persist [36]. In addition, ligands can give rise to new energy levels: thiols are known to quench the luminescence of CdSe QDs due to the emergence of an energy level superjacent to the first excited level of QDs [36].

The typical lifetime values of QD luminescence are 5–20 ns, being quite sufficient for efficient energy transfer. The kinetics of QD luminescence decay are characterized by two or three time components. There currently is no clear understanding of the reasons for the complexity of the decay kinetics of QD luminescence [35]. The most common hypothesis associates each time component with emissions from a specific energy state. This is evidenced by the complex structure of the exciton absorption peak of QDs [44]. In the simplest case (biexponential decay curve), the fast component corresponds to the radiative recombination of an exciton, while the slower one corresponds to the radiation mediated by crystal lattice defects [45, 46]. In this model, the QD luminescence spectrum consists of two overlapping bands, which sometimes cannot be separated. The contribution of the slow component declines with decreasing temperature [45] and luminescence quantum yield [40]. In this case, the luminescence decay curves of ideal QDs without defects would be monoexponential; indeed, only one time component was found in some QD samples [37, 47]. The more differentiated the defects in crystals are (especially in QDs with a core/shell structure), the more time components in the luminescence decay curves there are [39].

Particle size nonuniformity can be an alternative reason for the emergence of several time components in the decay curves of QD luminescence. Increasing the QD size not only leads to a bathochromic shift in the luminescence spectrum, but also causes a corresponding shift of the exciton band in the absorption spectrum [48], reduces the luminescence lifetime [49], and causes nonlinear changes in the quantum yield φ [50]. Consequently, a broadened luminescence spectrum will be observed for a sample containing several fractions of QDs of different sizes. Such a spectrum is a superposition of the spectra from different fractions of QDs, which have their own quantum yield and luminescence lifetime values. The average value weighted over all the components is typically used as the QD luminescence lifetime because of the complexity of interpreting the time components.

2. THE COMPLEXATION STRATEGIES

The following types of interactions make it possible to create hybrid LNP–PS complexes in aqueous solutions: electrostatic or covalent ones, or a group of interactions combined under the concept of sorption (*Fig. 3*). The spectral properties of PS change as bonds of any of these types form. The properties of LNPs change extremely rarely and are not associated with the HC formation process [51–53].

2.1. Electrostatic interaction

HCs are often formed by mixing the aqueous solutions of LNP and PS due to the electrostatic attraction of oppositely charged components (*Fig. 3*, 1.1–1.2). In this case, changes in the spectral properties of PS should be determined by electron density perturbation and may differ depending on the nature and the stoichiometric ratio of HC components. Information on the following complexation effects is available:

(1) a bathochromic shift in the absorption and/or fluorescence spectra of PS [54–59];
(2) a hypsochromic shift in the absorption and fluorescence spectra of PS [52, 60–62];
(3) hypochromism [52, 56, 57, 60];
(4) a reduced quantum yield of the PS fluorescence [60, 62];
(5) an increased [60, 63] quantum yield of the triplet state of PS; and
(6) an increased [60, 62] lifetime of the triplet state of PS.

The increased yield of the triplet states of PS is usually attributed to the so-called "heavy-atom effect."

According to it, the probability of intramolecular conversion of PS to the triplet state increases in the presence of heavy metal atoms (Cd, Te), which also reduces the quantum yield of PS fluorescence. In some cases, the cadmium ion from QD can be incorporated into the macrocycle of metal-free PS upon HC formation [62, 64]. It was noted [65] that the magnitude of the changes in the optical properties of PS increases with the size of the QD crystal. The presence of the ZnS protective shell is expected to reduce the effect of the heavy metal atoms in the QD core on the properties of PS.

2.2. Nonspecific sorption

HCs formed due to the electrostatic attraction of oppositely charged nanoparticles and photosensitizers do not require special preparation protocols and are quite stable. However, it was noted that mixing of like-charged components also leads to the formation of HC in some cases [66–70]. Consequently, the self-assembly of HCs can involve interactions other than electrostatic ones, which we will further combine under the term "sorption".

Depending on the structure of the organic shell of QD, there can be two variants of PS sorption. If the QD surface is coated with a layer of low-molecular-weight ligands, then PS molecules are incorporated into this monolayer due to peripheral [64] or axial [71–73] hydrophobic substituents. In this case, we talk about surface binding (*adsorption*, *Fig. 3*, 2.2). This kind of interaction weakens with increasing branching of the substituent [73]. Interestingly, the energy transfer efficiency increases with the substituent length as a result of stronger interaction, but then it decreases if the substituent length starts to exceed the length of the low-molecular-weight ligand on the QD surface [72].

Direct interaction between a PS molecule and a QD crystal is a special case of adsorption (*Fig. 3*, 4). The formation of a coordination bond between the tertiary nitrogen atom of the PS molecule and the atoms of the CdSe/ZnS QD crystal lattice in toluene can be considered proven [74–78]. In this case, a close contact is required between the PS and the QD crystal, which can be hindered by the outer organic shell of the nanoparticle. Meanwhile, the formation of a coordination bond should not be accompanied by the obligatory displacement of organic ligands by the PS molecule, since adsorption can occur on the ligand-free areas of the nanoparticle surface. A porphyrin molecule can obviously be adsorbed onto QDs both by the plane of the macrocycle involving all the side pyridyl rings and by its edge involving one or two pyridyl substituents. This is evidenced by the increased efficiency of energy transfer W in HC as the number of pyridyl substituents

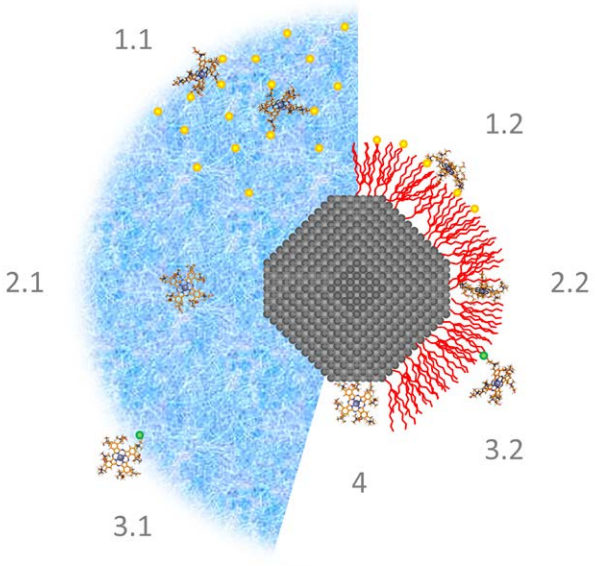

Fig. 3. The most common methods used to create a quantum dot–photosensitizer hybrid complex. 1.1–1.2 is the electrostatic interaction; 2.1–2.2 are absorption and adsorption, respectively; 3.1–3.2 are the covalent interactions; 4 corresponds to coordination. The nanocrystal core of QDs is shown in gray; the polymer shell is shown in blue; and the shell of low-molecular-weight ligands is shown in red. The orange dot indicates the charged functional groups on the polymer/ligand; the green dot shows the covalent bond

in the porphyrin molecule rises from 1 to 4, but the value of W is comparable for monopyridyl porphyrin and bipyridyl porphyrin with an opposite arrangement of pyridyl rings.

A hypsochromic shift in the fluorescence spectrum of porphyrin and an increase in its fluorescence lifetime were observed during the formation of HC [79]. According to Zenkevich et al. [79], the amplitude of the effects decreased with increasing porphyrin concentration in solution due to the rise in the proportion of porphyrin molecules not associated with QDs. In addition, during the formation of HC, a bathochromic shift of the Soret band was observed, which is possibly caused by changes in the structure of the π-system of electrons upon coordination of the pyridyl nitrogen atom to the QD zinc atom, or by a higher dielectric constant of the medium near the nanoparticle surface as compared to the toluene solution.

The feasibility of coordination interaction has been proposed to explain the formation of HC between a negatively charged CdTe quantum dot (coated with 3-mercaptopropionic acid) and aluminum tetrasulfophthalocyanine, which is also negatively charged [80]. It is

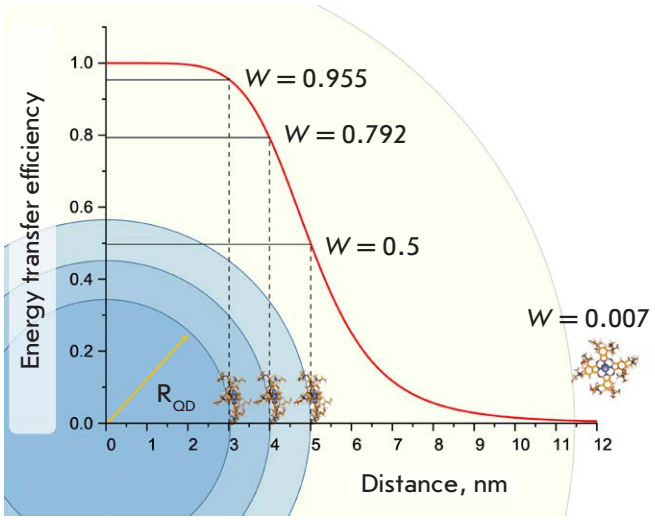

Fig. 4. Dependence of the energy transfer efficiency W in HC on the size R_{QD} of the QD core (here, we assume that the coordination bond forms directly between the PS molecule and the QD crystal). The Förster radius (R_0) was chosen to be equal to 5 nm. An example of HC with a photosensitizer covalently attached to the QD polymer shell (the total QD radius being 11.5 nm) is shown

assumed that the PS molecule is coordinated to the QD carboxyl group by an aluminum atom. The idea was extended to CdTe QDs coated with thioglycolic acid [81, 82].

The complexes of PS with LNPs coated with a polymer shell are of particular interest [70, 83–90]. It is believed that the PS molecules in such complexes can be incorporated into the bulk of the polymer; therefore, we talk about *absorption* in this case (*Fig. 3*, 2.1). This conclusion was drawn from the fact that the hydrodynamic radius of an LNP (together with the polymer shell) exceeds the distance between the donor and the acceptor required for efficient energy transfer via the FRET mechanism that is actually observed in these systems.

During the formation of HC through sorption, multidirectional changes in the spectral properties of PS were noted, depending on the type of PS molecule [78, 85, 87, 89, 91, 92]; there could also be no changes at all because of the adsorption occurring when incorporation was minimal [64]. Aggregation of PS molecules can be observed during sorption [93].

The triplet yield of PS typically increases upon sorption on LNP [67, 92]; however, some opposite results have also been obtained [68]: thus, a reduced lifetime of the triplet state of PS was observed in [91]. This could have been due to the fact that when a PS molecule is incorporated into the organic shell of a QD, the probability of quenching of the PS triplet state by oxygen decreases [78].

2.3. Covalent binding

The complexes between nanoparticles and PS formed via covalent interaction have a number of advantages over HCs stabilized by other types of interactions (*Fig. 3*, 3.1–3.2). First, the interaction occurs between specific functional groups of PS and the organic shell of QDs; therefore, exact localization of PS in HC is known. This makes it possible to predict some of the photophysical properties of HCs. Second, this HC potentially remains more stable in the presence of biological objects and environments. Therefore, there is a keen interest in covalently stabilized conjugates of PSs and nanoparticles [53, 65, 94–100].

Formation of a covalent bond can be easily monitored by the emergence of corresponding lines in the Raman spectra or absorption spectra in the IR region [65, 94, 96]. Meanwhile, it is difficult to control the PS : LNP ratio in the end product when routine crosslinking methods are used. In addition, when crosslinking is performed through amino and carboxyl groups, HCs of the electrostatically interacting components can form, which is difficult to prevent. For these reasons, a number of studies have failed to compare the properties of covalently crosslinked and electrostatically stabilized HCs based on the same components [94, 96, 98].

An even more important problem is that the linker that forms between the PS molecule and the LNP surface increases the distance between them. This fact negatively affects the energy transfer efficiency, which rapidly decreases with increasing distance between the energy donor and acceptor. *Figure 3* shows that the influence of this effect can be critical when a polymer shell is used.

In most studies, changes in the spectral characteristics of PS during HC formation are identical for the covalent and electrostatic binding methods: a hypsochromic shift in the absorption spectrum of PS and hypochromism [94, 95, 97] or a bathochromic shift in the absorption spectrum of PS and hypochromism [98]. There were no changes in the spectral properties of PSs during the formation of a covalent bond [96].

3. DESIGN OPTIMIZATION FOR HYBRID COMPLEXES

Designing hybrid complexes based on LNPs implies that the efficiency of ROS generation by a photosensitizer upon excitation is increased in the spectral regions where the PS itself has a low absorption capacity. Since such an enhancement of the photodynamic properties of PS is achieved due to nonradiative energy transfer, optimization of the HC design is primarily associated

with the optimization of energy transfer via the FRET mechanism. However, it should be noted that a set of properties of HC promoting efficient energy transfer may, generally speaking, not coincide with the set of properties of HC that enhances the photodynamic activity of PS in HC. For this reason, we will consider these two aspects of HC optimization separately.

3.1. Energy transfer efficiency

Since energy transfer increases the deactivation rate of the excited state of an energy donor, the degree of quenching of LNP luminescence is the main criterion in a quantitative assessment of the transfer efficiency.

Let us consider the simplest quantum dot–tetrapyrrolic PS system stabilized via coordination of the PS to the nanocrystal surface. The subject of optimization will be energy transfer, which contributes to the increase in the absorption capacity of PS in the blue-green spectral region. According to the nonradiative resonance energy transfer theory, the efficiency of this process (W) can be increased by

(A) increasing the overlap integral (J) of the LNP luminescence spectrum and PS absorption spectrum;
(B) increasing the quantum yield of LNP luminescence;
(C) decreasing the LNP–PS distance;
(D) increasing the molar extinction coefficient of a PS molecule; or
(E) increasing the PS : LNP stoichiometric ratio.

The J value can be increased by shifting the QD luminescence spectrum to longer wavelengths, closer to the absorption spectrum of the PS. Since the position of the luminescence spectrum of QDs is easily specified during their synthesis, a QD providing the maximum J value can be easily selected when the position of the PS absorption spectrum is fixed. However, the bathochromic shift in the QD luminescence spectrum occurs due to a rise in the particle size, which increases the QD–PS distance and reduces the energy transfer efficiency W (*Fig. 4*). This is typically accompanied by a reduction in the quantum yield of QD luminescence, which should also negatively affect the W value. Although the quantum yield of QD luminescence can be increased by growing a protective shell from a wider-gap semiconductor, such a modification will not only increase the luminescence yield, but also additionally increase the crystal size and, accordingly, increase the donor–acceptor distance. An alternative way is to choose materials for the crystal lattice of the QD core. On the one hand, an organic shell on the QD core protects the crystal surface against solvent molecules; therefore, the QD luminescence yield is expected to increase. On the other hand, additional defects may form on the crystal surface depending on the nature of the molecules comprising the organic shell, and the quantum yield of the QD luminescence will decrease.

It is possible to increase the J value due to the hypsochromic shift in the absorption spectrum of PS, since QDs of a smaller size can be used to create HCs in this case. Indeed, a smaller QD size will increase the quantum yield of QD luminescence and reduce the QD–PS distance, which will eventually increase the W value. However, applying such a strategy means that the red spectral region will not be used for ROS generation. In addition, if the spectra are ultimately shifted to the blue region, there is no need to use QDs, since many metal-free PSs absorb blue light perfectly due to the Soret band.

Therefore, complex QD-based systems have a number of parameters that cannot be optimized simultaneously due to their mutually exclusive influence on each other. Consequently, the highest energy transfer efficiency can be achieved only through compromise values of the PS and QD parameters.

Variation of only two parameters unambiguously increases the W value: increasing the molar extinction coefficient of PS and the PS : LNP stoichiometric ratio.

The molar extinction coefficient of PS in the visible region is usually increased by inserting a metal atom into the macrocycle. Since the formation of a metal complex significantly increases the lifetime of the triplet state of PS, this additionally enhances the photodynamic activity of the PS. Alternative ways for increasing the molar extinction coefficient of PS are to replace carbon with nitrogen in the methine bridges of the macrocycle, increase the macrocyclic aromaticity due to benzene rings, and hydrogenate double bonds. These ways also lead to an additional bathochromic shift in the absorption spectrum of PS. Consequently, it is necessary to additionally shift the luminescence spectrum of QD to longer wavelengths to preserve the maximum value of the overlap integral J. The effects caused by such a displacement can reduce the efficiency of energy transfer in HC.

The PS : LNP stoichiometric ratio can be increased to a certain limiting value that depends on the complexation method. If HC is formed by covalent crosslinking, then $[PS : LNP]_{max}$ is determined by the number of functional groups on the organic shell of the QD (i.e., their density and surface area of the QD). If HC is stabilized via electrostatic interactions, the $[PS : LNP]_{max}$ is determined by the number of charged groups on the organic shell of QD, as well as the number of charged groups on the PS molecule. There is ambiguity here: the more charges there are on the PS, the stronger the interaction is, but fewer PS molecules will bind to the QD surface.

If HC is stabilized trough sorption interactions, the $[PS : LNP]_{max}$ is determined by the LNP surface area, as

well as by the hydrophilic–hydrophobic balance of the PS molecule. For a bulk polymer shell of a nanoparticle, $[PS : LNP]_{max}$ will be much higher than that when a monolayer of low-molecular-weight ligands is used. However, additional PS molecules will be located far enough from the QD center so that the efficiency of energy transfer to these PS molecules should be minimal. *Figure 4* shows the situation where PS is covalently bound to the polymer shell of QD. One can see that for a total nanoparticle radius of 11.5 nm and Förster radius R_0 = 5 nm, the efficiency of energy transfer to a given PS molecule will be no more than 0.7%.

In theory, the increased factor χ^2 describing the mutual orientation of the transition dipole moments of the donor and acceptor can increase the energy transfer efficiency. The χ^2 values can vary from 0 to 4. In solutions, χ^2 is taken equal to 2/3 due to rotational diffusion and random orientation of the molecules. This is also used in the case of HCs, since most QDs do not have luminescence anisotropy. Nevertheless, in the general case, the orientation of transition dipole moments in the HC can be nonrandom. It is assumed that studies focusing on the anisotropy of the PS and LNPs fluorescence would potentially help estimate the possible mutual orientations of the transition dipole moments and thereby refine the χ^2 value [101].

3.2. Photodynamic properties of a photosensitizer

A successful energy transfer event causes a transition of the PS molecule to an excited state. Energy transfer can increase the ROS yield or increase the intensity of PS fluorescence. Increased absorption capacity of a PS manifesting itself as an increase in the intensity of its sensitized fluorescence can be used to calculate the energy transfer efficiency *W* [58, 75, 82]. However, it is considered more correct to use the spectral characteristics of the energy donor to calculate the *W* value, since enhancement of the photodynamic properties of PS in HC strongly depends on the PS : LNP stoichiometric ratio.

It is known that as the PS concentration in a dilute solution rises, its fluorescence intensity increases linearly in the initial period of time; however, it reaches a plateau and then decreases in sufficiently concentrated solutions (*Fig. 5*) [102]. This effect can be called "self-quenching of PS fluorescence". Self-quenching of the PS fluorescence can be caused by PS aggregation and the inner filter effects. PS aggregation was discussed in section 1.1. The inner filter effects consist in the shielding of the exciting light by layers of the PS solution, which lie closer to the front cell wall (a), and reabsorption of PS fluorescence (b). The latter is possible, since tetrapyrrolic PSs have a small Stokes shift (~ 10 nm) so that the absorption and fluorescence spectra of PSs largely overlap. In addition to the nonlinear dependence of PS fluorescence intensity on its concentration, this phenomenon leads to a bathochromic shift in the fluorescence spectrum of PS and increases the measured fluorescence lifetime of the PS [103].

Quenching of PS fluorescence in the presence of nanoparticles is common [55, 104–106]. The concentration dependence of the fluorescence intensity of PS

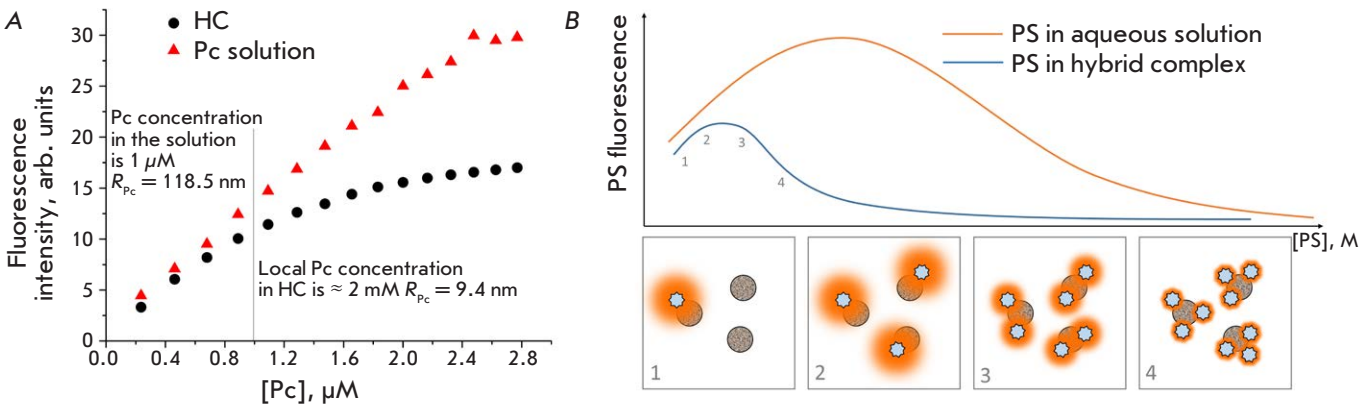

Fig. 5. (*A*) – The concentration dependence of the fluorescence intensity of polycationic aluminum Pc in an aqueous solution and in an electrostatically stabilized hybrid complex with a polymer-coated QD. R_{Pc} is the average distance between two Pc molecules in the medium (water in the case of a one-component Pc solution and the QD polymer shell in the case of a HC solution). The fluorescence excitation wavelength is 655 nm. (*B*) – The concentration dependence of the PS fluorescence intensity in water and in HC (LNP concentration being constant). (1–4) the schematic representation of HCs with a different stoichiometry and the fluorescence intensity of PS in such HCs

in HCs with semiconductor nanoparticles is also nonlinear [59, 70, 71, 87]; however, self-quenching starts at a much lower PS concentration compared to the PS in a single-component solution (*Fig. 5A*). Indeed, the maximum PS : LNP ratio in HC can exceed 1000, so the local PS concentration during complex formation can be as high as several mM [90].

An increasing PS : LNP ratio may result in the aggregation of PS in the organic shell of the LNP. This effect is observed in any type of interaction between PS and LNP, except for covalent crosslinking. Any PS in a solution exists in a state of monomer/aggregate dynamic equilibrium, which can be shifted upon binding to LNP. The probability of this process depends both on the structural properties of the PS molecule (the type of metal atom, the nature and number of peripheral substituents) and on the structural features of the organic shell of the LNP. Thus, we have shown that despite the presence of eight peripheral carboxyl groups, zinc and aluminum Pcs aggregate upon binding to upconversion LNPs coated with a polymer shell containing terminal amino groups; zinc Pcs undergo aggregation at lower concentrations than aluminum Pcs do [107]. In this case, the PS aggregates continue to accept the electronic excitation energy of the LNP and the efficiency of this process may increase due to the greater overlap of the absorption spectrum of the aggregates with the luminescence spectrum of the LNP.

In addition, concentrating PS from the solution onto the LNP surface leads to solution "bleaching" within the region of PS absorption. In this case, the photodynamic activity of PS in HC is further reduced.

Let us imagine that the number of PS molecules on the LNP surface can increase infinitely without an increase in the average PS–LNP distance that is equal to the Förster radius R_0. According to Förster's theory, at PS : LNP = x = 1, the energy transfer efficiency W is 50% at a distance R_0. When x = 10, W = 91%; at x = 100, W = 99%; and at x = 1000, W = 99.9%. It is clear that the highest increase in the W value is observed as the PS : LNP ratio rises from 1 to 10, which is much less than the characteristic $[PS : LNP]_{max}$ values are. It is fair to say that the absolute energy transfer efficiency W increases with a rising number of PS molecules in HC, while the energy transfer efficiency W for every separate PS molecule decreases.

Consequently, the more PS molecules there are in a complex with LNP, the less additional energy each of them receives, and, therefore, the enhancement of photodynamic properties of PS tends to zero. The photodynamic activity of PS in the HC at large PS : LNP ratios turns out to be lower than the activity of free PS due to self-quenching effects.

Finally, the use of some types of LNP shells can lead to the fact that ROS formed in a reaction between PS and molecular oxygen inside the organic shell of LNP cannot effectively damage the targets in the solution surrounding HC, since diffusion in the LNP shell is hindered. In this case, the most likely target of oxidation will be the PS molecule itself. Indeed, in electrostatically stabilized HCs based on aluminum phthalocyanines and QDs coated with a polymer shell, we observed rapid bleaching of the dye both under selective illumination of Pc and upon excitation of QD, followed by energy transfer [108]. As a result, the measured concentration of ROS is lower than the actual one. Nevertheless, the calculated ROS concentration corresponds to the effective concentration of ROS capable of exhibiting photodynamic activity outside the hybrid complex.

Therefore, the increased energy transfer efficiency in HCs due to a rise in the PS : LNP value contradicts the idea of enhancing the photodynamic activity of PS.

It should be noted that the interaction between PS and LNP can result in electron transfer. This phenomenon is observed quite rarely and is easily detected with strong changes in the spectral properties of PS due to the formation of radical anions and other derivatives [63, 109]. In addition, the electron transfer implies a QD transition to the "off" state, when the model of classical static quenching is appropriate. In this case, the QD luminescence intensity is quenched without a change in its lifetime. Unfortunately, the luminescence lifetime of LNPs has been estimated only in some studies and the absence of such an estimate may lead to a misinterpretation of the experimental results [52, 56].

CONCLUSIONS AND FUTURE PROSPECTS

All the mentioned functional relationships between the structural and spectral properties of PSs and LNPs, which can affect the efficiency of LNP as a light collector, and an enhancement of the photodynamic activity of PS in HC can be summarized in a single scheme shown in *Fig. 6*. One can see that all the key characteristics of PS and LNPs are interconnected. Therefore, the full set of parameters optimized so as to ensure the highest ROS yield must involve some degree of compromise.

Achieving this compromise is the primary task for PDT on its path to creating third-generation PSs. However, even though an impressive number of studies have been devoted to HCs, the data collected are too fragmentary and heterogeneous, making a global analysis and the selection of the required set of HC characteristics impossible. This would be feasible only by using an integrated approach, when all the connections shown in *Fig. 6* can be identified as quan-

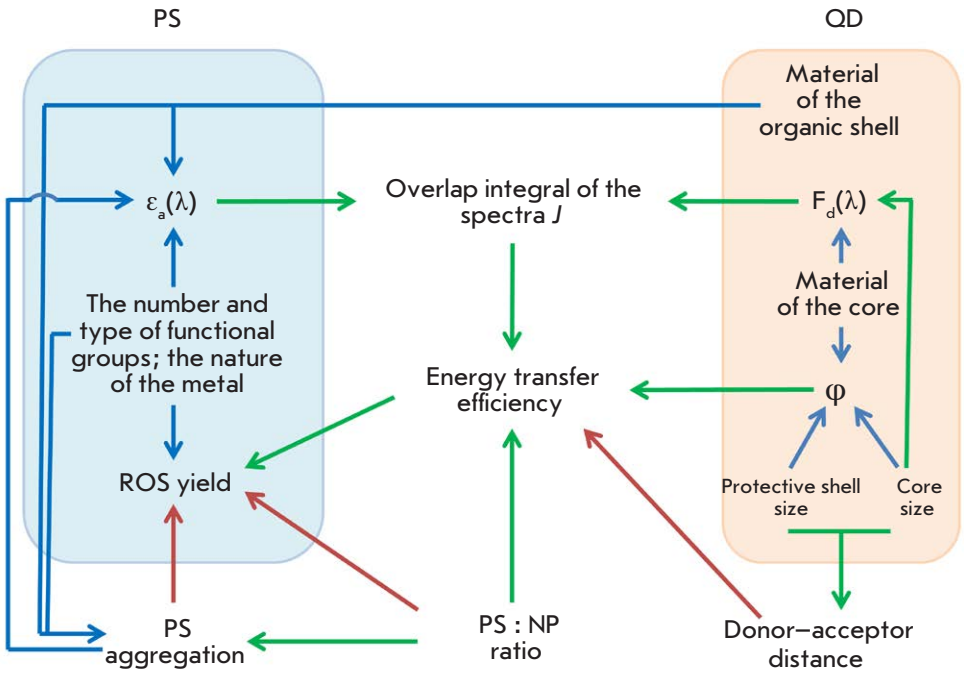

Fig. 6. Scheme showing the functional relationships between the structural parameters of PS/QD molecules and their photophysical properties, as well as the effect of these properties on the yield of reactive oxygen species through the parameters of energy transfer via the FRET mechanism. $F_d(\lambda)$ is the luminescence spectrum of QD; $\varepsilon_a(\lambda)$ is the absorption spectrum of PS; and φ is the luminescence quantum yield. Green arrows denote the positive correlation; red arrows denote the negative correlation; and blue arrows show the nonlinear dependences

titative dependences. Since most of these parameters are related to each other by the well-known formulas of the FRET theory, the difficulty arises only at the stage of uncovering the relationship between the structural and photophysical characteristics of the HC components. First of all, this concerns LNPs, since the relationship between the structural and spectral properties of tetrapyrrolic PSs has been studied quite thoroughly.

However, it is not enough to possess information about the properties of each component to optimize the design of the HC. Phenomena such as PS aggregation and static quenching of the luminescence of LNPs (as a result of the formation of nanocrystal surface defects involving PS) can be quantitatively studied only through experiments on HC formation. It should also be noted that electron density perturbation in a PS molecule during the formation of HC (even in the absence of the aforementioned aggregation and quenching effects) has some effect on the photophysical properties of PS and, thus, indirectly affects the energy transfer efficiency and the enhancement of the ROS yield. Failure to take into account any of the parameters described above leads to the following fact: even in the presence of PSs and LNPs with spectral characteristics optimal for FRET, it might not always be possible to obtain HC where enhanced PS fluorescence or the ROS generation rate is observed [87, 98, 104–106]. This usually leads to a rejection of the FRET mechanism as a model for describing the interactions between a nanoparticle and a PS [51, 56, 91, 93, 110].

It might be possible to find several variants of complexes significantly differing in terms of their set of internal characteristics but having comparable ROS yields (or comparable in terms of the efficiency of using certain spectral regions for ROS generation) by optimizing the HC design. Since the enhancement of the photodynamic characteristics of PS can be achieved only at low PS : LNP values, when the luminescence of the LNP is not completely quenched, the LNP luminescence can be used for diagnostic purposes. Such HCs can obviously be used to solve specific problems of PDT and fluorescence diagnostics depending on the properties of the target object. In this regard, it must be said that we have discussed the trends in optimizing the HC design exclusively with a view to enhancing the ROS yield. In fact, the overall photodynamic activity will depend not only on the absorption capacity of HC and the ROS yield, but also on the efficiency of interaction between HC and cells, the internalization mechanism, and the stability of HC in the presence of blood components when an HC-based drug is administered to a living being. It is highly likely that the approaches to optimizing HC for increasing the efficiency of targeted delivery will significantly affect the final set of HC pa-

rameters. Therefore, the scheme shown in *Fig. 6* should be expanded with allowance for all the aspects of the functional activity of HC as a third-generation photosensitizer. Building a complete scheme of this kind will allow one to take the prospects for using HC with energy transfer in PDT to a fundamentally new level and is, therefore, the main objective of modern medical biophysics. ●

This study was carried out with the financial support from the Russian Foundation for Basic Research (project No. 20-34-70042).

REFERENCES

1. Bissonnette L., Bergeron M.G. // Expert Rev. Mol. Diagn. 2006. V. 6. № 3. P. 433–450.
2. Kelkar S.S., Reineke T.M. // Bioconjug. Chem. 2011. V. 22. № 10. P. 1879–1903.
3. Frochot C., Mordon S. // J. Porphyr. Phthalocyanines. 2019. V. 23. № 04–05. P. 347–357.
4. Lucky S.S., Soo K.C., Zhang Y. // Chem. Rev. 2015. V. 115. № 4. P. 1990–2042.
5. Sobolev A.S. // Acta Naturae. 2020. V. 12. № 4. P. 47–56.
6. Sokolov A.V., Kostin N.N., Ovchinnikova L.A., Lomakin Y.A., Kudriaeva A.A., Shemyakin M.M., Ovchinnikov Yu.A. // Acta Naturae. 2019. V. 11. № 2. P. 28–41.
7. Zdobnova T.A., Lebedenko E.N., Deyev S.M. // Acta Naturae. 2011. V. 3. № 1. P. 29–47.
8. Wang X., Valiev R.R., Ohulchanskyy T.Y., Ågren H., Yang C., Chen G. // Chem. Soc. Rev. 2017. V. 46. № 14. P. 4150–4167.
9. Martynenko I.V., Litvin A.P., Purcell-Milton F., Baranov A.V., Fedorov A.V., Gun'Ko Y.K. // J. Mater. Chem. B. Royal Soc. Chem. 2017. V. 5. № 33. P. 6701–6727.
10. Algar W.R., Krull U.J. // Anal. Bioanal. Chem. 2008. V. 391. № 5. P. 1609–1618.
11. Khaydukov E.V., Mironova K.E., Semchishen V.A., Generalova A.N., Nechaev A.V., Khochenkov D.A., Stepanova E.V., Lebedev O.I., Zvyagin A.V., Deyev S.M., et al. // Sci. Rep. Nat. Publ. Group, 2016. V. 6. P. 35103.
12. Su Q., Feng W., Yang D., Li F. // Acc. Chem. Res. 2017. V. 50. № 1. P. 32–40.
13. Couleaud P., Morosini V., Frochot C., Richeter S., Raehm L., Durand J.-O. // Nanoscale. 2010. V. 2. № 7. P. 1083–1095.
14. Li Y., Bai G., Zeng S., Hao J. // ACS Appl. Mater. Interfaces. 2019. V. 11. № 5. P. 4737–4744.
15. Gao G., Guo Q., Zhi J. // Small. 2019. V. 15. № 48. P. 1902238.
16. Filali S., Pirot F., Miossec P. // Trends Biotechnol., 2020. V. 38. № 2. P. 163–177.
17. Gurinovich G.P., Sevchenko A.N., Solov'ev K.N. // Sov. Phys. Usp. 1963. V. 6. № 1. P. 67–105.
18. Bautista-Sanchez A., Kasselouri A., Desroches M.C., Blais J., Maillard P., de Oliveira D.M., Tedesco A.C., Prognon P., Delaire J. // J. Photochem. Photobiol. B Biol. 2005. V. 81. № 3. P. 154–162.
19. Idowu M., Nyokong T. // J. Photochem. Photobiol. A Chem. 2008. V. 200. № 2–3. P. 396–401.
20. Gonçalves P.J., De Boni L., Borissevitch I.E., Zílio S.C. // J. Phys. Chem. A. 2008. V. 112. № 29. P. 6522–6526.
21. Ogunsipe A., Nyokong T. // Photochem. Photobiol. Sci. 2005. V. 4. № 7. P. 510–516.
22. Kuznetsova N.A., Gretsova N.S., Derkacheva V.M., Mikhalenko S.A., Solov'eva L.I., Yuzhakova O.A., Kaliya O.L., Luk'yanets E.A. // Russ. J. Gen. Chem. 2002. V. 72. № 2. P. 300–306.
23. Çakır D., Göksel M., Çakır V., Durmuş M., Biyiklioglu Z., Kantekin H. // Dalt. Trans. 2015. V. 44. № 20. P. 9646–9658.
24. Oleinick N.L., Antunez A.R., Clay M.E., Rihter B.D., Kenney M.E. // Photochem. Photobiol. 1993. V. 57. № 2. P. 242–247.
25. Bonnett R., Charlambides A.A., Land E.J., Sinclair R.S., Tait D., Truscott T.G. // J. Chem. Soc. Faraday Trans. 1 Phys. Chem. Condens. Phases. 1980. V. 76. P. 852–859.
26. Wróbel D., Boguta A. // J. Photochem. Photobiol. A Chem. 2002. V. 150. № 1–3. P. 67–76.
27. Kadish K.M., Smith K.M., Guilard R. // The Porphyrin Handbook. San Diego: Acad. Press, 2003.
28. Gonçalves P.J., Corrêa D.S., Franzen P.L., De Boni L., Almeida L.M., Mendonça C.R., Borissevitch I.E., Zílio S.C. // Spectrochim. Acta – Part A Mol. Biomol. Spectrosc. 2013. V. 112. P. 309–317.
29. Maiti N.C., Mazumdar S., Periasamy N. // J. Phys. Chem. B. 1998. V. 102. № 9. P. 1528–1538.
30. Gandini S.C.M., Yushmanov V.E., Borissevitch I.E., Tabak M. // Langmuir. 1999. V. 15. № 9. P. 6233–6243.
31. Kaliya O.L., Kuznetsova N.A., Bulgakov R.A., Solovyova L.I., Shevchenko E.N., Slivka L.K., Lukyanets E.A. // Macroheterocycles. 2016. V. 9. № 2. P. 186–192.
32. Suchan A., Nackiewicz J., Hnatejko Z., Waclawek W., Lis S. // CHEMIK. 2014. V. 68. № 4. P. 369–376.
33. Suchan A., Nackiewicz J., Hnatejko Z., Waclawek W., Lis S. // Dye. Pigment. 2009. V. 80. № 2. P. 239–244.
34. Gandini S.C.M., Yushmanov V.E., Perussi J.R., Tabak M., Borissevitch I.E. // J. Inorg. Biochem. 1999. V. 73. № 1–2. P. 35–40.
35. Oleinikov V.A., Sukhanova A.V., Nabiev I.R. // Ross. Nanotekhnol. 2007. V. 2. № 1–2. P. 160–173.
36. Kim J.Y., Voznyy O., Zhitomirsky D., Sargent E.H. // Adv. Mater. 2013. № 25. P. 4986–5010.
37. Lane L.A., Smith A.M., Lian T., Nie S. // J. Phys. Chem. B. 2014. V. 118. № 49. P. 14140–14147.
38. Kortan A.R., Opila R.L., Bawendi M.G., Steigerwald M.L., Carroll P.J., Brus L.E. // J. Am. Chem. Soc. 1990. V. 112. № 4. P. 1327–1332.
39. Hines M.A., Guyot-Sionnest P. // J. Phys. Chem. 1996. V. 100. № 2. P. 468–471.
40. Wang X., Qu L., Zhang J., Peng X., Xiao M. // Nano Lett. 2003. V. 3. № 8. P. 1103–1106.
41. Grabolle M., Ziegler J., Merkulov A., Nann T., Resch-Genger U. // Ann. N. Y. Acad. Sci. 2008. V. 1130. P. 235–241.
42. Dabbousi B.O., Rodriguez-Viejo J., Mikulec F.V., Heine J.R., Mattoussi H., Ober R., Jensen K.F., Bawendi M.G. // J. Phys. Chem. B. 1997. V. 101. № 46. P. 9463–9475.
43. Hohng S., Ha T. // J. Am. Chem. Soc. 2004. V. 126. № 5. P. 1324–1325.
44. Kapitonov A.M., Stupak A.P., Gaponenko S.V., Petrov E.P., Rogach A.L., Eychmüller A. // J. Phys. Chem. B. 1999. V. 103. № 46. P. 10109–10113.
45. Bawendi M.G., Carroll P.J., Wilson W.L., Brus L.E. // J. Chem. Phys. 1992. V. 96. № 2. P. 946–954.

46. An L., Chao K., Zeng Q., Han X., Yuan Z., Xie F., Fu X., An W. // J. Nanosci. Nanotechnol. 2013. V. 13. P. 1368–1371.
47. Wuister S.F., Swart I., Van Driel F., Hickey S.G., Donega C. De Mello // Nano Lett. 2003. V. 3. № 4. P. 503–507.
48. Yu W.W., Qu L., Guo W., Peng X. // Chem. Mater. 2003. V. 15. № 14. P. 2854–2860.
49. Hong M., Guo-Hong M., Wen-Jun W., Xue-Xi G., Hong-Liang M. // Chinese Phys. B. 2008. V. 17. № 4. P. 1280.
50. Qu L., Peng X. // J. Am. Chem. Soc. 2002. V. 124. № 9. P. 2049–2055.
51. Zhang X., Liu Z., Ma L., Hossu M., Chen W. // Nanotechnology. 2011. V. 22. P. 195501.
52. Moeno S., Idowu M., Nyokong T. // Inorganica Chim. Acta. 2008. V. 361. № 9–10. P. 2950–2956.
53. Adegoke O., Khene S., Nyokong T. // J. Fluoresc. 2013. V. 23. № 5. P. 963–974.
54. Viana O.S., Ribeiro M.S., Rodas A.C.D., Rebouças J.S., Fontes A., Santos B.S. // Molecules. 2015. V. 20. № 5. P. 8893–8912.
55. Rotomskis R., Valanciunaite J., Skripka A., Steponkiene S., Spogis G., Bagdonas S., Streckyte G. // Lith. J. Phys. 2013. V. 53. № 1. P. 57–68.
56. Keane P.M., Gallagher S.A., Magno L.M., Leising M.J., Clark I.P., Greetham G.M., Towrie M., Gun'ko Y.K., Kelly J.M., Quinn S.J. // Dalt. Trans. 2012. V. 41. № 42. P. 13159.
57. Vaishnavi E., Renganathan R. // Analyst. 2014. V. 139. № 1. P. 225–234.
58. Martynenko I.V., Kuznetsova V.A., Orlova A.O., Kanaev P.A., Maslov V.G., Loudon A., Zaharov V., Parfenov P., Gun'ko Y.K., Baranov A.V., et al. // Nanotechnology. IOP Publ. 2015. V. 26. № 5. P. 055102.
59. Martynenko I.V., Kuznetsova V.A., Orlova A.O., Kanaev P.A., Gromova Y., Maslov V.G., Baranov A.V., Fedorov A. // Proc. SPIE. 2014. V. 9126. P. 91263C.
60. Idowu M., Chen J.Y., Nyokong T. // New J. Chem. 2008. V. 32. № 2. P. 290–296.
61. Duong H.D., Rhee J.I. // Chem. Phys. Lett. 2011. V. 501. № 4–6. P. 496–501.
62. Ahmed G.H., Aly S.M., Usman A., Eita M.S., Melnikov V.A., Mohammed O.F. // Chem. Commun. Royal Soc. Chem. 2015. V. 51. № 38. P. 8010–8013.
63. Moeno S., Nyokong T. // J. Photochem. Photobiol. A Chem. 2009. V. 201. № 2–3. P. 228–236.
64. Chambrier I., Banerjee C., Remiro-Buenamañana S., Chao Y., Cammidge A.N., Bochmann M. // Inorg. Chem. 2015. V. 54. № 15. P. 7368–7380.
65. Tshangana C., Nyokong T. // Spectrochim. Acta – Part A Mol. Biomol. Spectrosc. V. 2015. V. 151. P. 397–404.
66. Moeno S., Antunes E., Khene S., Litwinski C., Nyokong T. // Dalt. Trans. 2010. V. 39. P. 3460–3471.
67. Moeno S., Antunes E., Nyokong T. // J. Photochem. Photobiol. A Chem. Elsevier B.V., 2011. V. 218. № 1. P. 101–110.
68. Moeno S., Nyokong T. // Polyhedron. 2008. V. 27. № 8. P. 1953–1958.
69. Jhonsi M.A., Renganathan R. // J. Colloid Interface Sci. 2010. V. 344. № 2. P. 596–602.
70. Skripka A., Dapkute D., Valanciunaite J., Karabanovas V., Rotomskis R. // Nanomaterials. 2019. V. 9. № 1. P. 9.
71. Dayal S., Królicki R., Lou Y., Qiu X., Berlin J.C., Kenney M.E., Burda C. // Appl. Phys. B Lasers Opt. 2006. V. 84. № 1–2. P. 309–315.
72. Dayal S., Lou Y., Samia A.C.S., Berlin J.C., Kenney M.E., Burda C. // J. Am. Chem. Soc. 2006. V. 128. P. 13974–13975.
73. Dayal S., Li J., Li Y.S., Wu H., Samia A.C.S., Kenney M.E., Burda C. // Photochem. Photobiol. 2008. V. 84. № 1. P. 243–249.
74. Zenkevich E., Cichos F., Shulga A., Petrov E.P., Blaudeck T., von Borczyskowski C. // J. Phys. Chem. B. 2005. V. 109. P. 8679–8692.
75. Zenkevich E.I., Sagun E.I., Knyukshto V.N., Stasheuski A.S., Galievsky V.A., Stupak A.P., Blaudeck T., von Borczyskowski C. // J. Phys. Chem. C. 2011. V. 115. № 44. P. 21535–21545.
76. Zenkevich E.I., Stupak A.P., Goehler C., Krasselt C., von Borczyskowski C. // ACS Nano. 2015. V. 9. № 3. P. 2886–2903.
77. Blaudeck T., Zenkevich E.I., Abdel-Mottaleb M., Szwaykowska K., Kowerko D., Cichos F., Von Borczyskowski C. // ChemPhysChem. 2012. V. 13. № 4. P. 959–972.
78. Lemon C.M., Karnas E., Bawendi M.G., Nocera D.G. // Inorg. Chem. 2013. V. 52. № 18. P. 10394–10406.
79. Zenkevich E.I., Blaudeck T., Shulga A.M., Cichos F., von Borczyskowski C. // J. Lumin. 2007. V. 122–123. № 1–2. P. 784–788.
80. Ma J., Chen J.Y., Idowu M., Nyokong T. // J. Phys. Chem. B. 2008. V. 112. № 15. P. 4465–4469.
81. Orlova A.O., Martynenko I.V., Maslov V.G., Fedorov A.V., Gun'ko Y.K., Baranov A.V. // J. Phys. Chem. C. 2013. V. 117. № 44. P. 23425–23431.
82. Orlova A.O., Gubanova M.S., Maslov V.G., Vinogradova G.N., Baranov A.V., Fedorov A.V., Gounko I. // Opt. Spectrosc. 2010. V. 108. № 6. P. 927–933.
83. Narband N., Mubarak M., Ready D., Parkin I.P., Nair S.P., Green M.A., Beeby A., Wilson M. // Nanotechnology. 2008. V. 19. P. 445102.
84. Valanciunaite J., Skripka A., Streckyte G., Rotomskis R. // Laser Appl. Life Sci. 2010. V. 7376. P. 737607.
85. Valanciunaite J., Skripka A., Araminaite R., Kalantojus K., Streckyte G., Rotomskis R. // Chemija. 2011. V. 22. № 4. P. 181–187.
86. Borissevitch I.E., Parra G.G., Zagidullin V.E., Lukashev E.P., Knox P.P., Paschenko V.Z., Rubin A.B. // J. Lumin. 2013. V. 134. P. 83–87.
87. Skripka A., Valanciunaite J., Dauderis G., Poderys V., Kubiliute R., Rotomskis R. // J. Biomed. Opt. 2013. V. 18. № 7. P. 78002.
88. Kurabayashi T., Funaki N., Fukuda T., Akiyama S., Suzuki M. // Anal. Sci. 2014. V. 30. № 5. P. 545–550.
89. Yaghini E., Giuntini F., Eggleston I.M., Suhling K., Seifalian A.M., MacRobert A.J. // Small. 2014. V. 10. № 4. P. 782–792.
90. Gvozdev D.A., Maksimov E.G., Strakhovskaya M.G., Moysenovich A.M., Ramonova A.A., Moisenovich M.M., Goryachev S.N., Paschenko V.Z., Rubin A.B. // J. Photochem. Photobiol. B Biol. 2018. V. 187. P. 170–179.
91. Suchánek J., Lang K., Novakova V., Zimcik P., Zelinger Z., Kubát P. // Photochem. Photobiol. Sci. 2013. V. 12. № 5. P. 743.
92. Tekdaş D.A., Durmuş M., Yanik H., Ahsen V. // Spectrochim. Acta – Part A Mol. Biomol. Spectrosc. 2012. V. 93. P. 313–320.
93. Arvani M., Virkki K., Abou-Chahine F., Efimov A., Schramm A., Tkachenko N.V., Lupo D. // Phys. Chem. Chem. Phys. 2016. V. 18. № 39. P. 27414–27421.
94. Britton J., Antunes E., Nyokong T. // Inorg. Chem. Commun. 2009. V. 12. № 9. P. 828–831.
95. Britton J., Antunes E., Nyokong T. // J. Photochem. Photobiol. A Chem. 2010. V. 210. № 1. P. 1–7.
96. Chidawanyika W., Litwinski C., Antunes E., Nyokong T. // J. Photochem. Photobiol. A Chem. 2010. V. 212. № 1.

P. 27–35.
97. D'Souza S., Antunes E., Litwinski C., Nyokong T. // J. Photochem. Photobiol. A: Chem. 2011. V. 220. № 1. P. 11–19.
98. D'Souza S., Antunes E., Nyokong T. // Inorganica Chim. Acta. 2011. V. 367. № 1. P. 173–181.
99. Charron G., Stuchinskaya T., Edwards D.R., Russell D.A., Nann T. // J. Phys. Chem. C. 2012. V. 116. № 16. P. 9334–9342.
100. Tsolekile N., Ncapayi V., Obiyenwa G.K., Matoetoe M., Songca S., Oluwafemi O.S. // Int. J. Nanomedicine. 2019. V. 14. P. 7065–7078.
101. Lakowicz J.R. Principles of fluorescence spectroscopy. 3rd ed. Springer US, 2006. P. 449.
102. Ghosh M., Nath S., Hajra A., Sinha S. // J. Lumin. 2013. V. 141. P. 87–92.
103. Dhami S., de Mello A.J., Rumbles G., Bishop S.M., Phillips D., Beeby A. // Photochem. Photobiol. 1995. V. 61. № 4. P. 341–346.
104. Visheratina A.K., Martynenko I.V., Orlova A.O., Maslov V.G., Fedorov A.V., Baranov A.V., Gun'Ko Y.K. // J. Opt. Technol. 2014. V. 81. № 8. P. 444–448.
105. Rakovich A., Savateeva D., Rakovich T., Donegan J.F., Rakovich Y.P., Kelly V., Lesnyak V., Eychmüller A. // Nanoscale Res. Lett. 2010. V. 5. № 4. P. 753–760.
106. Dadadzhanov D.R., Martynenko I.V., Orlova A.O., Maslov V.G., Fedorov A.V., Baranov A.V. // Opt. Spectrosc. 2015. V. 119. № 5. P. 738–743.
107. Gvozdev D.A., Lukashev E.P., Gorokhov V.V., Pashchenko V.Z. // Biochem. 2019. V. 84. № 8. P. 911–922.
108. Gvozdev D.A., Maksimov E.G., Paschenko V.Z. // Moscow Univ. Biol. Sci. Bull. 2020. V. 75. № 1. P. 7–12.
109. Aly S.M., Ahmed G.H., Shaheen B.S., Sun J., Mohammed O.F. // J. Phys. Chem. Lett. 2015. V. 6. № 5. P. 791–795.
110. Tsay J.M., Trzoss M., Shi L., Kong X., Selke M., Jung E., Weiss S. // J. Am. Chem. Soc. 2008. V. 129. № 21. P. 6865–6871.

The Role of Non-coding RNAs in the Pathogenesis of Glial Tumors

T. F. Kovalenko#, T. D. Larionova#, N. V. Antipova, M. I. Shakhparonov, M. S. Pavlyukov*
Shemyakin-Ovchinnikov Institute of Bioorganic Chemistry Russian Academy of Sciences, Moscow, 117997 Russia
#Equal contribution
*E-mail: marat.pav@mail.ru
Received November 26, 2020; in final form, March 15, 2021
DOI: 10.32607/actanaturae.11270

ABSTRACT **Among the many malignant neoplasms, glioblastoma (GBM) leads to one of the worst prognosis for patients and has an almost 100% recurrence rate. The only chemotherapeutic drug that is widely used for treating glioblastoma is temozolomide, a DNA alkylating agent. Its impact, however, is only minor; it increases patients' survival just by 12 to 14 months. Multiple highly selective compounds that affect specific proteins and have performed well in other types of cancer have proved ineffective against glioblastoma. Hence, there is an urgent need for novel methods that could help achieve the long-awaited progress in glioblastoma treatment. One of the potentially promising approaches is the targeting of non-coding RNAs (ncRNAs). These molecules are characterized by extremely high multifunctionality and often act as integrators by coordinating multiple key signaling pathways within the cell. Thus, the impact on ncRNAs has the potential to lead to a broader and stronger impact on cells, as opposed to the more focused action of inhibitors targeting specific proteins. In this review, we summarize the functions of long noncoding RNAs, circular RNAs, as well as microRNAs, PIWI-interacting RNAs, small nuclear and small nucleolar RNAs. We provide a classification of these transcripts and describe their role in various signaling pathways and physiological processes. We also provide examples of oncogenic and tumor suppressor ncRNAs belonging to each of these classes in the context of their involvement in the pathogenesis of gliomas and glioblastomas. In conclusion, we considered the potential use of ncRNAs as diagnostic markers and therapeutic targets for the treatment of glioblastoma.**
KEYWORDS **glioma, glioblastoma, long noncoding RNAs, circRNAs, miRNAs, piRNAs, snRNAs, snoRNAs.**
ABBREVIATIONS **BBB – blood–brain barrier; ceRNA – competing endogenous RNA; circRNA – circular RNA; GBM – glioblastoma; lncRNA – long non-coding RNA; miRNA – microRNA; nc – nucleotide; ncRNA – non-coding RNA; piRNA – PIWI-interacting RNA; sncRNA – small non-coding RNA; snRNA – small nuclear RNA; snoRNA – small nucleolar RNA; TMZ – temozolomide.**

INTRODUCTION

Gliomas form a heterogeneous group of primary brain tumors, grade IV astrocytoma (also known as glioblastoma (GBM)) being the most aggressive amongst them [1]. Treatment of patients with GBM has remained almost unchanged over the past 20 years. First, maximal surgical resection of the tumor is performed, followed by a course of radiotherapy often supplemented with chemotherapy using temozolomide (TMZ), a DNA alkylating agent. However, despite this combination treatment, the mean survival rate of patients with GBM is extremely low compared to that for other cancer types. Thus, the 5-year survival rate of these patients is 4–5%, while the 2-year survival rate is approximately 26–33%.

Today, a mutation in the *IDH* gene and the level of *MGMT* promoter methylation are the key prognostic markers of gliomas widely used in clinical practice. The IDH^{R132H} mutation detected in almost 50% of all glioma specimens alters the metabolism and causes histone hypermethylation; strangely enough, this significantly increases patients' chances of survival [2]. The *MGMT* promoter methylation revealed in ~ 40% of all GBM specimens correlates with susceptibility to TMZ and is associated with a favorable outcome for patients receiving radiation therapy and chemotherapy [3]. Laboratory studies and an analysis of genome and transcriptome databases have allowed us to identify other survival-related markers and classify glioblastomas into phenotypic groups differing in terms of tumor

aggressiveness and susceptibility to therapy [4]. However, none of these approaches has gained a foothold in clinical practice thus far.

The past decades have witnessed a vigorous search for novel drugs for the treatment of glioblastoma. In particular, low-molecular-weight compounds inhibiting receptor tyrosine kinases such as EGFR (dacomitinib; phase II trials) and PDGFR (sunitinib; phase II/III trials), as well as epigenetic regulator proteins such as HDAC6 (panobinostat; phase II trials), are being studied. However, although similar drugs have proved highly effective in the treatment of various types of cancer, no encouraging results have been witnessed yet for glioblastoma [5, 6]. Along with low-molecular-compounds, a humanized monoclonal antibody against vascular endothelial growth factor A (VEGFA), known as bevacizumab, has been approved in a number of countries. However, it was shown later that bevacizumab, in combination with standard treatment, does not significantly increase a patient's survival [7]. Injecting immune cells exhibiting direct antitumor activity is another promising method to treat GBM. Some immunotherapy variants are currently undergoing different phases of clinical trials [8], but none of them is actively used in clinical practice.

Various classes of non-coding RNAs (ncRNAs) that often play an extremely important role in the regulation of the vitality of tumor cells are a rather promising target for developing new methods for glioblastoma treatment. An evident challenge related to the design of these drugs is that compounds capable of specifically interacting with a target nucleic acid sequence need to be used. This significantly increases the minimal size of a drug molecule and impedes its penetration through the cell membrane. In this review, we have made an attempt to systematize the data on the non-coding RNAs involved in the glioma pathogenesis and discuss the therapeutic strategies related to them.

Over the past two decades, it has become increasingly clear that non-coding transcripts play a crucial role both in natural physiological processes and in the development of various diseases, including cancer [9]. It has been found that ncRNAs are also involved in the pathogenesis of malignant glial tumors. Many ncRNAs have pro-oncogenic properties. Their level in malignant tumor tissues is significantly higher than in normal brain tissues. In many cases, expression of the respective ncRNA correlates with disease stage and (or) tumor phenotype [10, 11]. The ncRNAs associated with pro-neural to mesenchymal transition, proliferation of tumor stem cells, as well as ncRNAs facilitating tumor adaptation to hypoxia, are known [11–13]. Furthermore, it has been reported that oncogenic ncRNAs can both be synthesized in tumor cells and migrate to other cells within exosomes and microvesicles, which may contribute to further disease progression [14]. Meanwhile, numerous ncRNAs functioning as tumor suppressors have been reported [15–18]. Therefore, the information on the expression of numerous ncRNAs can theoretically be an important prognostic factor for patients. On the other hand, understanding the mechanism via which ncRNAs affect the key cellular processes can open up new prospects for the development of novel medications for the treatment of malignant glial tumors. In this review, we focus on long non-coding RNAs (lncRNAs), circular RNAs (circRNAs), microRNAs (miRNAs), PIWI-interacting RNAs (piRNAs), small nuclear RNAs (snRNAs), and small nucleolar RNAs (snoRNAs) in the context of their impact on the development of malignant glial tumors in humans (*Figure*). The roles played by transfer RNAs or ribosomal RNAs lie beyond the scope of our review; so, we will not discuss them.

1. LONG NON-CODING RNAS

1.1. Biosynthesis, classification, localization, and functions of lncRNAs

The group of lncRNAs includes nontranslated RNAs ≥ 200 nucleotides long. According to different estimates, 15,000 to 50,000 lncRNAs have been identified in humans [9, 25]. Most of these RNAs form with the involvement of RNA polymerase II; however, transcription of some lncRNAs can involve RNA polymerase III [26]. These RNAs are not translated for two reasons. First, their sequence usually does not contain open reading frames longer than 300 nucleotides. Second, these RNAs can contain various inactivating mutations that disable translation [27, 28]. As reported recently, some lncRNAs contain short open reading frames and can be translated to produce peptides whose function still needs to be elucidated in most cases [29]. Similar to mRNAs, lncRNAs can be capped and polyadenylated. Meanwhile, lncRNAs not carrying these modifications (e.g., lincROR) are also known [27]. According to the GenBank data, many lncRNAs (NEAT1, GAS5, and MALAT1) can undergo splicing, including alternative splicing, to produce several isoforms. Some lncRNAs (MALAT1 and GAS5) are widely expressed in most human tissues, while others (CRNDE and HOTAIR) are present only in certain types of tissues (the GenBank data). Furthermore, it is known that some lncRNAs (H19) are transcribed only during embryonic development, while their elevated level in the tissues of adult humans is indicative of pathology [30].

There are several criteria that are used for lncRNA classification: the position of the respective gene, the size, intracellular localization, and functions. The

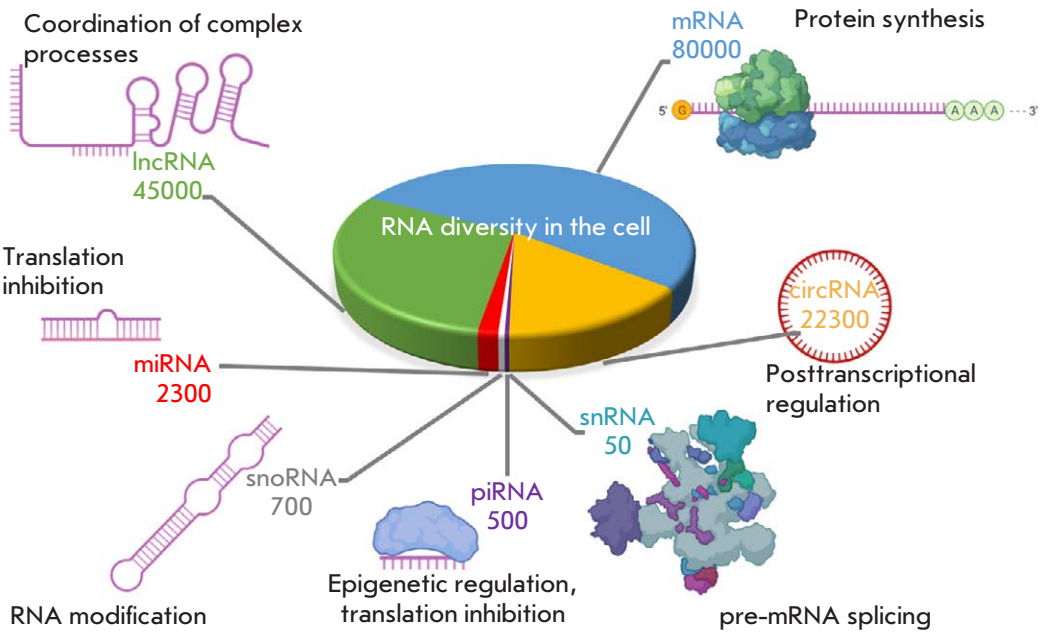

Functions of different types of ncRNAs in the cell. The diagram in the center and the numbers next to it indicate the approximate number of transcripts belonging to different classes of ncRNAs expressed in human cells [19–24]. The inscriptions indicate the main function of the corresponding group of ncRNAs

classification based on genomic localization of the lncRNA gene is provided below [9]. According to this classification, there are: (1) *intergenic* lncRNAs whose sequences do not overlap with those of protein-coding genes; (2) *antisense* lncRNAs that are transcribed in the direction opposite to the protein-coding genes and overlap with the gene sequences either partially or completely; (3) *bidirectional* (*or divergent*) lncRNAs whose transcription is initiated near the gene promoter and proceeds in the opposite direction; (4) *intronic* (sense and antisense) lncRNAs whose transcription is confined to gene introns; (5) *pseudogene-derived lncRNAs*, which are the transcripts of gene copies that have lost their coding potential due to inactivating mutations; (6) *telomeric and subtelomeric* lncRNAs that are transcribed from the telomeric chromosomal regions and contain telomeric sequences; (7) *centromeric* lncRNAs that are transcribed from centromeric regions and contain centromeric repeats; (8) *promoter-associated* lncRNAs; and (9) *enhancer-associated* lncRNAs that are expressed from these regulatory elements of the genome in both directions [9].

The lncRNAs can localize both inside the cell nucleus and in the cytoplasm [9]. Cytoplasmic lncRNAs can entrap regulatory miRNAs and various proteins, thus impeding their effects on the respective targets [31, 32]. The lncRNAs can ensure stability of other RNAs in the cytoplasm by binding to them [33]. Some lncRNAs act as precursors of regulatory miRNAs [34]. Nuclear lncRNAs can regulate gene expression by recruiting chromatin remodeling proteins and various activating or repressive complexes to gene promoters. Finally, due to their size, lncRNAs can act as scaffolds for the assembly of macromolecular protein complexes [35]. Furthermore, lncRNAs can stabilize chromosome loops by ensuring interaction between gene enhancers and promoters [36]. Some lncRNAs play a structure-forming role by being involved in the formation and maintenance of certain nuclear structures [37]. A number of lncRNAs have also been shown to play a crucial role in the occurrence of genomic imprinting and X chromosome inactivation [9].

The numerous lncRNAs that have been described can be viewed as prognostic markers for malignant glial tumors. Some of them have pro-oncogenic functions, while others act as tumor suppressors. However, existing data on many transcripts are very controversial. Some studies indicate that the same lncRNA can act as an oncogene for glioblastoma and as a tumor suppressor for other types of glioma that are less malignant. Thus, this finding is true for lincROR [38, 39]. We will focus on several lncRNAs that play different roles in the progression of GBM as an example. *Table 1* summarizes the remaining lncRNAs whose functions in glioblastoma cells have been studied.

1.2. Oncogenic lncRNAs

NEAT1 (nuclear enriched abundant transcript 1, or nuclear paraspeckle assembly transcript 1) is an interesting example of oncogenic lncRNAs that has been well studied in glioblastomas. The intron-lacking *NEAT1* gene resides on chromosome 11q13.1. A

Table 1. The role played by lncRNAs and circRNAs in the pathogenesis of malignant glial tumors

Name	Type of ncRNA	Role	Molecular mechanism of action	Reference
lncRNAs				
H19	Intergenic	Oncogene	Is a precursor of miR-675; acts as a ceRNA for microRNA Let-7.	[34, 40]
HOTAIR	Antisense	Oncogene	Recruits chromatin modeling complexes PRC2 and CoREST; acts as a ceRNA for many miRNAs (e.g., miR-326).	[35, 41]
CRNDE	Divergent	Oncogene	Recruits chromatin modeling complexes PRC2 and CoREST; acts as a ceRNA for many miRNAs (e.g., miR-186).	[42, 43]
XIST	Intergenic	Oncogene	Acts as a ceRNA for many miRNAs (e.g., miR-152).	[44]
NEAT1	Intergenic	Oncogene	Acts as a ceRNA for many miRNAs (e.g., miR-107); recruits EZH2 to promoters of the *AXIN2*, *ICAT* and *GSK3B* genes.	[45, 46]
PVT1	Intergenic	Oncogene	Acts as a ceRNA for many miRNAs (e.g., miR-128-3p); interacts with EZH2.	[47, 48]
CASC2	Divergent	Tumor suppressor	Acts as a ceRNA for miR-21.	[49]
GAS5	Divergent	Tumor suppressor	Acts as a ceRNA for miR-222.	[50]
PTENP1	Pseudogenic lncRNA	Tumor suppressor	Acts as a ceRNA for many miRNAs regulating *PTEN* expression.	[15, 31]
lincROR	Intergenic	Dual	Acts as a ceRNA for miR-145.	[51]
MEG3	Intergenic	Dual	Contributes to p53 stabilization; acts as a trap for miR-19a.	[52, 53]
NEAT2/ MALAT1	Intergenic	Dual	Acts as a ceRNA for many miRNAs (e.g., miR-384).	[54]
HOTTIP	Antisense	Dual	Acts as a ceRNA for miR-101.	[55]
circRNAs				
circHIPK3	Exonic	Oncogene	Acts as a ceRNA for some miRNAs (e.g., miR-654).	[56]
circPVT1	Exon-intronic	Oncogene	Acts as a ceRNA for miR-199a-5p.	[57]
circCFH	Exonic	Oncogene	Acts as a ceRNA for miR-149.	[58]
circTTBK2	Exonic	Oncogene	Acts as a ceRNA for some miRNAs (e.g., miR-761).	[59]
circSMARCA5	Exonic	Tumor suppressor	Interacts with splicing factor SRSF1, thus preventing the formation of oncogenic transcripts.	[60]
circFBXW7	Exonic	Tumor suppressor	Encodes the protein promoting ubiquitin-dependent degradation of c-Myc.	[16]
circSHPRH	Exonic	Tumor suppressor	Encodes the protein protecting SHPDH protein against ubiquitin-dependent degradation.	[17]
circPINT	Exonic	Tumor suppressor	Encodes the peptide increasing the affinity for the PAF1 complex to the target genes.	[18]
circITCH	Exonic	Tumor suppressor	Acts as a ceRNA for miR-214.	[61]

full-length 22,743-nucleotide-long non-polyadenylated transcript of NEAT1 and a 3735-nucleotide-long truncated polyadenylated lncRNA have been revealed (the GenBank data). NEAT1 is needed for the formation of paraspeckle nuclear condensates [37], ribonucleoprotein bodies sized 0.3–3 μm surrounded by chromatin [62]. Pro-oncogenic protein SRSF1 is an important posttranscriptional regulator of NEAT1: it interacts with this lncRNA, thus enhancing its stability [63].

The NEAT1 content in glioblastomas is more than twofold higher than that in less aggressive types of gliomas. Furthermore, the level of this lncRNA in glioblastoma stem cells ($CD133^+$) is twice higher than that in the less aggressive but better differentiated population of $CD133^-$ GBM cells [45]. Most often, NEAT1 exhibits its oncogenic effect in gliomas by binding to various miRNAs (e.g., miR-107) [45]. Moreover, NEAT1 recruits EZH2 to promoters of the *AXIN2*, *ICAT*, and *GSK3B* genes, thus facilitating H3K27 histone trimethylation and reducing the expression level of the aforementioned genes [46]. This example reveals a feature shared by all lncRNAs: they are able to activate different signaling pathways; these pathways eventually result in identical changes in the cellular phenotype and, thus, enhance each other's action.

1.3. Tumor-suppressive lncRNAs

GAS5 (grow arrest-specific 5) is one of the lncRNAs that suppress glioblastoma development. The *GAS5* gene residing on chromosome 1q25.1 partially overlaps with the 5' end of the *ZBTB37* gene transcribed in the opposite direction. Fifteen isoforms of lncRNA GAS5 differing in terms of length and the number of exons have been reported. The full-length non-polyadenylated transcript (725 nucleotides long) consists of 13 exons. The shorter isoforms contain 9–12 exons (the GenBank data). GAS5 interacts with the DNA-binding domain of the receptors of steroid hormones (glucocorticoids, mineralcorticoids, androgens, and progesterone), thus preventing them from impacting the target genes [64]. *In vitro* experiments have demonstrated that lncRNA GAS5 acts as a tumor suppressor in gliomas. Thus, X. Zhao *et al.* (2015) found that GAS5 inhibits the proliferation of U87 and U251 cells by binding to oncogenic miR-222 [50]. Furthermore, GAS5 overexpression increases the susceptibility of U87 cells to cisplatin [65]. Clinical trials also demonstrate that an increased GAS5 level correlates with a more favorable prognosis both in patients with glioblastoma and less malignant gliomas [66].

1.4. The lncRNAs exhibiting dual effect on glioma cells

Along with lncRNAs that play either an oncogenic or a tumor-suppressor role, there are several lncRNAs whose functions depend on the context. NEAT2/MALAT1 (metastasis associated lung adenocarcinoma transcript 1) is one of such lncRNAs. The *MALAT1* gene residing on chromosome 11q13 is expressed in various human tissues, including the brain. Three variants of lncRNA MALAT1 having a similar size (~ 8000 nucleotides) have been described; they are produced by splicing and differ in terms of the number of exons (the GenBank data). During MALAT1 processing, a small fragment is cleaved from the 3' end of the primary transcript and is transferred to the cytoplasm. The mature lncRNA MALAT1, ~ 7,000 nucleotides long, predominantly remains inside the nucleus and localizes in nuclear speckles [67]. MALAT1 does not contain poly(A) sequences; however, it is rather stable, since a special triplex structure forms at its 3' end. MALAT1 is associated with the splicing factors SRSF1, SRSF2, and SRSF3, and thus involved in mRNA processing. In addition, MALAT1 regulates gene expression at a transcriptional level. Thus, this lncRNA can bind to the nonmethylated protein Pc2 (polycomb 2 protein) to facilitate its interaction with the E2F transcription factor and transcriptional coactivators [67]. Meanwhile, the oncogenic role of MALAT1 in cancer is mainly related to its ability to affect the level of certain miRNAs (including miR-384) [54]. The meta-analysis conducted by Q. Zhou *et al.* (2018) demonstrated that an increased MALAT1 level correlates with an unfavorable prognosis in patients with glioma [68]. *In vitro* experiments have demonstrated that suppression of MALAT1 expression reduces cell resistance to temozolomide, as well as cell proliferation, migration, and invasion, and stimulates apoptosis [69]. Contrariwise, Y. Han *et al.* revealed that the MALAT1 level in gliomas is 1.5-fold lower than that in a normal brain. Furthermore, overexpression of MALAT1 reduces the proliferation of U87 and U251 cells [70]. It was also found that MALAT1 forms a complex with the RNA-binding protein HuR and ensures its recruitment to exon 2 of the *CD133* gene, the key marker of glioblastoma stem cells. As a result, *CD133* expression is suppressed at the transcriptional level [71]. Therefore, MALAT1 is involved in the fine tuning of the phenotype of glioblastoma cells while changes in the level of this RNA (both the increased and decreased levels) result in an unfavorable effect on cells.

2. CIRCULAR RNAs

2.1. General characteristics, biosynthesis, classification, and functions

circRNAs include transcripts whose 5' and 3' ends are linked by a phosphodiester bond yielding a circular structure. Inverted repeats contained in the precursors contribute to the formation of circRNAs [72, 73]. The circRNAs formed from RNA precursors via the so-called reverse splicing. Whereas the 5'-terminal donor site is bound to the 3'-terminal acceptor site in the case of canonical splicing, during reverse splicing, the 3'-donor site interacts with the 5'-acceptor site, thus producing a covalently closed circular transcript. According to some reports, reverse splicing (as well as the conventional forward one) occurs via the canonical spliceosome assembly pathway [73]. In a number of cases, both linear and circular RNAs can be transcribed from the same sequence [47, 57]. Depending on their origin and structure, there are: (1) *exonic circRNAs (ecircRNAs)*, (2) *exon–intronic circRNAs* (*eIcircRNAs*), (3) *intronic circRNAs* (*icircRNAs*), and (4) *intergenic circRNAs* (*igcircRNAs*). In the first case, circRNAs are formed from the mRNAs of protein-coding genes. As a result, this RNA can have the same exon composition as mRNA, but the 5' end of exon 1 is connected to the 3' end of the last exon in circRNAs. In the case of eicircRNAs, the circular transcripts contain some of the intronic sequences of RNA precursors. icircRNAs and igcircRNAs are formed upon transcription of the intronic and intergenic sequences, respectively [72]. Circular RNAs are neither polyadenylated nor capped.

They are more stable than linear lncRNAs, and thus more promising diagnostic markers and therapeutics [72]. Importantly, transcription of linear and circular RNAs of the same gene can occur independently of each other as it was demonstrated for lncRNA PVT1 and circPVT1 [47, 57].

In a manner similar to lncRNAs, circRNAs can interact with other RNAs, DNAs, and proteins, as well as perform various functions in the cell. Many circRNAs contain microRNA binding sites and act as a "sponge" by adsorbing these molecules [56–59, 61]. Circular transcripts can also compete with the mRNAs of protein-coding genes for splicing factors, thus reducing the efficiency of mRNA processing. A number of circRNAs act as adaptors and recruit various proteins, thus ensuring their interaction with each other. Furthermore, circRNAs can reside on gene promoters and regulate their transcription [73]. Although circRNAs are not capped, some of them contain short reading frames and are translated to produce small proteins and peptides [16–18]. The nucleotide sequences of these circRNAs contain the specific IRES elements required for the interaction with ribosomes and translation initiation factors [73].

It was not until recently that circRNAs were found to be involved in the pathogenesis of malignant glial tumors. Nevertheless, there already are several publications that have detected circular transcripts differentially expressed in patients with glioma and glioblastoma. These transcripts are now being actively studied, and many of them can be regarded as potential diagnostic markers. Some circRNAs playing a pro-oncogenic or tumor-suppressor role in the pathogenesis of malignant glial tumors will be listed below. *Table 1* provides a more detailed list of circRNAs with known functions.

2.2. Pro-oncogenic circRNAs

One of the pro-oncogenic circRNAs is circHIPK3. The *HIPK3* (homeodomain interacting protein kinase 3) gene resides on chromosome 11p13 (the GenBank data). Several circRNAs generated by noncanonical splicing of the primary *HIPK3* linear transcript are known. The 1099-nucleotide-long circular transcript involving only the *HIPK3* exon 2 is most abundant in human tissues (the CircBase data). This transcript increases cell proliferation and acts as a trap for several miRNAs. P. Jin *et al.* (2018) showed that the circHIPK3 level in gliomas is 1.5- to 5-fold higher than that in the normal brain tissue of the same patients. Furthermore, the increased circHIPK3 level reduces the mean survival time in patients almost twofold [56]. Suppression of this circRNA in *in vitro* experiments reduces proliferation of U87 and U251 cells. It was found that circHIPK3 acts as a "sponge" for miR-654, which in turn regulates the level of pro-oncogenic protein IGF2BP3 [56].

2.3. Tumor-suppressive circRNAs

circSMARCA5 is an example of tumor-suppressor circRNA. The *SMARCA5* protein-coding gene resides on chromosome 4 (4q31.21). The 269-nucleotide-long circSMARCA5 includes exons 15 and 16 (according to the CircBase data). This circRNA is highly transcribed in the human brain and plays an oncoprotective role. A reduced SMARCA5 level was shown to correlate with an unfavorable prognosis in patients with glioblastoma [60]. Overexpression of SMARCA5 contributes to reduced migration of U87MG cells. Circular RNA SMARCA5 contains binding sites for the splicing factor, which plays a pro-oncogenic role in many cancers, including glioblastomas. By interacting with SRSF1, SMARCA5 prevents its involvement in alternative splicing and the generation of oncogenic transcripts. In particular, this circRNA reduces the ratio between the oncogenic and anti-oncogenic VEGF-A isoforms [60].

3. SMALL NON-CODING RNAs

Small non-coding RNAs (sncRNAs) are small molecules 18–200 nucleotides long. Several types of sncRNAs have been identified thus far, namely, tRNAs, miRNAs, small interfering RNAs (siRNAs), small nuclear RNAs (snRNAs), small nucleolar RNAs (snoRNAs), telomerase RNA components (TERC), PIWI-interacting RNAs (piRNAs), small enhancer RNAs (seRNAs), and Y RNAs [74]. This list still continues to expand. By cooperating with other intracellular molecules, sncRNAs are involved in regulation of gene expression at all levels: the cotranscriptional, posttranscriptional, translational, and epigenetic ones. An improper amount and functions of sncRNAs alter the intracellular processes and trigger various diseases: not only cancer, but also neurodegenerative and cardiovascular diseases, etc. [75]. There are several reasons why the level of sncRNAs synthesized by the cell is altered. First, this occurs due to mutations in the genes encoding sncRNAs per se [76]. The second reason is the mutations and disrupted functions of the enzymes responsible for sncRNA biogenesis (e.g., Dicer and Drosha for miRNAs) [77]. The epigenetic, transcriptional, or posttranscriptional control over expression of both sncRNAs and enzymes processing them can also be disrupted [77]. In this section, we will focus on the types of sncRNAs involved in the pathogenesis of malignant glial tumors. *Table 2* provides brief characteristics of these sncRNAs.

3.1. microRNAs

microRNAs (miRNAs) are short RNAs (~ 22 nucleotides long) involved in posttranscriptional regulation of gene

Table 2. The key characteristics of the sncRNAs involved in glioblastoma pathogenesis

Parameter	miRNAs	piRNAs	snoRNAs	snRNAs
Length	~ 22 nucleotides	~ 24–30 nucleotides	~ 60–300 nucleotides	~ 80–350 nucleotides (on average, ~ 150 nucleotides)
Genomic localization	In the intronic regions of protein-coding genes, sometimes in exons	In PIWI clusters	In introns of protein-coding genes and polycistronic snoRNA clusters	In snRNA genes
Precursors	Double-stranded hairpin RNA	Single-stranded RNA	Single-stranded RNA	Single-stranded RNA
RNA polymerase performing transcription	RNA polymerase II	RNA polymerase II	RNA polymerase II	RNA polymerase II; for U6, RNA polymerase III
Mechanism of processing	Double-stage cleavage by Drosha and Dicer proteins	5'- and 3'-exonuclease-assisted truncation, followed by cleavage by Zucchini protein	Splicing of pre-mRNA, opening of the lariat structure, followed by its 5'- and 3'-exonuclease-assisted truncation	Capping and modification of the 3'-end of the molecule
Classes of RNA-binding proteins	Argonaute	PIWI	5.5 K, NOP56, NOP58, and firillarin	Spliceosomal proteins
Functions	Regulation of expression of protein-coding genes	Transposon silencing	Posttranscriptional modifications of the other types of cellular RNAs	pre-mRNA splicing

expression. The sequences encoding miRNAs in most cases reside inside introns, although exonic miRNAs are sometimes found. Transcription of miRNAs is performed by RNA polymerase II, which also transcribes the host gene [78]. After the multi-stage processing that has been described in detail in many reviews [78], miRNAs within the RNA-induced silencing complex (RISC) is involved in recognition of target gene mRNAs. The crucial criterion for choosing the target mRNA is the presence of a domain complementary to the so-called *seed sequence* of a miRNA, which is a region consisting of six nucleotides (nucleotides 2 through nucleotide 7) at the 5' end of a miRNA molecule [79]. These complementary domains are most typically found in the 3'-untranslated regions of mRNA (i.e., outside its protein-coding region). The complementarity (either complete or partial) ensures binding between the target mRNA and the RISC, which either causes mRNA degradation or represses its translation. In the former case, GW182 protein ensures the removal of poly(A) tail or 5' cap from the mRNA molecule [80] to give rise to a non-functional product that is degraded by 5'-3' exoribonuclease 1 (XRN1) [79]. There is currently no consensus regarding translational repression, but most studies indicate that the RISC causes dissociation of translation initiation factors eIF4AI and eIF4AII from the mRNA target, thus inhibiting mRNA scanning by the ribosome and formation of the translation initiation complex eIF4F [81]. Both the aforementioned gene silencing mechanisms are interrelated; however, according to the ribosome profiling data, 66–90% of gene silencing is caused by mRNA degradation [82]. The available estimates suggest that miRNAs are involved in expression regulation of approximately 30% of human genes [83]. The impact of a single miRNA on gene expression is usually appreciably weak. Therefore, miRNAs typically form large-scale networks of intracellular molecular interactions, thus exhibiting a synergistic effect. We would like to thoroughly describe several miRNAs playing different roles in progression of GBM as an example (*Table 3* lists miRNAs whose functions have been studied in glioblastoma cells).

3.1.1. Oncogenic microRNAs. The findings reported in numerous studies describing the role played by oncogenic miRNAs in the pathogenesis of gliomas have been published [94, 95]. Tumor suppressor genes usually act as targets for these miRNAs, while the disruption of miRNA expression causes uncontrolled cell proliferation, enhances cell migration and invasion, induces angiogenesis and blocks apoptosis. miR-21 is one of the best-studied oncogenic miRNAs; its level is elevated in many cancers and correlates with disease grade in gliomas [10]. This miRNA regulates numerous intracellular processes promoting glioma development [86]. The miR-21 targets include the genes promoting apoptosis (*PDCD4* and *LRRFIP1*) [99, 100], as well as the tumor suppressor genes inhibiting invasion (*RECK* and *TIMP3*) [101] and proliferation (*IGFBP3*) [87]. Furthermore, miR-21 can affect microglial be-

Table 3. sncRNAs associated with glioblastoma development

miRNA	Role	Target genes	Function	Reference
miRNAs				
let-7	Tumor suppressor	NRAS, KRAS, CCND1	Reduces proliferation and invasion; increases apoptosis and susceptibility to cisplatin	[84]
miR-7	Tumor suppressor	EGFR, FAK, PI3K, RAF1	Reduces invasion and migration	[84]
miR-17	Tumor suppressor	PTEN, MDM2, CCND1, AKT1	Reduces cell migration and viability	[84, 85]
miR-21	Oncogene	ANP32A, SMARCA4, RECK, TIMP3, IGFBP3	Enhances proliferation, invasion, and chemoresistance	[86, 87]
miR-24	Oncogene	ST7L, SOX7	Enhances proliferation and migration	[88]
miR-221/222	Oncogene	PTEN, PUMA, MGMT	Enhances proliferation, invasion, and treatment resistance	[84]
miR-326	Tumor suppressor	NOTCH1, NOTCH2	Reduces cell viability	[84, 89]
miR-451	Tumor suppressor	CAB39, LKB1, AMPK, PI3K, AKT	Inhibits proliferation	[84, 90]
piRNAs				
piR-30188	Tumor suppressor	lncRNAs OIP5-AS1	Reduces proliferation, migration, and invasion of glioma cells and stimulates apoptosis	[91]
piR-8041	Tumor suppressor	MAP3K7б, RASSF1	Induces cell cycle arrest and reduces proliferation	[92]
piR-DQ593109	Tumor suppressor	Causes degradation of miR-330-5p	Loosens the tight intercellular junctions	[93]
piR-598	Tumor suppressor	BAX, GOS2, JUN	Enhances apoptosis and reduces proliferation	[94]
snoRNAs				
SNORD44	Tumor suppressor	CASP3, CASP8, CASP9	Induces apoptosis, reduces proliferation and invasiveness	[95]
SNORD47	Tumor suppressor	CCNB1, CDK1, CDC25C, CTNNB1, CDH2, VIM, MMP2, MMP9, CDH1	Inhibits proliferation and increases patients' survival	[96]
SNORD76	Tumor suppressor	CCNA1, CCNB1	Inhibits growth and proliferation of glioma cells	[97]
snRNAs				
U1	Oncogene	The mutation in U1 inactivates *PTCH1* and activates *GLI2* and *CCND2*	Upregulates oncogene expression and inactivates tumor suppressor genes	[98]

havior, thus ensuring favorable conditions for tumor growth. miR-21 was detected in vesicles secreted by glioma cells [14]. Having entered microglia, the vesicles reduced expression of the target genes of miR-21 (*Bmpr2*, *Btg2*, *Kbtbd2*, *Pdcd4*, *Pten*, and *Rhob*). Some of these genes are involved in cell proliferation and differentiation. Therefore, their inhibition by vesicular miR-21 enhanced microglial proliferation, which may significantly affect the formation of tumor microenvironment and promote its progression as suggested in ref. [14].

Interestingly, more and more data on the important role played by exogenous miRNA molecules (the ones coming from neighboring cells) are being collected. Thus, oncogenic miRNAs can migrate between glioma cells and their microenvironment (astrocytes, oligodendrocytes, endothelial cells, and microglia/macrophages), thus being involved in intercellular communication, which contributes to tumor progression [14]. Co-culturing astrocytes with glioma cells increases the levels of nine miRNAs (miR-4519, miR-5096, miR-3178, etc.) in astrocytes; two miRNAs (miR-5096 and miR-4519) directly migrate to astrocytes from glioma cells through gap junctions [102]. The miRNA transfer in the opposite direction has also been reported: miR-19a is transferred from astrocytes to tumor cells by vesicles and inhibits PTEN activity in tumor cells, thus causing metastatic growth. Furthermore, the exosomes secreted by hypoxic glioma cells induce polarization of M2 macrophages and exhibit an immunosuppressive effect, thus promoting glioma proliferation, migration, and invasion *in vitro* and *in vivo*. This effect is attributed to the presence of miR-1246 in exosomes [103].

3.1.2. Tumor-suppressive miRNAs. A large number of tumor-suppressive microRNAs are known [84]. Thus, miR-7 inhibits signal transduction through the EGF receptor involved in the Akt protein kinase signaling pathway. However, miR-7 expression is suppressed (its level is reduced more than sixfold compared to the normal tissues) in glioblastoma, so the Akt signaling pathway is permanently activated and the viability and proliferation of tumor cells is increased [104]. It has also been demonstrated that exogenous administration of proapoptotic miR-218 suppresses expression of cyclin-dependent kinase 6 (CDK6), reduces proliferation, and causes apoptotic death of glioma cells [105]. Another target of miR-218 is EGFR-coamplified and overexpressed protein (ECOP), which regulates the transcriptional activity of NF-κB. Overexpression of miR-218 in glioma cells leads to a curb of the activity of NF-κB by ECOP by causing apoptosis and slowing down proliferation [106].

3.2. PIWI-interacting RNAs (piRNAs)

PIWI-interacting RNAs (piRNAs) are the non-coding RNAs approximately 24–35 nucleotides long which were initially detected in the Drosophila gonads. These RNAs have got their name because they bind to PIWI (P-element-induced wimpy testis) proteins [107, 108]. The so-called piRNA clusters that mainly reside in the intergenic or non-coding domains are the sources of piRNAs in the genome [109]. There are two mechanisms for piRNA formation in the cell: (1) via the primary processing pathway and (2) via the ping–pong mechanism resulting in amplification of secondary piRNAs. These mechanisms have been thoroughly described in reviews [110, 111]. It has been demonstrated that piRNAs are involved in the pathogenesis of various diseases, including malignant neoplasms [112, 113]. According to the profiling data, approximately 350 piRNAs are expressed in normal brain tissues and GBM, some piRNAs being typical of GBM only [92].

3.2.1. Oncogenic piRNAs. Because piRNAs have recently been studied in various types of malignant tumors, only a few publications focusing on piRNAs in gliomas are available, and there are no publications that would disclose the oncogenic role played by piRNAs in the development of glial tumors.

3.2.2. Tumor suppressor piRNAs. Database analysis has revealed that single-nucleotide polymorphisms in the piR-2799, piR-18913, piR-598, piR-11714, and piR-3266 genes are associated with the increased risk of glioma development; the piR-598 variants correlate with a risk level stronger than other variants do. The transcriptome profiling of cells transfected with wild-type piR-598 indicates that this piRNA affects expression of 518 genes involved in glioma cell death/survival. The presence of piR-598 reduced expression of most of the detected genes (71.2%). The gene encoding the oncogenic transcription factor Jun is one of the genes whose expression was significantly decreased. Simultaneously, piR-598 increases the level of BAX and GOS2 pro-apoptotic proteins. Studies focused on the effect of piR-598 on *in vitro* growth of glioma cells demonstrated that overexpression of wild-type piR-598 reduces cell proliferation and colony formation; contrariwise, overexpression of the mutant piR-598 increases them, which is consistent with the transcriptome analysis data [94]. However, the exact mechanisms underlying these processes have not been elucidated yet and need to be studied further. Other tumor suppressor piRNAs are listed in *Table 3*.

3.3. Small nucleolar RNAs

Small nucleolar RNAs (snoRNAs) are localized in the nucleolus and are 60–300 nucleotides long. Human snoRNAs reside in the intronic domains of the genes encoding proteins or lncRNAs and are cut out from them during splicing [114]. snoRNAs have several functions, their involvement in processing and maturation of other types of cellular RNAs being the best-known function. Therefore, three classes of snoRNAs have been differentiated: C/D box snoRNAs (involved in 2'-O-methylation of rRNAs), H/ACA box snoRNAs (involved in pseudouridination of RNA nucleotides), and small Cajal body-specific RNAs (cbsRNAs belonging to the class of box C/D–H/ACA RNAs and involved in 2'-O-methylation and pseudouridination of spliceosomal U1, U2, U4, and U5 snRNAs) [114]. snoRNAs were reported to act both as tumor suppressors and oncogenes. They are known to be involved in proliferation, apoptosis, metastasizing, and the development of drug resistance by tumor cells, while the mechanisms of action of these RNAs differ [115].

3.3.1. Oncogenic snoRNAs. No oncogenic snoRNAs involved in glioma development have been reported thus far.

3.3.2. Tumor suppressor snoRNAs. SNORD47 is one of the tumor suppressor snoRNAs whose level in gliomas is twice lower compared to that in normal brain tissues. A comparison of gliomas of different grades showed that most grade III–IV gliomas have a significantly reduced SNORD47 level (revealed in 71.4% of the analyzed specimens). Therefore, the survival of patients with a higher SNORD47 expression in glioma tissues is better compared to that in patients with lower SNORD47 expression. Overexpression of SNORD47

results in the inhibition of cell proliferation by inducing cell cycle arrest in the G2 phase. This possibly takes place due to a downregulated expression of such important cell cycle regulators as cyclin B1, CDK1 and CDC25C, β-catenin, and phospho-β-catenin. The levels of N-cadherin, vimentin, and metalloproteinases 2 and 9 decrease simultaneously, and the level of E-cadherin increases, thus indicating that SNORD47 prevents the pro-neural to mesenchymal transition of glioma cells. Furthermore, SNORD47 overexpression increases the susceptibility of glioma cells to temozolomide [96]. SNORD44 is another tumor-suppressor snoRNA. Its level and the level of the transcript of its host gene, lncRNA GAS5, in glioma cells are 2–3 times lower than those in a healthy brain. The levels of caspase 3, caspase 8, and caspase 9 are elevated upon SNORD44 overexpression, thus causing apoptosis. Moreover, cells transfected with SNORD44 are characterized by a noticeably lower proliferation and invasiveness [116]. However, the exact molecular mechanisms of these processes remain unknown. Other examples of tumor suppressor snoRNAs are listed in *Table 3*.

3.4. Small nuclear RNAs

Small nuclear RNAs (snRNAs) consist of approximately 150 nucleotides. The U6 and U6^{ATAC} snRNAs are synthesized by RNA polymerase III, while the remaining ones are by RNA polymerase II [117, 118]. During maturation, snRNAs undergo numerous processing and folding stages and bind to various proteins to form functional snRNPs. Mature snRNPs are imported back to the nucleus and travel to Cajal bodies to perform their functions. The snRNA biogenesis is discussed in more detail in review [119].

The key function of snRNAs is participation in pre-mRNA processing. snRNAs are the spliceosome components: U1, U2, U4, U5, and U6 are the components of the major spliceosome, while U5, U11, U12, U4^{ATAC}, and U6^{ATAC} are the components of the minor one. U7 and U8 have extra-spliceosomal functions: U7 is involved in the processing of histone pre-mRNA [120], while U8 is needed for rRNA maturation [121]. The involvement of snRNAs in splicing was thoroughly described earlier [122, 123]. The normal functioning of all components of the splicing machinery is critical for many biological processes: so, it is not surprising that splicing disruption is observed in multiple diseases, including glioblastoma [124].

3.4.1. Oncogenic snRNAs. Mutations in snRNAs are detected in various types of cancer [25], including brain tumors. Thus, mutations in the third nucleotide within the binding domain of the 5'-splice site in U1 were detected in medulloblastoma cells. Alternative splicing results in inactivation of tumor-suppressor genes (*PTCH1*) and activation of oncogenes (*GLI2* and *CCND2*) in medulloblastoma cells with mutant U1 snRNA [98]. Vesicles secreted by apoptotic glioblastoma cells were also shown to contain spliceosome components, including U2, U4, and U6 snRNAs. The exogenous spliceosome components alter pre-mRNA splicing in recipient cells, making the tumor more aggressive and treatment-resistant [126].

3.4.2. Tumor suppressor snRNAs. Data on the tumor suppressor functions of protein splicing factors has been obtained, but nothing is known yet about the tumor suppressor function of snRNAs in gliomas.

4. APPLICATION OF NON-CODING RNAs IN TREATMENT AND DIAGNOSIS OF BRAIN TUMORS

Protein molecules have long been viewed as potential targets for antitumor therapy and markers of malignant neoplasms. However, the role played by the non-coding part of the genome in cell functioning identified over the past decades has offered new insight into cancer development mechanisms. The number of reports on ncRNAs that can be used either as antitumor therapy targets or as prognostic markers increases year by year [127, 128]. Furthermore, ncRNA-based drugs effective in the treatment of some diseases have already been designed [129].

Thus, many sncRNAs are found in the body fluids (blood plasma and serum or cerebrospinal fluid) of patients with gliomas. sncRNAs usually reside in exosomes, so they are protected against degradation and can pass through the blood–brain barrier (BBB) [130]. For this reason, sncRNAs can be used as good biomarkers in non-invasive diagnostics. For example, the miR-221 level in glioma tissue specimens and the blood plasma of patients is elevated 2–11 times. Its level increases with tumor grade. Therefore, miR-221 can be viewed as a potential diagnostic marker of glial tumors [131]. Similar results have also been obtained for miR-21 [132, 133]. Along with miRNAs, other types of sncRNAs can also act as potential biomarkers. Thus, the miR-320/miR-574-3p/RNU6-1 combination or RNU6-1 isolated from serum exosomes is specific to patients with glioblastoma [134].

New cancer treatment strategies based on the use of antisense oligonucleotides with various RNAs (including lncRNAs) acting as targets are currently being developed [135, 136]. However, the BBB significantly reduces the bioavailability of such therapeutics in patients with brain tumors of glial origin. It is more promising to use low-molecular-weight compounds showing highly specific binding to certain sequences (or certain structural motifs) of lncRNAs for GBM treatment.

Thus, the compounds AC1NOD4Q and AC1Q3QWB bind to the region residing in the 5'-terminal domain of the oncogenic lncRNA HOTAIR and disrupt its interaction with EZH2, the catalytic subunit of the chromatin remodeling complex. These compounds significantly reduce the migration and invasion of glioma cells, as well as suppress their pro-neural to mesenchymal transition [137–139]. Compounds interacting with the specific triplex structure localized on the 3' end of lncRNA MALAT1 have also been identified. These low-molecular-weight compounds can reduce the MALAT1 level and slow tumor growth in a mouse model of breast cancer [140].

RNP complexes containing snRNAs are a promising therapeutic target. It has been demonstrated that activity of U2-snRNP is needed for glioblastoma stem cells to survive and pass through the mitotic phase. Pladienolide B, a macrolide inhibiting activity of the SF3b subcomplex, disturbs the normal interaction between U2 snRNA and pre-mRNA, thus disrupting splicing and causing tumor cell death [141]. Two other antitumor agents, spliceostatin A and E7107, have the same effect [142, 143]. These agents disrupt mRNA splicing in such cell-cycle regulators as cyclin A2 and Aurora A kinase [144] by inhibiting the proliferation of tumor cells [145]. Furthermore, disrupted splicing results in the emergence of aberrant proteins, which may also cause tumor cell death [142]. Novel drugs aimed at splicing inhibition are being actively developed. For example, agent H3B-8800 is currently undergoing phase I clinical trials and is expected to become the first antitumor splicing inhibitor [146].

piRNA can become another potential target for the development of new therapy protocols. Drug delivery poses a significant problem relative to the treatment of brain tumors. Because of the blood–brain barrier, most agents cannot be delivered to the tumor at sufficient concentrations. However, S. Shen *et al.* have recently demonstrated that the penetrability of the blood–brain barrier can be increased by inhibiting the PIWIL1/piR-DQ593109 complex in the endothelial cells lining tumor blood vessels in gliomas [147]. This complex plays a crucial role in the degradation of oncogenic lncRNA MEG3, which in turn regulates the formation of tight intercellular junctions. PIWIL1/piR-DQ593109 knockdown increases the MEG3 level, eventually enhancing the permeability of the capillaries supplying the tumor with blood. This approach can be used to elaborate novel glioma treatment regimens.

CONCLUSIONS

The research conducted over the past decades has made it clear that the roles of RNAs are not confined to protein coding. Due to their complex architecture and an ability to get involved in highly specific complementary interactions with a number of various molecules, ncRNAs can act as master regulators of crucial intercellular processes. Furthermore, ncRNAs were found to play a key role in intercellular interplay. It is therefore not surprising that more and more scholars are focusing their attention on the role played by these molecules in cancer, as well as the prospects of using them as a target for the development of novel antitumor agents. Unfortunately, it is much more challenging today to design a drug that would inhibit a specific ncRNA than to develop novel low-molecular-weight protein inhibitors. However, for aggressive cancer types such as glioblastoma, these very approaches can yield the long-awaited progress in patient treatment. ●

This study was supported by the Russian Science Foundation (grant No. 19-44-02027) and the Russian Foundation for Basic Research (grant No. 20-14-50306).

REFERENCES

1. Ostrom Q.T., Gittleman H., Truitt G., Boscia A., Kruchko C., Barnholtz-Sloan J.S. // Neuro Oncol. 2018. V. 20. P. iv1–iv86.
2. Aquilanti E., Miller J., Santagata S., Cahill D.P., Brastianos P.K. // Neuro Oncol. 2018. V. 20. P. vii17–vii26.
3. Kitange G.J., Carlson B.L., Schroeder M.A., Grogan P.T., Lamont J.D., Decker P.A., Wu W., James C.D., Sarkaria J.N. // Neuro Oncol. 2009. V. 11. № 3. P. 281–291.
4. Phillips H.S., Kharbanda S., Chen R., Forrest W.F., Soriano R.H., Wu T.D., Misra A., Nigro J.M., Colman H., Soroceanu L., et al. // Cancer Cell. 2006. V. 9. № 3. P. 157–173.
5. Sepúlveda-Sánchez J.M., Vaz M.Á., Balañá C., Gil-Gil M., Reynés G., Gallego Ó., Martínez-García M., Vicente E., Quindós M., Luque R., et al. // Neuro Oncol. 2017. V. 19. № 11. P. 1522–1531.
6. Lee E.Q., Reardon D.A., Schiff D., Drappatz J., Muzikansky A., Grimm S.A., Norden A.D., Nayak L., Beroukhim R., Rinne M.L., et al. // Neuro Oncol. 2015. V. 17. № 6. P. 862–867.
7. Castro B.A., Aghi M.K. // Neurosurg. Focus. 2014. V. 37. № 6. P. E9.
8. Weenink B., French P.J., SillevisSmitt P.A.E., Debets R., Geurts M. // Cancers (Basel). 2020. V. 12. № 3. P. 751.
9. Rao M.R.S. Long non-coding RNA biology. Singapore: Springer Nature, 2017. 323 p.
10. Li C., Sun J., Xiang Q., Liang Y., Zhao N., Zhang Z., Liu Q., Cui Y. // J. Neurooncol. 2016. V. 130. P. 11–17.

11. Guardia G.D.A., Correa B.R., Araujo P.R., Qiao M., Burns S., Penalva L.O.F., Galante P.A.F. // NPJ Genom. Med. 2020. V. 5. P. 2.
12. Li W., Jiang P., Sun X., Xu S., Ma X., Zhan R. // Cell Mol. Neurobiol. 2016. V. 36. № 8. P. 1219–1227.
13. Muz B., de la Puente P., Azab F., Azab A.K. // Hypoxia (Auckl.) 2015. V. 3. P. 83–92.
14. Abels E.R., Maas S.L.N., Nieland L., Wei Z., Cheah P.S., Tai E., Kolsteeg C.J., Dusoswa S.A., Ting D.T., Hickman S., et al. // Cell Rep. 2019. V. 28. № 12. P. 3105–3119.
15. Hu S., Xu L., Li L., Luo D., Zhao H., Li D., Peng B. // Onco Targets Ther. 2019. V. 12. P. 147–156.
16. Yang Y., Gao X., Zhang M., Yan S., Sun C., Xiao F., Huang N., Yang X., Zhao K., Zhou H., et al. // J. Natl. Cancer Inst. 2018. V. 110. № 3. P. 304–315.
17. Zhang M., Huang N., Yang X., Luo J., Yan S., Xiao F., Chen W., Gao X., Zhao K., Zhou H., et al. // Oncogene. 2018. V. 37. № 13. P. 1805–1814.
18. Zhang M., Zhao K., Xu X., Yang Y., Yan S., Wei P., Liu H., Xu J., Xiao F., Zhou H., et al. // Nat. Commun. 2018. V. 9. № 1. P. 4475.
19. Jorjani H., Kehr S., Jedlinski D.J., Gumienny R., Hertel J., Stadler P.F., Zavolan M., Gruber A.R. // Nucl. Acids Res. 2016. V. 44. № 11. P. 5068–5082.
20. Yu Y., Xiao J., Hann S.S. // Cancer Manag. Res. 2019. V. 11. P. 5895–5909.
21. Alles J., Fehlmann T., Fischer U., Backes C., Galata V., Minet M., Hart M., Abu-Halima M., Grässer F.A., Lenhof H.P., et al. // Nucl. Acids Res. 2019. V. 47. № 7. P. 3353–3364.
22. Xu T., Wu J., Han P., Zhao Z., Song X. // BMC Genomics. 2017. V. 18. (Suppl 6). P. 680.
23. Kosmyna B., Gupta V., Query C. // bioRxiv. 2020. P. 01.24.917260.
24. Ruan X., Li P., Chen Y., Shi Y., Pirooznia M., Seifuddin F., Suemizu H., Ohnishi Y., Yoneda N., Nishiwaki M., et al. // Nat. Commun. 2020 V. 11. № 1. P. 45.
25. Jalali S., Gandhi S., Scaria V. // Hum. Genomics. 2016. V. 10. № 1. P. 35.
26. Massone S., Ciarlo E., Vella S., Nizzari M., Florio T., Russo C., Cancedda R., Pagano A. // Biochim. Biophys. Acta. 2012. V. 1823. № 7. P. 1170–1177.
27. Loewer S., Cabili M.N., Guttman M., Loh Y.H., Thomas K., Park I.H., Garber M., Curran M., Onder T., Agarwal S., et al. // Nat. Genet. 2010. V. 42. № 12. P. 1113–1117.
28. Dahia P.L., FitzGerald M.G., Zhang X., Marsh D.J., Zheng Z., Pietsch T., von Deimling A., Haluska F.G., Haber D.A., Eng C. // Oncogene. 1998. V. 16. № 18. P. 2403–2406.
29. Ruiz-Orera J., Messeguer X., Subirana J.A., Alba M.M. // Elife. 2014. P. e03523.
30. Yoshimura H., Matsuda Y., Yamamoto M., Kamiya S., Ishiwata T. // Front. Biosci. (Landmark Ed.). 2018. V. 23. P. 614–625.
31. Poliseno L., Salmena L., Zhang J., Carver B., Haveman W.J., Pandolfi P.P. // Nature. 2010. V. 465. № 7301. P. 1033–1038.
32. Bier A., Oviedo-landaverde I., Zhao J., Mamane Y., Kandouz M., Batist G. // Mol. Cancer Ther. 2009. V. 8. № 4. P. 786–793.
33. Bier A., Oviedo-landaverde I., Zhao J., Mamane Y., Kandouz M., Batist G. // Mol. Cancer Ther. 2009. V. 8. № 4. P. 786–793.
34. Cai X., Cullen B.R. // RNA. 2007. V. 13. № 3. P. 313–316.
35. Tsai M.C., Manor O., Wan Y., Mosammaparast N., Wang J.K., Lan F., Shi Y., Segal E., Chang H.Y. // Science. 2010. V. 329. № 5992. P. 689–693.
36. Lai F., Orom U.A., Cesaroni M., Beringer M., Taatjes D.J., Blobel G.A., Shiekhattar R. // Nature. 2013. V. 494. № 7438. P. 497–501.
37. Yamazaki T., Hirose T. // Front. Biosci. (Elite Ed.). 2015. V. 7. P. 1–41.
38. Feng S., Yao J., Chen Y., Geng P., Zhang H., Ma X., Zhao J., Yu X. // J. Mol. Neurosci. 2015. V. 56. № 3. P. 623–630.
39. Toraih E.A., El-Wazir A., Hussein M.H., Khashana M.S., Matter A., Fawzy M.S., Hosny S. // Int. J. Biol. Markers. 2019. V. 34. № 1. P. 69–79.
40. Kallen A.N., Zhou X.B., Xu J., Qiao C., Ma J., Yan L., Lu L., Liu C., Yi J.S., Zhang H., et al. // Mol. Cell. 2013. V. 52. № 1. P. 101–112.
41. Ke J., Yao Y.L., Zheng J., Wang P., Liu Y.H., Ma J., Li Z., Liu X.B., Li Z.Q., Wang Z.H., et al. // Oncotarget. 2015. V. 6. № 26. P. 21934–21949.
42. Ellis B.C., Molloy P.L., Graham L.D. // Front. Genet. 2012. № 3. P. 270.
43.Zheng J., Li X.D., Wang P., Liu X.B., Xue Y.X., Hu Y., Li Z., Li Z.Q., Wang Z.H., Liu Y.H. // Oncotarget. 2015. V. 6. № 28. P. 25339–25355.
44. Yao Y., Ma J., Xue Y., Wang P., Li Z., Liu J., Chen L., Xi Z., Teng H., Wang Z., et al. // Cancer Lett. 2015. V. 359. № 1. P. 75–86.
45. Yang X., Xiao Z., Du X., Huang L., Du G. // Oncol. Rep. 2017. V. 37. № 1. P. 555–562.
46. Chen Q., Cai J., Wang Q., Wang Y., Liu M., Yang J., Zhou J., Kang C., Li M., Jiang C. // Clin. Cancer Res. 2018. V. 24. № 3. P. 684–695.
47. Fu C., Li D., Zhang X., Liu N., Chi G., Jin X. // Neurotherapeutics. 2018. V. 15. № 4. P. 1139–1157.
48. Yang A., Wang H., Yang X. // Biosci. Rep. 2017. V. 37. № 6. P. BSR20170871.
49. Wang P., Liu Y.H., Yao Y.L., Li Z., Li Z.Q., Ma J., Xue Y.X. // Cell Signal. 2015. V. 27. № 2. P. 275–282.
50. Zhao X., Wang P., Liu J., Zheng J., Liu Y., Chen J., Xue Y. // Mol. Ther. 2015. V. 23. № 12. P. 1899–1911.
51. Wang Y., Xu Z., Jiang J., Xu C., Kang J., Xiao L., Wu M., Xiong J., Guo X., Liu H. // Dev. Cell. 2013. V. 25. № 1. P. 69–80.
52. Uroda T., Anastasakou E., Rossi A., Teulon J.M., Pelleq-uer J.L., Annibale P., Pessey O., Inga A., Chillón I., Marcia M. // Mol. Cell. 2019. V. 75. № 5. P. 982–995.
53. Qin N., Tong G.F., Sun L.W., Xu X.L. // Oncol. Res. 2017. V. 25. № 9. P. 1471–1478.
54. Ma R., Zhang B.W., Zhang Z.B., Deng Q.J. // Eur. Rev. Med. Pharmacol. Sci. 2020. V. 24. № 5. P. 2601–2615.
55. Zhang S., Wang W., Liu G., Xie S., Li Q., Li Y., Lin Z. // Biomed. Pharmacother. 2017. № 95. P. 711–720.
56. Jin P., Huang Y., Zhu P., Zou Y., Shao T., Wang O. // Biochem. Biophys. Res. Commun. 2018. V. 503. № 3. P. 1570–1574.
57. Chi G., Yang F., Xu D., Liu W. // Artif. Cells Nanomed. Biotechnol. 2020. V. 48. № 1. P. 188–196.
58. Bian A., Wang Y., Liu J., Wang X., Liu D., Jiang J., Ding L., Hui X. // Med. Sci. Monit. 2018. V. 24. P. 5704–5712.
59. Zhang H.Y., Zhang B.W., Zhang Z.B., Deng Q.J. // Eur. Rev. Med. Pharmacol. Sci. 2020. V. 24. № 5. P. 2585–2600.
60. Barbagallo D., Caponnetto A., Brex D., Mirabella F., Barbagallo C., Lauretta G., Morrone A., Certo F., Broggi G., Caltabiano R., et al. // Cancers (Basel). 2019. V. 11. № 2. P. E194.
61. Li F., Ma K., Sun M., Shi S. // Am. J. Transl. Res. 2018. V. 10. № 5. P. 1373–1386.
62. Chen Y., Belmont A.S. // Curr. Opin. Genet. Dev. 2019.

V. 55. P. 91–99.
63. Zhou X., Li X., Yu L., Wang R., Hua D., Shi C., Sun C., Luo W., Rao C., Jiang Z., et al. // Int. J. Biochem. Cell. Biol. 2019. № 113. P. 75–86.
64. Kino T., Hurt D.E., Ichijo T., Nader N., Chrousos G.P. // Sci. Signal. 2010. V. 3. № 107. P. ra8.
65. Huo J.F., Chen X.B. // J. Cell Biochem. 2019. V. 120. № 4. P. 6127–6136.
66. Shen J., Hodges T.R., Song R., Gong Y., Calin G.A., Heimberger A.B., Zhao H. // Mol. Carcinog. 2018. V. 57. № 1. P. 137–141.
67. Zhang X., Hamblin M.H., Yin K.J. // RNA Biol. 2017. V. 14. № 12. P. 1705–1714.
68. Zhou Q., Liu J., Quan J., Liu W., Tan H., Li W. // Gene. 2018. № 668. P. 77–86.
69. Xiang J., Guo S., Jiang S., Xu Y., Li J., Li L., Xiang J. // J. Korean Med. Sci. 2016. V. 31. № 5. P. 688–694.
70. Han Y., Wu Z., Wu T., Huang Y., Cheng Z., Li X., Sun T., Xie X., Zhou Y., Du Z. // Cell Death Dis. 2016. V. 7. № 3. P. e2123.
71. Latorre E., Carelli S., Raimondi I., D'Agostino V., Castiglioni I., Zucal C., Moro G., Luciani A., Ghilardi G., Monti E., et al. // Cancer Res. 2016. V. 76. № 9. P. 2626–2636.
72. Chen B., Huang S. // Cancer Lett. 2018. V. 418. P. 41–50.
73. Li X., Yang L., Chen L.L. // Mol. Cell. 2018. V. 71. № 3. P. 428–442.
74. Zhang P., Wu W., Chen Q., Chen M. // J. Integr. Bioinform. 2019. V. 16. № 3. P. 20190027.
75. Deogharia M., Majumder M. // Biology (Basel). 2018. V. 8. № 1. P. 1.
76. Calin G.A., Dumitru C.D., Shimizu M., Bichi R., Zupo S., Noch E., Aldler H., Rattan S., Keating M., Rai K., et al. // Proc. Natl. Acad. Sci. USA. 2002. V. 99. № 24. P. 15524–15529.
77. Adams B.D., Kasinski A.L., Slack F.J. // Curr. Biol. 2014. V. 24. № 16. P. 762–776.
78. Macfarlane L.A., Murphy P.R. // Curr. Genom. 2010. V. 11. № 7. P. 537–561.
79. Braun J.E., Truffault V., Boland A., Huntzinger E., Chang C.T., Haas G., Weichenrieder O., Coles M., Izaurralde E. // Nat. Struct. Mol. Biol. 2012. V. 19. № 12. P. 1324–1331.
80. Liu J., Rivas F.V., Wohlschlegel J., Yates J.R. 3rd, Parker R., Hannon G.J. // Nat. Cell Biol. 2005. V. 7. P. 1261–1266.
81. Meijer H.A., Kong Y.W., Lu W.T., Wilczynska A., Spriggs R.V., Robinson S.W., Godfrey J.D., Willis A.E., Bushell M. // Science. 2012. V. 340. P. 82–85.
82. Guo H., Ingolia N.T., Weissman J.S., Bartel D.P. // Nature. 2010. V. 466. P. 835–840.
83. Lewis B.P., Burge C.B., Bartel D.P. // Cell. 2005. V. 120. № 1. P. 15–20.
84. Shea A., Harish V., Afzal Z., Chijioke J., Kedir H., Dusmatova S., Roy A., Ramalinga M., Harris B., Blancato J., et al. // Cancer Med. 2016. V. 5. № 8. P. 1917–1946.
85. Sun G., SiMa G., Wu C., Fan Y., Tan Y., Wang Z., Cheng G., Li J. // PLoS One. 2018. V. 13. № 1. P. e0190515.
86. Papagiannakopoulos T., Shapiro A., Kosik K.S. // Cancer Res. 2008. V. 68. № 19. P. 8164–8172.
87. Yang C.H., Yue J., Pfeffer S.R., Fan M., Paulus E., Hosni-Ahmed A., Sims M., Qayyum S., Davidoff A.M., Handorf C.R., et al. // J. Biol. Chem. 2014. V. 289. P. 25079–25087.
88. Xiuju C., Zhen W., Yanchao S. // Open Med. (Wars.). 2016. V. 11. № 1. P. 133–137.
89. Kefas B., Comeau L., Floyd D.H., Seleverstov O., Godlewski J., Schmittgen T., Jiang J., di Pierro C.G., Li Y., Chiocca E.A., et al. // J. Neurosci. 2009. V. 29. № 48. P. 15161–15168.
90. Tian Y., Nan Y., Han L., Zhang A., Wang G., Jia Z., Hao J., Pu P., Zhong Y., Kang C. // Int. J. Oncol. 2012. V. 40. № 4. P. 1105–1112.
91. Liu X., Zheng J., Xue Y., Yu H., Gong W., Wang P., Li Z., Liu Y. // Theranostics. 2018. V. 8. № 4. P. 1084.
92.Jacobs D.I., Qin Q., Fu A., Chen Z., Zhou J., Zhu Y. // Oncotarget. 2018. V. 9. P. 37616–37626.
93. Shen S., Yu H., Liu X., Liu Y., Zheng J., Wang P., Gong W., Chen J., Zhao L., Xue Y. // Mol. Ther. Nucl. Acid. 2018. V. 10. P. 412–425.
94. Jacobs D.I., Qin Q., Lerro M.C., Fu A., Dubrow R., Claus E.B., DeWan A.T., Wang G., Lin H., Zhu Y. // Cancer Epidemiol. Biomarkers Prev. 2016. V. 25. № 7. P. 1073–1080.
95. Xia X.-R., Li W.-C., Yu Z.-T., Li J., Peng C.-Y., Jin L., Yuan G.-L. // Histochem. Cell Biol. 2020. V. 153. P. 257–269.
96. Xu B., Ye M.H., Lv S.G., Wang Q.X., Wu M.J., Xiao B., Kang C.S., Zhu X.G. // Oncotarget. 2017. V. 8. № 27. P. 43953–43966.
97. Chen L., Han L., Wei J., Zhang K., Shi Z., Duan R., Li S., Zhou X., Pu P., Zhang J., Kang C. // Sci. Rep. 2015. V. 5. P. 8588.
98. Suzuki H., Kumar S.A., Shuai S. // Nature. 2019. V. 574. № 7780. P. 707–711.
99. Gaur A.B., Holbeck S.L., Colburn N.H., Israel M.A. // Oncol. 2011. V. 13. P. 580–590.
100. Li Y., Li W., Yang Y., Lu Y., He C., Hu G., Liu H., Chen J., He J., Yu H. // Brain Res. 2009. V. 1286. P. 13–18.
101. Gabriely G., Wurdinger T., Kesari S., Esau C.C., Burchard J., Linsley P.S., Krichevsky A.M. // Mol. Cell. Biol. 2008. V. 28. P. 5369–5380.
102. Hong X., Sin W.C., Harris A.L., Naus C.C. // Oncotarget. 2015. V. 6. № 17. P. 15566–15577.
103. Qian M., Wang S., Guo X., Wang J., Zhang Z., Qiu W., Gao X., Chen Z., Xu J., Zhao R., et al. // Oncogene. 2020. V. 39. P. 428–442.
104. Kefas B., Godlewski J., Comeau L., Li Y., Abounader R., Hawkinson M., Lee J., Fine H., Chiocca E.A., Lawler S., et al. // Cancer Res. 2008. V. 68. № 10. P. 3566–3572.
105. Jun G.J., Zhong G.G., Ming Z.S. // Oncol. Lett. 2015. V. 9. № 6. P. 2743–2749.
106. Xia H., Yan Y., Hu M., Wang Y., Wang Y., Dai Y., Chen J., Di G., Chen X., Jiang X. // Neuro Oncol. 2013. V. 15. № 4. P. 413–422.
107. Saito K., Nishida K.M., Mori T., Kawamura Y., Miyoshi K., Nagami T., Siomi H., Siomi M.C. // Genes Dev. 2006. V. 20. P. 2214–2222.
108. Aravin A.A. // Nature. 2006. V. 442. P. 203–207.
109. Yamanaka S., Siomi M.C., Siomi H. // Mob. DNA. 2014. V. 5. P. 22.
110. Weick E.M., Miska E.A. // Development. 2014. V. 141. № 18. P. 3458–3471.
111. Ozata D.M., Gainetdinov I., Zoch A., O'Carroll D., Zamore P.D. // Nat. Rev. Genet. 2019. V. 20. № 2. P. 89–108.
112. Weng W., Li H., Goel A. // Biochim. Biophys. Acta Rev. Cancer. 2019. V. 1871. № 1. P. 160–169.
113. Cheng Y., Wang Q., Jiang W., Bian Y., Zhou Y., Gou A., Zhang W., Fu K., Shi W. // Aging (Albany NY). 2019. V. 11. № 21. P. 9932–9946.
114. Kufel J., Grzechnik P. // Trends Genet. 2019. V. 35. № 2. P. 104–117.
115. Liu Y., Dou M., Song X., Dong Y., Liu S., Liu H., Tao J., Li W., Yin X., Xu W. // Mol. Cancer. 2019. V. 18. № 1. P. 123.
116.Xia X.R., Li W.C., Yu Z.T., Li J., Peng C.Y., Jin L., Yuan G.L. // Histochem. Cell Biol. 2020. V. 153. № 4. P. 257–269.
117. Reddy R., Henning D., Das G., Harless M., Wright D. //

J. Biol. Chem. 1987. V. 262. P. 75–81.
118. Huang Y., Maraia R.J. // Nucl. Acids Res. 2001. V. 29. P. 2675–2690.
119. Fischer U., Englbrecht C., Chari A. // Wiley Interdiscip. Rev. RNA. 2011. V. 2. № 5. P. 718–731.
120. Godfrey A.C., Kupsco J.M., Burch B.D., Zimmerman R.M., Dominski Z., Marzluff W.F., Duronio R.J. // RNA. 2006. V. 12. № 3. P. 396–409.
121. Peculis B.A., Steitz J.A. // Cell. 1993. V. 73. № 6. P. 1233–1245.
122. Wilkinson M.E., Charenton C., Nagai K. // Annu. Rev. Biochem. 2020. V. 89. P. 359–388.
123. Fica S.M., Nagai K. // Nat. Struct. Mol. Biol. 2017. V. 24. № 10. P. 791–799.
124. Bielli P., Pagliarini V., Pieraccioli M., Caggiano C., Sette C. // Cells. 2019. V. 9. № 1. P. 10.
125. Shuai S., Suzuki H., Diaz-Navarro A., Nadeu F., Kumar S.A., Gutierrez-Fernandez A., Delgado J., Pinyol M., López-Otín C., Puente X.S., et al. // Nature. 2019. V. 574. № 7780. P. 712–716.
126. Pavlyukov M.S., Yu H., Bastola S., Minata M., Shender V.O., Lee Y., Zhang S., Wang J., Komarova S., Wang J. // Cancer Cell. 2018. V. 34. № 1. P. 119–135.e10.
127. Rasool M., Malik A., Zahid S., Basit Ashraf M.A., Qazi M.H., Asif M., Zaheer A., Arshad M., Raza A., Jamal M.S. // Noncoding RNA Res. 2016. V. 1. № 1. P. 69–76.
128. Hanna J., Hossain G.S., Kocerha J. // Front. Genet. 2019. V. 10. P. 478.
129. Adams D., Gonzalez-Duarte A., O'Riordan W.D., Yang C.C., Ueda M., Kristen A.V., Tournev I., Schmidt H.H., Coelho T., Berk J.L., et al. // N. Engl. J. Med. 2018. V. 379. № 1. P. 11–21
130. Cheng J., Meng J., Zhu L., Peng Y. // Mol. Cancer. 2020. V. 19. № 1. P. 66.
131. Yang J.K., Yang J.P., Tong J., Jing S.Y., Fan B., Wang F., Sun G.Z., Jiao B.H. // J. Neurooncol. 2017. V. 131. № 2. P. 255–265.
132. Shi R., Wang P.Y., Li X.Y., Chen J.X., Li Y., Zhang X.Z., Zhang C.G., Jiang T, Li W.B., Ding W., et al. // Oncotarget. 2015. V. 6. № 29. P. 26971–26981.
133. Akers J.C., Ramakrishnan V., Kim R., Skog J., Nakano I., Pingle S., Kalinina J., Hua W., Kesari S., Mao Y., et al. // PLoS One. 2013. V. 8. № 10. P. e78115.
134. Manterola L., Guruceaga E., Gállego Pérez-Larraya J., González-Huarriz M., Jauregui P., Tejada S., Diez-Valle R., Segura V., Samprón N., Barrena C., et al. // Neuro Oncol. 2014. V. 16. № 4. P. 520–527.
135. Springfeld C., Jäger D., Büchler M.W, Strobel O., Hackert T., Palmer D.H., Neoptolemos J.P. // Presse Med. 2019. V. 48 (3 Pt 2). P. e159–e174.
136. Valencia-Serna J., Aliabadi H.M., Manfrin A., Mohseni M., Jiang X., Uludag H. // Eur. J. Pharm. Biopharm. 2018. V. 130. P. 66–70.
137. Ren Y., Wang Y.F., Zhang J., Wang Q.X., Han L., Mei M., Kang C.S. // Clin. Epigenetics. 2019. V. 11. № 1. P. 29.
138. Li Y., Ren Y., Wang Y., Tan Y., Wang Q., Cai J., Zhou J., Yang C., Zhao K., Yi K., et al. // Theranostics. 2019. V. 9. № 16. P. 4608–4623.
139. Shi J., Lv S., Wu M., Wang X., Deng Y., Li Y., Li K., Zhao H., Zhu X., Ye M. // Clin. Transl. Med. 2020. V. 1. P. 182–198.
140. Abulwerdi F.A., Xu W., Ageeli A.A., Yonkunas M.J., Arun G., Nam H., Schneekloth J.S.Jr., Dayie T.K., Spector D., Baird N., et al. // ACS Chem. Biol. 2019. V. 14. № 2. P. 223–235.
141. Kotake Y., Sagane K., Owa T., Mimori-Kiyosue Y., Shimizu H., Uesugi M., Ishihama Y., Iwata M., Mizui Y. // Nat. Chem. Biol. 2007. V. 3. № 9. P. 570–575.
142. Kaida D., Motoyoshi H., Tashiro E., Nojima T., Hagiwara M., Ishigami K., Watanabe H., Kitahara T., Yoshida T., Nakajima H., et al. // Nat. Chem. Biol. 2007. V. 3. № 9. P. 576–583.
143. Folco E.G., Coil K.E., Reed R. // Genes Dev. 2011. V. 25. № 5. P. 440–444.
144. Corrionero A., Miñana B., Valcárcel J. // Genes Dev. 2011. V. 25. № 5. P. 445–459.
145. Roybal G.A., Jurica M.S. // Nucl. Acids Res. 2010. V. 38. № 19. P. 6664–6672.
146. Steensma D.P., Wermke M., Klimek V.M., Greenberg P.L., Font P., Komrokji R.S., Yang J., Brunner A.M., Carraway H.E., Ades L., et al. // Blood. 2019. V. 134. P. 673.
147. Shen S., Yu H., Liu X., Liu Y., Zheng J., Wang P., Gong W., Chen J., Zhao L., Xue Y. // Mol. Ther. Nucl. Acids. 2018. V. 10. P. 412–425.

Molecular Tools for Targeted Control of Nerve Cell Electrical Activity. Part I

D. V. Kolesov, E. L. Sokolinskaya, K. A. Lukyanov, A. M. Bogdanov*
Shemyakin-Ovchinnikov Institute of Bioorganic Chemistry, Moscow, 117997 Russia
*E-mail: noobissat@ya.ru
Received August 24, 2020; in final form, May 14, 2021
DOI: 10.32607/actanaturae.11414

ABSTRACT **In modern life sciences, the issue of a specific, exogenously directed manipulation of a cell's biochemistry is a highly topical one. In the case of electrically excitable cells, the aim of the manipulation is to control the cells' electrical activity, with the result being either excitation with subsequent generation of an action potential or inhibition and suppression of the excitatory currents. The techniques of electrical activity stimulation are of particular significance in tackling the most challenging basic problem: figuring out how the nervous system of higher multicellular organisms functions. At this juncture, when neuroscience is gradually abandoning the reductionist approach in favor of the direct investigation of complex neuronal systems, minimally invasive methods for brain tissue stimulation are becoming the basic element in the toolbox of those involved in the field. In this review, we describe three approaches that are based on the delivery of exogenous, genetically encoded molecules sensitive to external stimuli into the nervous tissue. These approaches include optogenetics (Part I) as well as chemogenetics and thermogenetics (Part II), which are significantly different not only in the nature of the stimuli and structure of the appropriate effector proteins, but also in the details of experimental applications. The latter circumstance is an indication that these are rather complementary than competing techniques.**
KEYWORDS **optogenetics, chemogenetics, thermogenetics, action potential, membrane voltage, neurointerface, ion channels, rhodopsin, chemoreceptors, GPCR, neuronal activity stimulation, neuronal excitation, neuronal inhibition.**
ABBREVIATIONS **AAV – adeno-associated virus; BLUF – blue-light sensors using flavin-adenine dinucleotide; ChR – channelrhodopsin; CIB1 – cryptochrome interacting BHLH 1; COP1 – coat protein complex 1; DBS – deep brain stimulation; FAD – flavin adenine dinucleotide; GFP – green fluorescent protein; IR – infra red; LOV – light-oxygen-voltage; PhoCl – photocleavable; PHR – photolyase homology related domain; PICCORO – PIxD complex dependent control of transcription; PIF – phytochrome-interacting factor; ROS – reactive oxygen species; UVR8 – UV-B resistance 8 protein.**

INTRODUCTION

Deciphering the principles of the nervous system functioning in higher multicellular organisms is a fundamental problem in neuroscience. For many decades, the traditional approach to its solution has been reductionism; i.e., extrapolation of the results observed in simple model systems to complex neuronal assemblies that cannot be directly analyzed (e.g., mammalian brain). The numerous disadvantages of such an approach and the emergence of revolutionary techniques for imaging and stimulation of cellular processes have pushed neuroscientists to look for ways to directly investigate the entire organizational nomenclature of the nervous system and the complex biological phenomena associated with its functioning.

Today, minimally invasive methods for a selective stimulation of the activity of nerve cells and brain structures are among the major tools used in neuroscience. Here, we describe the main ones: optogenetics (the first part of this review), chemogenetics and thermogenetics (the second part), with an emphasis on the nature, physicochemical properties, and principles for developing effector molecules that mediate cellular stimulation and are used in biochemical and neurobiological experiments. We will also focus on the molecular mechanisms underlying the functioning of these genetically encoded tools.

The review focuses on the key characteristics of the described approaches (spatial and temporal resolution, toxicity, invasiveness, etc.), provides a compara-

tive analysis of these characteristics in relation to the topical problems of modern neuroscience, and discusses the prospects for improving these neurostimulation tools.

OPTOGENETICS

Optogenetics is a group of techniques that use visible light to control the functional activity of cells by means of light-sensitive proteins whose genes are introduced into the biological system in advance (for a detailed review, see [1–7]). Light is not only the primary energy source for anabolic processes in the entire biota, but also the most important physical stimulus playing a key role in the physiology and biochemistry of the representatives of all living kingdoms. During evolution, a rich repertoire of light-sensitive molecules has emerged. They differ in their physical and biochemical properties, structure, and functions [8–14]. This circumstance provides the prerequisites for the use of a wide range of genetically encoded effector molecules in optogenetics to affect a wide variety of biochemical targets [2, 3, 7].

Before the advent of optogenetic tools, chemical compounds with photolabile bonds were used to mediate light-driven effects on a cell physiology. Such photoeffectors, which include photoactivatable amino acids, oligonucleotides, and compounds for a light-dependent release of other molecules, have been engineered in abundance and remained in use until now, developing independently of the genetically encoded tools [15–17].

Optogenetics in molecular biology

In molecular biology, the optogenetic approach is primarily used for the control and manipulation of protein–protein interactions [2, 18, 19]. In this case, effector molecules are natural proteins or individual domains whose oligomeric state or interaction with other proteins changes upon absorption of light: e.g., phytochromes, bacteriophytochromes, and cryptochromes.

Phytochromes are plant photoreceptors containing a covalently bound tetrapyrrole chromophore that is sensitive in the red region of the spectrum [18, 20]. The optogenetic use of these proteins is primarily based on the natural light-dependent reversible interaction between phytochrome PhyB and the transcription factors PIF3 and PIF6, and the most striking examples are the systems for optical control of Gal4 transcription factor activity [21], protein splicing activation [22] in yeast cells, and rapid reversible translocation of Rho family GTPase activators to the plasma membrane of mammalian cells [23]. Cryptochromes are FAD-containing, blue and violet sensitive photoreceptors found in all cellular life forms, which are also capable of photodimerization with partner proteins. In particular, photodimerization of the plant cryptochrome CRY2 with the transcription factor CIB1 [24–27] was used to demonstrate light-dependent DNA recombination [28] and to control the epigenetic status of chromatin [29] in mammalian cells. There are reports on the use of the CRY/CIB system for controlling transcription in yeast [30] and the activity of the phosphoinositide metabolism in COS-7 cells with a high spatial resolution [31]. The light-sensitive PHR domains of CRY2 were used to develop tools for controlling the release of intracellular calcium [32], including those operating in single T-cells *in vivo* [33].

The three-dimensional conformation of some photoproteins can change significantly in response to light absorption [2, 18, 19]. In optogenetics, this property is used to manipulate molecular targets. A striking example is light-oxygen-voltage (LOV) proteins from a large family of light-sensitive flavoproteins found in plant, fungal, and bacterial cells [34–36]. LOV domains have been used to develop dozens of optogenetic techniques [2, 18]; e.g., control of gene expression [37, 38], modulation of enzymatic activity [39] and signaling involving cyclic nucleotides [40], regulation of genome editing [41], and photosensitization [42].

BLUF (blue-light sensors using flavin-adenine dinucleotide) family flavoproteins, which are mainly of bacterial origin, similarly to LOV-domains, undergo photoactivation accompanied by structural rearrangements [43–47]. Optogenetic applications of these flavoproteins include the PICCORO transcription activation system [48] and photoactivation of adenylate cyclases [49, 50] and guanylate cyclases [51].

A separate group of optogenetic effectors is constituted by UVR8 photoreceptors that absorb in the UV range owing to their intrinsic tryptophan residues and are involved in photoprotective reactions in plants [52]. In plant cells, UVR8 homodimers dissociate in response to ultraviolet light irradiation and monomers bind to the E3-ubiquitin ligase COP1 [52–56]. There are reports on the use of this protein for targeted regulation of transcription [19, 57, 58] and control of intracellular transport of proteins and their secretion [59]. Optogenetic control of transcription also uses prokaryotic proteins of the xanthopsin family [60, 61], which carry a covalently bound *p*-coumaric acid chromophore and have an unusual photocycle [62].

The reversible light-induced interaction of the bacterial phytochrome BphP1 and its natural partner protein PpsR2 form the basis of another platform for optogenetic experiments using bacterial proteins [63]. The unique characteristics of the BphP1–PpsR2 system include its activation in the near-IR wavelength

range (740–780 nm), ability to use endogenous biliverdin of eukaryotes, including mammals, as a chromophore, and spectral compatibility with blue light-based optogenetic systems [63]. Further studies of the system led to the designing of its updated version, where the Q-PAS protein, produced using genetic engineering methods, is used instead of natural PpsR2 as a BphP1 partner [64]. The Q-PAS-based system has no limitations related to the PpsR2 properties, such as a large size, multidomain structure, and tendency to oligomerize [64].

The system based on the bacterial phytochrome BphP1 was also used for optogenetic control of the activity of receptor tyrosine kinases [65]. For this purpose, the catalytic domain of the tropomyosin kinases TrkA and TrkB, which are present on the cell membrane as inactivated dimers, was fused with a photosensitive core of BphP1. BphP1 dimerization under illumination with far red (640–680 nm) and near-IR (740–780 nm) light activated the kinase dimer and enabled light-driven reversible modulation of the enzyme activity [65].

Green fluorescent protein (GFP) family members are widely used as fully genetically encoded fluorescent probes. In addition, there are several examples of the use of GFP-like proteins in optogenetics. For example, the reversibly switchable Dronpa protein was found to simultaneously change its fluorescent properties and oligomeric state: it monomerizes after exposure to blue light [66]. This property was used for light-dependent induction of the activity of target proteins (e.g., protein kinases) flanked at the N- and C-termini by Dronpa monomers and inactive in the dark due to steric blocking by a fluorescent protein dimer [66, 67]. Another example is the engineering of a photocleavable protein based on mMaple [68] that is characterized by irreversible photoconversion from a green to red fluorescent state. Although this photoconversion is accompanied by a cleavage of the polypeptide chain before the chromophore, two parts of the protein remain tightly bound through many non-covalent interactions. There is a permuted mMaple variant, called PhoCl (PhotoCleavable) [69], which spontaneously dissociates into two parts after exposure to 405-nm light. PhoCl was used to design the proteins with light-induced activity: Cre recombinase, Gal4 transcription factor, HCVp viral protease, and photocleavable cadherin to study the transfer of mechanical tension between cells [69, 70].

A separate area of optogenetics is the use of phototoxic proteins: i.e., proteins that produce significant amounts of reactive oxygen species (ROS) in response to irradiation with light [71, 72]. The most popular objects are the phototoxic proteins KillerRed (GFP-like red fluorescent protein) and miniSOG (LOV-based flavin-binding protein), as well as their mutated variants [42, 73–75]. The advantages of such genetically encoded photosensitizers (in comparison with conventional chemical ones) include the possibility to guide them toward any cell compartments and subcompartments using protein localization signals and, at the level of the organism, to target cell populations using tissue-specific or inducible promoters. Local ROS production enables targeted manipulation of biological systems: e.g., inactivating target proteins [73, 76], triggering various pathways of cell death [77–79], damaging genomic DNA [80], and destroying target cells in model organisms [81–83].

Protein engineering is widely used in the design of optogenetic systems [2, 18], which makes it possible not only to integrate effector molecules into the context of target intracellular interactions, but also to adapt their activity to a particular experimental task. This adaptation may be exemplified by the optobody, an optogenetically activated intracellular antibody (intrabody, iB) built on the basis of modified LOV domains (namely, the so-called Magnets, chimeric variants of the Vivid photoreceptor which are capable of light-dependent heterodimerization [84]) and anti-GFP nanobody fragments [85]. A composite optogenetic tool based on recombinant iBs was used for reversible regulation of the activity of endogenous proteins in mammalian cells [86]. The activity of endogenous actin and RAS GTPase can be manipulated by guiding effectors of two optogenetic systems (BphP1-Q-PAS, which is sensitive to near IR light, and LOV, which is activated by blue light) with a fluorescently labeled iB [86].

According to their molecular mechanism, there are two groups of optogenetic manipulations in molecular biology: allosteric manipulations, where the photosensitive domain affects enzymatic activity or access to the substrate binding site, and dimerization-based manipulations: i.e., those associated with a light-dependent change in the oligomeric status of effector domains, which affects the activity of target proteins comprising the chimeric molecule. Combinations of the two approaches are also possible [18]. As we have illustrated above, such indirect involvement of optical effectors comes handy in a wide range of model systems, but it is not typical of neurobiological optogenetics. The activity of electrically excitable cells is controlled by effector molecules that directly affect the physiological status of cells.

Optogenetics in neurobiology

The activity of electrically excitable cells is closely related to the electrical potential on their plasma

membrane [87]. The potential is generated, in particular, thanks to the activity of voltage-gated selective ion channels; i.e., channels that allow passage of certain ions at a certain level of membrane polarization [87]. The transmembrane gradient of ions, for which voltage-gated channels are selective (primarily Na^+, K^+, Cl^-), causes a short-term shift of the membrane potential, termed the action potential. When the membrane is depolarized below the threshold level or is hyperpolarized, the arising current rapidly decays or integrates with other ionic currents, which can, depending on the direction of integrated currents, initiate or, on the contrary, prevent the generation of a new action potential. Therefore, by changing transmembrane ionic currents and the ratio of ion concentrations inside and outside the cell, it becomes possible to control the functional activity of cells using various ionic transporters.

The first report on an instance of activation of neurons by light dates back to 1971, when laser light was found to nonspecifically stimulate nerve cells in tissues of the mollusk Aplysia [88]. The ability of genetically encoded effector molecules to influence transmembrane ionic currents upon light activation was first observed during heterologous expression of bacteriorhodopsin in *Xenopus laevis* oocytes [89]. The same system was used to demonstrate the induction of photocurrents upon expression of channelrhodopsin 1 (channelopsin-1) [90], a retinal-containing proton channel from the single-cell green alga *Chlamydomonas reinhardtii*. It is noteworthy that this photoreceptor, which has a high homology with bacteriorhodopsins, plays a role in the phototaxis of algal cells [91]. Later, channelrhodopsin 2 (ChR2) from *C. reinhardtii* was functionally expressed in mammalian cells and its activity as a light-dependent cationic channel capable of depolarizing the cell membrane was described [92]. One of the first examples of use of an optogenetic tool for stimulating neurons was associated with the expression of rhodopsin from *Drosophila* in a primary culture of rat neurons [93]. But in this case, the minimum set of transgenes that ensured the activity of the effector consisted of three coding sequences (rhodopsin, arrestin-2, and the α-subunit of the G-protein), the latency of the stimulation ranged from hundreds of milliseconds to seconds, and addition of a retinal solution to the cells was required in the experiment. Finally, control of neuronal activity using single-component optogenetic effectors based on channelrhodopsin 2 (ChR2) was shown almost simultaneously in four studies [94–97]. From a methodological point of view, these studies form the basis of modern neurobiological optogenetics. It is noteworthy that due to the efficiency of channelrhodopsin, yet early experiments could use complex model systems, in particular to control the behavior of the *Caenorhabditis elegans* nematode [96] and partially restore the visual sensitivity of transgenic mice with degenerative retinal disorders [97]. These pioneering works reported a high spatial and temporal resolution of activation: stimulation on a millisecond time scale [94] or at frequencies of up to 20 Hz [96], and the possibility of targeted manipulation of fine subcellular neuronal structures.

Effector molecules

Thuswise, rhodopsins constitute the major class of effector molecules in optogenetics of electrically excitable cells [1, 3, 98, 99] (the diversity of rhodopsins is illustrated in *Fig. 1*). These light-sensitive transmembrane proteins bear a retinal-based chromophore that, as a protonated Schiff base, is covalently (via a lysine residue) attached to the seventh transmembrane helix of the protein backbone [100, 101]. Rhodopsins form two independent families: microbial rhodopsins (type 1 rhodopsins) and animal rhodopsins (type 2 rhodopsins). Despite their structural similarity, representatives of these two rhodopsin types are characterized by an extremely low homology of amino acid sequences, apparently arising independently during convergent evolution [102]. Type 2 rhodopsins are known primarily as visual pigments that are specifically expressed in the cells (rods) of the animal retina; however, the proteins of this family are involved in other physiological processes, both associated and not associated with photoreception [100, 102]. The mechanism of signal transduction during photoreception is an important distinguishing feature of type 2 rhodopsins. For example, the functional cycle of visual (rod) rhodopsin involves at least three cytoplasmic proteins: G-protein transducin, rhodopsin kinase, and arrestin. This circumstance complicates the use of animal rhodopsins in heterologous systems and thereby reduces their value as optogenetic effectors. Microbial rhodopsins are found in archaea, bacteria, eukaryotic microorganisms (algae and fungi), and even giant viruses [100–105]. The molecules of this family perform a wide range of functions associated with photosensitivity: light-dependent enzymatic activity, photoreception, and ion transport [100, 103, 106]. According to their working principle, rhodopsins involved in ion transport are, in turn, subdivided into ion pumps and channels. It is ion-transporting rhodopsins, which are capable of generating currents in the cell membrane and changing its polarization, that are used in optogenetics as effectors (*Fig. 1*). Among wild-type microbial rhodopsins, these include bacteriorhodopsins, proton pumps that pump these cations

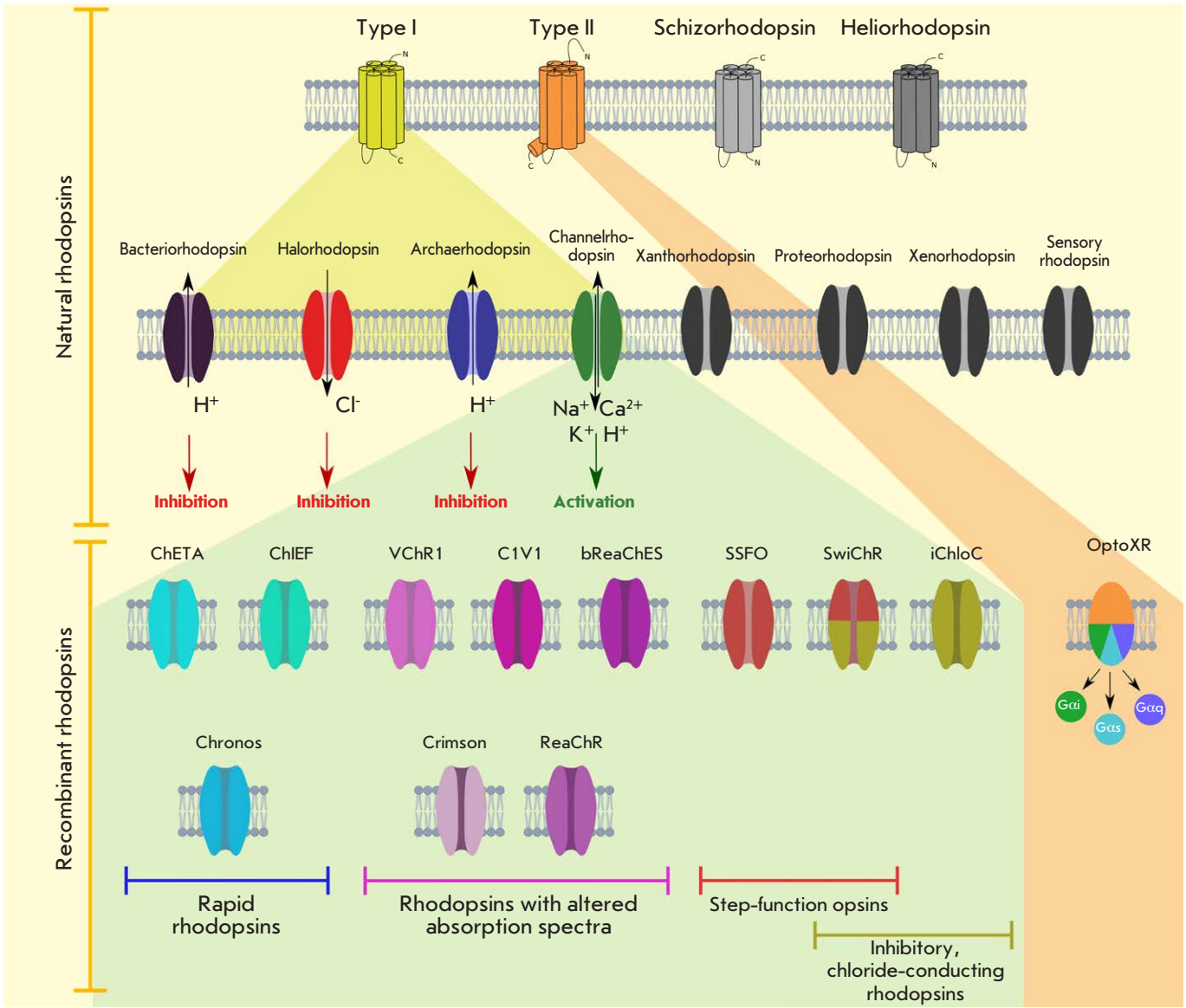

Fig. 1. The diversity of rhodopsins and their use in optogenetics. The top row depicts the four largest families of natural rhodopsins. The second row from the top presents the main groups of microbial rhodopsins. The next row presents chimeric channelrhodopsins (left) and type 2 rhodopsin-derived molecules (right) optimized for performing special optogenetic tasks. In the top two rows, families/types of rhodopsins that have not yet been used in optogenetic applications are shown in gray; those involved in optogenetics are represented by spectral colors. Chimeric molecules are differentiated by colors depending on their functional features (the color legend is described in the lower part of the figure)

out of the cell; halorhodopsins, chloride pumps that transport Cl^- into the cell; and channelrhodopsins that are non-selective cation channels allowing passage of H^+, Na^+, K^+, and Ca^{2+} ions through the membrane [3, 107, 108]. The proteins of the first two groups, upon photoactivation (by green and yellow light, respectively), cause membrane hyperpolarization, which in the case of electrically excitable cells leads to inhibition of the action potential, thereby acting as inhibitory effectors [107] *(Fig. 1)*. Channelrhodopsins

absorbing blue light, on the contrary, depolarize the membrane and promote the stimulation of nerve cells. Determination of channelrhodopsins' spatial structure [109] has enabled the application of rational design principles to the development of chimeric variants of these proteins and the switch from cationic to anionic selectivity of the ionic pore [110, 111], expanding the repertoire of optogenetic inhibitors. Later, natural chloride anion-conducting channelrhodopsins were also discovered [112]. In addition to the abovementioned inhibitory channelrhodopsins, a rich palette of artificial channelrhodopsins optimized for solving particular optogenetic tasks has been developed using protein engineering methods. These include: fast channelrhodopsins (e.g., ChETA, ChIEF, Chronos) that provide, in particular, high-frequency (up to 200 Hz) stimulation of neurons [1, 113–115]; the so-called step-function opsins [116] that have a significantly increased inactivation time and are therefore able to maintain a corresponding transmembrane current for a relatively long time at a short duration of the light stimulus (there are both variants causing membrane depolarization [117]; and inhibitory hyperpolarizing variants [110]).

Wild-type channelrhodopsins are activated by blue light, which has a small penetration depth in animal tissue and can be toxic to neurons. In addition, blue light excites most of the existing fluorescent calcium ion indicators that can be used in conjunction with optogenetic tools. In this regard, a number of spectrally optimized variants of channelrhodopsins with absorption maxima shifted to the red region have been developed (these include VChR1, C1V1, Chrimson, ReaChR, etc.) [1, 114, 117–120] (*Fig. 1*). Rhodopsins with artificially altered cationic permeability are represented, in particular, by calcium-translocating channelrhodopsin (CatCh) that preferentially conducts Ca^{2+} ions and is in demand in studies of calcium signaling [121]. In addition, unique rhodopsins, Na^+ pumps, were found in marine bacteria [122], and they were used to develop selective transporters of potassium, rubidium, and cesium cations [123, 124]. Recently, an elegant method for a genetically engineered modification of a ChR2 mutant was proposed, which led to inverted topology of the insertion of this protein into the cell membrane and its conversion from an activator into an inhibitor upon photoactivation [125, 126].

The last few years have been full of discoveries of new groups and even families of rhodopsins which can be considered as promising optogenetic tools. For example, channelrhodopsins *Gt*_CCR1–4 from the flagellate unicellular alga *Guillardia theta*, which are light-sensitive cationic channels, proved structurally closer to the rhodopsins of haloarchaea than to classical ChR2 [106, 127, 128]. Recently, *Gt*_CCR4, which has activation/inactivation kinetics similar to those of ChR2, was shown to have a significantly higher photosensitivity, as well as higher selectivity for sodium cations [106, 129]. In 2018, a new rhodopsin family, heliorhodopsins, was discovered using functional metagenomics methods [103]. These proteins, like type 1 rhodopsins, bind retinal in the all-*trans* conformation and are abundant in archaea, bacteria, microalgae, and their viruses. Data on the spatial structure of heliorhodopsins [130, 131] confirm their structural homology with bacteriorhodopsins and an unusual, inverted compared to other rhodopsins, orientation in the membrane (with cytoplasmic N- and extracellular C-termini, *Fig. 1*). The biological function of these pigments is still unknown, but the inability of heliorhodopsins to transfer ions and their relatively slow (on a second scale) photocycle is evidence pointing to their photoreceptor role [103]. The availability of high-resolution structural data provides hope that, in the near future, heliorhodopsins may become an object of protein engineering aimed, in particular, at optimizing their molecules for the needs of optogenetics. Representatives of two families of light-dependent proton pumps, xenorhodopsins [132] and schizorhodopsins [133], may also become optogenetic actuators. Interestingly, the proteins of both families pump protons into the cell, which distinguishes them from the previously described bacterio- and archaerhodopsins, which transport H^+ in the opposite direction.

Finally, chimeric photosensitive G-protein-coupled receptors (Opto GPCRs), such as optoXR, constitute a distinctive class of optogenetic tools. These molecules are built on the basis of type 2 rhodopsins (visual rhodopsins of animals), in which the intracellular loops of rhodopsin are replaced by loops from, e.g., adrenergic or dopamine receptors [134, 135]. In this case, photostimulation of rhodopsin can initiate various intracellular signaling cascades, depending on the type of receptor donating intracellular loop regions (*Fig. 1*) [136–139]. Detailed information about Opto GPCR studies can be found in a dedicated review [5].

The biophysical properties of the rhodopsins used in optogenetics have been studied in detail [100, 140, 141]. For example, the three-dimensional structures of channelrhodopsins from *C. reinhardtii* have been resolved [109, 142] and the photocycle of microbial rhodopsins has been investigated not only by time-resolved spectroscopy [100], but also by time-resolved X-ray diffraction analysis [143, 144] (their detailed description is beyond the scope of this review). How-

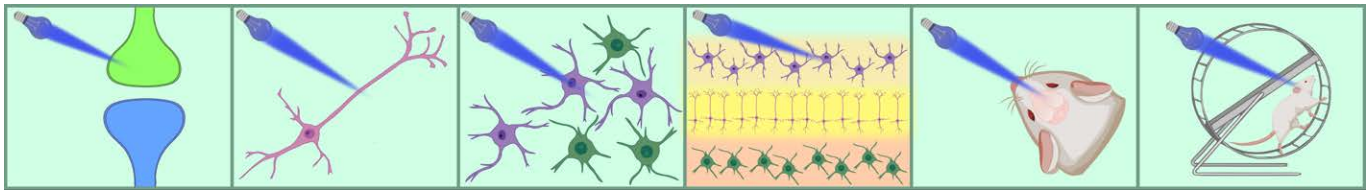

Fig. 2. Optogenetics applications at different levels of the nervous system organization. The figure illustrates rhodopsin photoactivation in (left to right): a synaptic axon terminal; a single neuron *in cellulo*; a neuronal population *in cellulo*; a fresh brain tissue slice *ex vivo*; and the brain of a live and freely moving mouse *in vivo*. Adapted from [159]

ever, it is worth mentioning two facts that are of fundamental value for the optogenetic use of microbial rhodopsins: (i) all type 1 rhodopsins use the all-*trans* retinal stereoisomer as a chromophore. The successful development of the so-called single-component (i.e., using an effector encoded by a single transgene) optogenetics is largely related to the presence of a sufficient amount of endogenous retinal in the nerve tissues of vertebrates, which excludes addition of this cofactor from the outside [145]; (ii) during the photocycle, retinal is photoisomerized into the 13-*cis*-conformation and then, remaining covalently bound to the protein backbone, spontaneously returns to its initial all-*trans* state [108]. This process lacks a dissociation stage, which enables multiple usage of the effector molecule, while its timescale – 10–20 ms – ensures a high temporal resolution of optical stimulation.

Optogenetic experiment

According to the key researchers involved in the implementation of neurobiological optogenetics, about the first 5 years of its development were devoted to the design and refinement of optogenetic experimental techniques [3]. In addition to the selection of successful photoeffector molecules (see the previous section), the delivery of a transgene to the target model system and the design features of an experimental setup play an important role in the matter. Here, we will briefly discuss these aspects.

Generally, strategies for the delivery and introduction of the genetic material of rhodopsin effectors may be reduced either to a transient expression in specific populations of nerve cells using viral vectors carrying rhodopsin genes [3] or to a stable expression of these genes in the brain of transgenic animals [3, 146–148]. In the former case, viral particles are usually injected into the animal's brain. Early optogenetic studies gave preference to retroviral vectors. Modern studies usually use high titers of adeno-associated viruses (AAVs), whose genome sequences are often optimized to ensure a high expression level in specific types of brain cells [1]. In the last few years, modified rabies viruses have been used for the so-called retrograde (i.e., directed into the bodies of presynaptic neurons) targeted expression of rhodopsins [149, 150]. To increase the selectivity of "labeling" during heterologous expression of rhodopsins, promoters specific to a certain cell type [1, 3] (e.g., the hypocretin promoter (Hcrt) [151]) are used. In experiments on live embryonic brain slices, the transgene can be delivered using *in utero* electroporation; while in the body of transgenic animals, rhodopsin is expressed from birth. An increase in the specificity of optogenetic stimulation, which is effective in both the transient and stable expression of rhodopsins, can be provided by genetic manipulations using site-specific recombination [1, 3]. For example, Cre or Flp recombinases, which can be delivered to the brain by a separate vector or be stably expressed in the cells of transgenic animals, allow for highly selective turning on/off of the expression of a photoeffector gene in the studied cell populations [152].

The tissue and cell specificity of optogenetics as applied to the stimulation of the intact brain of experimental animals is provided by a combination of the genetic approach (specific targeted expression) and instrumental solutions for precision optical exposure. For example, light is delivered to the brain by means of a fiber-optic cable fixed to the animal's skull, through an implanted optical cannula. The fiber-optic neurointerface is one of the key technological solutions that ensure success of the optogenetic approach [151, 153, 154]. The most important invention in the field of neurointerfaces for freely moving animals is autonomous wireless implants [155–157].

An essential aspect of the experiments on the optical manipulation of neuronal activity is the control of stimulation outputs at the level of individual cells and cell populations. Along with classical approaches to the di-

rect monitoring of electrical activity (e.g., patch-clamp), which are often of limited applicability in stimulating an intact brain, fluorescent methods, such as imaging of genetically encoded calcium and voltage indicators, can be used [1, 3]. According to some authors, optogenetic tools include not only photoeffector molecules, but also fluorescent probes for neuroscience [158, 159]. The concept of combining optical stimulation and the monitoring of neuronal activity within one experiment, or all-optical electrophysiology, has been developed [4, 158, 160].

Modern applications

A unique feature of the optogenetic approach is its versatile character and applicability in model systems of varying complexity (*Fig. 2*). This approach is used to investigate all levels of nervous system organization: in a culture of neurons *in cellulo*, live brain slices *ex vivo*, and the whole brain *in vivo* (in particular, awake, freely moving mammals) [159, 161]. Molecules mediating optical stimulation can be delivered to most highly specialized cells of the nervous system and their subcellular compartments, and the functional parameters induced by optogenetic stimulation range from the electrical activity of a single excitable cell to higher behavioral functions of mammals, such as learning, memory, etc.

Optogenetic tools have allowed neuroscientists to control the activity of neurons and neuroglial cells with high temporal and spatial resolution. This advantage of the method is especially important when studying *in vivo* tissue physiology and animal behavior. The resolution typical of optogenetic tools could not previously have been achieved using other neurobiological methods, such as deep brain stimulation (DBS) or administration of various drugs. The emergence of optogenetic methods in the arsenal of neuroscientists has enabled significant progress in understanding the formation and functioning of neural networks and signaling pathways in the mammalian brain [1, 3, 162]. They have been used to identify causal relationships between cellular activity and functional response, in particular, in experiments on a relationship between the activity of neural networks and the specific behavior of animals [163] and gain new information about various behavioral patterns in health and disease [164, 165].

Small rodents (mice and rats) are the main model objects in neurobiological research involving optogenetic tools. There are hundreds of studies on neuronal ensembles, networks, rhythmic brain activity, transmission, memorizing, and storage of information in the brain, learning, synaptic plasticity, neurogenesis, regulation of motor activity, hunger and thirst, sleep and wakefulness, sensory organs, biological rhythms, respiratory activities, and social behavior of these animals [1, 3, 6, 148, 164, 166, 167]. The optogenetic toolbox is also used to explore the neurobiology of fish [168], birds [169], and primates [170, 171]. Of course, the use of microbial rhodopsins in medicine and human neurophysiology research is of particular interest. Here, there are several closely related research areas: the study of the mechanisms of neurodegenerative diseases (Alzheimer's disease [172, 173] and Parkinson's disease [174, 175], epilepsy [176], etc.), mental disorders, and heart diseases in animal models and human neurons, finding approaches to the diagnosis of these pathologies using collected data, and screening of compounds potentially suitable for their therapy [3, 158]. Also, approaches to the therapeutic use of optogenetic tools are being developed. Currently, two clinical trials in the field of gene therapy for vision recovery using channelrhodopsins are being carried out in the U.S. [177]. Therapy for epilepsy [176] and hearing impairment [178] is coming soon.

Method limitations

Paradoxically, it is the extraordinary diversity and efficacy of the optogenetic approach that prompts researchers to pay significant attention to its shortcomings and limitations. In this case, we are dealing with a tool that has become a *de facto* standard for dozens of research areas, and its issues should thus draw more attention than the theoretical downsides in exotic techniques which can be reproduced by only a few laboratories in the world.

Below, we list the most significant problems associated with single-component optogenetics:

· Expression of microbial rhodopsins has limited applicability when working with invertebrates. As already mentioned, mammalian neurons contain a sufficient amount of retinal for inclusion in heterologically expressed rhodopsins, but in models, such as *Drosophila* or *Caenorhabditis*, at minimum addition of retinal to the diet of experimental animals is required [3].

· The spectral repertoire of microbial rhodopsins (at least, if activating and inhibiting molecules are considered separately) is rather poor. Even new variants of channelrhodopsins with absorption maxima shifted to the red region have a large spectral overlap with wild-type pigments. Although the use of several effectors with different activation profiles enables selective simulation of separate neuronal populations in the brain [179], this opportunity is rarely used in practice.

· Overexpression of microbial rhodopsins in nervous tissue can negatively affect the physiology of neurons

[180], and their activation by blue light is potentially phototoxic.

· An obvious limitation of the method is the need to use complex fiber-optic devices fixed on the skull of animals. Methods of brain tissue irradiation without a special interface [181, 182] are less effective and have not yet become widespread [3].

· Finally, the intensity of optogenetic stimulation (both excitation and inhibition of neurons) cannot always be precisely controlled, and it can spill beyond the physiological limits. The problem is complicated by the heterogeneity of effector expression and light energy distribution in brain tissue, while precise stimulation is completely impossible in the depth of the tissue [159].

In the second part of this review, we will acquaint the reader with alternative approaches to specific neurostimulation: thermogenetics and chemogenetics. ●

The reported study was funded by the Russian Foundation for Basic Research, project No. 19-14-50116.

REFERENCES

1. Kim C.K., Adhikari A., Deisseroth K. // Nat. Rev. Neurosci. 2017. V. 18. № 4. P. 222–235.
2. Losi A., Gardner K.H., Möglich A. // Chem. Rev. 2018. V. 118. № 21. P. 10659–10709.
3. Deisseroth K. // Nat. Neurosci. 2015. V. 18. № 9. P. 1213–1225.
4. Cohen A.E. // Biophys. J. 2016. V. 110. № 5. P. 997–1003.
5. Lesca E. // J. Membr. Biol. 2020. V. 253. № 2. P. 81–86.
6. Prestori F., Montagna I., D'Angelo E., Mapelli L. // Int. J. Mol. Sci. 2020. V. 21. № 7. P. 2494.
7. Tischer D., Weiner O.D. // Nat. Rev. Mol. Cell Biol. 2014. V. 15. № 8. P. 551–558.
8. Fraikin G.Y., Strakhovskaya M.G., Rubin A.B. // Biochemistry. (Moscow). 2013. V. 78. № 11. P. 1238–1253.
9. Nowicka B., Kruk J. // Microbiol. Res. 2016. V. 186–187. P. 99–118.
10. Hohmann-Marriott M.F., Blankenship R.E. // Annu. Rev. Plant Biol. 2011. V. 62. P. 515–548.
11. Tisch D., Schmoll M. // Appl. Microbiol. Biotechnol. 2010. V. 85. № 5. P. 1259–1277.
12. Cronin T.W., Johnsen S. // Integr. Comp. Biol. 2016. V. 56. № 5. P. 758–763.
13. Besharse J.C., McMahon D.G. // J. Biol. Rhythms. 2016. V. 31. № 3. P. 223–243.
14. Palczewski K. // J. Biol. Chem. 2012. V. 287. № 3. P. 1612–1619.
15. Gardner L., Deiters A. // Curr. Opin. Chem. Biol. 2012. V. 16. № 3–4. P. 292–299.
16. Feng Z., Zhang W., Xu J., Gauron C., Ducos B., Vriz S., Volovitch M., Jullien L., Weiss S., Bensimon D. // Rep. Prog. Phys. 2013. V. 76. № 7. P. 072601.
17. Li J., Wang L., Tian J., Zhou Z., Li J., Yang H. // Chem. Soc. Rev. 2020. V. 49. № 5. P. 1545–1568.
18. Kim B., Lin M.Z. // Biochem. Soc. Trans. 2013. V. 41. № 5. P. 1183–1188.
19. Pathak G.P., Vrana J.D., Tucker C.L. // Biol. Cell. 2013. V. 105. № 2. P. 59–72.
20. Riggsbee C.W., Deiters A. // Trends Biotechnol. 2010. V. 28. № 9. P. 468–475.
21. Shimizu-Sato S., Huq E., Tepperman J.M., Quail P.H. // Nat. Biotechnol. 2002. V. 20. № 10. P. 1041–1044.
22. Tyszkiewicz A.B., Muir T.W. // Nat. Methods. 2008. V. 5. № 4. P. 303–305.
23. Levskaya A., Weiner O.D., Lim W.A., Voigt C.A. // Nature. 2009. V. 461. № 7266. P. 997–1001.
24. Liu H., Yu X., Li K., Klejnot J., Yang H., Lisiero D., Lin C. // Science. 2008. V. 322. № 5907. P. 1535–1539.
25. Shao K., Zhang X., Li X., Hao Y., Huang X., Ma M., Zhang M., Yu F., Liu H., Zhang P. // Nat. Struct. Mol. Biol. 2020. V. 27. № 5. P. 480–488.
26. Ma L., Wang X., Guan Z., Wang L., Wang Y., Zheng L., Gong Z., Shen C., Wang J., Zhang D., et al. // Nat. Struct. Mol. Biol. 2020. V. 27. № 5. P. 472–479.
27. Wang Q., Lin C. // Nat. Struct. Mol. Biol. 2020. V. 27. № 5. P. 401–403.
28. Kennedy M.J., Hughes R.M., Peteya L.A., Schwartz J.W., Ehlers M.D., Tucker C.L. // Nat. Methods. 2010. V. 7. № 12. P. 973–975.
29. Konermann S., Brigham M.D., Trevino A., Hsu P.D., Heidenreich M., Cong L., Platt R.J., Scott D.A., Church G.M., Zhang F. // Nature. 2013. V. 500. № 7463. P. 472–476.
30. Hughes R.M., Bolger S., Tapadia H., Tucker C.L. // Methods. 2012. V. 58. № 4. P. 385–391.
31. Idevall-Hagren O., Dickson E.J., Hille B., Toomre D.K., De Camilli P. // Proc. Natl. Acad. Sci. USA. 2012. V. 109. № 35. P. E2316–E2323.
32. Kyung T., Lee S., Kim J.E., Cho T., Park H., Jeong Y.-M.,

Kim D., Shin A., Kim S., Baek J., et al. // Nat. Biotechnol. 2015. V. 33. № 10. P. 1092–1096.
33. Bohineust A., Garcia Z., Corre B., Lemaître F., Bousso P. // Nat. Commun. 2020. V. 11. № 1. P. 1143.
34. Huala E., Oeller P.W., Liscum E., Han I.S., Larsen E., Briggs W.R. // Science. 1997. V. 278. № 5346. P. 2120–2123.
35. Christie J.M., Reymond P., Powell G.K., Bernasconi P., Raibekas A.A., Liscum E., Briggs W.R. // Science. 1998. V. 282. № 5394. P. 1698–1701.
36. Glantz S.T., Carpenter E.J., Melkonian M., Gardner K.H., Boyden E.S., Wong G.K.-S., Chow B.Y. // Proc. Natl. Acad. Sci. USA. 2016. V. 113. № 11. P. E1442–E1451.
37. Strickland D., Moffat K., Sosnick T.R. // Proc. Natl. Acad. Sci. USA. 2008. V. 105. № 31. P. 10709–10714.
38. Motta-Mena L.B., Reade A., Mallory M.J., Glantz S., Weiner O.D., Lynch K.W., Gardner K.H. // Nat. Chem. Biol. 2014. V. 10. № 3. P. 196–202.
39. Lee J., Natarajan M., Nashine V.C., Socolich M., Vo T., Russ W.P., Benkovic S.J., Ranganathan R. // Science. 2008. V. 322. № 5900. P. 438–442.
40. Jansen V., Jikeli J.F., Wachten D. // Curr. Opin. Biotechnol. 2017. V. 48. P. 15–20.
41. Richter F., Fonfara I., Bouazza B., Schumacher C.H., Bratovič M., Charpentier E., Möglich A. // Nucleic Acids Res. 2016. V. 44. № 20. P. 10003–10014.
42. Shu X., Lev-Ram V., Deerinck T.J., Qi Y., Ramko E.B., Davidson M.W., Jin Y., Ellisman M.H., Tsien R.Y. // PLoS Biol. 2011. V. 9. № 4. P. e1001041.
43. Gauden M., Yeremenko S., Laan W., van Stokkum I.H.M., Ihalainen J.A., van Grondelle R., Hellingwerf K.J., Kennis J.T.M. // Biochemistry. 2005. V. 44. № 10. P. 3653–3662.
44. Domratcheva T., Hartmann E., Schlichting I., Kottke T. // Sci. Rep. 2016. V. 6. P. 22669.
45. Domratcheva T., Grigorenko B.L., Schlichting I., Nemukhin A.V. // Biophys. J. 2008. V. 94. № 10. P. 3872–3879.
46. Stelling A.L., Ronayne K.L., Nappa J., Tonge P.J., Meech S.R. // J. Am. Chem. Soc. 2007. V. 129. № 50. P. 15556–15564.
47. Gauden M., Grinstead J.S., Laan W., van Stokkum I.H.M., Avila-Perez M., Toh K.C., Boelens R., Kaptein R., van Grondelle R., Hellingwerf K.J., et al. // Biochemistry. 2007. V. 46. № 25. P. 7405–7415.
48. Masuda S., Nakatani Y., Ren S., Tanaka M. // ACS Chem. Biol. 2013. V. 8. № 12. P. 2649–2653.
49. Iseki M., Matsunaga S., Murakami A., Ohno K., Shiga K., Yoshida K., Sugai M., Takahashi T., Hori T., Watanabe M. // Nature. 2002. V. 415. № 6875. P. 1047–1051.
50. Schröder-Lang S., Schwärzel M., Seifert R., Strünker T., Kateriya S., Looser J., Watanabe M., Kaupp U.B., Hegemann P., Nagel G. // Nat. Methods. 2007. V. 4. № 1. P. 39–42.
51. Barends T.R.M., Hartmann E., Griese J.J., Beitlich T., Kirienko N.V., Ryjenkov D.A., Reinstein J., Shoeman R.L., Gomelsky M., Schlichting I. // Nature. 2009. V. 459. № 7249. P. 1015–1018.
52. Brown B.A., Cloix C., Jiang G.H., Kaiserli E., Herzyk P., Kliebenstein D.J., Jenkins G.I. // Proc. Natl. Acad. Sci. USA. 2005. V. 102. № 50. P. 18225–18230.
53. Favory J.-J., Stec A., Gruber H., Rizzini L., Oravecz A., Funk M., Albert A., Cloix C., Jenkins G.I., Oakeley E.J., et al. // EMBO J. 2009. V. 28. № 5. P. 591–601.
54. Rizzini L., Favory J.-J., Cloix C., Faggionato D., O'Hara A., Kaiserli E., Baumeister R., Schäfer E., Nagy F., Jenkins G.I., et al. // Science. 2011. V. 332. № 6025. P. 103–106.
55. Christie J.M., Arvai A.S., Baxter K.J., Heilmann M., Pratt A.J., O'Hara A., Kelly S.M., Hothorn M., Smith B.O., Hitomi K., et al. // Science. 2012. V. 335. № 6075. P. 1492–1496.
56. Wu D., Hu Q., Yan Z., Chen W., Yan C., Huang X., Zhang J., Yang P., Deng H., Wang J., et al. // Nature. 2012. V. 484. № 7393. P. 214–219.
57. Crefcoeur R.P., Yin R., Ulm R., Halazonetis T.D. // Nat. Commun. 2013. V. 4. P. 1779.
58. Müller K., Engesser R., Schulz S., Steinberg T., Tomakidi P., Weber C.C., Ulm R., Timmer J., Zurbriggen M.D., Weber W. // Nucl. Acids Res. 2013. V. 41. № 12. P. e124.
59. Chen D., Gibson E.S., Kennedy M.J. // J. Cell Biol. 2013. V. 201. № 4. P. 631–640.
60. Morgan S.-A., Al-Abdul-Wahid S., Woolley G.A. // J. Mol. Biol. 2010. V. 399. № 1. P. 94–112.
61. Fan H.Y., Morgan S.-A., Brechun K.E., Chen Y.-Y., Jaikaran A.S.I., Woolley G.A. // Biochemistry. 2011. V. 50. № 7. P. 1226–1237.
62. Genick U.K., Borgstahl G.E., Ng K., Ren Z., Pradervand C., Burke P.M., Srajer V., Teng T.Y., Schildkamp W., McRee D.E., et al. // Science. 1997. V. 275. № 5305. P. 1471–1475.
63. Kaberniuk A.A., Shemetov A.A., Verkhusha V.V. // Nat. Methods. 2016. V. 13. № 7. P. 591–597.
64. Redchuk T.A., Omelina E.S., Chernov K.G., Verkhusha V.V. // Nat. Chem. Biol. 2017. V. 13. № 6. P. 633–639.
65. Leopold A. V, Chernov K.G., Shemetov A.A., Verkhusha V.V. // Nat. Commun. 2019. V. 10. № 1. P. 1129.
66. Zhou X.X., Chung H.K., Lam A.J., Lin M.Z. // Science. 2012. V. 338. № 6108. P. 810–814.
67. Zhou X.X., Fan L.Z., Li P., Shen K., Lin M.Z. // Science. 2017. V. 355. № 6327. P. 836–842.
68. McEvoy A.L., Hoi H., Bates M., Platonova E., Cranfill P.J., Baird M.A., Davidson M.W., Ewers H., Liphardt J., Campbell R.E. // PLoS One. 2012. V. 7. № 12. P. e51314.
69. Zhang W., Lohman A.W., Zhuravlova Y., Lu X., Wiens M.D., Hoi H., Yaganoglu S., Mohr M.A., Kitova E.N., Klassen J.S., et al. // Nat. Methods. 2017. V. 14. № 4. P. 391–394.
70. Endo M., Iwawaki T., Yoshimura H., Ozawa T. // ACS Chem. Biol. 2019. V. 14. № 10. P. 2206–2214.
71. Lukyanov K.A., Serebrovskaya E.O., Lukyanov S., Chudakov D.M. // Photochem. Photobiol. Sci. 2010. V. 9. № 10. P. 1301–1306.
72. Jiang H.N., Li Y., Cui Z.J. // Front. Physiol. 2017. V. 8. P. 191.
73. Bulina M.E., Chudakov D.M., Britanova O.V., Yanushevich Y.G., Staroverov D.B., Chepurnykh T.V., Merzlyak E.M., Shkrob M.A., Lukyanov S., Lukyanov K.A. // Nat. Biotechnol. 2006. V. 24. № 1. P. 95–99.
74. Takemoto K., Matsuda T., Sakai N., Fu D., Noda M., Uchiyama S., Kotera I., Arai Y., Horiuchi M., Fukui K., et al. // Sci. Rep. 2013. V. 3. P. 2629.
75. Westberg M., Bregnhøj M., Etzerodt M., Ogilby P.R. // J. Phys. Chem. B. 2017. V. 121. № 40. P. 9366–9371.
76. Lin J.Y., Sann S.B., Zhou K., Nabavi S., Proulx C.D., Malinow R., Jin Y., Tsien R.Y. // Neuron. 2013. V. 79. № 2. P. 241–253.
77. Ryumina A.P., Serebrovskaya E.O., Shirmanova M.V, Snopova L.B., Kuznetsova M.M., Turchin I.V., Ignatova N.I., Klementieva N.V., Fradkov A.F., Shakhov B.E., et al. // Biochim. Biophys. Acta. 2013. V. 1830. № 11. P. 5059–5067.
78. Wang B., van Veldhoven P.P., Brees C., Rubio N., Nordgren M., Apanasets O., Kunze M., Baes M., Agostinis P., Fransen M. // Free Radic. Biol. Med. 2013. V. 65. P. 882–894.
79. Serebrovskaya E.O., Ryumina A.P., Boulina M.E., Shirmanova M.V., Zagaynova E.V., Bogdanova E.A., Lukyanov S.A., Lukyanov K.A. // J. Biomed. Opt. 2014. V. 19. № 7. P. 071403.

80. Petrova N.V., Luzhin A., Serebrovskaya E.O., Ryumina A.P., Velichko A.K., Razin S.V., Kantidze O.L. // Aging (Albany. NY). 2016. V. 8. № 10. P. 2449–2462.
81. Del Bene F., Wyart C., Robles E., Tran A., Looger L., Scott E.K., Isacoff E.Y., Baier H. // Science. 2010. V. 330. № 6004. P. 669–673.
82. Williams D.C., Bejjani R.El, Ramirez P.M., Coakley S., Kim S.A., Lee H., Wen Q., Samuel A., Lu H., Hilliard M.A., et al. // Cell Rep. 2013. V. 5. № 2. P. 553–563.
83. Young L.E.A., Shoben C., Ricci K., Williams D.C. // J. Neurogenet. 2019. V. 33. № 1. P. 1–9.
84. Kawano F., Suzuki H., Furuya A., Sato M. // Nat. Commun. 2015. V. 6. P. 6256.
85. Yu D., Lee H., Hong J., Jung H., Jo Y., Oh B.-H., Park B.O., Heo W. D. // Nat. Methods. 2019. V. 16. № 11. P. 1095–1100.
86. Redchuk T.A., Karasev M.M., Verkhusha P.V., Donnelly S.K., Hülsemann M., Virtanen J., Moore H.M., Vartiainen M.K., Hodgson L., Verkhusha V.V. // Nat. Commun. 2020. V. 11. № 1. P. 605.
87. Alberts B., Johnson A., Lewis J., Raff M., Roberts K., Walter P. Molecular biology of the cell. Sixth ed. New York: Garland Science, 2015. 1464 p.
88. Fork R.L. // Science. 1971. V. 171. № 3974. P. 907–908.
89. Nagel G., Möckel B., Büldt G., Bamberg E. // FEBS Lett. 1995. V. 377. № 2. P. 263–266.
90. Nagel G., Ollig D., Fuhrmann M., Kateriya S., Musti A.M., Bamberg E., Hegemann P. // Science. 2002. V. 296. № 5577. P. 2395–2398.
91. Harz H., Hegemann P. // Nature. 1991. V. 351. № 6326. P. 489–491.
92. Nagel G., Szellas T., Huhn W., Kateriya S., Adeishvili N., Berthold P., Ollig D., Hegemann P., Bamberg E. // Proc. Natl. Acad. Sci. USA. 2003. V. 100. № 24. P. 13940–13945.
93. Zemelman B.V., Lee G.A., Ng M., Miesenböck G. // Neuron. 2002. V. 33. № 1. P. 15–22.
94. Boyden E.S., Zhang F., Bamberg E., Nagel G., Deisseroth K. // Nat. Neurosci. 2005. V. 8. № 9. P. 1263–1268.
95. Li X., Gutierrez D.V., Hanson M.G., Han J., Mark M.D., Chiel H., Hegemann P., Landmesser L.T., Herlitze S. // Proc. Natl. Acad. Sci. USA. 2005. V. 102. № 49. P. 17816–17821.
96. Nagel G., Brauner M., Liewald J.F., Adeishvili N., Bamberg E., Gottschalk A. // Curr. Biol. 2005. V. 15. № 24. P. 2279–2284.
97. Bi A., Cui J., Ma Y.-P., Olshevskaya E., Pu M., Dizhoor A.M., Pan Z.-H. // Neuron. 2006. V. 50. № 1. P. 23–33.
98. Knöpfel T., Lin M.Z., Levskaya A., Tian L., Lin J.Y., Boyden E.S. // J. Neurosci. 2010. V. 30. № 45. P. 14998–15004.
99. Rein M.L., Deussing J.M. // Mol. Genet. Genomics. 2012. V. 287. № 2. P. 95–109.
100. Ernst O.P., Lodowski D.T., Elstner M., Hegemann P., Brown L.S., Kandori H. // Chem. Rev. 2014. V. 114. № 1. P. 126–163.
101. Govorunova E.G., Sineshchekov O.A., Li H., Spudich J.L. // Annu. Rev. Biochem. 2017. V. 86. P. 845–872.
102. Spudich J.L., Yang C.S., Jung K.H., Spudich E.N. // Annu. Rev. Cell Dev. Biol. 2000. V. 16. P. 365–392.
103. Pushkarev A., Inoue K., Larom S., Flores-Uribe J., Singh M., Konno M., Tomida S., Ito S., Nakamura R., Tsunoda S.P., et al. // Nature. 2018. V. 558. № 7711. P. 595–599.
104. Yutin N., Koonin E.V. // Biol. Direct. 2012. V. 7. P. 34.
105. Philosof A., Béjà O. // Environ. Microbiol. Rep. 2013. V. 5. № 3. P. 475–482.
106. Hososhima S., Shigemura S., Kandori H., Tsunoda S.P. // Biophys. Rev. 2020. V. 12. № 2. P. 453–459.
107. Chow B.Y., Han X., Dobry A.S., Qian X., Chuong A.S., Li M., Henninger M.A., Belfort G.M., Lin Y., Monahan P.E., et al. // Nature. 2010. V. 463. № 7277. P. 98–102.
108. Zhang F., Vierock J., Yizhar O., Fenno L.E., Tsunoda S., Kianianmomeni A., Prigge M., Berndt A., Cushman J., Polle J., et al. // Cell. 2011. V. 147. № 7. P. 1446–1457.
109. Kato H.E., Zhang F., Yizhar O., Ramakrishnan C., Nishizawa T., Hirata K., Ito J., Aita Y., Tsukazaki T., Hayashi S., et al. // Nature. 2012. V. 482. № 7385. P. 369–374.
110. Berndt A., Lee S.Y., Ramakrishnan C., Deisseroth K. // Science. 2014. V. 344. № 6182. P. 420–424.
111. Wietek J., Wiegert J.S., Adeishvili N., Schneider F., Watanabe H., Tsunoda S.P., Vogt A., Elstner M., Oertner T.G., Hegemann P. // Science. 2014. V. 344. № 6182. P. 409–412.
112. Govorunova E.G., Sineshchekov O.A., Janz R., Liu X., Spudich J.L. // Science. 2015. V. 349. № 6248. P. 647–650.
113. Gunaydin L.A., Yizhar O., Berndt A., Sohal V.S., Deisseroth K., Hegemann P. // Nat. Neurosci. 2010. V. 13. № 3. P. 387–392.
114. Klapoetke N.C., Murata Y., Kim S.S., Pulver S.R., Birdsey-Benson A., Cho Y.K., Morimoto T.K., Chuong A.S., Carpenter E.J., Tian Z., et al. // Nat. Methods. 2014. V. 11. № 3. P. 338–346.
115. Berndt A., Schoenenberger P., Mattis J., Tye K.M., Deisseroth K., Hegemann P., Oertner T.G. // Proc. Natl. Acad. Sci. USA. 2011. V. 108. № 18. P. 7595–7600.
116. Berndt A., Yizhar O., Gunaydin L.A., Hegemann P., Deisseroth K. // Nat. Neurosci. 2009. V. 12. № 2. P. 229–234.
117. Yizhar O., Fenno L.E., Prigge M., Schneider F., Davidson T.J., O'Shea D.J., Sohal V.S., Goshen I., Finkelstein J., Paz J.T., et al. // Nature. 2011. V. 477. № 7363. P. 171–178.
118. Zhang F., Prigge M., Beyrière F., Tsunoda S.P., Mattis J., Yizhar O., Hegemann P., Deisseroth K. // Nat. Neurosci. 2008. V. 11. № 6. P. 631–633.
119. Lin J.Y., Knutsen P.M., Muller A., Kleinfeld D., Tsien R.Y. // Nat. Neurosci. 2013. V. 16. № 10. P. 1499–1508.
120. Rajasethupathy P., Sankaran S., Marshel J.H., Kim C.K., Ferenczi E., Lee S.Y., Berndt A., Ramakrishnan C., Jaffe A., Lo M., et al. // Nature. 2015. V. 526. № 7575. P. 653–659.
121. Kleinlogel S., Feldbauer K., Dempski R.E., Fotis H., Wood P.G., Bamann C., Bamberg E. // Nat. Neurosci. 2011. V. 14. № 4. P. 513–518.
122. Inoue K., Ono H., Abe-Yoshizumi R., Yoshizawa S., Ito H., Kogure K., Kandori H. // Nat. Commun. 2013. V. 4. P. 1678.
123. Kato H.E., Inoue K., Abe-Yoshizumi R., Kato Y., Ono H., Konno M., Hososhima S., Ishizuka T., Hoque M.R., Kunitomo H., et al. // Nature. 2015. V. 521. № 7550. P. 48–53.
124. Konno M., Kato Y., Kato H.E., Inoue K., Nureki O., Kandori H. // J. Phys. Chem. Lett. 2016. V. 7. № 1. P. 51–55.
125. Brown J., Behnam R., Coddington L., Tervo D.G.R., Martin K., Proskurin M., Kuleshova E., Park J., Phillips J., Bergs A.C.F., et al. // Cell. 2018. V. 175. № 4. P. 1131–1140.e11.
126. Gao K. // Nat. Methods. 2018. V. 15. № 12. P. 1003.
127. Govorunova E.G., Sineshchekov O.A., Spudich J.L. // Biophys. J. 2016. V. 110. № 11. P. 2302–2304.
128. Yamauchi Y., Konno M., Ito S., Tsunoda S.P., Inoue K., Kandori H. // Biophys. Physicobiol. 2017. V. 14. P. 57–66.
129. Shigemura S., Hososhima S., Kandori H., Tsunoda S.P. // Appl. Sci. 2019. V. 9. № 17. P. 3440.
130. Shihoya W., Inoue K., Singh M., Konno M., Hososhima S., Yamashita K., Ikeda K., Higuchi A., Izume T., Okazaki S., et al. // Nature. 2019. V. 574. № 7776. P. 132–136.
131. Kovalev K., Volkov D., Astashkin R., Alekseev A., Gushchin I., Haro-Moreno J.M., Chizhov I., Siletsky S., Mamedov

M., Rogachev A., et al. // Proc. Natl. Acad. Sci. USA. 2020. V. 117. № 8. P. 4131–4141.
132. Inoue K., Ito S., Kato Y., Nomura Y., Shibata M., Uchihashi T., Tsunoda S.P., Kandori H. // Nat. Commun. 2016. V. 7. P. 13415.
133. Inoue K., Tsunoda S.P., Singh M., Tomida S., Hososhima S., Konno M., Nakamura R., Watanabe H., Bulzu P.-A., Banciu H.L., et al. // Sci. Adv. 2020. V. 6. № 15. P. eaaz2441.
134. Kim J.-M., Hwa J., Garriga P., Reeves P.J., RajBhandary U.L., Khorana H.G. // Biochemistry. 2005. V. 44. № 7. P. 2284–2292.
135. Airan R.D., Thompson K.R., Fenno L.E., Bernstein H., Deisseroth K. // Nature. 2009. V. 458. № 7241. P. 1025–1029.
136. Siuda E.R., Copits B.A., Schmidt M.J., Baird M.A., Al-Hasani R., Planer W.J., Funderburk S.C., McCall J.G., Gereau R.W., Bruchas M.R. // Neuron. 2015. V. 86. № 4. P. 923–935.
137. Gunaydin L.A., Grosenick L., Finkelstein J.C., Kauvar I.V., Fenno L.E., Adhikari A., Lammel S., Mirzabekov J.J., Airan R.D., Zalocusky K.A., et al. // Cell. 2014. V. 157. № 7. P. 1535–1551.
138. Oh E., Maejima T., Liu C., Deneris E., Herlitze S. // J. Biol. Chem. 2010. V. 285. № 40. P. 30825–30836.
139. van Wyk M., Pielecka-Fortuna J., Löwel S., Kleinlogel S. // PLoS Biol. 2015. V. 13. № 5. P. e1002143.
140. Kandori H. // Biophys. Rev. 2020. V. 12. № 2. P. 355–361.
141. Deisseroth K., Hegemann P. // Science. 2017. V. 357. № 6356. P. eaan5544.
142. Volkov O., Kovalev K., Polovinkin V., Borshchevskiy V., Bamann C., Astashkin R., Marin E., Popov A., Balandin T., Willbold D., et al. // Science. 2017. V. 358. № 6366. P. eaan8862.
143. Nango E., Royant A., Kubo M., Nakane T., Wickstrand C., Kimura T., Tanaka T., Tono K., Song C., Tanaka R., et al. // Science. 2016. V. 354. № 6319. P. 1552–1557.
144. Nogly P., Weinert T., James D., Carbajo S., Ozerov D., Furrer A., Gashi D., Borin V., Skopintsev P., Jaeger K., et al. // Science. 2018. V. 361. № 6398. P. eaat0094.
145. Zhang F., Wang L.-P., Boyden E.S., Deisseroth K. // Nat. Methods. 2006. V. 3. № 10. P. 785–92.
146. Wang H., Peca J., Matsuzaki M., Matsuzaki K., Noguchi J., Qiu L., Wang D., Zhang F., Boyden E., Deisseroth K., et al. // Proc. Natl. Acad. Sci. USA. 2007. V. 104. № 19. P. 8143–8148.
147. Arenkiel B.R., Peca J., Davison I.G., Feliciano C., Deisseroth K., Augustine G.J., Ehlers M.D., Feng G. // Neuron. 2007. V. 54. № 2. P. 205–218.
148. Hägglund M., Borgius L., Dougherty K.J., Kiehn O. // Nat. Neurosci. 2010. V. 13. № 2. P. 246–252.
149. Lammel S., Lim B.K., Ran C., Huang K.W., Betley M.J., Tye K.M., Deisseroth K., Malenka R.C. // Nature. 2012. V. 491. № 7423. P. 212–217.
150. Reardon T.R., Murray A.J., Turi G.F., Wirblich C., Croce K.R., Schnell M.J., Jessell T.M., Losonczy A. // Neuron. 2016. V. 89. № 4. P. 711–724.
151. Adamantidis A.R., Zhang F., Aravanis A.M., Deisseroth K., de Lecea L. // Nature. 2007. V. 450. № 7168. P. 420–424.
152. Fenno L.E., Mattis J., Ramakrishnan C., Hyun M., Lee S.Y., He M., Tucciarone J., Selimbeyoglu A., Berndt A., Grosenick L., et al. // Nat. Methods. 2014. V. 11. № 7. P. 763–772.
153. Aravanis A.M., Wang L.-P., Zhang F., Meltzer L.A., Mogri M.Z., Schneider M.B., Deisseroth K. // J. Neural Eng. 2007. V. 4. № 3. P. S143–156.
154. Warden M.R., Cardin J.A., Deisseroth K. // Annu. Rev. Biomed. Eng. 2014. V. 16. P. 103–129.
155. Montgomery K.L., Yeh A.J., Ho J.S., Tsao V., Mohan Iyer S., Grosenick L., Ferenczi E.A., Tanabe Y., Deisseroth K., Delp S.L., et al. // Nat. Methods. 2015. V. 12. № 10. P. 969–974.
156. Goncalves S.B., Ribeiro J.F., Silva A.F., Costa R.M., Correia J.H. // J. Neural Eng. 2017. V. 14. № 4. P. 041001.
157. Park S., Brenner D.S., Shin G., Morgan C.D., Copits B.A., Chung H.U., Pullen M.Y., Noh K.N., Davidson S., Oh S.J., et al. // Nat. Biotechnol. 2015. V. 33. № 12. P. 1280–1286.
158. Song C., Knöpfel T. // Nat. Rev. Drug Discov. 2016. V. 15. № 2. P. 97–109.
159. Häusser M. // Nat. Methods. 2014. V. 11. № 10. P. 1012–1014.
160. Hochbaum D.R., Zhao Y., Farhi S.L., Klapoetke N., Werley C.A., Kapoor V., Zou P., Kralj J.M., Maclaurin D., Smedemark-Margulies N., et al. // Nat. Methods. 2014. V. 11. № 8. P. 825–833.
161. Deisseroth K. // Nat. Methods. 2011. V. 8. № 1. P. 26–29.
162. Sizemore R.J., Seeger-Armbruster S., Hughes S.M., Parr-Brownlie L.C. // J. Neurophysiol. 2016. V. 115. № 4. P. 2124–2146.
163. Bernstein J.G., Boyden E.S. // Trends Cogn. Sci. 2011. V. 15. № 12. P. 592–600.
164. Kravitz A.V., Freeze B.S., Parker P.R.L., Kay K., Thwin M.T., Deisseroth K., Kreitzer A.C. // Nature. 2010. V. 466. № 7306. P. 622–626.
165. Aquili L., Liu A.W., Shindou M., Shindou T., Wickens J.R. // Learn. Mem. 2014. V. 21. № 4. P. 223–231.
166. Mager T., Lopez de la Morena D., Senn V., Schlotte J., D Errico A., Feldbauer K., Wrobel C., Jung S., Bodensiek K., Rankovic V., et al. // Nat. Commun. 2018. V. 9. № 1. P. 1750.
167. Proville R.D., Spolidoro M., Guyon N., Dugué G.P., Selimi F., Isope P., Popa D., Léna C. // Nat. Neurosci. 2014. V. 17. № 9. P. 1233–1239.
168. Thiele T.R., Donovan J.C., Baier H. // Neuron. 2014. V. 83. № 3. P. 679–691.
169. Roberts T.F., Gobes S.M.H., Murugan M., Ölveczky B.P., Mooney R. // Nat. Neurosci. 2012. V. 15. № 10. P. 1454–1459.
170. Lu Y., Truccolo W., Wagner F.B., Vargas-Irwin C.E., Ozden I., Zimmermann J.B., May T., Agha N.S., Wang J., Nurmikko A.V. // J. Neurophysiol. 2015. V. 113. № 10. P. 3574–3587.
171. Galvan A., Stauffer W.R., Acker L., El-Shamayleh Y., Inoue K.-I., Ohayon S., Schmid M.C. // J. Neurosci. 2017. V. 37. № 45. P. 10894–10903.
172. Yamamoto K., Tanei Z.-I., Hashimoto T., Wakabayashi T., Okuno H., Naka Y., Yizhar O., Fenno L.E., Fukayama M., Bito H., et al. // Cell Rep. 2015. V. 11. № 6. P. 859–865.
173. Suberbielle E., Sanchez P.E., Kravitz A. V, Wang X., Ho K., Eilertson K., Devidze N., Kreitzer A.C., Mucke L. // Nat. Neurosci. 2013. V. 16. № 5. P. 613–621.
174. Gradinaru V., Mogri M., Thompson K.R., Henderson J.M., Deisseroth K. // Science. 2009. V. 324. № 5925. P. 354–359.
175. Steinbeck J.A., Choi S.J., Mrejeru A., Ganat Y., Deisseroth K., Sulzer D., Mosharov E.V., Studer L. // Nat. Biotechnol. 2015. V. 33. № 2. P. 204–209.
176. Walker M.C., Kullmann D.M. // Neuropharmacology. 2020. V. 168. P. 107751.
177. Shen Y., Campbell R.E., Côté D.C., Paquet M.-E. // Front. Neural Circuits. 2020. V. 14. P. 41.
178. DiGuiseppi J., Zuo J. // Neurosci. Lett. 2019. V. 701. P. 175–179.
179. Han X., Boyden E.S. // PLoS One. 2007. V. 2. № 3. P. e299.

180. Miyashita T., Shao Y.R., Chung J., Pourzia O., Feldman D.E. // Front. Neural Circuits. 2013. V. 7. P. 8.
181. Gradinaru V., Thompson K.R., Zhang F., Mogri M., Kay K., Schneider M.B., Deisseroth K. // J. Neurosci. 2007. V. 27. № 52. P. 14231–14238.
182. Huber D., Petreanu L., Ghitani N., Ranade S., Hromádka T., Mainen Z., Svoboda K. // Nature. 2008. V. 451. № 7174. P. 61–64.

The p53 Protein Family in the Response of Tumor Cells to Ionizing Radiation: Problem Development

O. A. Kuchur[1*], D. O. Kuzmina[1], M. S. Dukhinova[1], A. A. Shtil[1,2]
[1] ITMO University, Saint-Petersburg, 191002 Russia
[2] Blokhin National Medical Research Center of Oncology, Moscow, 115478 Russia
*E-mail: kuchur@scamt-itmo.ru
Received October 27, 2020; in final form, December 24, 2020
DOI: 10.32607/actanaturae.11247

ABSTRACT **Survival mechanisms are activated in tumor cells in response to therapeutic ionizing radiation. This reduces a treatment's effectiveness. The p53, p63, and p73 proteins belonging to the family of proteins that regulate the numerous pathways of intracellular signal transduction play a key role in the development of radioresistance. This review analyzes the p53-dependent and p53-independent mechanisms involved in overcoming the resistance of tumor cells to radiation exposure.**
KEYWORDS **p53 family protein, cell death, radioresistance, radiation therapy, malignant tumors.**
ABBREVIATIONS **EMT – epithelial–mesenchymal transition; NF-κB – nuclear factor kappa-light-chain-enhancer of activated B cells; CDK – cyclin-dependent kinases; TAp63/73 – p63/p73 isoforms with N-terminal transactivation domain (TA); ΔNp63/73 – p63/p73 isoform with N-terminal transactivation domain deletion.**

INTRODUCTION

Ionizing radiation, which ranges from the original use of photons to modern sources of ionizing particles (protons, electrons, neutrons, and carbon atoms), is a key tool in treating tumors. Its effectiveness has been proven for more than 50 years. However, the problem related to the resistance of tumor cells to ionizing radiation (either primary resistance or that acquired during treatment) remains to be solved. Identically to drug resistance, resistance to radiation is an unfavorable prognostic factor of treatment effectiveness. There are numerous reasons why resistance to ionizing radiation develops. This review analyzes the molecular mechanisms forming a synergistic response from tumor cells to radiation therapy with gamma photons. The response needs to cause cell death rather than immune evasion, which may result in cancer cell survival and the formation of a recurrent, radioresistant tumor.

The genotoxic effect (disruption of DNA structure and functions) is considered to be the primary reason why ionizing radiation damages tumor cells. This effect can either be caused by direct rupturing of molecular bonds due to the ionization of atoms in DNA or be an indirect process occurring due to water radiolysis. In the latter case, the interaction between the radiation energy and water molecules gives rise to reactive radicals that cause single- or double-strand DNA breaks. This process can be accompanied by the altering of the expression of the genes whose products are involved in homeostasis regulation [1–3]. Therefore, the biological effect of radiation is implemented through the regulation of gene transcription. It is plasticity, a shared feature of all living systems that is especially marked in tumor cells, that allows for the rearranging (reprogramming) of the transcription machinery for adaptation to stress. It is quite expected that the transcriptional protein p53, a prototype of the family comprising p63 and p73, is the primary and key sensor regulating the cellular response to radiation-induced DNA damage [4, 5]. The p53-family proteins regulate the cellular response to radiation, thus maintaining the balance between cell survival and apoptosis [6–8].

The research into the p53 family started in 1979, when independent researchers discovered the protein forming a complex with the known tumor-associated protein, the polyomavirus SV40 large T antigen [9]. The new protein was examined as an auxiliary protein involved in cell malignization by the SV40 virus and expression of small T and large T antigens of the virus in host cells. Back then, serum containing a previously unstudied factor with a molecular weight of 53–54 kDa was also obtained [10]. The era of p53 had arrived: new functions for this protein were being discovered,

including such functions as regulation of the cell cycle and the balance between cell survival and death, as well as control over tumor emergence and progression. While previously recognized as a common regulator of cell transformation, p53 and the processes mediated by it have become some of the main topics of discussion in modern molecular oncobiology [11]. The problem remains relevant, as it remains impossible to investigate the novel mechanisms of tumor cell response to ionizing radiation (and largely, the radioresistance mechanisms) without taking into account the significant role played by the p53 family.

Has this problem been solved over the past decades of research? What remains to be clarified in a broad range of questions regarding the role played by the p53 family as the main molecular mechanism in the cell response to ionizing radiation? In this review, we have analyzed the available data on p53-family proteins as regulators (sensors) of therapeutic photons. These mechanisms determine the fate of an irradiated cell: whether it dies or becomes radioresistant.

THE STRUCTURE AND FUNCTIONS OF p53 FAMILY PROTEINS

The p53 protein (393 a.a.r.) consists of five domains; the key ones are the transcriptional activation domain, the DNA-binding domain, and the tetramerization domain [12, 13]. Expression of the *p53* gene and the activity of the p53 protein are regulated by diverse stress signals, DNA damage being the main one (but not the only one). After single- or double-strand DNA breaks are induced in cells by radiation, ATM and ATR protein kinases activate the transcriptional competence of p53 via phosphorylation at Ser15 [14, 15].

Two other proteins belonging to this family, p63 and p73, also contain domains similar to those found in p53. All three proteins in homotetrameric form regulate transcription [16, 17]. The p73 protein is activated upon exposure to ionizing radiation, DNA-damaging drugs, and medications that disrupt microtubule dynamics through the pathways regulated by c-Abl tyrosine kinase [18]. In all likelihood, there is cooperation between c-Abl and apoptosis activation by the p73 protein [19]. Much less is known about the features of p63 functions. It has been reported that this protein can also be activated in response to UV and gamma radiation and mediates apoptosis even if p53 is inactivated [20]; upregulated p63 expression in some types of tumors reduces cellular sensitivity to ionizing radiation [21]. Since there is a high level of structural similarity between the proteins belonging to this family, full-length p73 and p63 are capable of binding and activating the transcription of most of the p53-dependent promoters [22].

MUTATIONS AND ISOFORMS OF p53-FAMILY PROTEINS IN TUMOR CELLS

The disruption of the functions of p53-family proteins can be caused by mutations in the *TP53*, *TP63*, and *TP73* genes or the genes whose products are involved in the modification of these proteins (e.g., protein kinases phosphorylating p53 (Cdc2, JNK1, protein kinase C)) [23]. The *p53* gene encodes nine protein isoforms (p53, p53β, p53γ, Δ133p53, Δ133p53β, Δ133p53γ, Δ40p53, Δ40p53β, and Δ40p53γ); this diversity is determined by alternative mRNA splicing, alternative use of the promoter, or translation initiation sites [24]. An analysis of the biopsy specimens of 29,346 tumors derived from different tissues showed that most of these tumors carry a mutant p53 (*Fig. 1*). Most malfunctions of p53 in tumor cells are caused by missense and/or point mutations; there can also be deletions and splicing errors [25]. Approximately 15% of the mutations in the *p53* gene are frameshift or nonsense mutations [26]. In most tumors, *TP53* mutations are found in exons 5–8 encoding the DNA-binding domain. Because of this, 80% of missense p53 mutations are associated with the pro-oncogenic function [27, 28].

The main difference between most mutant forms of p53 and wild-type p53 (whose half-life in dormant cells does not exceed 5–10 min) consists in enhanced stability because of the disrupted negative feedback with E3 ligase Mdm2 and binding to Hsp90 and Hsc70, which stabilizes p53 and causes its accumulation in cells [29, 30]. Importantly, mutant p53 can form oligomeric complexes with wild-type p53. This binding can inactivate the intact protein and explains why mutant p53 can transform cells in the presence of wild-type protein [31].

A wide range of the isoforms of two other proteins belonging to the p53 family are known: the *p63* and *p73* genes contain an internal promoter in intron 3 and, due to alternative splicing, express the 6 and 35 mRNA variants, respectively. The *p63* gene is located in the 3q27-ter locus; three C-terminal isoforms (α, β, and γ) formed as a result of alternative splicing are expressed from it. The *p73* gene is located in the 1p36 locus; its alternatively spliced transcripts encode the C-terminal isoforms α–η [32]. *p63* and *p73* mRNA can be transcribed from the distal and internal (in intron 3) promoters. The distal promoter regulates *TAp63* and *TAp73* expression (the transactivation domains are homologous to *p53*), whereas the ΔNp63 and ΔNp73 isoforms, which are N-terminal truncated proteins (ΔN) with properties in opposition to those of the p63/TAp73 isoforms, are transcribed from the internal promoter [33]. These results indicate that the p53 family is exceptionally diverse. It is little surprise that the problem under examination remains relevant while also acquiring new layers of complexity.

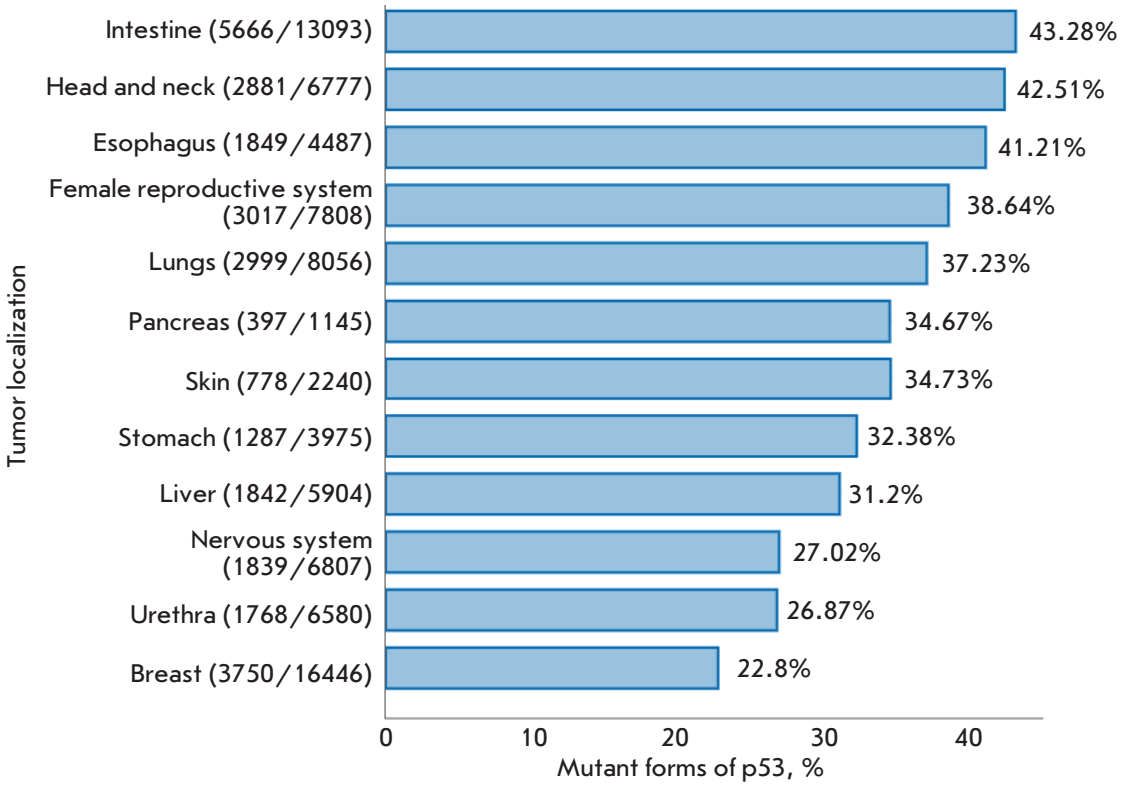

Fig. 1. Prevalence of mutant p53 forms in tumors based on DNA sequencing (IARCTP53 Database, 2019). X-axis: the number of biopsy specimens with identified mutations; Y-axis: the number of analyzed biopsy specimens

RESPONSE TO THERAPEUTIC IONIZING RADIATION

The p53 protein

As mentioned above, p53 is activated in response to stressful conditions (primarily, to DNA damage caused by oxidative stress, ionizing radiation, etc.) The proteins activating the protein kinases ATM (ataxia telangiectasia mutated kinase) and ATR (ATM- and Rad3-related kinase) bind to the DNA damage site [34]. In turn, the latter group of proteins activates the checkpoint kinases Chk1 and Chk2 phosphorylating p53 at Ser15. Activation of p53 results in the induction of Mdm2, its functional antagonist. Binding between Mdm2 and the N-terminus of p53 promotes monoubiquitination of p53 and nuclear export or polyubiquitination and p53 hydrolysis in the proteasome [35, 36]. *Figure 2* shows a generalized scheme of the intracellular responses to ionizing radiation involving p53-family proteins.

The "choice" between cell survival and death is regulated by post-translational modifications of p53 and its isoforms, partner proteins, and a set of activated genes [37]. The p53 protein activates the transcription of $p21^{Cip1/Waf1}$, blocker of the cell cycle at the G_1 phase that inhibits binding of cyclins A and B to CDK1 and CDK2 protein kinases [38, 39]. There is insufficient data on the role played by p53 in the regulation of the S phase of the cell cycle. During the S phase, Chk2 phosphorylates phosphatase CDC25A, causing its degradation and cell cycle arrest [40]. The p53 protein can delay the G2/M progression through repression of *CDC2* and cyclin B promoters [41].

In response to radiation, p53 can stimulate apoptosis through the induction of proapoptotic (Bax) and repression of antiapoptotic (Bcl-2) proteins, as well as the activation or inhibition of the other target genes involved in cell cycle regulation. It is known that low-dose radiation induces p21 and Hdm2 (an Mdm2 homolog), while high-dose radiation increases the Bax : Bcl-2 ratio, thus promoting apoptosis [42]. Radioresistance is caused by the activity of antiapoptotic proteins (overexpression of the Bcl-2 family proteins), loss of the components of apoptotic cell signaling, or inhibition of the genes encoding caspases.

The efficiency of DNA damage repair in response to radiation depends on the histological origin of the cells and cell cycle phase. The G_2 and mitotic phases are most sensitive to it. Importantly, p53 may play a dual role in response to radiation exposure. In some cases, an increased p53 expression level enhances sensitivity to radiation, while correlation between an increased p53 expression level and radioresistance has been demonstrated in other cases [43]. Under minor stress, p53 can act as a survival factor, since it promotes DNA damage repair; therefore, *p53* knockout in a colon adenocar-

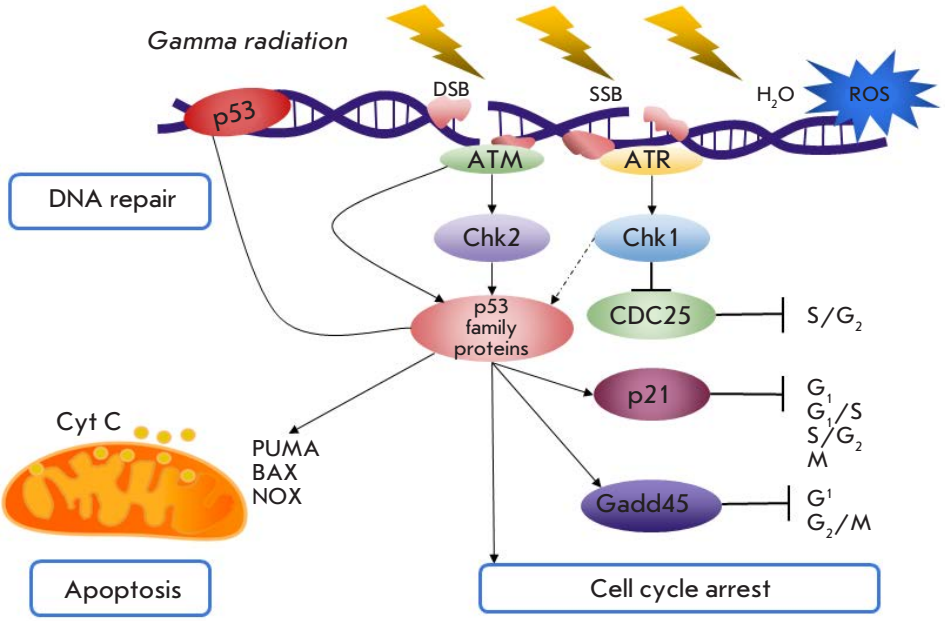

Fig. 2. The response mechanisms to ionizing radiation involving p53-family proteins

cinoma cell line (HCT116) increases the sensitivity of cells to radiation and causes the "mitotic catastrophe," the aberrant chromosome segregation resulting in cell death. A significantly increased number of cells undergoing mitotic catastrophe was also observed in irradiated human fibrosarcoma cells (HT1080) after p53 was inactivated by a dominant negative mutant [44].

The transcription factors Slug and Snail regulate the epithelial–mesenchymal transition (EMT) and invasion by tumor cells of the subjacent tissues [45]. A research team from Seoul National University found that p53 induces Slug and Snail degradation by Mdm2-mediated ubiquitination [46]. Importantly, Snail activity depends on the p53 status. Thus, the mutant forms of p53 cause overexpression of Snail and Slug, which is related to the acquisition of radioresistance by ovarian cancer cells: these proteins increase the survivability of precursor cells thanks to the activation of the SCF/c-Kit signaling pathway [47].

Polo-like serine/threonine protein kinase 3 (PLK3) is one of the components of p53-mediated regulatory signals. PLK3 interacts with p53, Chk2, and CDC25C in response to DNA damage. p53 can bind to *PLK3* promoter and induce expression of its gene, which is followed by a delay in G_2/M progression and cell cycle arrest. Another p53-regulated gene, *GPX1*, encodes the antioxidant protein glutathione peroxidase. After irradiation, cells accumulate highly active oxygen free radicals. Due to *GPX1* induction and rapid catabolism of H_2O_2, p53 can protect cells against the oxidative damage that accompanies radiation treatment [48, 49]. The dual role of p53 upon radiation exposure manifests itself here: this protein protects cells in some cases, while in other cases it promotes their death.

Halacli *et al.* revealed that in colon adenocarcinoma cells with non-functional p53, telomerase activity drops after irradiation, while it increases in the wild-type isogenic line ($p53^{+/+}$). An opposite effect was observed for the catalytic subunit of telomerase (TERT). After irradiation, TERT activity decreases as p53 induction increases, while TERT activity in $p53^{-/-}$ cells is increases. Whereas irradiation does not alter telomerase activity, accelerated senescence is observed in cells with normally functioning p53. Therefore, telomerase activity and G1-phase arrest of cell cycle progression in irradiated cells are regulated depending on the p53 status [50].

The equally important features of cell cycle regulation have been demonstrated for connective tissue cells. Thus, mouse embryonic fibroblasts (MEF $p53^{+/+}$) accumulated in the G_1 phase after irradiation (5 Gy): the p53-dependent promoter of the *p21* gene was activated in them. However, irradiated p53 knockout cells did not undergo apoptosis and remained in the premitotic phase [51]. In $p53^{-/-}$ cells, p21 and Cdc25 regulated p53-independent cell cycle arrest at the G_2 phase [52].

The p63 and p73 proteins

The role played by p73 in the cellular response to ionizing radiation has been studied more thoroughly compared to that of p63. It was found that *p73* expression level is higher in patients with radiosensitive cervical cancer compared to that in patients with radioresistant cervical cancer. The p73 protein is a positive regulator

of *p21* transcription upon irradiation and can potentially take on the role of p53 protein in the regulation of cell cycle checkpoints. Hence, p73 is involved in the regulation of radiosensitivity [53].

Increased p73 expression induced by radiation activates the transcription of the p53-dependent genes *Bax*, *Mdm2*, and *GADD45*, thus promoting apoptosis or cell cycle arrest and inhibiting proliferation. It has been assumed that p73 can be induced by irradiation and take on some of the functions of p53 in tumor cells with disrupted p53 expression or activity. Furthermore, activation of p53 suppresses p73 expression in irradiated breast and lung cancer cells [54–56]. It has been shown recently that nutlin, a low-molecular-weight agent uncoupling the p53-Mdm2 interaction, can induce apoptosis in p53-negative cells through activation of p73 upon irradiation. These results justify the use of nutlin for treating tumors with non-functional p53 [57].

The antitumor drug cisplatin and ionizing radiation cause Tyr99 phosphorylation of p73 and the accumulation of this protein. This post-translational modification occurs due to the interaction between p73 and tyrosine kinase Abl; it promotes the apoptotic activity of p73. Furthermore, it has been demonstrated that treatment with cisplatin can result in the acetylation of p73 by the p300 protein. These data attest to the importance of p73 in cellular response to a combination of chemotherapy and radiation therapy [58].

A genome-wide association study (GWAS) in p63 and p73 knockout cells has shown that these proteins regulate the transcription of the *BRCA2*, *Rad51*, *Rad50*, and *Mre11* genes, whose products are involved in the repair of single- and double-strand DNA breaks. This mechanism can be responsible for tumor survival. Interestingly, the ΔNp63 and ΔNp73 isoforms are stronger transactivators of the aforelisted genes than the TA isoforms. An analysis of the mutations in the *p63/p73* genes can be important in choosing a radiation therapy strategy [59].

Therefore, the mutant p53-family forms are regulated through numerous pathways, which are far from obvious in some cases. Proteins belonging to this family mediate the signaling cascades that regulate the establishment of stable phenotypes or death of irradiated cells. The use of platinum-based drugs in combination with mTOR inhibitors or other intracellular signal blockers opens up the potential for modulating p53-family proteins and enhancing the response to ionizing radiation.

RADIORESISTANCE MEDIATED BY p53-FAMILY PROTEINS

A pioneer study focused on the role played by p53 in the radioresistance of tumor cells was the paper by Lee and Bernstein [60], who used transgenic mice carrying $p53^{Pro193}$ and $p53^{Val135}$ mutations and showed that the expression of both mutant variants of the *p53* gene significantly increases the gamma radiation resistance of hematopoietic cells. They uncovered an association between mutations in the p53 gene and radioresistance [60]. The radiosensitivity of rat embryonic fibroblasts (REF) transfected with a mutant form of *p53* ($MTp53^{Pro193}$), either individually or in combination with *H-Ras* and *E7* oncogenes, was studied later. The results of the experiments involving transfection with $p53^{Pro193}$ have confirmed the previous data showing that radioresistance of cells increases. Cotransfection with the mutant *p53* and *H-Ras* genes or transfection with $p53^{Pro193}$, *H-Ras* and *E7* yielded clones with an even higher radioresistance and overexpression of mutant p53 [61].

The ovarian adenocarcinoma cell lines SKOV-3 and CaOV-3 acquired radioresistance if the mutant p53 was overexpressed; irradiation caused neither activation nor accumulation of the mutant p53 form. It turned out that p-53-regulated expression of *Bcl-2* in these cell lines was associated with gamma radiation resistance and cisplatin sensitivity. It is possible that mutations in the *p53* gene causing the increased protein expression level and radioresistance are associated with greater p53 stability and cell cycle blockage; cells have time to repair DNA damage [62].

It has been shown for melanoma cells that the Chk2/hCds1-independent signaling pathway of DNA damage dephosphorylating Ser376 in the C-terminal region of p53 enhances p53 activity upon irradiation. In cells with functional p53, Ser376 phosphorylation is not regulated by DNA damage: so, these cells do not develop radioresistance. Contrariwise, the defects in the superjacent mechanisms of p53 activation in response to DNA damage (e.g., mutations in Chk2/hCds1 disabling Ser376 phosphorylation of p53 upon irradiation) are associated with the development of radioresistance by melanoma cells. The same feature was also observed for the mutant p53, which was unable to interact with the 14-3-3 protein [43].

In cooperation with p53, the Ki-67 nuclear protein, which is expressed in proliferating cells and is non-functional in dormant (G_0) cells, is also a predictor of radioresistance. In specimens of head and neck squamous cell carcinoma, the p53 expression level correlates with the absence of a tumor response to radiation therapy. A combination of p53 accumulation and low Ki-67 level is associated with tumor recurrence in patients with early-stage cancer. Therefore, p53 and Ki-67 can play a key role in the choice of radiation therapy strategies for patients with head and neck tumors [63]. Multiple mutations, including changes in p53-dependent

proapoptotic proteins Bcl-2, PUMA, and Bax, increase resistance to radiation therapy and chemotherapy [64].

The activity of focal adhesion kinase (FAK) is increased in patients with various tumors. In the FAK knockout cell line of squamous cell carcinoma of the skin, radiation suppresses transcription of the *p21* gene and other p53 target genes mediating cell cycle arrest and DNA damage repair. Suppression of *p53* and *p21* activation promotes radiosensitization of tumor cells; this was not observed for intact FAK [65]. The experiments on FAK inhibition in p53-negative lung cancer cells showed encouraging results: *in vitro* migration and invasion were reduced, and *in vivo* survivability tended to increase [66]. Modulation of FAK activity, in combination with radiation, seems quite promising.

Overexpression and the accumulation of p53 in endometrial cancer cells are caused by the fact (among others) that mutant p53 is refractory to ubiquitin-mediated proteasomal degradation. Simultaneous accumulation of p53 and PTEN phosphatase renders endometrial cells insensitive to radiation therapy, which is associated with disease progression [67].

Since ionizing radiation induces oxidative stress [68], reactive oxygen species (ROS) are involved in radiation damage to mitochondria. Activation of mitochondrial BNIP3, a proapoptotic protein belonging to the Bcl-2 family and regulating the generation of ROS in irradiated cells and mitophagy, did not take place in the cells with non-functional p53. Thus, p53 acts as a key mechanism in the regulation of BNIP3; the absence of functional p53 can affect the survivability of irradiated tumor cells by maintaining mitochondrial integrity [69]. The p53 status turns out to be an important biomarker for predicting the therapeutic value of drugs targeted at mitochondrial proteins.

There are insufficient data on the role played by p63 and p73 in the formation of radioresistance phenotypes. Since the proteins belonging to this family are interchangeable or complement each other in some cases, it is fair to assume that p63 and p73 can also regulate radioresistance via mechanisms similar to those employed by p53. Indeed, Moergel *et al.* [21] studied p63 in specimens of oral squamous cell carcinoma. The expression level of the transactivated form TAp63 before treatment is a marker of radioresistance; the high levels of TAp63 expression are associated with poor treatment effectiveness and unfavorable prognosis [70, 71]. These results were confirmed by studies of biopsy specimens of squamous cell carcinoma of the head and neck collected from 33 patients; the increased level of p63 expression before treatment in these tumors is also considered a predictor of radioresistance, but studies involving a larger patient cohort are needed [21].

Expression of the ΔNp63α isoform upon irradiation for the cell lines of squamous cell carcinoma of the larynx, head, and neck (PCI-I-1, PCI-13, SCC-68, and SCC-4), as well as primary oral mucosal keratinocytes, has also been studied. The level of ΔNp63α expression was dependent on the radiation dose in all the cell lines. ΔNp63 knockdown induced by small interfering RNA (siRNA) increased radiation sensitivity [72]. However, an opposite effect was also observed: expression of TAp73 and caspase 7 in colorectal cancer cells after radiation therapy correlated with radiosensitivity. The *Rb1* gene was then knocked down using microRNA miR-622. Rb1 knockdown inhibited the formation of the Rb-E2F1-P/CAF complex, thus reducing the expression of *TAp73* and caspase 7, and the cells acquired radioresistance [73].

It is also known that upon the irradiation of cells, p63/p73 bind to the mutant form of p53 in some cases and cannot activate the proapoptotic genes: so, the cells survive. Inhibitors of mutant p53 forms, p63/p73 overexpression, or disruption of physical interactions between proteins belonging to this family using peptidomimetics or low-molecular-weight compounds (see text below) are used to enhance p63/p73 activity [74, 75].

WAYS TO OVERCOME RADIORESISTANCE UPON MODULATION OF p53-FAMILY PROTEINS

Modulation of p53

The key approaches to modulating p53 for the radiosensitizing effect include (*Fig. 3*):

1. Low-molecular-weight p53 stabilizers [76];
2. Modulators of chaperones/stabilizers of wild-type and mutant p53 [77];
3. Regulators of E3 ubiquitin ligases;
4. Modulators of components of the p53 signaling pathway (e.g., CDK and Bcl-2) [78].

Stictic acid, which restores the functions of p53 by binding to its mutant form, is one of the examples of low-molecular-weight stabilizers [79]. Carbazole-based compounds also exhibit a similar effect. Thus, PK083 binds to the mutant form $p53^{Y220C}$ and restores its transcriptional activity, causing apoptosis [36, 80, 81]. Analogs of quinazoline (2-styryl-4-aminoquiazoline, CP-31398) [82–84] reactivate p53. Alkylating agents are involved in the restoration of the structure of the p53 protein by directly binding to and modifying its mutant forms [85]. PRIMA-1 and its more efficient analog, PRIMA-1Met (APR-246), are among such agents that restore p53. Inside the cells, these agents are converted into an active compound, methylene quinuclidinone (MQ), a Michael acceptor that binds covalently to cysteine residues in the DNA-binding domain of p53. Cys277 is essential for the MQ-mediat-

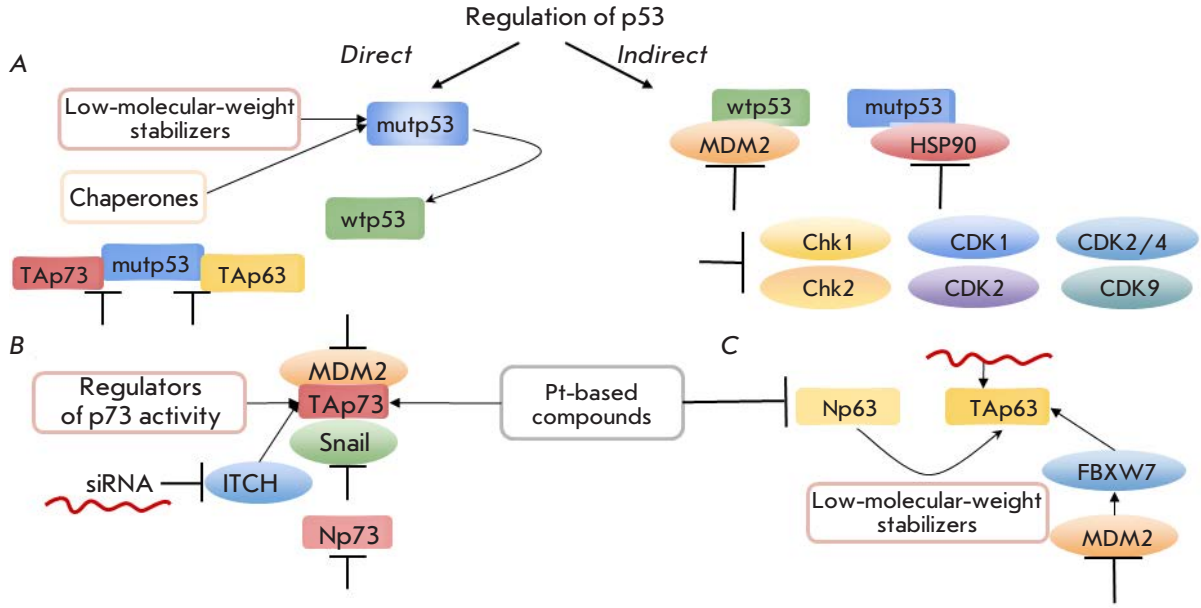

Fig. 3. Methods for enhancing the sensitivity of tumor cells to ionizing radiation by modulating the p53-family proteins. (*A*) – Modulation of p53 by low-molecular-weight-stabilizing molecules and chaperones. (*B*) – Regulation of p73 by acting on Snail family proteins and E3 ubiquitin ligase (MDM2, ITCH). (*C*) – The impact on p63 isoforms via Pt-containing compounds, low-molecular-weight stabilizers and ubiquitin ligase activity (MDM2, FBXW7). See explanation in the text

ed thermal stabilization of the mutant $p53^{R273H}$, while Cys124 is needed for APR-246-mediated functional restoration of the mutant $p53^{R175H}$ in tumor cells and the normalizing activity of the wild-type protein. These studies are especially important for a rational design of p53-targeting molecules [86–88].

The activity of p53 can also be regulated indirectly, through stabilizers of the intact or mutant forms of p53. Blanden *et al.* [89, 90] showed that the low-molecular-weight compound ZMC1 (NSC319726) acts as a metallochaperone and restores the functions of $p53^{R175H}$ [89, 90]. In the case of the stabilization of mutant pro-oncogenic forms of p53 by Hsp90, the activity of this chaperone needs to be suppressed in order to sensitize the cell to chemotherapy and radiation therapy. Hsp90 inhibitors (ganetespib and geldanamycin) are used for this purpose, which allows one to suppress the proliferation of tumor cells carrying mutant p53. AUY922 and other candidate drugs destabilize the mutant protein by suppressing the chaperone activity [91–94]. Cerivastatin, one of the members of the class of statins, inhibits the mevalonate pathway. By inhibiting HMG-CoA reductase (an enzyme catalyzing the synthesis of mevalonic acid), this compound reduces the activity of histone deacetylase HDAC6, resulting in dissociation of the Hsp90–mutant p53 complex [95]. Therefore, it is reasonable to assume that destabilization of mutant p53 and restoration of p53 functions can increase cell sensitivity to radiation.

Agents that regulate the interaction between E3 ligases and p53 are being designed. Among the numerous agents uncoupling the Mdm2-p53 interaction, the family of *cis*-imidazolines (nutlins) is universally recognized. AMG-232 is currently undergoing clinical trials [96]. Anthraquinones activating p53 via Mdm2 suppression also possess a high therapeutic potential [97, 98]. There is a diverse range of Mdm2 inhibitors: genisteins, curcumins, ginsenosides, SP141, and NFAT1-Mdm2 dual inhibitors. Thus, curcumin, a natural compound exhibiting antioxidant properties, can stabilize p53 by forming a stable complex between p53 and (NAD(P)H:quinone oxidoreductase 1 [99], while genistein can amplify cell death through p53-dependent apoptosis [100–102]. Ma *et al.* [103] investigated USP14, a signalosome COPS5 activator enhancing the activity of E3 ligase, as a potentially promising target for therapy and endeavored to choose inhibitors for it (e.g., IU1 and AP15).

Modulation of p53 can occur indirectly via the regulation of the components of the p53 signaling pathway. One of the promising strategies can involve affecting cyclin-dependent kinases, which regulate the cell cycle and transcription [104]. Treatment with roscovitine, a CDK1 and CDK2 inhibitor, has induced the apoptosis of cells expressing mutant p53 [105, 106]. Chemical inhibitors of mTOR (mammalian target of rapamycin), the cyclin-dependent protein kinases CDK1, CDK7, and CDK9, as well as poly(ADP-riboso)polymerases

(PARP), also affect p53 functions. Roscovitine and flavopiridol increase the p53 expression level in cells and reduce *Mdm2* transcription, possibly by inhibiting CDK7 or CDK9, which are components of the general transcription machinery [107]. The effect of CDK inhibitors flavopiridol, THZ1 and YKL-1-116 on *Mdm2* transcription and p53 induction was studied using an Mdm2:T2A-GFP reporter; its transactivation in breast cancer cells (MCF-7 cell line) was quantified. Flavopiridol and roscovitine increased p53 transactivation as a result of Mdm2 depletion. Although p53 is probably inactive in these situations (since transcription in the presence of an inhibitor of transcriptional protein kinases is either disrupted or absent), after CDK7 and CDK9 inhibitors (THZ1 and YKL-1-116, respectively) are removed, p53 activates the targets (DR5, Fas and p21) and enhances the antitumor effect of irradiation [108, 109].

Treatment with dinaciclib (an inhibitor of CDK1, CDK2, CDK5, CDK9, and CDK12) also resulted in a switch to p53-dependent apoptosis [110, 111]. Furthermore, AT7519 (an inhibitor of CDK1, CDK2, CDK4, CDK6, and CDK9) and SNS-032 (an inhibitor of CDK2, CDK7, and CDK9) increases sensitivity to irradiation through p53 activation and Chk1 suppression [112]. Compound YM155 affects the cell cycle regulation through Chk1 and Chk2 by stabilizing p53 and p21 [113]. The thiazole derivative of quinone RO-3306, an inhibitor of CCNB1/Cdk1, induces p53-mediated apoptosis of p53-intact neuroblastoma cells [114]. Luteolin, which causes Mdm2 degradation, can inhibit cyclin D1 and CDK2/4, thus increasing the level of p53 expression in the cell [115]. Therefore, it is promising to use a combination of CDK inhibitors and radiation therapy. *Figure 4* shows the chemical formulas of CDK inhibitors listed above.

Gene therapeutics and synergistic impacts on cellular metabolism, which may restore or evade the disrupted functions of mutant p53 through the regulation of the metabolism of tumor cells, are also used for tumor treatment, along with chemotherapeutic agents. In the cells with intact p53, ATP is synthesized via oxidative phosphorylation. The loss of normal functions by p53 leaves the cell relying on glycolysis; cells become able to survive under hypoxic conditions. Recent findings indicate that treatment with a glycolysis inhibitor can increase the sensitivity of the tumor to radiation therapy [116].

Alteration of p73 and p63 activity

Sensitivity to chemotherapy and radiation therapy can be increased by impacting p53 and other p53-family proteins. Thus, some chemotherapy regimens increase the expression level of p73 [117]. Platinum-based drugs (cisplatin, oxaliplatin, etc.) help the cell overcome drug resistance by increasing activity of the TAp73 protein and inducing the apoptosis of tumor cells [118]. In addition, cisplatin suppresses the pro-oncogenic form ΔNp63α, which can also inhibit tumor growth [119, 120] and presumably enhance its radiosensitivity.

These p53-like strategies can also be applied to p73 and p63 (to regulate the activity of E3 ligases). E3 ligase

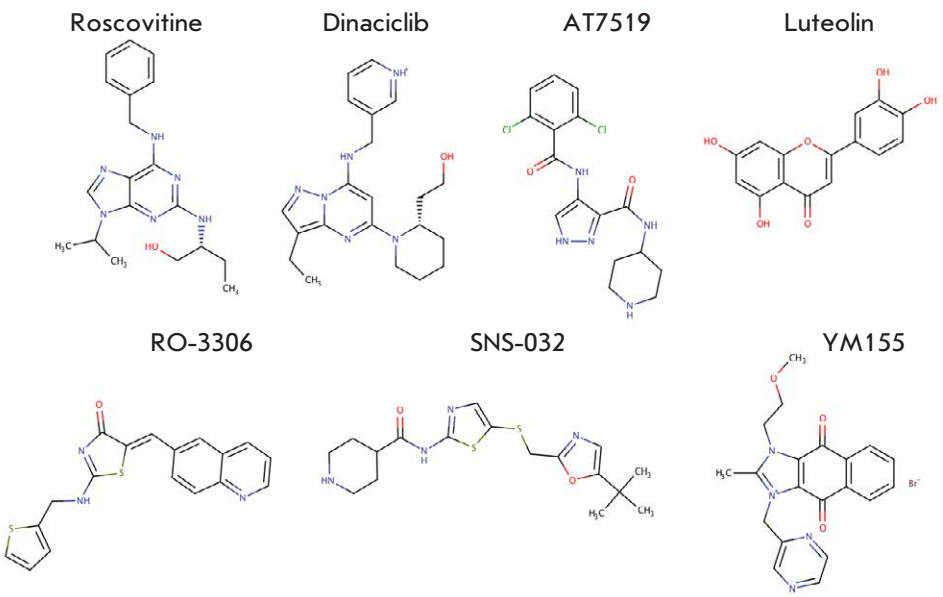

Fig. 4. Therapeutically promising inhibitors of the cyclin-dependent protein kinases modulating the activity of p53

ITCH negatively regulates p73; ITCH knockout using a combination of nanoparticles and siRNA enhances the stabilization of p73 in p53-mutant cells [121]. Agents directly regulating p53 activity can also be effective in the case of p63 and p73. Curcumin, a p53 stabilizer, activates *p73* expression [99, 122].

By activating the AMP-activated protein kinase (AMPK), metformin affects all three p53-family proteins: it increases the expression level of p53 and p73, while reducing the expression level of the pro-oncogenic form of p63 (ΔNp63α) [123, 124]. Prodigiosin has a positive effect on *p53* expression by activating its reporter via induction of p73 and reduction of the expression level of oncogenic ΔNp73, a suppressor of the *p53* gene [125]. Compound NSC59984 destabilizes the mutant p53 and causes its degradation, which is accompanied by induction of p73-dependent apoptosis [126].

Along with the regulators affecting all proteins belonging to the p53 family, agents with selectivity to individual proteins have also been proposed. *Abrus agglutinin* (AGG), a plant-derived lectin inhibiting translation, leads to p73 induction [127]. The p73 induced by lectin suppresses the expression of Snail and inhibits the EMT in the cells of squamous cell carcinoma of the larynx. It is noteworthy that AGG promotes Snail transfer from the nucleus into the cytoplasm and induces its degradation via ubiquitination. Therefore, AGG stimulates p73 and suppresses the EGF-induced EMT and invasiveness by inhibiting the ERK/Snail pathway [128]. Protoporphyrin IX (PpIX), a metabolite of aminolevulinic acid, which is used in photodynamic cancer therapy, stabilizes TAp73 and activates TAp73-dependent apoptosis in tumor cells lacking p53. TAp73 is activated through the disruption of TAp73/MDM2 and TAp73/MDMX interactions, as well as the inhibition of TAp73 degradation by ubiquitin ligase ITCH [129]. Similar properties were also observed for 1-carbaldehyde-3,4-dimethoxyxantone, which stabilizes TAp73 by inhibiting its binding to Mdm2 [130]. Diallyl disulfide (DADS) enhances the sensitivity to ionizing radiation by increasing the expression level of TAp73 and reducing the expression level of the ΔNp73 isoform. The DADS-mediated balance between TAp73 and ΔNp73 is associated with the radiosensitivity of cervical cancer cells [131].

The results of the use of microRNA for p63 modulation have been published [132]. miR-130b activates the antitumor p63 isoform (TAp63) by binding directly to the protein [133]. Special attention should be paid to the study of the response of p63 to irradiation and the acquisition of p63-mediated radioresistance, as well as the choice of drugs targeted at a respective gene/protein for designing novel therapy methods, especially for patients with cross-resistance to chemotherapeutics.

The important problem related to the design of methods for targeted drug delivery using liposomes and nanoparticles remains poorly studied. The mesoporous nanoparticles UCNPs(BTZ)@ mSiO2-H2A/p53, which contain the proteasome inhibitor bortezomib along with cDNA of p53, increased cell sensitivity to this drug and induced a more pronounced apoptosis compared to the situation in the control cells without nanoparticles in [134]. Not only gene fragments, but also antagonists of E3 ligases for p53 (Mdm2 and MdmX) can be delivered inside cells as a part of gold nanoparticles. Furthermore, the low-molecular-weight agents VIP116 and PM2 inhibiting the p53-Mdm2 and p53-Mdm4 interactions, which were delivered inside lipodisks (the nanosized bilayer structures stabilized into flat circular shapes by lipids linked to polyethylene glycol), significantly reduced the viability of tumor cells [136]. This approach can be used to precipitate the death of tumor cells exposed to ionizing radiation.

CONCLUSIONS: THE NEW APPROACHES TO AN OLD PROBLEM

Despite the many decades of research, the role played by the p53 protein as a molecular target and a prognostic marker in radiation therapy remains controversial. The situation is complicated by the variability of the p53-dependent responses elicited by the radiation treatment of different tumors (even cell lines originating from the same tissue) [137]. Nonetheless, the p53 protein was reported to be an informative, predictive genetic marker of acute toxicity or response to the radiation therapy of native tumors [138]. By analyzing the expression of p53 and a number of other genes, researchers have predicted the absorbed dose at which a particular tumor response is elicited [139, 140]. Gendicine (Ad-*p53*), a recombinant adenovirus engineered to express wild-type p53 in the tumor where this protein is mutated, can be considered a successful application of p53-targeting therapy. Ad-*p53* is used in clinical practice and shows a good result when combined with radiation therapy, especially in patients with breast, pancreatic, cervical, or ovarian cancer [141].

Information regarding the application of p63 and p73 in radiation oncology remains so far confined to experimental data and the hypothesis on their practical use [142]. This gap needs filling, since a general analysis of the p53-protein family reveals a more detailed, and more complex, mechanism of radiation response regulation.

The problem related to p53-negative tumors remains unsolved. One of the pathways that allow one to evade the non-functional p53-dependent mechanism is

to use nanostructured silver particles that can induce mitochondrial stress and apoptosis independently of p53 [143]. The question of whether these materials can be combined with radiation therapy remains to be elucidated[144]. Finally, the impact on p63 and p73 should be considered justified if their functions are preserved in p53-negative tumors [145]. ●

This work was supported by the Russian Foundation for Basic Research (research project No. 20-34-90046).

REFERENCES

1. Seidlitz A., Combs S.E., Debus J., Baumann M. // Oxford Textbook of Oncology. 2016. P. 173.
2. Snyder A.R., Morgan W.F. // Cancer Metastasis Rev. 2004. V. 23. № 3–4. P. 259–268.
3. Finnberg N., Wambi C., Ware J.H., Kennedy A.R. // Cancer Biol. Ther. 2008. V. 7. № 12. P. 2023–2033.
4. McIlwrath A.J., Vasey P.A., Ross G.M., Brown R. // Cancer Res. 1994. V. 54. № 14. P. 3718–3722.
5. Mallya S.M., Sikpi M.O. // Mutat. Res. 1999. V. 434. № 2. P. 119–132.
6. Moergel M., Abt E., Stockinger M., Kunkel M. // Oral Oncol. 2010. V. 46. № 9. P. 667–671.
7. Akervall J., Nandalur S., Zhang J., Qian C.N., Goldstein N., Gyllerup P., Resau J. // Eur. J. Cancer. 2014. V. 50. № 3. P. 570–581.
8. Dietz S., Rother K., Bamberger C., Schmale H., Mössner J., Engeland K. // FEBS Lett. 2002. V. 525. № 1–3. P. 93–99.
9. Lane D.P., Crawford L.V. // Nature. 1979. V. 278. № 5701. P. 261–263.
10. Linzer D.I., Levine A.J. // Cell. 1979. V. 17. № 1. P. 43–52.
11. Ryan K.M., Phillips A.C., Vousden K.H. // Curr. Opin. Cell Biol. 2001. V. 13. № 3. P. 332–337.
12. Joerger A.C., Fersht A.R. // CSH Perspect. Biol. 2010. V. 2. № 6. P. a000919.
13. Sullivan K.D., Galbraith M.D., Andrysik Z., Espinosa J.M. // Cell Death Differ. 2018. V. 25. № 1. P. 133–143.
14. May P., May E. // Oncogene. 1999. V. 18. № 53. P. 7621–7636.
15. Tibbetts R.S., Brumbaugh K.M., Williams J.M., Sarkaria J.N., Cliby W.A., Shieh S.Y., Abraham R.T. // Genes Dev. 1999. V. 13. № 2. P. 152–157.
16. Harms K.L., Chen X. // Cell Death Differ. 2006. V. 13. № 6. P. 890–897.
17. Joerger A.C., Rajagopalan S., Natan E., Veprintsev D.B., Robinson C.V., Fersht A.R. // Proc. Natl. Acad. Sci. USA. 2009. V. 106. № 42. P. 17705–17710.
18. Yang A., McKeon F. // Nat. Rev. Mol. 2000. V. 1. № 3. P. 199–207.
19. Wang X., Zeng L., Wang J., Chau J.F.L., Lai K.P., Jia D., He L. // Cell Death Differ. 2011. V. 18. № 1. P. 5–15.
20. Johnson J., Liu Y., Lawson S., Kulesz-Martin M. // Proc. Am. Assoc. Cancer Res. 2005. V. 46. P. 5691.
21. Moergel M., Abt E., Stockinger M., Kunkel M. // Oral Oncol. 2010. V. 46. № 9. P. 667–671.
22. Dötsch V., Bernassola F., Coutandin D., Candi E., Melino G. // CSH Perspect. Biol. 2010. V. 2. № 9. a004887.
23. Harris C.C. // J. Natl. Cancer Inst. 1996. V. 88. № 20. P. 1442–1455.
24. Bourdon J.C. // Br. J. Cancer. 2007. V. 97. № 3. P. 277–282.
25. Allred D.C., Clark G.M., Elledge R., Fuqua S.A., Brown R.W., Chamness G.C., McGuire W.L. // J. Natl. Cancer Inst. 1993. V. 85. № 3. P. 200–206.
26. Freed-Pastor W.A., Prives C. // Genes Dev. 2012. V. 26. № 12. P. 1268–1286.
27. Garcia C.A., Ahmadian A., Gharizadeh B., Lundeberg J., Ronaghi M., Nyrén P. // Gene. 2000. V. 253. № 2. P. 249–257.
28. Hartmann A., Blaszyk H., McGovern R.M., Schroeder J.J., Cunningham J., De Vries E.M., Sommer S.S. // Oncogene. 1995. V. 10. № 4. P. 681–688.
29. Quinlan D.C., Davidson A.G., Summers C.L., Warden H.E., Doshi H.M. // Cancer Res. 1992. V. 52. № 17. P. 4828–4831.
30. Yue X., Zhao Y., Xu Y., Zheng M., Feng Z., Hu W. // J. Mol. Biol. 2017. V. 429. № 11. P. 1595–1606.
31. Davidoff A.M., Humphrey P.A., Iglehart J.D., Marks J.R. // Proc. Natl. Acad. Sci. USA. 1991. V. 88. № 11. P. 5006–5010.
32. Inoue K., Fry E.A. Mutant p53 and MDM2 in Cancer. Dordrecht, Heidelberg, New York, London: Springer, 2014. P. 17–40.
33. Bénard J., Douc-Rasy S., Ahomadegbe J.C. // Hum. Mutat. 2003. V. 21. № 3. P. 182–191.
34. Maréchal A., Zou L. // CSH Perspect. Biol. 2013. V. 5. № 9. P. 012716.
35. Gajjar M., Candeias M.M., Malbert-Colas L., Mazars A., Fujita J., Olivares-Illana V., Fahraeus R. // Cancer Cell. 2012. V. 21. № 1. P. 25–35.
36. Joerger A.C., Fersht A.R. // Annu. Rev. Biochem. 2016. V. 85. P. 375–404.
37. Saito S.I., Goodarzi A.A., Higashimoto Y., Noda Y., Lees-Miller S.P., Appella E., Anderson C.W. // J. Biol. Chem. 2002. V. 277. № 15. P. 12491–12494.
38. Cmielova J., Rezáčová M. // J. Cell. Biochem. 2011. V. 112. № 12. P. 3502.
39. Kreis N.N., Sanhaji M., Rieger M.A., Louwen F., Yuan J. // Oncogene. 2014. V. 33. № 50. P. 5716–5728.
40. Jinno S., Suto K., Nagata A., Igarashi M., Kanaoka Y., Nojima H., Okayama H. // EMBO J. 1994. V. 13. № 7. P. 1549–1556.
41. Fei P., El-Deiry W.S. // Oncogene. 2003. V. 22. № 37. P. 5774–5783.
42. Latonen L., Yoichi T., Marikki L. // Oncogene. 2001. V. 20. № 46. P. 6784–6793.
43. Palazzo J.P., Kafka N.J., Grasso L., Chakrani F., Hanau C., Cuesta K.H., Mercer W.E. // Hum. Pathol. 1997. V. 28. № 10. P. 1189–1195.
44. Gudkov A.V., Komarova E.A. // Nat. Rev. Cancer. 2003. V. 3. № 2. P. 117–129.
45. Muller P.A., Vousden K.H., Norman J.C. // J. Cell. Biol. 2011. V. 192. № 2. P. 209–218.
46. Lim S.O., Kim H., Jung G. // FEBS Lett. 2010. V. 584. № 11. P. 2231–2236.
47. Kurrey N.K., Jalgaonkar S.P., Joglekar A.V., Ghanate A.D., Chaskar P.D., Doiphode R.Y., Bapat S.A. // Stem Cells. 2009. V. 27. № 9. P. 2059–2068.
48. Jen K.Y., Cheung V.G. // Cancer Res. 2005. V. 65. № 17. P. 7666–7673.
49. Budanov A.V. Mutant p53 and MDM2 in Cancer. Dordrecht, Heidelberg, New York, London: Springer, 2014. P. 337–358.
50. Halacli S.O., Canpinar H., Cimen E., Sunguroglu A. //

Oncol. Lett. 2013. V. 6. № 3. P. 807–810.
51. Pohl F., Grosse J., Grimm D., Brockhoff G., Westphal K., Moosbauer J., Schoenberger J. // Thyroid. 2010. V. 20. № 2. P. 159–166.
52. Attardi L.D. // Mutat. Res. 2005. V. 569. № 1–2. P. 145–157.
53. Liu S.S., Leung R.C.Y., Chan K.Y.K., Chiu P.M., Cheung A.N.Y., Tam K.F., Ngan H.Y.S. // Clin. Cancer Res. 2004. V. 10. № 10. P. 3309–3316.
54. Wakatsuki M., Ohno T., Iwakawa M., Ishikawa H., Noda S., Ohta T., Nakano T. // Int. J. Radiat. Oncol. Biol. Phys. 2008. V. 70. № 4. P. 1189–1194.
55. Lin K.W., Nam S.Y., Toh W.H., Dulloo I., Sabapathy K. // Neoplasia. 2004. V. 6. № 5. P. 546–557.
56. Ramadan S., Terrinoni A., Catani M.V., Sayan A.E., Knight R.A., Mueller M., Candi E. // Biochem. Biophys. Res. Commun. 2005. V. 331. № 3. P. 713–717.
57. Impicciatore G., Sancilio S., Miscia S., Di Pietro R. // Curr. Pharm. Des. 2010. V. 16. № 12. P. 1427–1442.
58. Adamovich Y., Adler J., Meltser V., Reuven N., Shaul Y. // Cell Death Differ. 2014. V. 21. № 9. P. 1451–1459.
59. Lin Y.L., Sengupta S., Gurdziel K., Bell G.W., Jacks T., Flores E.R. // PLoS Genet. 2009. V. 5. № 10. e1000680.
60. Lee J.M., Bernstein A. // Proc. Natl. Acad. Sci. USA. 1993. V. 90. № 12. P. 5742–5746.
61. Bristow R.G., Jang A., Peacock J., Chung S., Benchimol S., Hill R.P. // Oncogene. 1994. V. 9. № 6. P. 1527–1536.
62. Concin N., Zeillinger C., Stimpfel M., Schiebel I., Tong D., Wolff U., Zeillinger R. // Cancer Lett. 2000. V. 150. № 2. P. 191–199.
63. Couture C., Raybaud-Diogène H., Têtu B., Bairati I., Murry D., Allard J., Fortin A. // Cancer. 2002. V. 94. № 3. P. 713–722.
64. Perri F., Pacelli R., Della Vittoria Scarpati G., Cella L., Giuliano M., Caponigro F., Pepe S. // Head. Neck. 2015. V. 37. № 5. P. 763–770.
65. Graham K., Moran-Jones K., Sansom O.J., Brunton V.G., Frame M.C. // PLoS One. 2011. V. 6. № 12. e27806
66. Dragoj M., Bankovic J., Sereti E., Stojanov S.J., Dimas K., Pesic M., Stankovic T. // Invest. New Drugs. 2017. V. 35. № 6. P. 718–732.
67. Akiyama A., Minaguchi T., Fujieda K., Hosokawa Y., Nishida K., Shikama A., Satoh T. // Oncol. Lett. 2019. V. 18. № 6. P. 5952–5958.
68. Yoshida T., Goto S., Kawakatsu M., Urata Y., Li T.S. // Free Radic. Res. 2012. V. 46. № 2. P. 147–153.
69. Chang H.W., Kim M.R., Lee H.J., Lee H.M., Kim G.C., Lee Y.S., Lee J.C. // Oncogene. 2019. V. 38. № 19. P. 3729–3742.
70. Somerville T.D., Xu Y., Miyabayashi K., Tiriac H., Cleary C.R., Maia-Silva D., Vakoc C.R. // Cell Rep. 2018. V. 25. № 7. P. 1741–1755.
71. Ding R., Cai X., Xu F., Wang H., Zhang B. // Die Pharmazie. 2017. V. 72. № 7. P. 414–418.
72. Moergel M., Goldschmitt J., Stockinger M., Kunkel M. // Clin. Oral Investig. 2014. V. 18. № 4. P. 1259–1268.
73. Ma W., Yu J., Qi X., Liang L., Zhang Y., Ding Y., Ding Y. // Oncotarget. 2015. V. 6. № 18. P. 15984.
74. Li Y., Prives C. // Oncogene. 2007. V. 26. № 15. P. 2220–2225.
75. Johnson J.L., Lagowski J.P., Sundberg A., Lawson S., Liu Y., Kulesz-Martin M. // Proc. Amer. Assoc. Cancer Res. 2006. V. 47. P. 5183.
76. Doveston R.G., Kuusk A., Andrei S.A., Leysen S., Cao Q., Castaldi M.P., Ottmann C. // FEBS Lett. 2017. V. 591. № 16. P. 2449–2457.
77. Li C., Xiao Z.X. // BioMed Res. Int. 2014. V. 14. P. 1–9.
78. Chen B., Wen P., Hu G., Gao Y., Qi X., Zhu K., Zhao G. // Front. Cell Dev. Biol. 2020. V. 8. P. 408.
79. Wassman C.D., Baronio R., Demir Ö., Wallentine B.D., Chen C.K., Hall L.V., Chamberlin A.R. // Nat. Commun. 2013. V. 4. № 1. P. 1–9.
80. Bauer M.R., Kraämer A., Settanni G., Jones R.N., Ni X., Khan T.R., Joerger A.C. // ACS Chem. Biol. 2020. V. 15. № 3. P. 657–668.
81. Synnott N.C., O'Connell D., Crown J., Duffy M.J. // Breast Cancer Res. Treat. 2020. V. 179. № 1. P. 47–56.
82. Wang H., Liao P., Zeng S.X., Lu H. // Cancer Biol. Ther. 2020. V. 21. № 3. P. 269–277.
83. Liu L., Yu Z.Y., Yu T.T., Cui S.H., Yang L., Chang H., Ren C.C. // J. Cell. Physiol. 2020. V. 235. № 11. P. 8768–8778.
84. Wei X.W., Yuan J.M., Huang W.Y., Chen N.Y., Li X.J., Pan C.X., Su G.F. // Eur. J. Med. Chem. 2020. V. 186. P. 111851.
85. Loh S.N. // Biomolecules. 2020. V. 10. № 2. P. 303.
86. Zhang Q., Bykov V.J., Wiman K.G., Zawacka-Pankau J. // Cell Death Dis. 2018. V. 9. № 5. P. 1–12.
87. Duffy M.J., Synnott N.C., McGowan P.M., Crown J., O'Connor D., Gallagher W.M. // Cancer Treat. Rev. 2014. V. 40. № 10. P. 1153–1160.
88. Ramraj S.K., Elayapillai S.P., Pelikan R.C., Zhao Y.D., Isingizwe Z.R., Kennedy A.L., Benbrook D.M. // Int. J. Cancer. 2020. V. 147. № 4. P. 1086–1097.
89. Blanden A.R., Yu X., Wolfe A.J., Gilleran J.A., Augeri D.J., O'Dell R.S., Carpizo D.R. // Mol. Pharmacol. 2015. V. 87. № 5. P. 825–831.
90. Garufi A., D'Orazi V., Crispini A., D'Orazi G. // Int. J. Oncol. 2015. V. 47. № 4. P. 1241–1248.
91. Li D., Yallowitz A., Ozog L., Marchenko N. // Cell Death Dis. 2014. V. 5. № 4. P. e1194–e1194.
92. Alexandrova E.M., Yallowitz A.R., Li D., Xu S., Schulz R., Proia D.A., Moll U.M. // Nature. 2015. V. 523. № 7560. P. 352–356.
93. McLaughlin M., Barker H.E., Khan A.A., Pedersen M., Dillon M., Mansfield D.C., Nutting C.M. // BMC Cancer. 2017. V. 17. № 1. P. 86.
94. Mantovani F., Collavin L., Del Sal G. // Cell Death Differ. 2019. V. 26. № 2. P. 199–212.
95. Ingallina E., Sorrentino G., Bertolio R., Lisek K., Zannini A., Azzolin L., Rosato A. // Nat. Cell Biol. 2018. V. 20. № 1. P. 28–35.
96. Gluck W.L., Gounder M.M., Frank R., Eskens F., Blay J.Y., Cassier P.A., Siegel D. // Invest. New Drugs. 2020. V. 38. № 3. P. 831–843.
97. Anifowose A., Yuan Z., Yang X., Pan Z., Zheng Y., Zhang Z., Wang B. // Bioorganic Med. Chem. Lett. 2020. V. 30. № 2. P. 126786.
98. Anifowose A., Agbowuro A.A., Tripathi R., Lu W., Tan C., Yang X., Wang B. // Med. Chem. Res. 2020. V. 29. P. 1199–1210.
99. Patiño-Morales C.C., Soto-Reyes E., Arechaga-Ocampo E., Ortiz-Sánchez E., Antonio-Véjar V., Pedraza-Chaverri J., García-Carrancá A. // Redox Biol. 2020. V. 28. P. 101320.
100. Morris S.M., Chen J.J., Domon O.E., McGarrity L.J., Bishop M.E., Manjanatha M.G., Casciano D.A. // Mutation Res./Fund. Mol. Mech. Mutagenesis. 1998. V. 405. № 1. P. 41–56.
101. Wang W., Zafar A., Rajaei M., Zhang R. // Cells. 2020. V. 9. № 5. P. 1176.
102. Rasafar N., Barzegar A., Aghdam E.M. // Life Sci. 2020. V. 245. P. 117358.
103. Ma Y.S., Wang X.F., Zhang Y.J., Luo P., Long H.D., Li L., Chang Z.Y. // Mol. Ther. Oncolytics. 2020. V. 16. P. 147–157.

104. Lee B., Sandhu S., McArthur G. // Curr. Opin. Oncol. 2015. V. 27. № 2. P. 141–150.
105. Jabbour-Leung N.A., Chen X., Bui T., Jiang Y., Yang D., Vijayaraghavan S., Keyomarsi K. // Mol. Cancer Ther. 2016. V. 15. № 4. P. 593–607.
106. Gary C., Hajek M., Biktasova A., Bellinger G., Yarbrough W.G., Issaeva N. // Oncotarget. 2016. V. 7. № 25. P. 38598.
107. Stewart-Ornstein J., Lahav G. // Sci. Signal. 2017. V. 10. № 476. P. 1–10.
108. Bagashev A., Fan S., Mukerjee R., Paolo Claudio P., Chabrashvili T., Leng R.P., Sawaya B.E. // Cell Cycle. 2013. V. 12. № 10. P. 1569–1577.
109. Kalan S., Amat R., Schachter M.M., Kwiatkowski N., Abraham B.J., Liang Y., Gray N.S. // Cell Rep. 2017. V. 21. № 2. P. 467–481.
110. Mita M.M., Mita A.C., Moseley J.L., Poon J., Small K.A., Jou Y.M., Sankhala K.K. // Br. J. Cancer. 2017. V. 117. № 9. P. 1258–1268.
111. Desai B.M., Villanueva J., Nguyen T.T.K., Lioni M., Xiao M., Kong J., Smalley K.S. // PLoS One. 2013. V. 8. № 3. P. e59588.
112. Kang M., Kim W., Jo H.R., Shin Y.J., Kim M.H., Jeong J.H. // Int. J. Oncol. 2018. V. 53. № 2. P. 703–712.
113. Sim M.Y., Go M.L., Yuen J.S.P. // Life Sci. 2018. V. 203. P. 282–290.
114. Schwermer M., Lee S., Köster J., van Maerken T., Stephan H., Eggert A., Schramm A. // Oncotarget. 2015. V. 6. № 17. P. 15425.
115. Ambasta R.K., Gupta R., Kumar D., Bhattacharya S., Sarkar A., Kumar P. // Brief. Funct. Genom. 2019. V. 18. № 4. P. 230–239.
116. Wilkie M.D., Anaam E.A., Lau A.S., Rubbi C.P., Jones T.M., Boyd M.T., Vlatković N. // Cancer Lett. 2020. V. 478. P. 107–121.
117. Naseer, F., Saleem M. // Oncol. Rev. 2019. V. 13(2). № 421. P. 83–87.
118. Tonino S.H., Mulkens C.E., van Laar J., Derks I.A., Suo G., Croon-de Boer F., Kater A.P. Leuk. Lymphoma. 2015. V. 56. № 8. P. 2439–2447.
119. Fomenkov A., Zangen R., Huang Y.P., Osada M., Guo Z., Fomenkov T., Ratovitski E.A. // Cell Cycle. 2004. V. 3. № 10. P. 1285–1295.
120. Deyoung M.P., Ellisen L.W. // Oncogene. 2017. V. 26. № 36. P. 5169–5183.
121. Meng J., Tagalakis A.D., Hart S.L. // Sci. Rep. 2020. V. 10. № 1. P. 1–12.
122. Huang L., Li A., Liao G., Yang F., Yang J., Chen X., Jiang X. // Oncol. Lett. 2020. V. 14. № 1. P. 1080–1088.
123. Yudhani R.D., Astuti I., Mustofa M., Indarto D., Muthmainah M. // APJCP. 2019. V. 20. № 6. P. 1667.
124. Yi Y., Zhang W., Yi J. Xiao Z.X. // J. Cancer. 2019. V. 10. № 11. P. 2434.
125. Prabhu V.V., Hong B., Allen J.E., Zhang S., Lulla A.R., Dicker D.T., El-Deiry W.S. // Cancer Res. 2016. V. 76. № 7. P. 1989–1999.
126. Zhang S., Zhou L., Hong B., van den Heuvel A.P.J., Prabhu V.V., Warfel N.A., El-Deiry W.S. // Cancer Res. 2015. V. 75. № 18. P. 3842–3852.
127. Sinha N., Panda P.K., Naik P.P., Das D.N., Mukhopadhyay S., Maiti T.K., Sethi G. // Mol. Carcinog. 2017. V. 56. № 11. P. 2400–2413.
128. Sinha N., Meher B.R., Naik P.P., Panda P.K., Mukhapadhyay S., Maiti T.K., Bhutia S.K. // Phytomedicine. 2019. V. 55. P. 179–190.
129. Sznarkowska A., Kostecka A., Kawiak A., Acedo P., Lion M., Inga A., Zawacka-Pankau J. // Cell Div. 2018. V. 13. № 1. P. 1–12.
130. Gomes S., Raimundo L., Soares J., Loureiro J.B., Leão M., Ramos H., Chlapek P. // Cancer Lett. 2019. V. 446. P. 90–102.
131. Di C., Sun C., Li H., Si J., Zhang H., Han L., Gan L. // Cell Cycle. 2015. V. 14. № 23. P. 3725–3733.
132. Novelli F., Lena A.M., Panatta E., Nasser W., Shalom-Feuerstein R., Candi E., Melino G. // Cell Death Dis. 2016. V. 7. № 5. P. e2227.
133. Gunaratne P.H., Pan Y., Rao A.K., Lin C., Hernandez–Herrera A., Liang K., Kim S.S. // Cancer. 2019. V. 125. № 14. P. 2409–2422.
134. Rong J., Li P., Ge Y., Chen H., Wu J., Zhang R., Zhang Y. // Colloids Surf. B. 2020. V. 186. P. 110674.
135. He W., Yan J., Li Y., Yan S., Wang S., Hou P., Lu W. // J. Control. Release. 2020. V. 325. P. 293–303.
136. Lundsten S., Hernández V.A., Gedda L., Sarén T., Brown C J., Lane D.P., Nestor M. // Nanomaterials. 2020. V. 10. № 4. P. 783.
137. Viktorsson K., De Petris L., Lewensohn R. // Biochem. Biophys. Res. Commun. 2005. V. 331. № 3. P. 868–880.
138. Mayer C., Popanda O., Greve B., Fritz E., Illig T., Eckardt-Schupp F., Schmezer P. // Cancer Lett. 2011. V. 302. № 1. P. 20–28.
139. Paul S., Barker C.A., Turner H.C., McLane A., Wolden S.L., Amundson S.A. // Radiat. Res. 2011. V. 175. № 3. P. 257–265.
140. Akiyoshi T., Kobunai T., Watanabe T. // Surg. Today. 2011. V. 42. № 8. P. 713–719.
141. Zhang W.W., Li L., Li D., Liu J., Li X., Li W., Hu A. // Hum. Gene Ther. 2018. V. 29. № 2. P. 160–179.
142. Orth M., Lauber K., Niyazi M., Friedl A.A., Li M., Maihöfer C., Belka C. // Radiat. Environ. Biophys. 2014. V. 53. № 1. P. 1–29.
143. Kovács D., Igaz N., Keskeny C., Bélteky P., Tóth T., Gáspár R., Kiricsi M. // Sci. Rep. 2016. V. 6. P. 27902.
144. Swanner J., Mims J., Carroll D.L., Akman S.A., Furdui C.M., Torti S.V., Singh R.N. // Int. J. Nanomedicine. 2016. V. 10. P. 3937.
145. Merkel O., Taylor N., Prutsch N., Staber P.B., Moriggl R., Turner S.D., Kenner L. // Mutat. Res. Rev. Mutat. Res. 2017. V. 773. P. 1–13.

Genetic Diversity and Evolution of the Biological Features of the Pandemic SARS-CoV-2

A. A. Nikonova*, E. B. Faizuloev, A. V. Gracheva, I. Yu. Isakov, V. V. Zverev
Mechnikov Research Institute for Vaccines and Sera, Moscow, 105064 Russia
*E-mail: aa.nikonova@nrcii.ru
Received January 19, 2021; in final form, April 13, 2021
DOI: 10.32607/actanaturae.11337

ABSTRACT **The new coronavirus infection (COVID-19) represents a challenge for global health. Since the outbreak began, the number of confirmed cases has exceeded 117 million, with more than 2.6 million deaths worldwide. With public health measures aimed at containing the spread of the disease, several countries have faced a crisis in the availability of intensive care units. Currently, a large-scale effort is underway to identify the nucleotide sequences of the SARS-CoV-2 coronavirus that is an etiological agent of COVID-19. Global sequencing of thousands of viral genomes has revealed many common genetic variants, which enables the monitoring of the evolution of SARS-CoV-2 and the tracking of its spread over time. Understanding the current evolution of SARS-CoV-2 is necessary not only for a retrospective analysis of the new coronavirus infection spread, but also for the development of approaches to the therapy and prophylaxis of COVID-19. In this review, we have focused on the general characteristics of SARS-CoV-2 and COVID-19. Also, we have analyzed available publications on the genetic diversity of the virus and the relationship between the diversity and the biological properties of SARS-CoV-2, such as virulence and contagiousness.**
KEYWORDS **coronaviruses, SARS-CoV-2, pathogenicity, virulence, contagiousness, virus evolution, viral genome.**

INTRODUCTION

After the first cases of infection were reported in Wuhan, China, in December 2019, the novel coronavirus infection COVID-19 caused by SARS-CoV-2 spread throughout the world and became the first coronavirus pandemic in human history [1]. As of March 2021, COVID-19 had been diagnosed in more than 117 million people worldwide, with more than 2.6 million deaths [2]. Currently, preventive vaccines are far from available in all countries or to all segments of their populations; therefore, quarantine, social distancing, and special sanitary precautions have remained the most potent measures to prevent the further spread of the infection.

The rapid and worldwide spread of the new coronavirus is inevitably associated with its divergence and the emergence of strains with various biological properties, the most significant of which is virulence. Very little is known about the phenotypic diversity of SARS-CoV-2, given the short period during which it has been investigated. Unfortunately, the available reports on genomic sequences provide limited information about the patient and are confined to age and gender, while, often, information on the severity, manifestations, and outcome of the disease is lacking.

One of the topical issues of fundamental and medical virology is the identification of the nature of the pathogenicity and virulence of viruses, including those of animal origin. Despite the progress made in understanding the evolution of viruses, the question of the evolution of virulence resulting from interspecies transmission remains open. Does the virus become more or less virulent in a new host? How is the degree of virulence modulated by natural selection and why? Are there regularities in the evolution of virus virulence in a new host which can allow one to predict the direction of this process? A simplified interpretation of virulence evolution is that natural selection optimizes the level of virulence in a way that increases the efficiency of viral transmission, which is characterized by the basic reproduction number (R0) [3]. The adaptation of a virus to a new host is affected by a complex set of host–pathogen interactions. According to modern concepts, during interspecies transmission, the initial virulence of a virus can vary from an absence of pathogenicity (asymptomatic carriage) to a high pathogenicity, while it remains very difficult to predict the direction in which virulence will evolve. Mankind has rarely faced a highly virulent pandemic virus of

animal origin – once every several decades – but the consequences of such an occurrence are dire and often global in scope. In such a context, it is of extreme importance to understand and predict how the biological properties of the SARS-CoV-2 coronavirus can evolve. The purpose of this review is to analyze the results of scientific studies that have focused on the relationship between genetic changes in the SARS-CoV-2 virus and its biological properties, including pathogenicity, virulence, and contagiousness.

The *pathogenicity* of a virus is defined as its ability to cause a disease. The term "virulence" can have different meanings depending on the context. In this review, the *virulence* of a virus means the measure of its pathogenicity; i.e., its ability to cause more or less severe diseases; the degree of virulence is determined by the mortality rate. The *contagiousness* (transmissibility) of a virus is its ability to move from infected organisms to healthy ones. Contagiousness is assessed with two interrelated indicators: the contagiousness index (the proportion of susceptible persons infected after contact with a source of the pathogen) and the basic reproduction number R0 (the average number of cases directly infected by one case during the entire infectious period in a completely susceptible population).

GENERAL CHARACTERIZATION OF SARS-CoV-2

The pandemic SARS-CoV-2, along with the SARS-CoV virus, belongs to the Coronaviridae family, Orthocoronavirinae subfamily, *Betacoronavirus* genus, *Sarbecovirus* subgenus, and *Severe acute respiratory syndrome-related coronavirus* species [4]. It should be noted that, along with the listed pathogens, the *Sarbecovirus* subgenus also includes coronaviruses isolated from bats; in particular, horseshoe bats (*Rhinolophus* genus) [5]. The genome sequence of SARS-CoV-2 was found to be 96.2 and 93.3% identical to that of the raTG13 [6] and RmYN02 [7] bat coronaviruses, respectively. The degree of nucleotide sequence similarity and evolutionary analysis lends credibility to the hypothesis that bats are the natural reservoir of the SARS-CoV-2 that was transmitted to humans through unknown intermediate hosts [8, 9]. In addition, the SARS-CoV-2 genome has been shown to be 85.5–92.4% similar to that of coronaviruses isolated from pangolins [10], 80% to SARS-CoV [6], and 50% to MERS-CoV (*Merbecovirus* subgenus) [11]. However, the degree of genome homology varies greatly depending on genes and genomic loci [5]. In this case, the main differences between these viruses reside in the *ORF1a* sequence and the gene encoding the spike protein S that plays a key role in the interaction of the virus with the cell [12]. These features of genome organization may be a result of some interviral recombination [13].

SARS-CoV-2 virions are pleiomorphic (usually spherical), with an average diameter of 108 ± 8 nm, ranging from 84 to 126 nm [14]. The spikes on the surface of viral particles, about 9–12 nm long, give the virus its characteristic crown appearance. The morphology of SARS-CoV-2 virions is similar to that of other members of the Coronaviridae family, including SARS-CoV and MERS-CoV [15].

The SARS-CoV-2 genome is a nonsegmented, single-stranded, positive sense RNA, 29.9 kb in size, and consists of six main open reading frames (ORF) (*Fig. 1*). Translation of virus-encoded RNA-dependent RNA polymerase (replicase) is necessary for the initiation of viral replication in the cell and the synthesis of the subgenomic viral RNAs that, in turn, serve as a matrix for the synthesis of viral structural and accessory proteins [16]. The size of *ORF1ab*, which encodes replicase, is 2/3 of the size of the entire viral genome. *ORF1ab* is followed by the genes for the spike protein (*S*), *ORF3a*, envelope protein (*E*), membrane protein (*M*), *ORF6*, *ORF7a*, *ORF7b*, *ORF8*, nucleocapsid (*N*), and *ORF10*. In addition, Nelson *et al.* proved that SARS-CoV-2 contains a new overlapping gene (OLG) *ORF3d* [17] that is also present in coronaviruses isolated from pangolins in the Guangxi region of Southern China, but that it is not found in other coronaviruses isolated from pangolins and bats.

The spike protein S of the SARS-CoV and SARS-CoV-2 coronaviruses initiates a fusion of the viral envelope with the cell membrane of the host cell, and the angiotensin-converting enzyme 2 (ACE2) serves as a cellular receptor for the attachment of the virus. The receptor for MERS-CoV is hDPP4 (human dipeptidyl peptidase 4 or CD26) [18]. The S protein comprises two domains, S1 and S2. The S1 domain mediates the binding to ACE2, while the S2 domain mediates subsequent fusion of the viral envelope with a cell's membrane [19]. The receptor binding domain (RBD) is a key functional component of S1, which is responsible for the binding of SARS-CoV-2 to ACE2 [20]. In addition, the SARS-CoV RBD contains a core motif and a receptor binding motif (RBM) that mediates the contacts with ACE2. The surface of ACE2 contains two virus-binding hotspots that are essential for SARS-CoV-2 binding [21]. The stage of adsorption and penetration of SARS-CoV-2 into a cell depends not only on the ACE2 receptor, but also on the transmembrane serine protease TMPRSS2 and proprotein convertase furin, whose role is to prime the SARS-CoV-2 S protein [22, 23]. Thus, SARS-CoV-2 can enter a cell in two different ways (*Fig. 2*): through the late endosome where the S protein is cleaved by cathepsins, or through the cell membrane or early endosome using trypsin-like proteases to cleave the S protein [23, 24].

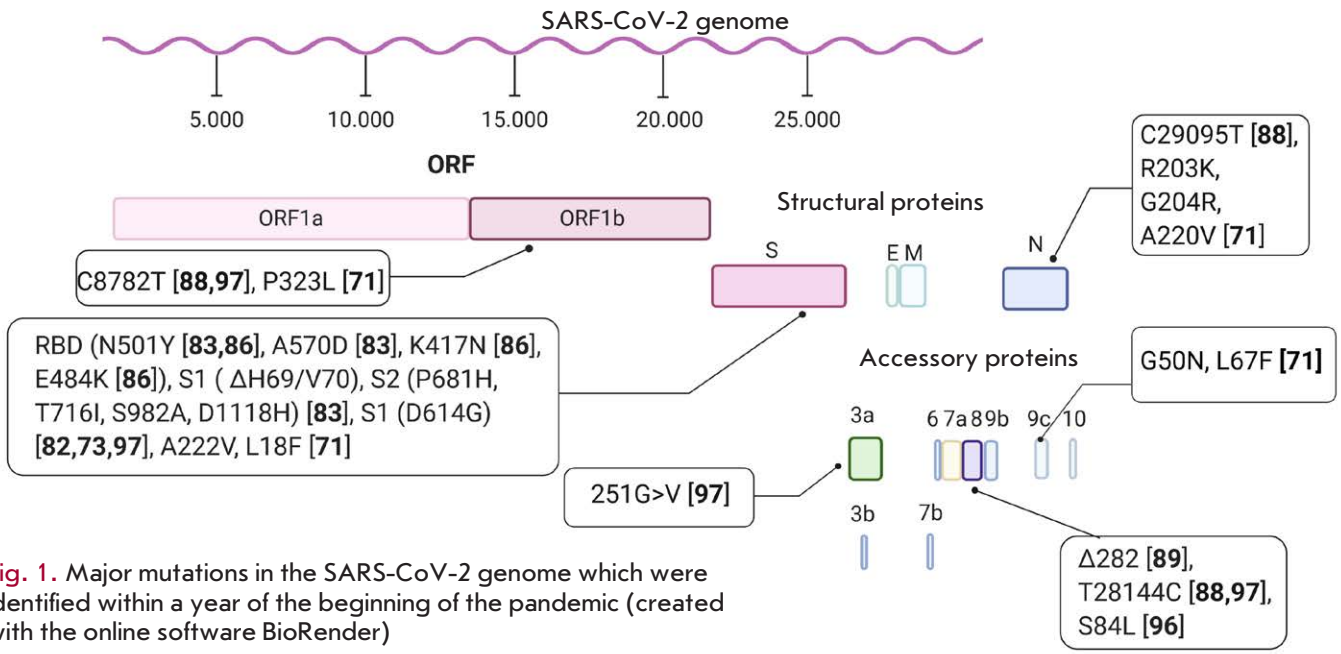

Fig. 1. Major mutations in the SARS-CoV-2 genome which were identified within a year of the beginning of the pandemic (created with the online software BioRender)

The E protein forms ion channels and regulates the assembly of virions [25]. The M protein is also involved in the assembly of viral particles [26], while the N protein forms a ribonucleoprotein complex with viral RNA and performs several functions, such as enhancing the transcription of the viral genome and interacting with the viral membrane protein during virion assembly [27].

The receptor of target cells, which is used by the virus to enter a cell, is a factor in determining which organs and tissues are susceptible to infection. The ACE2 receptor is expressed on the surface of epithelial cells of the alveoli, trachea, bronchi, and bronchial glands, as well as on alveolar macrophages. In addition, ACE2 is present on mucous membranes, such as the cornea of the eye and goblet and ciliary cells in the nasal cavity [28], which appear to be the gateway to infection. The life cycle of the virus with the host consists of the following steps: the virus enters the cell using the ACE2 receptor and releases the single-stranded viral RNA that binds to the target cell's ribosome and initiates the synthesis of the RNA replicase that, in turn, reproduces copies of genomic and subgenomic RNA, as well as RNA fragments that serve as templates for the synthesis of viral envelope proteins. Positive-sense viral RNA molecules, together with structural viral proteins, form new SARS-CoV-2 virions that are released from the cell and infect intact target cells (*Fig. 2*) [29].

VARIETY OF CLINICAL MANIFESTATIONS OF COVID-19

The severity of the disease caused by SARS-CoV-2 can vary significantly [30]. There is great variability in the clinical presentations of COVID-19 even among close contacts of an infected person or members of the same family [30]. The spectrum of COVID-19 symptoms ranges from mild/moderate to critical and fatal [31–33]. Also, an asymptomatic course of the disease is often observed. The rate of asymptomatic cases can amount to 40–50%, and an infected person remains a source of infection for more than 14 days [34]. In addition, an asymptomatic course of the infection can be associated with subclinical changes in the lungs, which are detected during computed tomography [34]. Therefore, SARS-CoV-2 possesses increased virulence with a tactical advantage – the ability to maintain human-to-human transmission even in asymptomatic carriers [35], which allows the virus to spread rapidly.

According to a report issued by the Chinese Center for Disease Control and Prevention [36], an analysis of 44,500 confirmed cases of infection with an assessment of the disease severity revealed that a mild form of COVID-19 (nonpneumonia and mild pneumonia) is observed in 81% of cases. A severe form (dyspnea, hypoxia, or lung involvement of >50%) was reported in 14% of cases. And 5% of cases were critical (respiratory failure, shock, or multiple organ dysfunction). In this case, the overall mortality rate was 2.3% (no deaths among non-critical cases).

A severe form of the COVID-19 disease can be observed in any healthy person of any age, but it occurs mainly in people over 65 years of age and/or with concomitant diseases (cardiovascular diseases, diabetes mellitus, hypertension, chronic lung and kidney diseases, cancer, obesity, smoking) [32, 36, 37], while, in

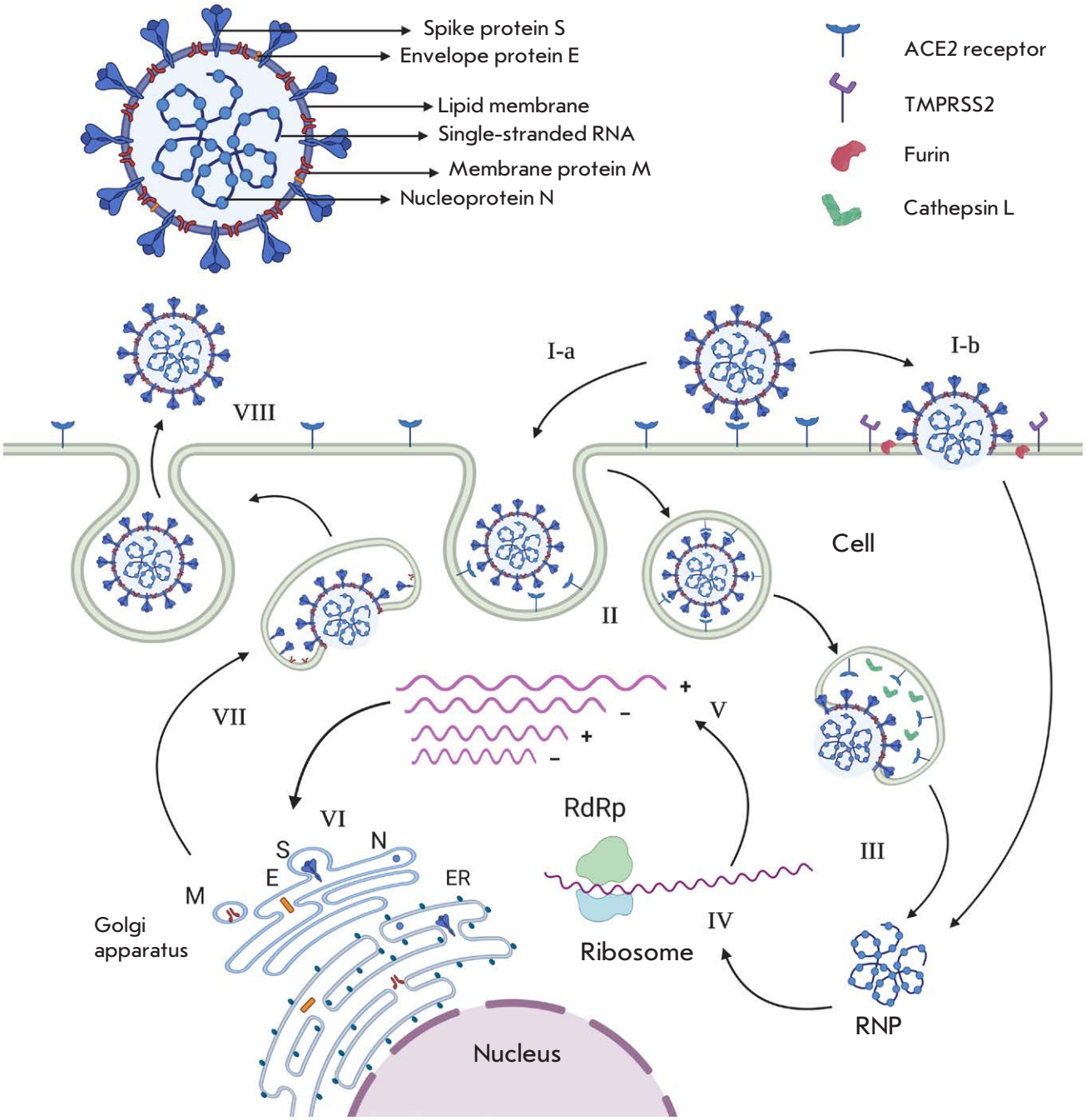

Fig. 2. The SARS-CoV-2 virion and life cycle (created with the online software BioRender)
I. Virus binding. After adsorption, the virus can enter the cell in two ways: through the endosome (I-a) or through fusion with the cell membrane (I-b)
II. Receptor-mediated endocytosis
III. Fusion of the virus envelope with the endosome membrane results in virus uncoating. Release of the ribonucleoprotein complex (RNP)
IV. Viral genome translation. Synthesis of the viral proteins (including RNA-dependent RNA polymerase (RdRp) involved in genome replication and transcription
V. Replication and transcription of the viral genome
VI. Viral proteins are synthesized at the endoplasmic reticulum (ER) lumen
VII. Assembly and transport of the virions to the cell membrane
VIII. Release of the virions by exocytosis

most young adults, the infection is mild and without complications.

There are several complications associated with COVID-19. These include the acute respiratory distress syndrome, which is a type of respiratory failure that requires critical care support, including artificial ventilation of the lungs. This care is required in 12 to 24% of hospitalized patients [38, 39]. Also, cardiovascular [40] and thromboembolic complications [41], inflammatory reactions [42], and superinfections [43] are observed.

Children are the least susceptible to infection. They account for 1 to 6.3% of COVID-19 cases [44, 45]. According to a report by China's Center for Disease Control and Prevention, of the 72,314 cases reported as of February 11, 2020, only 2% were under the age of 19 [36]. Multisystem inflammatory syndrome with clinical signs similar to Kawasaki's disease and toxic shock syndrome were reported in children with COVID-19 [46]. Monitoring of children infection by Meskina [45] showed that the rate of asymptomatic COVID-19 cases in children was 62%, with that in newborns being 73.1%, and the rate of severe forms being as low as 0.38%.

GENETIC DETERMINANTS OF SARS-CoV-2 VIRULENCE

The question of the causes behind the diverse clinical presentations of COVID-19 in different categories of the population remains open. It may be that this diversity depends on certain genetic profiles of a host organism. In accordance with this hypothesis, the genetic basis of the susceptibility to infection may be explained by the polymorphism of the functional receptors required for virus entry into target cells. In particular, multiple organ dysfunctions in COVID-19, including fatal damage to the lungs and myocardium, may be associated with the functional characteristics of the ACE2 receptors in the population [47–49]. For example, Hou *et al.*, based on an analysis of ~ 81,000 human genomes, investigated the association between the polymorphism of the *ACE2* and *TMPRSS2* genes (two key host factors of SARS-CoV-2) and susceptibility to COVID-19. *ACE2* polymorphisms (p.) (e.g., p.Arg514Gly in the African/African American population) were found to be associated with the cardiovascular and pulmonary diseases through altered angiotensinogen–ACE2 interactions. Unique but prevalent polymorphisms (including p.Val160Met (rs12329760)) in *TMPRSS2* have the potential to cause differential genetic susceptibility to COVID-19 [50].

A genome-wide association study (GWAS) analyzed 8,582,968 single nucleotide polymorphisms (SNPs) from 1,980 severe COVID-19 patients from the Italian and Spanish epicenters of the pandemic in Europe. The study did not reveal any significant associations of a severe form of the disease with a single gene. Rather, it did so with a multigene cluster on chromosome 3 (*SLC6A20*, *LZTFL1*, *CCR9*, *FYCO1*, *CXCR6*, and *XCR1* genes) [51].

Chinese scientists analyzed the genetic profiles of 332 patients with varying severity of COVID-19 using NGS techniques. The results of a genome-wide association study (GWAS) indicated that the most significant locus associated with disease severity was located in *TMEM189–UBE2V1*, which is involved in the interleukin-1 (IL-1) signaling pathway. The rate of p.Val197Met missense variants of the *TMPRSS2* gene, which affect the stability of the protein, is lower in patients with a severe infection than in patients with a mild form of the disease and the general population. In addition, the HLA-A*11:01, B*51:01, and C*14:02 alleles were found to significantly predispose people to a severe course of COVID-19 [52].

Selectivity for host genetic profiles (as a factor of SARS-CoV-2 virulence) may be one of the viral features. This property was not reported in the influenza virus which caused the global pandemic in 1918. This may be because, in the early 1900s, the level of technological evolution and knowledge did not allow for conducting research on the topic. There is data indicating that susceptibility to HIV-1 is genetically determined by variations in the host chemokine receptors [53]. This data suggests that this selectivity may determine the virulence and tissue specificity of other viruses, including SARS-CoV-2.

Studies of the molecular mechanisms of the pathogenicity and contagiousness of coronaviruses have focused on the determinants of coronavirus tropism to the cells of the human respiratory tract, which is associated with receptor-mediated virus entry into the cell. These determinants are present on the surface S protein of coronaviruses. Mutations in S protein epitopes, which are responsible for the binding to viral receptors, are believed to determine the efficiency of interspecies transmission and adaptation of the virus to a new host [54]. There is experimental evidence that the bat coronavirus, whose S-protein can be modified by reverse genetics methods, is able to overcome the species barrier (to infect human cells) [55]. However, to date, there has been no experimental confirmation that the SARS-CoV-2 S protein alone mediates contagiousness or the high virulence of the virus in humans. Previously, a highly pathogenic avian influenza A virus, H5N1, was used to prove that an ability to recognize the viral receptors of epithelial cells in the respiratory tract of mammals could be achieved by introducing two to four amino acid substitutions into hemagglutinin (HA), which are essential for the binding of HA to α-2,6-sialic receptors [56, 57]. However, these mu-

tations alone were not enough for a virus to acquire contagiousness and high virulence for ferrets [56, 57]. This indicates that additional determinants of contagiousness and virulence are likely encoded in the internal genes of the virus. The pathogenicity of the virus is mediated not only by its ability to effectively penetrate target cells, but also by many other viral factors. An example of this is vaccine strains that are used as live, attenuated vaccines. According to Klimov *et al.* [58], the determinants of the attenuation of the cold-adapted vaccine strain of influenza A/Leningrad/134/47/17 are mutations in the genes of the polymerase complex proteins (PB1, PB2, PA, NP), M-protein, and the nonstructural protein NS2, but not in the genes of the surface proteins neuraminidase N and hemagglutinin H. Review [3] provides more than 10 examples of changes in the virulence of various mammalian viruses which are caused by only one or two amino acid substitutions. Most of these examples concern RNA viruses (influenza A and B viruses, enteroviruses, Ebola virus, HIV, West Nile virus, Newcastle disease virus, porcine reproductive and respiratory syndrome virus, etc.).

Viruses of the same biological species can significantly differ in virulence, something associated with divergence in the course of evolution. The mortality rate from an infection with seasonal influenza A viruses (*Influenza A virus* species of the Orthomyxoviridae family) of the H3N2 and H1N1 serotypes is 0.04–1.0%, while that from diseases caused by some strains of the avian influenza A virus, including H5N1, H7N7, H9N2, H7N3, and H7N9, reaches 60% [59, 60]. Human coronaviruses are no exception. The so-called seasonal coronaviruses (HCoV-NL63, -229E, -OC43, -HKU1) are associated mainly with mild and moderate forms of acute respiratory viral infections, while coronaviruses of animal origin (SARS-CoV, MERS-CoV, and SARS-CoV-2) are associated with the development of a severe acute respiratory syndrome and a higher risk of mortality (according to various estimates, 1 to 40% of the number of laboratory-confirmed cases).

Recently, the Koonin's group identified possible genetic determinants for the increased mortality from an infection with the highly virulent coronaviruses SARS-CoV, MERS-CoV, and SARS-CoV-2 compared to that from the low-virulent seasonal HCoV-NL63, -229E, -OC43, and -HKU1 [61]. An analysis of more than 3,000 coronavirus genomes revealed that the genome of the highly pathogenic coronaviruses SARS-CoV, MERS-CoV, and SARS-CoV-2 contains four regions (three in the N nucleoprotein gene and one in the S protein gene) significantly different in amino acid sequences from seasonal coronaviruses [61]. The differences in the *N* gene presumably determine the enhancement of signals for nuclear localization and export of this protein. Differences in the *S* gene occur at the site of receptor recognition and fusion of the viral envelope with the cell membrane and are hypothetically responsible for enhancing the stage of virus attachment and entry into the cell. The obtained results shed light on the potential determinants of coronavirus virulence, but they have not yet been empirically confirmed, because the work was performed using computer-based analysis methods.

New mutations constantly occur in the genome of any virus, and some of these are capable of changing the biological properties of the virus, including the degree of contagiousness, ability to evade the host's immune response, and virulence. The viral RNA genome of SARS-CoV-2 is characterized by a high mutation rate (but lower than that of other RNA viruses) [62].

To date, hundreds of thousands of genome sequences for the SARS-CoV-2 coronavirus are known. The results of multiple studies have enriched the GISAID genome sequence database, which, as of January 2021, includes information on more than 323,493 sequences. In addition to SARS-CoV-2, GISAID contains the genome sequences of coronaviruses isolated from bats and pangolins. Based on data from viral sequences and information on the geographical origin of the samples in GISAID, another information resource, Nextstrain (https://nextstrain.org) [63] publishes hosts phylogenetic, geographic, and genomic analyses of SARS-CoV-2. Using the GISAID database and Nextstrain resource, the evolution of a virus can be monitored in real time. The Nextstrain analysis predicts the occurrence of approximately 26 substitutions in the SARS-CoV-2 genome per year. Given the SARS-CoV-2 genome size (29.9 kb), the estimated evolutionary rate is approximately 0.90×10^{-3} substitutions/site/year [5]. This value is comparable with values reported for SARS-CoV ($0.80–2.38 \times 10^{-3}$) [64], MERS-CoV ($0.63–1.12 \times 10^{-3}$) [65], and HCoV-OC43 (0.43×10^{-3}) [66]. Since the coronavirus genome encodes a 3'–5'-exoribonuclease (nsp14-ExoN) that has editing activity, the mutation rate (the number of single nucleotide substitutions per site per replication cycle) is likely to be lower in SARS-CoV-2 than in other RNA viruses, such as influenza viruses [67]. This underlies the high stability of the genome of coronaviruses, including SARS-CoV-2. An analysis of the nucleotide sequences of 48,635 virus isolates confirmed the low mutation rate, which was 7.23 mutations per sample, on average, compared with the reference SARS-CoV-2 genome (NC_0455122) [68].

In addition, the SARS-CoV-2 genome was shown to have a much lower mutation rate and genetic diversity compared to those of the SARS-CoV virus that caused the outbreak of SARS in 2002–2003 [69]. It should also be noted that the S protein RBD domain (~90 amino

Table 1. Major genetic variants of SARS-CoV-2

Genetic SARS-CoV-2 variant	Region where it was first detected	Typical mutations	Characteristic features
B.1.1.7	United Kingdom	S protein: RBD (N501Y, A570D), S1 (ΔH69/V70) S2 (P681H, T716I, S982A, and D1118H)	High contagiousness
B.1.351 (N501Y.V2)	Republic of South Africa	S protein: RBD (K417N, E484K, and N501Y)	Some vaccines are less effective against this variant, high contagiousness
P1 descendant of B.1.1.28	Brazil	S protein: RBD (E484K, K417T, and N501Y)	High contagiousness
Fin-796H	Finland	S protein: RBD (E484K, K417T, and N501Y)	Not detectable in PCR

acids) of SARS-CoV-2, which reacts directly with the ACE2 receptor on the surface of target cells, differs significantly from the SARS-CoV RBD, especially in two regions that interact with ACE2, and is the part of SARS-CoV-2 most susceptible to variations [70]. The latter suggests the participation of several mechanisms involved in virus entry into the cell. Six amino acid residues of the S protein RBD (Leu455, Phe486, Gln493, Ser494, Asn501, and Tyr505) were found to play a key role in the binding to ACE2. In this case, five of them differ from the SARS-CoV RBD, which should be considered in the development of specific antiviral agents that block virus entry into the cell [70].

It should be noted that numerous elements of the virus genome are mutated at different rates. For example, an analysis of about 223,000 full-length sequences of the SARS-CoV-2 proteome was used to calculate the mutation rate of each viral protein. The highest mutation rates were observed in the S, NSP12, NS9c, and N proteins [71].

An analysis of the nucleotide sequences of SARS-CoV-2 isolates revealed several genome regions with an increased mutation rate [72–81]. One of these regions is D614G, in the C-terminal region of the S1 domain [72–74, 77, 81]. A mutant virus with a D614G substitution in the S1 domain was shown to be prevalent in Europe [68]. Comparison of the functional properties of the S protein with aspartic acid at position 614 (S^{D614}) and glycine (S^{G614}) showed that pseudoviruses carrying S^{G614} enter ACE2-expressing cells more efficiently than viruses with S^{D614} [82]. While evidence continues to accumulate, a growing proportion of the virus with the D614G substitution suggests that viruses with this mutation are characterized by a more efficient person-to-person transmission. Interestingly, this mutation does not appear to significantly affect the severity of the disease [73, 79].

In December 2019, isolation of a new SARS-CoV-2 strain with an increased level of contagiousness was reported in the UK [83]. According to the data of a phylogenetic analysis, this strain forms a distinct phylogenetic cluster (lineage B.1.1.7) [84]. Seven characteristic mutations were identified in the S protein of this virus: RBD (N501Y, A570D), S1 (ΔH69/V70), and S2 (P681H, T716I, S982A, and D1118H) [83]. The N501Y mutation in the receptor binding domain (RBD) provides increased affinity for human and mouse ACE2 [85]. The ΔH69/V70 deletion in S1 enhances the ability of the virus to evade the immune response. The P681H mutation is directly adjacent to the furin cleavage site between S1 and S2 in the S protein. In addition, there is data pointing to the existence of several independent SARS-CoV-2 lineages that are characterized by the ΔH69/V70 deletion in the S protein and an increase in the circulation of these viruses in some European countries since August 2020 [83].

In January 2021, a new SARS-CoV-2 (501Y.V2) lineage emerged in South Africa. It quickly spread and became prevalent in several regions of the country. There are eight S protein mutations characteristic of this lineage; in particular three in the RBD (K417N, E484K, and N501Y) which may be of functional value. Two of these (E484K and N501Y) are located in the receptor binding motif (RBM) that directly interacts with ACE2 [86]. The N501Y mutation is also characteristic of the B.1.1.7 lineage identified in the UK. Perhaps, this mutation determines the level of SARS-CoV-2 contagiousness.

There are also reports of a new SARS-CoV-2 P.1. lineage in Brazil [87]. It is necessary to note the emergence of convergent mutations common to the P1, B.1.1.7, and B.1.351 lineages (*Table 1*). These are the N501Y mutation in the S protein and a deletion in ORF1b (del11288–11296 (3675–3677 SGF)) common to P.1. and the British B.1.1.7, as well as mutations in the RBD (K417N/T, E484K, N501Y) typical of both P.1. and the South African B.1.351.

The set of mutations/deletions characteristic of the P.1., B.1.1.7, and B.1.351 lineages appeared, probably, quite independently. In addition, mutations common to P.1. and B.1.351 are probably associated with a rapid increase in the number of infection cases in areas where high morbidity rates were previously observed. Therefore, it is imperative to establish if there is an increased risk of re-infection in people who have had COVID-19 [87]. There is information about isolation of a new SARS-CoV-2 strain (Fin-796H) that is similar to both the British and South African variants of the virus, but identification of this variant by PCR can be difficult.

It should be noted that mutations in the *S* gene are of particular interest to researchers. The GISAID resource regularly updates data on variants of the S protein gene of the SARS-CoV-2 virus. The most common variants as of January 2021 are shown in *Fig. 1*.

An analysis of 95 full-length SARS-CoV-2 genome sequences available in GenBank for the period from December 2019 to April 2020 revealed 116 mutations, with the most frequent mutations being 8782C > T in the *ORF1ab* gene, 28144T > C in the *ORF8* gene, and 29095C > T in the *N* gene. The identified mutations are supposed to affect the virulence and contagiousness of SARS-CoV-2 [88].

Another attempt to investigate a relationship between certain mutations in the SARS-CoV-2 genome and the virulence of the virus was made by Young *et al.* [89]. In particular, they studied how a 382-nucleotide deletion (Δ382) in the *ORF8* region of the SARS-CoV-2 genome affects the clinical features of infection. The Δ382 variant of SARS-CoV-2 was found to be probably associated with a milder infection.

Currently, the collection and analysis of data on any relationship between mutations in the SARS-CoV-2 genome and the virulence and contagiousness of the virus is underway. The main mutations identified during the year of circulation of the pandemic virus are presented in *Fig. 1*. Obviously, a significant proportion of the mutations affecting the transmissibility of the virus are present in the gene encoding the S protein. This very important finding should be considered by developers of vaccines against SARS-CoV-2, the overwhelming majority of which are based on the S protein [90]. Sera from 20 people vaccinated with BNT162b2 (RNA vaccine encoding the S protein) was shown to neutralize SARS-CoV-2 pseudoviruses with N501 and Y501 mutations [91]. Probably, other proteins of the virus, including the nucleocapsid N protein, should be considered during the development of vaccines. For example, 90% of the epitopes in the T-cell response are located in ORF1ab of the SARS-CoV-2 nucleocapsid protein gene [92].

SYSTEMATIZATION AND GEOGRAPHIC DISTRIBUTION OF SARS-CoV-2 GENETIC VARIANTS

Molecular genetic monitoring of the new coronavirus infection and phylogenetic analysis has enabled us to identify various genetic SARS-CoV-2 variants different in their geographic distribution. There are several approaches to a comparative genomic analysis of SARS-CoV-2 variants. One of them, proposed by Forster *et al.*, distinguishes three main SARS-CoV-2 variants (A, B, C) that differ in their amino acid substitutions. During a phylogenetic analysis, the closely related bat coronavirus BatCoVRaTG13 isolated in Yunnan Province [93] was identified as ancestral and placed at the base of the phylogenetic tree (cluster A) [94]. There are two subclusters of A which distinguish themselves by the synonymous mutation T29095C. Variant B is derived from A by two mutations: the synonymous mutation T8782C and the nonsynonymous mutation C28144T changing a leucine to a serine. In this case, type C differs from its parent type by the nonsynonymous mutation G26144T which changes a glycine into a valine [94]. Types A and C circulate mainly in Europe and America. On the contrary, type B is most prevalent in East Asia and its ancestral genome has not, apparently, spread beyond East Asia, which suggests the existence of immunological or ecological resistance to this type outside Asia [94]. These studies were complemented by the work of a group of scientists from Hong Kong [95] who performed a phylogenetic and philodynamic analysis of 247 SARS-CoV-2 genome sequences available in the GISAID database as of March 5, 2020. Among them, four genetic viral clusters, called "super-spreaders" (SSs), were identified, which were responsible for the major outbreaks of COVID-19 in various countries. For example, SS1 was widely disseminated in Asia and the United States and was mainly responsible for the outbreaks in the states of Washington and California, as well as South Korea, while SS4 contributed to the pandemic in Europe. Using the signature mutations of each SS as markers, the authors further analyzed 1,539 SARS-CoV-2 genome sequences reported after February 29, 2020 and found that 90% of these genomes were super-spreaders, with SS4 being prevalent [95]. Drawing parallels with the study [94], it should be noted that the virus identified as SS1 is equivalent to type B, SS2 is equivalent to type C, and type A is an ancestral variant. The results of a geographic distribution of different viral types are the same in both studies.

A population genetic analysis of 103 SARS-CoV-2 genomes revealed [96] that viruses may be divided into two main types (L and S) that differ in two point mutations in the amino acid sequence of site 84 (S84L) of the *ORF8* gene. Although the L type (~70%) is more preva-

Table 2. Modern approaches to the subspecies classification of SARS-CoV-2

Clades (GISAID [101]) and characteristic mutations		Lineages (Rambaut [103])	Clades (Hodcroft [105]) and characteristic mutations	
S	C8782T, T28144C, including NS8-L84S	A	19A 19B	C8782T T28144C
L	C241, C3037, A23403, C8782, G11083, G26144, T28144 (reference sequence is strain WIV04, GISAID: hCoV-19/Wuhan/WIV04/2019)	B.2	20A	C3037T, C14408T, and A23403G
V	G11083T, G26144T NSP6-L37F + NS3-G251V	B.1		
G	C241T, C3037T, A23403G, including S-D614G	B.1*		
GH	C241T, C3037T, A23403G, G25563T including S-D614G + NS3-Q57H	B.1.1.	20C	C1059T and G25563T
GR	C241T, C3037T, A23403G, G28882A, including S-D614G + N-G204R		20B	G28881A, G28882A, and G28883C
GV	C241T, C3037T, A23403G, C22227T, including S-D614G + S-A222V			

lent than the S type (~30%), the results of an evolutionary analysis suggest that the S type is most likely the ancestral SARS-CoV-2 version. In addition, the L type might be more aggressive and spread faster than S and human intervention may have changed the L/S ratio soon after the first outbreak of SARS-CoV-2. However, it is currently unclear whether the L type originated from the evolution of the human S type coronavirus or intermediate hosts. It is also unclear whether the L type is more virulent than the S type [96].

To assess the relationship between genetic mutations and the level of virus virulence, Zhang *et al.* analyzed clinical, molecular, and immunological data from 326 patients with a confirmed SARS-CoV-2 infection in Shanghai [97]. They identified two major clades. Clade I included several subclades characterized by differences in ORF3a: p.251G> V (subclade V) or S: p.614D> G (subclade G). Clade II differs from clade I in two linked mutations in ORF8: p.84L> S (28144T> C) and ORF1ab: p.2839S (8782C> T). This classification is inconsistent with the S/L classification [96] despite the fact that it is based on the same two related polymorphisms. In addition, the authors did not find any significant differences in the mutation rate and transmissibility in viruses belonging to clade I or II or in the clinical features of the diseases they cause.

Another approach to the systematization of genetic SARS-CoV-2 variants is offered in a preprint [98]. The authors compared viruses at a genome-wide level using the Jaccard similarity coefficient. In this case, they did not include information on the geographical origin of the samples into the analysis and did not try to model the evolutionary relationships of different SARS-CoV-2 genomes using a phylogenetic analysis. Nonetheless, the results of their analysis reflect the chronological spread of SARS-CoV-2 around the globe, from the first cases detected in China to the current outbreaks in Europe and North America. In addition, the use of the nucleotide sequences of 7,640 SARS-CoV-2 genomes presented in the GISAID database revealed that viruses cluster in four distinct genetic subgroups [98].

An analysis of tens of thousands of SARS-CoV-2 genomes, performed by a team of scientists from Temple University, identified an ancestral strain (preprint [99] published on the bioRxiv.org website). Over time, mutations in the ancestral virus genome gave rise to seven dominant lineages that spread across different continents. The use of molecular barcoding technology revealed that the genome sequences of the North American coronaviruses differed from those of the coronaviruses in circulation in Europe and Asia at that time [99].

An analysis of 75 whole genomes revealed six clusters, named Wuhan, Diamond Princess, Asian, European, USA, and Beijing [100]. Mutations in the gene encoding the spike glycoprotein S found in samples from South Korea, India, Greece, Spain, Australia, Sweden, and Yunnan may suggest a predominance of mutated strains with varying virulence.

Despite the variety of approaches to the classification of SARS-CoV-2, the GISAID consortium has developed its own generalized classification system [101] that distinguishes seven major clades (based on characteristic sets of mutations): S, L, V, G, GH, GR, and GV (*Table 2*).

According to [68], the G and GR clades are prevalent in Europe, while S and GH are predominant in North and South America. The reference clade L is represented mainly by sequences from Asia. Currently, the clade G and its offspring, GH and GR, are the most common clades among the sequenced SARS-CoV-2 genomes, globally accounting for 74% of all known sequences. In

particular, the GR clade, which carries a combination of S protein D614G and N protein RG203KR mutations, is currently the most abundant representative of SARS-CoV-2 worldwide. The original viral strain, represented by the clade L, still accounts for just 7% of the sequenced genomes [68].

An analysis of 1,566 SARS-CoV-2 genome sequences isolated in 10 Asian countries was carried out in [102]. The sequences were compared with the reference sequence of the WIV04 strain (Accession No. MN996528.1) to identify potential mutations in different regions of the genome. An *in silico* analysis showed that isolates from 10 Asian countries form clades G, GH, GR, L, S, O, and V. The highest mutation rate was detected in the GH and GR clades [102].

The GISAID classification is complemented with a more detailed, dynamic nomenclature system proposed by Rambaut *et al.* [103]. According to this system, 81 SARS-CoV-2 lineages can be distinguished, with most of them belonging to the A, B, and B.1 lineages. Six lineages derived from lineage A (A.1–A.6) and two descendant sublineages of A.1 (A.1.1 and A.3) are identified. Also, there are 16 lineages derived from lineage B. Lineage B.1, comprising 70 sublineages as of April 2020, is predominant. Lineage B.2 has six descendant sublineages. According to this classification, clades S, V, G, GH, GR, and GV correspond to lineages A, B.2, B.1, B.1*, and B.1.1 (*Table 2*) [68]. Based on this system, the pangolin software was developed [104]. It allows automatic classification of new genomes.

Another approach to systematization is described in a work by Hodcroft *et al.* [105]. The authors propose to name major clades by the year they emerged. In this case, the clade is formed from strains that have circulated for several months and have a characteristic geographic distribution. According to this classification, the following clades can currently be distinguished: 19A, 19B, 20A, 20B, and 20C (*Table 1*). Clades 19A and 19B were prevalent in Asia at the start of the pandemic, while 20A was detected in Europe in early 2020. 20B is another European clade, while 20C is a largely North American clade.

Therefore, efforts to develop a convenient and understandable classification system for the pandemic SARS-CoV-2 continue. It should be noted that at the time of preparation of our manuscript, no official ICTV guidelines for SARS-CoV-2 subspecies taxonomy had been published.

At the end of January 2020, the first cases of SARS-CoV-2 infection were detected in Russia, and since May 2020, Russia has been among the four countries with the largest number of confirmed COVID-19 cases. As of March 2021, 4.3 million cases of COVID-19 and 87,000 deaths have been reported in Russia. However, the outbreak in Russia began later than that in many neighboring European countries, possibly due to the measures taken to restrict transport links with China. A phylogenetic analysis of SARS-CoV-2 isolates from Russia showed that most samples correspond to the B.1, B.1.1, and B.1* lineages (PANGOLIN nomenclature) or to the G, GR, and GH clades (GISAID nomenclature), which are widespread in Europe [106]. In this case, the most prevalent genetic lineage is GR/20B/B.1.1 (GISAID/Nextstrain/Pangolin nomenclature, respectively) [107]. A phylogenetic analysis of Russian strains revealed that, as elsewhere, Russian SARS-CoV-2 isolates were characterized by a low mutation rate. However, a high rate of nonsynonymous mutations leading to non-conservative substitutions was found. Most of the nonsynonymous substitutions were found in nucleotide sequences encoding the N nucleoprotein. This finding may serve as indirect evidence of intensive circulation of the virus in the human population and its adaptation to new carriers [108].

CONCLUSION

The global spread of SARS-CoV-2 with the abrupt onset of a pandemic of viral infection new to the human immune system has created conditions where it is possible to collect sufficiently convincing data on whether the structure of clinical COVID-19 forms depends on dynamic changes in the genetically determined biological properties of the virus, or if it is determined only by the characteristics of the host. This issue is fundamental to vaccine development and public health resource planning. Twelve months since the start of the spread of the new coronavirus in the human population, there is less and less doubt about the divergence of SARS-CoV-2; i.e. about the emergence of strains that differ in their biological properties, which is due to the high plasticity of the genomes of RNA viruses and favorable conditions for their evolution.

Any changes in the viral genome that disrupt the interaction with the host cell or alter the conditions of coronavirus reproduction, expression of the host's genes, or resistance to the host's immunity can change the degree of virus contagiousness and virulence. Furthermore, the biological properties of the virus can be altered by one or more point mutations, as has been shown in a number of studies. In this case, the interaction between the coronavirus and the host is the key to the pathogenesis of the coronavirus diseases and, ultimately, determines the outcome of the infection. ●

This study was supported by the Russian Foundation for Basic Research (project No. 20-04-60079).

REFERENCES

1. Liu Y.C., Kuo R.L., Shih S.R. // Biomed. J. 2020. V. 43. № 4. P. 328–333.
2. COVID-19 Dashboard by the Center for Systems Science and Engineering (CSSE) at Johns Hopkins University (JHU). https://gisanddata.maps.arcgis.com/apps/opsdashboard/index.html#/bda7594740fd40299423467b48e9ecf6.
3. Geoghegan J.L., Holmes E.C. // Nat. Rev. Genet. 2018. V. 19. № 12. P. 756–769.
4. ICTV (International Committee on Taxonomy of Viruses). https://talk.ictvonline.org/ictv-reports/ictv_9th_report/positive-sense-rna-viruses-2011/w/posrna_viruses/222/coronaviridae.
5. Nakagawa S., Miyazawa T. // Inflamm. Regen. 2020. V. 40. № 1. P. 17.
6. Zhou P., Yang X.L., Wang X.G., Hu B., Zhang L., Zhang W., Si H.R., Zhu Y., Li B., Huang C.L., et al. // Nature. 2020. V. 579. № 7798. P. 270–273.
7. Zhou H., Chen X., Hu T., Li J., Song H., Liu Y., Wang P., Liu D., Yang J., Holmes E.C., et al. // Curr. Biol. 2020. V. 30. № 11. P. 2196–2203 e2193.
8. Guo Y.R., Cao Q.D., Hong Z.S., Tan Y.Y., Chen S.D., Jin H.J., Tan K.S., Wang D.Y., Yan Y. // Mil. Med. Res. 2020. V. 7. № 1. P. 11.
9. Yuan S., Jiang S.C., Li Z.L. // Front. Vet. Sci. 2020. V. 7. P. 379.
10. Lam T.T., Jia N., Zhang Y.W., Shum M.H., Jiang J.F., Zhu H.C., Tong Y.G., Shi Y.X., Ni X.B., Liao Y.S., et al. // Nature. 2020. V. 583. № 7815. P. 282–285.
11. Wu C., Liu Y., Yang Y., Zhang P., Zhong W., Wang Y., Wang Q., Xu Y., Li M., Li X., et al. // Acta Pharm. Sin B. 2020. V. 10. № 5. P. 766–788.
12. Chen Y., Liu Q., Guo D. // J. Med. Virol. 2020. V. 92. № 4. P. 418–423.
13. Li X., Giorgi E.E., Marichannegowda M.H., Foley B., Xiao C., Kong X.P., Chen Y., Gnanakaran S., Korber B., Gao F. // Sci. Adv. 2020. V. 6. № 27. P. eabb9153.
14. Liu C., Mendonca L., Yang Y., Gao Y., Shen C., Liu J., Ni T., Ju B., Liu C., Tang X., et al. // Structure. 2020. V. 28. № 11. P. 1218–1224 e1214.
15. Zhu N., Zhang D., Wang W., Li X., Yang B., Song J., Zhao X., Huang B., Shi W., Lu R., et al. // N. Engl. J. Med. 2020. V. 382. № 8. P. 727–733.
16. Lim Y.X., Ng Y.L., Tam J.P., Liu D.X. // Diseases. 2016. V. 4. № 3. P. 26.
17. Nelson C.W., Ardern Z., Goldberg T.L., Meng C., Kuo C.-H., Ludwig C., Kolokotronis S.-O., Wei X. // eLife. 2020. V. 9. P. e59633.
18. Davidson A.M., Wysocki J., Batlle D. // Hypertension. 2020. V. 76. № 5. P. 1339–1349.
19. Li W., Choe H., Farzan M. // Nidoviruses. 2006. doi: 10.1007/978-0-387-33012-9-36
20. Walls A.C., Park Y.J., Tortorici M.A., Wall A., McGuire A.T., Veesler D. // Cell. 2020. V. 181. №. 2. P. 281–292 e6.
21. Shang J., Ye G., Shi K., Wan Y., Luo C., Aihara H., Geng Q., Auerbach A., Li F. // Nature. 2020. V. 581. № 7807. P. 221–224.
22. Hoffmann M., Kleine-Weber H., Schroeder S., Kruger N., Herrler T., Erichsen S., Schiergens T.S., Herrler G., Wu N.H., Nitsche A., et al. // Cell. 2020. V. 181. № 2. P. 271–280 e8.
23. Bestle D., Heindl M.R., Limburg H., Van Lam van T., Pilgram O., Moulton H., Stein D.A., Hardes K., Eickmann M., Dolnik O., et al. // Life Sci. Alliance. 2020. V. 3. № 9. P. e202000786.
24. Tang T., Bidon M., Jaimes J.A., Whittaker G.R., Daniel S. // Antiviral Res. 2020. V. 178. P. 104792.
25. Ruch T.R., Machamer C.E. // Viruses. 2012. V. 4. № 3. P. 363–382.
26. Neuman B.W., Kiss G., Kunding A.H., Bhella D., Baksh M.F., Connelly S., Droese B., Klaus J.P., Makino S., Sawicki S.G., et al. // J. Struct. Biol. 2011. V. 174. № 1. P. 11–22.
27. McBride R., van Zyl M., Fielding B.C. // Viruses. 2014. V. 6. № 8. P. 2991–3018.
28. Sungnak W., Huang N., Becavin C., Berg M., Queen R., Litvinukova M., Talavera-Lopez C., Maatz H., Reichart D., Sampaziotis F., et al. // Nat. Med. 2020. V. 26. № 5. P. 681–687.
29. Zhang X.Y., Huang H.J., Zhuang D.L., Nasser M.I., Yang M.H., Zhu P., Zhao M.Y. // Infect. Dis. Poverty. 2020. V. 9. № 1. P. 99.
30. Khan F.A. // New Microbes New Infect. 2020. V. 36. P. 100697.
31. Russell C.D., Millar J.E., Baillie J.K. // Lancet. 2020. V. 395. № 10223. P. 473–475.
32. Yang X., Yu Y., Xu J., Shu H., Xia J.a., Liu H., Wu Y., Zhang L., Yu Z., Fang M., et al. // Lancet Respiratory Med. 2020. V. 8. №. 5. P. 475–481.
33. Liu K., Fang Y.Y., Deng Y., Liu W., Wang M.F., Ma J.P., Xiao W., Wang Y.N., Zhong M.H., Li C.H., et al. // Chin. Med. J. (Engl.). 2020. V. 133. № 9. P. 1025–1031.
34. Oran D.P., Topol E.J. // Ann. Intern. Med. 2020. V. 173. № 5. P. 362–367.
35. Abduljalil J.M., Abduljalil B.M. // New Microbes New Infect. 2020. V. 35. P. 100672.
36. Wu Z., McGoogan J.M. // J. Am. Med. Ass. 2020. V. 323. № 13. P. 1239–1242.
37. Harrison S.L., Fazio-Eynullayeva E., Lane D.A., Underhill P., Lip G.Y.H. // PLoS Med. 2020. V. 17. № 9. P. e1003321.
38. Richardson S., Hirsch J.S., Narasimhan M., Crawford J.M., McGinn T., Davidson K.W., the Northwell C.-R.C., Barnaby D.P., Becker L.B., Chelico J.D., et al. // J. Am. Med. Ass. 2020. V. 323. № 20. P. 2052–2059.
39. Petrilli C.M., Jones S.A., Yang J., Rajagopalan H., O'Donnell L., Chernyak Y., Tobin K.A., Cerfolio R.J., Francois F., Horwitz L.I. // Brit. Med. J. 2020. V. 369. P. m1966.
40. Wang D., Hu B., Hu C., Zhu F., Liu X., Zhang J., Wang B., Xiang H., Cheng Z., Xiong Y., et al. // J. Am. Med. Ass. 2020. V. 323. № 11. P. 1061–1069.
41. Zhang Y., Xiao M., Zhang S., Xia P., Cao W., Jiang W., Chen H., Ding X., Zhao H., Zhang H., et al. // N. Engl. J. Med. 2020. V. 382. № 17. P. e38.
42. Mehta P., McAuley D.F., Brown M., Sanchez E., Tattersall R.S., Manson J.J., Hlh Across Speciality Collaboration U.K. // Lancet. 2020. V. 395. № 10229. P. 1033–1034.
43. Rawson T.M., Moore L.S.P., Zhu N., Ranganathan N., Skolimowska K., Gilchrist M., Satta G., Cooke G., Holmes A. // Clin. Infect. Dis. 2020. V. 71. № 9. P. 2459–2468.
44. Ludvigsson J.F. // Acta Paediatrica. 2020. V. 109. № 6. P. 1088–1095.
45. Meskina E.R. // J. Microbiol. Epidemiol. Immunobiol. 2020. V. 97. № 3. P. 202–215.
46. Ahmed M., Advani S., Moreira A., Zoretic S., Martinez J., Chorath K., Acosta S., Naqvi R., Burmeister-Morton F., Burmeister F., et al. // EClin.Med. 2020. V. 26. P. 100527.
47. Hamming I., Timens W., Bulthuis M.L., Lely A.T., Navis G., van Goor H. // J. Pathol. 2004. V. 203. № 2. P. 631–637.
48. LoPresti M., Beck D.B., Duggal P., Cummings D.A.T.,

Solomon B.D. // Am. J. Hum. Genet. 2020. V. 107. № 3. P. 381–402.
49. Fujikura K., Uesaka K. // J. Clin. Pathol. 2021. V. 74. № 5. P. 307–313.
50. Hou Y., Zhao J., Martin W., Kallianpur A., Chung M.K., Jehi L., Sharifi N., Erzurum S., Eng C., Cheng F. // BMC Med. 2020. V. 18. № 1. P. 216.
51. Ellinghaus D., Degenhardt F., Bujanda L., Buti M., Albillos A., Invernizzi P., Fernandez J., Prati D., Baselli G., Asselta R., et al. // N. Engl. J. Med. 2020. V. 383. № 16. P. 1522–1534.
52. Wang F., Huang S., Gao R., Zhou Y., Lai C., Li Z., Xian W., Qian X., Li Z., Huang Y., et al. // Cell Discov. 2020. V. 6. № 1. P. 83.
53. Zimmerman P.A., Buckler-White A., Alkhatib G., Spalding T., Kubofcik J., Combadiere C., Weissman D., Cohen O., Rubbert A., Lam G., et al. // Mol. Med. 1997. V. 3. № 1. P. 23–36.
54. de Wilde A.H., Snijder E.J., Kikkert M., van Hemert M.J. // Curr. Top. Microb. Immunol. 2018. V. 419. P. 1–42.
55. Menachery V.D., Yount B.L., Debbink K., Agnihothram S., Gralinski L.E., Plante J.A., Graham R.L., Scobey T., Ge X.-Y., Donaldson E.F., et al. // Nat. Med. 2015. V. 21. № 12. P. 1508–1513.
56. Imai M., Watanabe T., Hatta M., Das S.C., Ozawa M., Shinya K., Zhong G., Hanson A., Katsura H., Watanabe S., et al. // Nature. 2012. V. 486. № 7403. P. 420–428.
57. Maines T.R., Chen L.-M., Van Hoeven N., Tumpey T.M., Blixt O., Belser J.A., Gustin K.M., Pearce M.B., Pappas C., Stevens J., et al. // Virology. 2011. V. 413. № 1. P. 139–147.
58. Klimov A.I., Cox N.J., Yotov W.V., Rocha E., Alexandrova G.I., Kendal A.P. // Virology. 1992. V. 186. № 2. P. 795–797.
59. Lin J.-H., Wu H.-S. // BioMed Research International. 2015. V. 2015. P. 805306.
60. Jernigan D.B., Cox N.J. // Annu. Rev. Med. 2015. V. 66. № 1. P. 361–371.
61. Gussow A.B., Auslander N., Faure G., Wolf Y.I., Zhang F., Koonin E.V. // Proc. Natl. Acad. Sci. USA. 2020. V. 117. № 26. P. 15193–15199.
62. Islam M.R., Hoque M.N., Rahman M.S., Alam A., Akther M., Puspo J.A., Akter S., Sultana M., Crandall K.A., Hossain M.A. // Sci. Rep. 2020. V. 10. № 1. P. 14004.
63. Hadfield J., Megill C., Bell S.M., Huddleston J., Potter B., Callender C., Sagulenko P., Bedford T., Neher R.A. // Bioinformatics. 2018. V. 34. № 23. P. 4121–4123.
64. Zhao Z., Li H., Wu X., Zhong Y., Zhang K., Zhang Y.P., Boerwinkle E., Fu Y.X. // BMC Evol. Biol. 2004. V. 4. P. 21.
65. Cotten M., Watson S.J., Zumla A.I., Makhdoom H.Q., Palser A.L., Ong S.H., Al Rabeeah A.A., Alhakeem R.F., Assiri A., Al-Tawfiq J.A., et al. // mBio. 2014. V. 5. № 1. P. e01062–01013.
66. Vijgen L., Keyaerts E., Moës E., Thoelen I., Wollants E., Lemey P., Vandamme A.-M., van Ranst M. // J. Virol. 2005. V. 79. № 3. P. 1595–1604.
67. Smith E.C., Blanc H., Surdel M.C., Vignuzzi M., Denison M.R. // PLoS Pathog. 2013. V. 9. № 8. P. e1003565.
68. Mercatelli D., Giorgi F.M. // Front. Microbiol. 2020. V. 11. P. 1800.
69. Jia Y., Shen G., Zhang Y., Huang K.-S., Ho H.-Y., Hor W.-S., Yang C.-H., Li C., Wang W.-L. // bioRxiv. 2020. doi: 10.1101/2020.04.09.034942.
70. Naqvi A.A.T., Fatima K., Mohammad T., Fatima U., Singh I.K., Singh A., Atif S.M., Hariprasad G., Hasan G.M., Hassan M.I. // Biochim. Biophys. Acta Mol. Basis. Dis. 2020. V. 1866. № 10. P. 165878.
71. Vilar S., Isom D.G. // bioRxiv. 2020. doi: 10.1101/2020.12.16.423071.
72. Morais I.J., Polveiro R.C., Souza G.M., Bortolin D.I., Sassaki F.T., Lima A.T.M. // Sci. Rept. 2020. V. 10. № 1. P. 18289.
73. Korber B., Fischer W.M., Gnanakaran S., Yoon H., Theiler J., Abfalterer W., Hengartner N., Giorgi E.E., Bhattacharya T., Foley B., et al. // Cell. 2020. V. 182. № 4. P. 812–827 e819.
74. Laha S., Chakraborty J., Das S., Manna S.K., Biswas S., Chatterjee R. // Infection, Genetics and Evolution. 2020. V. 85. P. 104445.
75. Alouane T., Laamarti M., Essabbar A., Hakmi M., Bouricha E.M., Chemao-Elfihri M.W., Kartti S., Boumajdi N., Bendani H., Laamarti R., et al. // Pathogens. 2020. V. 9. № 10. P. 829.
76. Lokman S.M., Rasheduzzaman M., Salauddin A., Barua R., Tanzina A.Y., Rumi M.H., Hossain M.I., Siddiki A.M.A.M.Z., Mannan A., Hasan M.M. // Infect.Genet. Evol. 2020. V. 84. P. 104389.
77. Comandatore F., Chiodi A., Gabrieli P., Biffignandi G.B., Perini M., Ricagno S., Mascolo E., Petazzoni G., Ramazzotti M., Rimoldi S.G., et al. // bioRxiv. 2020. doi: 10.1101/2020.04.30.071027.
78. Zhang L., Wang S., Ren Q., Yang J., Lu Y., Zhang L., Gai Z. // medRxiv. 2020. doi: 10.1101/2020.04.27.20081349.
79. van Dorp L., Richard D., Tan C.C., Shaw L.P., Acman M., Balloux F. // bioRxiv. 2020. doi: 10.1101/2020.05.21.108506.
80. Bhowmik D., Pal S., Lahiri A., Talukdar A., Paul S. // bioRxiv. 2020. doi: 10.1101/2020.04.26.062471.
81. Cortey M., Li Y., Díaz I., Clilverd H., Darwich L., Mateu E. // bioRxiv. 2020. doi: 10.1101/2020.05.16.099499.
82. Zhang L., Jackson C.B., Mou H., Ojha A., Peng H., Quinlan B.D., Rangarajan E.S., Pan A., Vanderheiden A., Suthar M.S., et al. // Nat. Commun. 2020. V. 11. № 1. P. 6013.
83. Kemp S., Harvey W., Datir R., Collier D., Ferreira I., Carabelli A., Robertson D., Gupta R. // bioRxiv. 2020. doi: 10.1101/2020.12.14.422555.
84. Preliminary genomic characterisation of an emergent SARS-CoV-2 lineage in the UK defined by a novel set of spike mutations. 2020. https://virological.org/t/preliminary-genomic-characterisation-of-an-emergent-sars-cov-2-lineage-in-the-uk-defined-by-a-novel-set-of-spike-mutations/563.
85. Starr T.N., Greaney A.J., Hilton S.K., Crawford K.H.D., Navarro M.J., Bowen J.E., Tortorici M.A., Walls A.C., Veesler D., Bloom J.D. // bioRxiv. 2020. doi: 10.1101/2020.06.17.157982.
86. Tegally H., Wilkinson E., Giovanetti M., Iranzadeh A., Fonseca V., Giandhari J., Doolabh D., Pillay S., San E.J., Msomi N., et al. // medRxiv. 2020. doi: 10.1101/2020.12.21.20248640.
87. Genomic characterisation of an emergent SARS-CoV-2 lineage in Manaus: preliminary findings. 2021. https://virological.org/t/genomic-characterisation-of-an-emergent-sars-cov-2-lineage-in-manaus-preliminary-findings/586.
88. Khailany R.A., Safdar M., Ozaslan M. // Gene Rep. 2020. V. 19. P. 100682.
89. Young B.E., Fong S.-W., Chan Y.-H., Mak T.-M., Ang L.W., Anderson D.E., Lee C.Y.-P., Amrun S.N., Lee B., Goh Y.S., et al. // Lancet. 2020. V. 396. № 10251. P. 603–611.
90. Krammer F. // Nature. 2020. V. 586. № 7830. P. 516–527.
91. Xie X., Zou J., Fontes-Garfias C.R., Xia H., Swanson K.A., Cutler M., Cooper D., Menachery V.D., Weaver S., Dormitzer P.R., et al. // bioRxiv. 2021. doi: 10.1101/2021.01.07.425740.
92. Ferretti A.P., Kula T., Wang Y., Nguyen D.M.V., Weinheimer A., Dunlap G.S., Xu Q., Nabilsi N., Perullo C.R.,

Cristofaro A.W., et al. // Immunity. 2020. V. 53. № 5. P. 1095–1107 e1093.
93. Wahba L., Jain N., Fire A.Z., Shoura M.J., Artiles K.L., McCoy M.J., Jeong D.E. // mSphere. 2020. V. 5. № 3. P. e00160-20.
94. Forster P., Forster L., Renfrew C., Forster M. // Proc. Natl. Acad. Sci. USA. 2020. V. 117. № 17. P. 9241–9243.
95. Yang X., Dong N., Chan E.W., Chen S. // Emerg. Microbes Infect. 2020. V. 9. № 1. P. 1287–1299.
96. Tang X., Wu C., Li X., Song Y., Yao X., Wu X., Duan Y., Zhang H., Wang Y., Qian Z., et al. // Nat. Sci. Rev. 2020. V. 7. № 6. P. 1012–1023.
97. Zhang X., Tan Y., Ling Y., Lu G., Liu F., Yi Z., Jia X., Wu M., Shi B., Xu S., et al. // Nature. 2020. V. 583. № 7816. P. 437–440.
98. Hahn G., Lee S., Weiss S.T., Lange C. // bioRxiv. 2020. doi: 10.1101/2020.05.05.079061.
99. Kumar S., Tao Q., Weaver S., Sanderford M., Caraballo-Ortiz M.A., Sharma S., Pond S.L.K., Miura S. // bioRxiv. 2020. doi: 10.1101/2020.09.24.311845.
100. Sundru Manjulata D., Annapurna P., Balakuntalam K., Kumar S. // Res. Square. 2021. doi: 10.21203/rs.3.rs-29557/v1.
101. GISAID: Clade and lineage nomenclature, July 4, 2020. https://www.gisaid.org/references/statements-clarifications/clade-and-lineage-nomenclature-aids-in-genomic-epidemiology-of-active-hcov-19-viruses/
102. Sengupta A., Hassan S.S., Choudhury P.P. // bioRxiv. 2020. doi: 10.1101/2020.11.30.402487.
103. Rambaut A., Holmes E.C., Hill V., O'Toole Á., McCrone J., Ruis C., du Plessis L., Pybus O.G. // bioRxiv. 2020. doi: 10.1101/2020.04.17.046086.
104. Phylogenetic Assignment of Named Global Outbreak LINeages (PANGOLIN) updated 2020. https://github.com/cov-lineages/pangolin.
105. Hodcroft E. B, Hadfield J., Neher R. A, Bedford T. Year-letter genetic clade naming for SARS-CoV-2 on nextstain.org. 2020. https://nextstrain.org/blog/2020-06-02-SARSCoV2-clade-naming
106. Komissarov A.B., Safina K.R., Garushyants S.K., Fadeev A.V., Sergeeva M.V., Ivanova A.A., Danilenko D.M., Lioznov D., Shneider O.V., Shvyrev N., et al. // Nat. Commun. 2021. V. 12. № 1. P. 649.
107. Shchetinin A.M., Tsyganova E.V., Protsenko D.N. // Cureus. 2021. V. 13. № 3. P. e13733.
108. Kozlovskaya L., Piniaeva A., Ignatyev G., Selivanov A., Shishova A., Kovpak A., Gordeychuk I., Ivin Y., Berestovskaya A., Prokhortchouk E., et al. // Int. J. Infect. Dis. 2020. V. 99. P. 40–46.

Chemiluminescence Detection in the Study of Free-Radical Reactions. Part 1

L. A. Romodin*
Moscow State Academy of Veterinary Medicine and Biotechnology – MVA named after K.I. Skryabin, Departmental affiliation is Ministry of Agriculture of the Russian Federation, Moscow, 109472 Russia
*E-mail: rla2904@mail.ru
Received March 18, 2020; in final form, June 11, 2020
DOI: 10.32607/actanaturae.10912

ABSTRACT **The present review, consisting of two parts, considers the application of the chemiluminescence detection method in evaluating free radical reactions in biological model systems. The first part presents a classification of experimental biological model systems. Evidence favoring the use of chemiluminescence detection in the study of free radical reactions, along with similar methods of registering electromagnetic radiation as electron paramagnetic resonance, spectrophotometry, detection of infrared radiation (IR spectrometry), and chemical methods for assessing the end products of free radical reactions, is shown. Chemiluminescence accompanying free radical reactions involving lipids has been the extensively studied reaction. These reactions are one of the key causes of cell death by either apoptosis (activation of the cytochrome *c* complex with cardiolipin) or ferroptosis (induced by free ferrous ions). The concept of chemiluminescence quantum yield is also discussed in this article. The second part, which is to be published in the next issue, analyzes the application of chemiluminescence detection using luminescent additives that are called activators, a.k.a. chemiluminescence enhancers, and enhance the emission through the triplet–singlet transfer of electron excitation energy from radical reaction products, followed by light emission with a high quantum yield.**
KEYWORDS **free radical reactions, apoptosis, ferroptosis, chemiluminescence, lipid peroxidation, reactive oxygen species.**
ABBREVIATIONS **MDA – malonic dialdehyde; EES – electronically excited state; EPR – electron paramagnetic resonance.**

INTRODUCTION

Biochemiluminescence is the generation of photons in biological systems. There is also the term "bioluminescence," which is, strictly speaking, meaningless, since it stands for light emission produced by chemical reactions in living organisms. The luminescence in these systems results from reactions involving free radicals. Chemiluminescence detection is used to study the reactions and the impact of various factors such as antioxidants on this process. Prior to directly describing chemiluminescence and its mechanisms of occurrence in biological systems, several words should be said about the systematization of biological model systems.

BIOLOGICAL MODEL SYSTEMS IN THE STUDY OF FREE RADICAL REACTIONS

An experimental model system is a material system that, once affected by a physical, chemical, biological or any other factor, can provide information about the effect of the factor on the original system. Here, we present a classification of the experimental model systems used in biological studies.

A. Biological model systems:

A1. Laboratory animals. This model most fully represents the properties of the human body. However, the taxonomic characteristics of the animals used (e.g., the ability to synthesize vitamin C) should be taken into account. This will allow for understanding how the result obtained in this model can be applied to the human body. An example is the study of free radical processes in mice carried out by the M.V. Listov research team [1, 2] and a model of acetaminophen- (paracetamol-) induced liver cirrhosis in rats [3];

A2. Animal embryos. The main difference of this model from the previous one is that it allows for reducing the experimental time and studying a more com-

plete set of effects thanks to the fact that regulations regarding laboratory animals do not apply to embryos at early developmental stages. An example is the work on the effects of vitamin E deficiency and hypervitaminosis on *Brachydanio rerio* (zebrafish) parents studied in fish embryos [4];

A3. Neuromuscular agent. The free radical nature of excitation and inhibition in neuronal tissue was demonstrated using this model [5];

A4. Cell cultures. This model is used to determine the formaldehyde level by registering chemiluminescence enhanced by coumarin derivatives under conditions of artificially induced stress [6];

A5. Mitochondrial culture. This model allows for the study of mitochondrial processes. An example is the works on chemiluminescence detection in mitochondrial suspension conducted by Yu.A. Vladimirov *et al*. [7–9]. The results of those studies suggest that peroxidation of lipids in mitochondrial membranes is initiated in condition of deficiency of the enzymes that catalyze β-oxidation of fatty acids. Another example is an isolated culture of plant plastids: e.g., chloroplasts [10];

A6. Tissue samples. In the study of tissues obtained directly from animals, a laboratory animal serves as an experimental model. Biochemiluminescence was first detected in a tissue sample [11]. The method of detecting the chemiluminescence of blood and its fractions is used in many studies [12–16];

A7. Fungi model. The most commonly used experimental model is baker's yeast (*Saccharomyces cerevisiae*). This model was used to study oxidative stress by detecting chemiluminescence [17];

A8. Plant models. This group of models includes both whole plants, seedlings, individual organs, and cultures of plant cells and tissues. An increase in the concentration of the superoxide anion radical upon enhanced activity of lipoxygenases was shown in bean cotyledons [18]. Another example is the use of the chemiluminescence detection method in the study of a peptide ligand binding to a cell receptor [19].

A large group of models called molecular models can be also distinguished; it includes two groups of systems.

B. Conditionally biological experimental models:

B1. Models based on biological molecules isolated from living organisms. Examples include cytochrome *c* and cardiolipin isolated from animals [20] and *Escherichia coli* DNA [1];

B2. Molecular models based on biological molecules isolated from living organisms and artificially synthesized molecules identical to them. Examples are the study of the participation of coumarin derivatives in the reaction catalyzed by the cytochrome *c* complex with cardiolipin using cytochrome *c* isolated from the horse's heart and artificially synthesized tetraoleyl cardiolipin [21];

C. Models based on synthetic polymers and low-molecular-weight organic compounds. Technically, these models cannot be considered biological. However, some data obtained with their use can be applied to living systems. In addition, these models are often the most suitable choice for studying the basic principles of free radical reactions:

C1. A molecular model that uses biomolecules and their non-biological analogue. For instance, the dodecyl sulfate anion is used as a cardiolipin analogue to study changes in cytochrome *c* properties upon its binding to phospholipids [22]. This model makes it possible to study the complex of cytochrome *c* with cardiolipin, which induces peroxidation of lipids in mitochondrial membranes, resulting in the activation of apoptosis through the mitochondrial pathway [23];

C2. Molecular model using a synthetic polymer. This model was used to study chemiluminescence produced by polymer decomposition [24] and the kinetics of alkyl radical decay in polyethylene [25];

C3. Molecular model based only on low-molecular-weight organic compounds. The use of this model made it possible to obtain data on the nature of the chemiluminescence caused by reactions involving hydrocarbon radicals through the action of the products of thermal decomposition of α_1,α_2-azobisisobutyronitrile [26]. Hydrocarbons can be considered a very convenient model for studying free radical reactions involving lipids, since the tails of lipid molecules are hydrocarbons. The results of such work have been published [26, 27] and contributed to the study of the mechanisms of lipid peroxidation [28–31].

CHEMILUMINESCENCE AND ITS MECHANISM

Emission of light of very low intensity by biological objects was first noticed at the end of the first third of the previous century: V.V. Lepeshkin discovered the emission from photographic plates lying on biological samples. He considered this radiation to be ultraviolet emitted during protoplast coagulation upon cell death and called it necrobiotic radiation [32, 33]. A.G. Gurvich, who detected luminescence of a suspension of fission yeast, suggested the signaling role of the luminescence of biological samples in the ultraviolet spectral region. He further called this luminescence "mitogenetic radiation" [34].

Subsequenly, with the help of photomultipliers, in the third quarter of the 20th century visible light emission of extremely low intensity produced by biological objects of plant origin [36] and animal tissues [11] was detected and called *ultraweak chemiluminescence* in the English language literature [35]. Chemilu-

minescence of intact tissues, mitochondria [7–9], and chloroplasts [10] was discovered. In the early 1970s, R. Allen discovered chemiluminescence of human blood leukocytes during bacterial phagocytosis [37, 38]. This discovery made it possible to use chemiluminescence as a clinical method for determining immunoreactivity.

Chemiluminescence is luminescence caused by the transition of various metabolites of free radical reactions from an electronically excited state (EES) to the ground state [39, 40].

Free radical reactions in biological systems

A free radical is a particle with a free valence that is due to the presence of an unpaired electron. M. Gomberg was the first to describe radicals at the beginning of the 20th century [41–43]. Free radicals are highly reactive, meaning that they are chemically unstable and have a short lifetime. The molecular structure of a radical can affect its stability. For example, methyl groups [44, 45] and an iminoacetyl group in the *para* position [44] stabilize the quinone radical.

Radical forms of the respiratory chain components were discovered in the middle of the 20th century: single-electron energy transfer was described [46–48]. Previously, redox reactions in biological systems were believed to involve only the release and acceptance of two electrons simultaneously [31].

One of the most important radicals in oxidative stress is the superoxide anion radical ($O_2^{\bullet -}$), resulting from the interaction between a semiquinone radical (semi-reduced ubiquinone) and molecular oxygen at the inner side of the mitochondrial membrane, in the respiratory complexes III [49] and I [29], and in the cytoplasm (in the NADPH oxidase complex in the endoplasmic reticulum membrane or plasmalemma) [50, 51]. In addition, the superoxide radical is formed during the oxidation of hemoglobin to hemin [2]. The resulting superoxide radical participates in neurohumoral regulation [1, 2, 5, 52]. M.V. Listov *et al*. found that the superoxide anion radical formed in the blood promotes the generation of cell surface potentials, acting as a trigger for effectors [5]. In particular, the superoxide radical contributes to automatic contractions of the myocardium, acting on the sinoatrial node of the cardiac conduction system [52] and serving as a major factor in the depolarization and hyperpolarization of the cell membrane. Thus, the superoxide radical triggers the mechanisms of excitation and inhibition on the surface of conducting fibers [5]. Along with nitrogen monoxide formed by NO-synthases, the superoxide anion radical was called primary in the classification proposed by Yu.A. Vladimirov [29]. This term indicates that formation of both radicals is catalyzed by enzymatic systems [29, 53].

Primary radicals form the following molecular products: $O_2^{\bullet -}$ is either converted to hydrogen peroxide by superoxide dismutase or reacts with $NO^{\bullet}$ producing the toxic peroxynitrite ion $ONOO^-$ [54]. Superoxide can also reduce the ferric iron in ferritin and the iron-sulfur clusters of electron transport chains to a bivalent ion, which further reacts with hydrogen peroxide or hypochlorite to form an extremely reactive hydroxyl radical ($^{\bullet}OH$) and can branch lipid oxidation chains by reacting with lipid hydroperoxides. The hydroxyl radical can activate lipid peroxidation with formation of lipid radicals [29]. The resulting reactive oxygen and nitrogen species, as well as hypochlorite at low concentrations, act as secondary messengers. When cellular antioxidant systems are impaired (the major role is played by glutathione and glutathione peroxidase [56]), these radicals induce oxidative stress, leading to wither apoptosis [23, 58] or ferroptosis [59–61] through lipid peroxidation. It should be noted that lipid peroxidation leading to apoptosis is usually induced by cytochrome *c* complexed with cardiolipin. Binding of cytochrome *c* to cardiolipin changes its conformation so that the protein acquires the ability to catalyze lipid peroxidation [62–64]. Ferroptosis is induced by initiation of the Fenton reaction by Fe^{2+} ions, followed by lipid peroxidation initiated by hydroxyl radicals [59–61]. Both hydroxyl and lipid radicals are secondary in the Yu.A. Vladimirov classification [53]. The diagram in *Fig. 1* shows major metabolic pathways involving free radicals. It should be noted that there is no unified system of terms describing free radical reactions in biological systems and oxidative stress.

Detection of free radicals in biological systems, intrinsic chemiluminescence

The method of chemiluminescence detection makes it possible to estimate the rate of free radical formation [28, 31]. This physical method is used to study free radical reactions together with chemical methods for detecting the molecular products of radical reactions. The most common marker of free radical reactions and the state of oxidative stress is one of the products of lipid peroxidation, malondialdehyde (MDA), whose concentration is determined using thiobarbituric acid (TBA) [65, 66]. In order to obtain more reliable results, the concentration of Schiff bases [67, 68], diene [69, 70], and triene [67] conjugates should be also measured. Other methods are based on the use of radical scavengers: antioxidant enzymes such as catalase (H_2O_2) [71] and superoxide dismutase ($O_2^{\bullet -}$) [69], phenolic antioxidants for hydroxyl/lipid radicals, and other organic molecules [71]. The main disadvantage of chemical methods is the impossibility of determining the nature and concentration of free radicals [29].

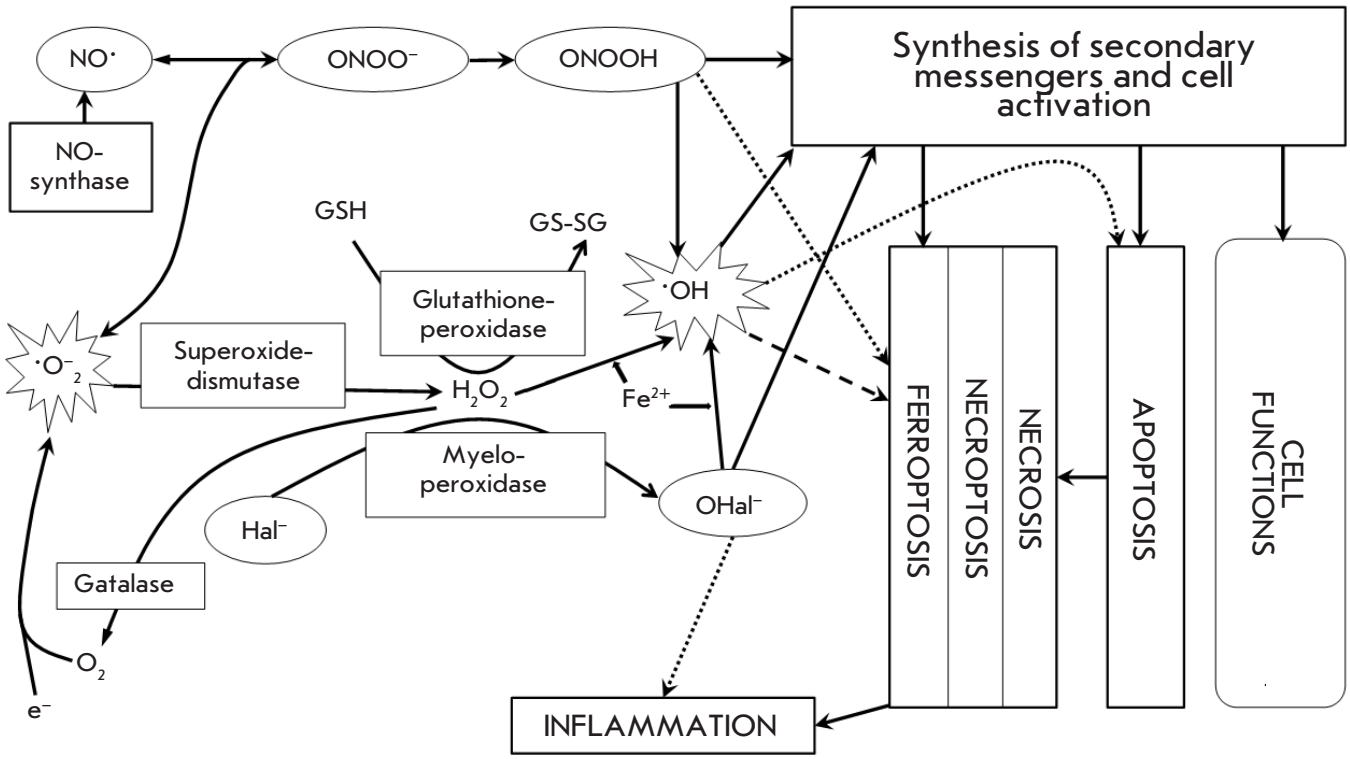

Fig. 1. Metabolic pathways involving free radicals [29, 54–57]

The method of electron paramagnetic resonance (EPR), developed in the middle of the 20th century [72], makes it possible to detect and identify many radicals by analyzing the hyperfine structure of EPR signals [73, 74]. However, the use of EPR is hampered by the short lifespan and, thus, low concentration of free radicals [75]. For this reason, only the use of a flow-through system with a high consumption of reagents made it possible to detect radicals formed in the reaction between Fe^{2+} cations and lipid hydroperoxides [76]. Reagent consumption can be reduced by using spin traps [1, 77], which, however, can affect the biochemical reactions in the system, and also be destroyed in some of them [29]. Free radical reactions in heme-dependent exophthalmos were studied using EPR and infrared (IR) spectroscopy [1]. Another physical method, spectrophotometry, should be also mentioned. This method was used to determine the concentration of oxidation products when studying the mechanisms of heteroauxin (β-indoleacetic acid) oxidation by horseradish peroxidase and tobacco anionic peroxidase [78]. The concentration of lipid peroxidation markers in the overwhelming majority of cases is also determined using spectrophotometry. Coumarin derivatives used as a luminescent additive to assess the peroxidase properties of the cytochrome *c* complex with cardiolipin were studied using spectrophotometry and chemiluminescence detection [21].

The method of chemiluminescence detection makes it possible to study the intensity of reactions involving short-lived radicals. This is possible thanks to the large amount of energy produced in a radical reaction and partially released in the form of photons [40].

Here we present widely available information on the kinetics of reactions accompanied by chemiluminescence. In these reactions, the initial substances R form free radicals R$^{\bullet}$, which can generate electronically excited products P* in a subsequent reaction, which, in turn, when converted to the ground state P, can emit a photon ($h\nu$). The chance of formation of an EES product is very high if the activated complex of reagents and reaction products has states with different multiplicities [40]. For the convenience of further description of the processes under consideration, we present the general scheme of a chain reaction with the formation and participation of free radicals, followed by photon emission:

$$R \xrightarrow{k_1} R^{\bullet} \xrightarrow{k_2} P^{*} \xrightarrow{k_3} P + h\nu. \quad (1)$$

It should be noted that, in most cases, the chemiluminescence spectrum does not correspond to the fluorescence spectrum of the product P* but corresponds to its phosphorescence spectrum [79]. This clearly indicates that products P* are in a triplet excited state.

The intensity of chemiluminescence (J) is proportional to the rate of the third reaction in the abovementioned scheme (1): $J \propto k_3[P^*]$.

Due to the high rate of free radical conversion to reaction products, the steady state, when the rates of all reactions in the reaction chain are equal, is quickly established in the system. Thus, the luminescence intensity is proportional to the rate of free radical formation v_1 (reaction with the rate constant k_1). Hence, the chemiluminescence intensity is also proportional to the steady-state concentration of free radicals, which can be determined based on the rate of their formation and the rate constant of conversion to EES products [40, 80]:

$$J \propto v_1 = k_2\left[R^{\cdot}\right] \quad (2)$$

$$\left[R^{\cdot}\right] = \frac{v_1}{k_2}. \quad (3)$$

It is important to note that both the EPR method and fluorimetry/spectrometry are used to determine the concentrations of substances, which are free radicals [R˙] in our case. The [R˙] value, and thus the recorded signal, decreases with the growth of radical reactivity; i.e., with an increase in k_2. Therefore, active radicals, even with an extremely high production rate, are not detected by EPR because of the high k_2 value: i.e. high rate of their conversion to reaction products. However, the chemiluminescence intensity does not depend on the concentration of radicals but rather on the rate of free radical reactions. For this reason, this method can be used to detect even the most reactive radicals at extremely low concentrations [80].

Quantum yield of intrinsic chemiluminescence

Two concepts of the quantum yield should be mentioned when considering chemiluminescence: the quantum yield of excitation (Q_{ex}), which is the ratio of reaction product molecules in EES to the total number of reaction product molecules; and the luminescence quantum yield (Q_{lum}), which is the ratio of molecules in EES emitting a photon to the total number of molecules in EES. The total yield of luminescence, namely chemiluminescence (Q_{ChLum}), is equal to their multiplication: $Q_{ChLum} = Q_{ex} \cdot Q_{lum}$ [40].

Let us consider the reactions presented in scheme (1) with the rate constants k_2 and k_3 in more detail:

$$A + B \xrightarrow{k_2} P^* + \text{other products}. \quad (4)$$

A chemiluminescent reaction [40].

$$P^* \xrightarrow{k_3} P + h\nu. \quad (5)$$

A luminescenct reaction [40].

$$P^* \xrightarrow{k_{3_{not}}} P. \quad (6)$$

Nonradiative transition [40].

The quantum yield Q_{lum} of reaction (5) is the quantum yield of the product photoluminescence, which is close to zero in most biochemical reactions. However, the quantum yield Q_{ex} in the case of formation of EES products is also extremely low, since most chemical reactions in aqueous solutions at ambient temperature result in the formation of unexcited molecules in the ground electronic state [29] ("other products" in reaction (4) with the constant k_2). The total quantum yield of chemiluminescence evaluating the rate of free radical formation is calculated using the following formula: $Q_{ChLum} = Q_{ex} \cdot Q_{lum}$ [40]. This luminescence is called superweak due to such a low value of the quantum yield of biochemiluminescence [31, 81].

The quantum yield value, and hence, the resulting chemiluminescence intensity, can be calculated using the formulas [40]:

$$Q_{lum} = \frac{k_3}{k_3 + k_{3_{not}}} \quad (7)$$

$$J = k_3\left[P^*\right] = Q_{ex}\frac{k_3}{k_3 + k_{3_{not}}} k_2\left[A\right]\left[B\right], \quad (8)$$

where k_3 is the rate constant of reaction (5), $k_{3_{not}}$ is the rate constant of reaction (6), k_2 is the rate constant of reaction (4), and J is the chemiluminescence intensity.

Apparently, not every light quantum entering the luminometer is capable of ejecting an electron from the photocathode of the photomultiplier tube [31]. Therefore, the software of modern luminometers takes into account the light collection coefficient (the ratio of quanta reaching the photocathode to the total number of quanta emitted by the system [82]) and the quantum yield of the photocathode (the ratio of electrons ejected from the cathode to the number of quanta reaching the cathode).

Chemiluminescence mechanism in the peroxidation of biological molecules

Lipid peroxidation is one of the main processes contributing to ferroptosis [60, 61, 83] and apoptosis through

the mitochondrial pathway [23]. Therefore, most attention in the study of these processes is focused on radical reactions involving lipids. However, the scheme describing lipid radical reactions accompanied by chemiluminescence is generally valid and can be applied to chemiluminescent reactions involving proteins, as shown by I.I. Sapezhinskij and E.A. Lissi [75, 84–86], and nucleic acids in solutions exposed to low-frequency electromagnetic radiation [87, 88]. It should be noted that, for luminescence to occur, the energy yield of the reaction must be ⩾ 40 kcal/mol (167.5 kJ/mol) [40]. The mechanisms of luminescence were initially discovered and studied in model systems based on synthetic polymers [24, 89] and low-molecular-weight organic compounds [26, 90, 91]. For instance, alkyl radical decay in polyethylene was studied [25] and the results of a spectrometric study of the chemiluminescence accompanying the oxidation of polycarbonate, polystyrene, and polyethyl methacrylate by the products of thermal decomposition of dicyclohexylperoxydicarbonate with the total quantum yield of chemiluminescence equal to 10^{-9} were published [24].

Lipid peroxidation, which mostly involves polyunsaturated acyl chains, is presented not as a single reaction, but a cascade of branched chain reactions [92–94]. Below is the detailed scheme of reaction (4) with the overall rate constant k_2:

$$R_1H \xrightarrow{k_1;\ -H} R_1^{\bullet} \xrightarrow{+[O_2];\ k_{2a}} R_1OO^{\bullet} \quad (9)$$

$$R_1OO^{\bullet} + R_2H \xrightarrow{k_{2b}} R_1OOH + R_2^{\bullet} \quad (10)$$

$$R_2^{\bullet} + [O_2] \xrightarrow{k_{2a}} R_2OO^{\bullet}. \quad (11)$$

Lipid hydroperoxides ROOH very easily become the source of new lipid oxidation chains, according to the general principles of such reactions [95, 96]:

$$e^- + ROOH \xrightarrow{k_{2c}} RO^{\bullet} + OH^- \quad (12)$$

$$RO^{\bullet} + RH \rightarrow 2R^{\bullet} + OH^-. \quad (13)$$

Formation of oxygen radicals is a key step in a cascade of reactions producing chemiluminescence. Despite the well-known fact that molecular oxygen is a luminescence quencher [97], the presence of oxygen in a system with proteins and hydrocarbons enhances the chemiluminescence intensity, as shown in the middle of the 20th century [26, 40, 75, 80, 90, 98]. This allows one to assume that the excited particles that ultimately emit light result from the recombination of oxygen radicals. It should be also noted that, in addition to proteins and hydrocarbon groups, luminol can also serve as a substrate for oxidation followed by photon emission [99, 100]. However, the resulting luminescent product is in a singlet but not triplet EES, which is typical of excited products of free radical reactions involving hydrocarbon groups. Luminol is widely used as an additive enhancing the chemiluminescence intensity.

The chemiluminescence accompanying lipid peroxidation reactions is caused by the disproportionation of $ROO^{\bullet}$ radicals [27, 90]. Generally speaking, this process can be described as follows [90]:

$$2ROO^{\bullet} \xrightarrow{k_{2e}} ROH + Q_{ex}R{=}O^* + (1 - Q_{ex})R{=}O + O_2. \quad (14)$$

The mechanism of disproportionation of peroxyl radicals with the formation of a carbonyl compound, alcohol, and an oxygen molecule was first described by G.A. Russell [101] and later named after him. The reaction (14) is termination of the radical oxidation chain, while reaction (10) is a chain extension reaction. G.A. Russell determined the average ratio of the rate of reaction (10) to the rate of reaction (14), which is equal to 7.4 for the hydrocarbon model system [101].

Reaction (14) is a second-order reaction. Thus, it is described by a known mathematical equation:

$$\frac{1}{C} - \frac{1}{C_0} = k_{2e}t, \quad (15)$$

where t is the time from the beginning of the reaction, C and C_0 are concentrations of $ROO^{\bullet}$ radicals at time t and at the beginning of the reaction, respectively. However, M. Dole [102] states that some $ROO^{\bullet}$ radicals in the system may not undergo disproportionation. The concentration of these radicals is further denoted by letter A. According to [102], the resulting formula for (15) is the following (the equation is presented in two forms for convenience):

$$\frac{t}{C_0 - C} = \frac{1}{(C_0 - A)^2 4\pi D r_0} + \frac{t}{C_0 - A} - \frac{1}{2\pi D(C_0 - A)^2\left(2r_0 + \sqrt{\pi D t}\right)}$$

$$\frac{t}{C_0 - C} = \frac{\sqrt{\pi D t} + 4\pi D r_0 t(C_0 - A)\left(2r_0 + \sqrt{\pi D t}\right)}{4\pi D r_0 (C_0 - A)^2\left(2r_0 + \sqrt{\pi D t}\right)}, \quad (16)$$

where r_0 is the distance between radicals they react within, and D is the sum of diffusion coefficients of the reagents.

Photon emission occurs during the transition of ketone formed in reaction (14) from triplet EES to the ground state:

$$R{=}O^{*} \xrightarrow{k_3} R{=}O + \text{photon}. \qquad (17)$$

The emitted light has a maximum intensity in the region of 450–550 nm [103].

Reaction (14) proceeds with tetroxide formation, followed by its decomposition to alcohol and a diradical due to mechanical stress in the molecule skeleton: this is the time point when electrons are separated in the molecule. Next, an oxygen molecule is released and a triplet EES ketone is generated [27, 80]. However, there is a high chance that tetroxide can decompose again to two lipid peroxyl radicals. This is supported by the fact that the diffusion rate constant for these radicals is orders of magnitude higher than the rate constant of their disproportionation [27]. A graphic representation of the Russell mechanism is presented in *Fig. 2A*. The resulting oxygen can be in singlet EES. According to [104], the quantum yield of O_2 excitation is ≈11%. Luminescence with a maximum at 634 and 703 nm is observed upon transition of oxygen to the ground state [103, 105].

Due to extremely low values of the quantum yields of formation of excited ketone molecules and their luminescence (in this case, phosphorescence), the total quantum yield of chemiluminescence is only 10^{-8} [80].

The relationship between the concentration of lipid peroxyl radicals and luminescence intensity J is determined by the equation [24, 40]:

$$J = Q_{\text{ChLum}} k_{2e} \left[\text{ROO}^{\cdot}\right]^2, \qquad (18)$$

where J is the total light input at all wavelengths and in all directions and Q_{ChLum} is the quantum yield of chemiluminescence.

Apart from the Russell mechanism, there is another path of formation of carbonyl compounds in triplet EES: decomposition of the dioxetane group resulting from peroxide cyclization [86]. This process is presented graphically in *Fig. 2B*.

E.J. Bechara *et al.* investigated the mechanisms of dioxetane formation and decomposition [103]. The obtained data showed that, in addition to the classical non-radical decomposition of dioxetane to two carbonyl compounds in a triplet EES and the ground state, a radical containing a carbonyl group is formed instead of the second compound, as well as either lipid peroxide or lipid peroxyl radicals. Having avoided the Russell mechanism, these radicals can form a lipoxyl radical RO$^{\cdot}$, which can convert to an alkyl radical and a carbonyl compound or a radical with a either oxetane or oxirane structure, which rapidly decomposes, producing a tertiary radical bound to an alkoxy group [103]. The review by G. Cilento and W. Adam [106]

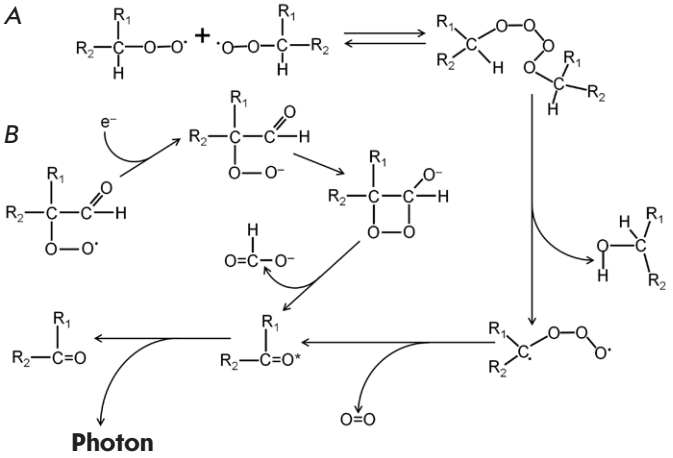

Fig. 2. The main mechanisms of photon emission in lipid oxidation [81, 102, 104, 107]. (*A*) –disproportionation of peroxyl radicals. (*B*) – formation and decomposition of the dioxetane group (dioxetanone is presented in the diagram)

presents various mechanisms of production of dioxetanes, with their subsequent cleavage to an excited product. In addition to the classical reaction scheme, the mechanism of aldehyde oxidation by oxygen through the formation of dioxetane, followed by the production of formic acid and excited aldehyde in the form of the next lower homolog, was shown [106]. The mechanism of formation of an excited ketone during oxidation and decomposition of diethylstilbestrol and other similar mechanisms were also described. Dioxetane can result from the oxidation of a phenol radical, which is produced during the interaction between phenol and a lipid peroxyl radical, by oxygen. This reaction is part of the mechanism of action of phenolic antioxidants [107]. Other ways of formation of excited products, such as recombination of two tertiary alcohol α-radicals, formation of excited products upon "sticking" of radicals due to free valences, formation of an excited ketone upon dehydration of hydrocarbon hydroperoxide (including lipid hydroperoxides), etc., were also presented [107].

Let us return to lipid peroxidation. The rate of peroxide oxidation is the rate of formation of the products of lipid oxidation by hydroperoxide in reaction (10) with the rate constant k_{2b}:

$$\frac{d\left[\text{ROOH}\right]}{dt} = k_{2b}\left[\text{RH}\right]\left[\text{ROO}^{\cdot}\right] = k_{2b}\left[\text{RH}\right]\sqrt{\frac{J}{Q_{\text{ChLum}} k_{2e}}}. \qquad (19)$$

Hence, the peroxidation rate is to a certain extent proportional to the steady-state concentration of free radicals in the system and depends on the chemiluminescence intensity. Therefore, measuring the chemiluminescence intensity allows one to assess the changes in the lipid peroxidation rate over time and, thus, study the kinetics and the mechanism of this process [24].

The described relationship between the intensity of the intrinsic chemiluminescence accompanying free radical oxidation of lipids and the rate of this oxidation was confirmed by the study of successive stages of chemiluminescence in model systems containing lipids (liposomes and mitochondria) with the addition of salts dissociating to Fe^{2+} cations [108, 109]. A study of the kinetics of such chemiluminescence with determination of the level of oxygen consumption, Fe^{2+} to Fe^{3+} oxidation, and mathematical modeling of reactions [110] made it possible to determine the equations of the lipid oxidation cascade, identify the rate constants of its main reactions, and also study the effect of various antioxidants on it. The method of chemiluminescence detection is a convenient tool to study lipid peroxidation. This method was widely used by R.F. Vasil'ev [111–116], Yu.A. Vladimirov [62, 117–119], A.I. Zhuravlev [31], and other researchers [17, 30, 120–127].

As things stand, the study of the kinetics of lipid peroxidation caused by free iron ions is becoming relevant again. This is due to the discovery of another type of programmed cell death in 2012: ferroptosis [61], which is necrosis-like cell death caused by the oxidation of mitochondrial structures, primarily membranes, induced by iron ions through the Fenton reaction [59, 83, 93].

Detection of intrinsic chemiluminescence is used in the study of various biological model systems [29, 128, 129]. In addition to lipid peroxidation, NO synthesis also causes tissue chemiluminescence, as shown by J.F. Turrens *et al.* in perfused lung and model systems [130, 131]. Interaction of peroxynitrite with proteins is another source of chemiluminescence [132], with interaction of peroxynitrite with tryptophan making the greatest contribution to luminescence, while reaction with phenylalanine provides a somewhat smaller yield [131]. This method for detecting intrinsic chemiluminescence has been successfully used in the study of the peroxidation of lipids comprising low-density lipoproteins in blood plasma stimulated by neutrophils [133].

However, the intensity of intrinsic chemiluminescence is extremely low in the majority of cases [29, 31, 134], which significantly complicates its detection. In addition, a study often requires the analysis of specific radicals. For example, lipid peroxidation reactions require an assessment of the presence of lipid radicals in the system. However, the method of chemiluminescence detection has no specificity [29]. Therefore, most studies require the use of specific luminescent additives that enhance the signal through a migration of the electronic excitation energy from the molecules resulting from free radical reactions to them, followed by the emission of photons with a higher quantum yield than that of the products. These substances can be called enhancers or chemiluminescence activators; they will be discussed in the next part of the review. ●

The author of this review is grateful to N.P. Lysenko, Professor of the Department of Radiobiology and Virology n.a. A.D. Belov and V.N. Syurin at K.I. Scriabin Moscow State Academy of Veterinary Medicine and Biotechnology, for help in preparing the English version of the article.

REFERENCES

1. Listov M.V., Mamykin A.I., Rassadina A.A. // Journal of new medical technologies. Electronic edition. 2017. V. 2. P. 259–266.
2. Listov M.V., Mamykin A.I. // Bulletin of the Russian military medical academy. 2018. V. 4(64). P. 117–122
3. Tropskaya N.S., Kislyakova E.A., Vilkova I.G., Kislicyna O.S., Gurman Yu.V., Popova T.S., Bajmatov V.N. // Bulletin of Experimental Biology and Medicine. 2020. V. 169. № 3. P. 391–396.
4. Miller G.W., Labut E.M., Lebold K.M., Floeter A., Tanguay R.L., Traber M.G. // J. Nutr Biochem. 2012. V. 23(5). P. 478–486.
5. Listov M.V., Mamykin A.I. // Clinical Pathophysiology. 2014. V. 3. P. 34–39.
6. Liang X.G., Cheng J., Qin S., Shao L.X., Huang M.Z., Wang G., Han Y., Han F., Li X. // Chem. Commun. 2018. V. 54. № 85. P. 12010–12013.
7. Vladimirov Yu.A., L'vova O.F. // Biophysics. 1964. № 9(4). P. 506–507.
8. Vladimirov Yu.A., L'vova O.F., Cheremisina Z.P. // Biochemistry (Moscow). 1966. V. 31(3). P. 507–514.
9. L'vova O.F., Vladimirov Yu.A. // Proceedings of the Moscow Society of Nature Experts. 1966. V. 16. P. 214–217.
10. Mayne B.C. // Brookhaven Symposia Biology. 1966. V. 19. P. 460–466.
11. Tarusov B.N., Polivoda A.I., Zhuravlyov A.I. // Biophysics. 1961. V. 6. № 4. P. 490–492.
12. Bajmatov V.N., Hromova E.V., Rybkova O.O. // Rabbit breeding and fur farming. 2016. №6. P. 27–28.
13. Hughes D.L., Richards R.S., Lexis L.A. // Luminescence: J. Biol. Chem. Luminescence. 2018. V. 33. № 4. P. 764–770.

14. Ding L., Wu Y., Duan Y., Yu S., Yu F., Wang J., Tian Y., Gao Z., Wan Z., He L. // ACS Sensors. 2020. V. 5. № 2. P. 440–446.
15. Jantan I., Harun N.H., Septama A.W., Murad S., Mesaik M.A. // J. Nat. Med. 2011. V. 65. № 2. P. 400–405.
16. Karazhaeva M.I., Saksonova E.O., Klebanov G.I., Lyubickij O.B., Gur'eva N.V. // Vestnik oftal'mologii. 2004. V. 120. № 4. P. 14–18.
17. Krasowska A., Piasecki A., Murzyn A., Sigler K. // Folia Microbiol. 2007. V. 52. № 1. P. 45–51.
18. Lynch D.V., Thompson J.E. // FEBS Lett. 1984. V. 173. № 1. P. 251–254.
19. Wildhagen M., Albert M., Butenko M.A. // Meth. Mol. Biol. 2017. V. 1610. P. 287–295.
20. Romodin L.A., Vladimirov Yu.A., Lysenko N.P., Zarudnaya E.N. // Izvestia MAAO. 2018. V. 42. № 1. P. 112–117.
21. Romodin L.A., Shangin S.V., Vladimirov Yu.A., Lysenko N.P., Hramov A.P. // Izvestia MAAO. 2018. V. 42. № 1. P. 118–123.
22. Jain R., Sharma D., Kumar R. // J. Biochem. 2019. V. 165. № 2. P. 125–137.
23. Vladimirov Yu.A., Proskurnina E.V., Alekseev A.V. // Biochemistry (Moscow). 2013. V. 78. № 10. P. 1391–1404.
24. Phillips D., Anissimov V., Karpukhin O., Shlyapintokh V. // Photochem. Photobiol. 1969. V. 9. № 2. P. 183–187.
25. Wen W.Y., Johnson D.R., Dole M. // Am. Chem. Soc. 1974. V. 7. № 2. P. 199–204.
26. Vassil'ev R.F., Vichutinskii A.A. // Nature. 1962. V. 194. № 4835. P. 1276–1277.
27. Belyakov V.A., Vassil'ev R.F. // Photochem. Photobiol. 1970. V. 11. № 3. P. 179–192.
28. Vladimirov Yu.A., Archakov A.I. Lipid peroxidation in biological membranes. M.: Science. 1972. 252 p.
29. Vladimirov Yu.A., Proskurnina E.V. // Advances in biological chemistry. 2009. V. 49. P. 341–388.
30. Bajmatov V.N., Bagautdinov A.M., Bajmatov N.V. Mechanisms for correcting free radical oxidation with antioxidants. Ufa: Publishing house of the Bashkir Agrarian University, 2008. 312 p.
31. Zhuravlyov A.I., Zubkova S.M. Antioxidants. Free radical pathology, aging. Second edition, revised and enlarged. M.: White Alves, 2014. 304 p.
32. Lepeschkin W.W. // Science. 1932. V. 76. № 1975. P. 409.
33. Lepeschkin W.W. // Science. 1932. V. 76. № 1964. P. 168.
34. Gurvich A.G. Mitogenetic radiation. M.: Gosmedizdat, 1934.
35. Boveris A., Cadenas E., Chance B. // Fed. Proc. 1981. V. 40. № 2. P. 195–198.
36. Colli L., Facchini U. // Nuovo Cimento. 1954. V. 12. № 1. P. 150–153.
37. Allen R.C., Stjernholm R.L., Steele R.H. // Biochem. Biophys. Res. Commun. 1972. V. 47. № 4. P. 679–684.
38. Stjernholm R.L., Allen R.C., Steele R.H., Waring W.W., Harris J.A. // Infection Immunity. 1973. V. 7. № 2. P. 313–314.
39. Vassil'ev R.F. // Nature. 1962. V. 196. № 4855. P. 668–669.
40. Shlyapintoh V.YA., Karpuhin O.N., Postnikov L.M., Zaharov I.V., Vichutinskij A.A., Cepalov V.F. Chemiluminescent methods for studying slow chemical processes. M.: Science, 1966. 300 p.
41. Gomberg M. // J. Chem. Edu. 1932. V. 9. № 3. P. 439–451.
42. Gomberg M. // J. Am. Chem. Soc. 1903. V. 25. № 12. P. 1274–1277.
43. Gomberg M. // J. Am. Chem. Soc. 1901. V. 23. № 7. P. 496–502.
44. Fischer V., Mason R.P. // J. Biol. Chem. 1984. V. 259. № 16. P. 10284–10288.
45. Fischer V., West P.R., Harman L.S., Mason R.P. // Envi. Hlth Persp. 1985. V. 64. P. 127–137.
46. Michaelis L. // Am. Sci. 1946. V. 34. № 4. P. 573–596.
47. Michaelis L., Schubert M.P., Smythe C.V. // Science. 1936. V. 84. № 2171. P. 138–139.
48. Granick S., Michaelis L., Schubert M.P. // Science. 1939. V. 90. № 2340. P. 422–423.
49. Dysregulatory Pathology: A Guide for Physicians and Biologists. M.: Medicine, 2002. P. 140–151.
50. Babior B.M. // Adv. Enzymol. Related Areas Mol. Biol. 1992. V. 65. P. 49–95.
51. Babior B.M. // J. Clin. Invest. 1984. V. 73. № 3. C. 599–601.
52. Listov M.V., Mamykin A.I. // Clinical Pathophysiology. 2015. №2. P. 54–58.
53. Vladimirov Yu.A. // Annals of the Russian academy of medical sciences. 1998. №7. P. 43–51.
54. Lobachev V.L., Rudakov E.S. // Russian chemical reviews. 2006. V. 75. № 5. P. 422–444.
55. Uzbekov M.G. // Social and Clinical Psychiatry. 2014. V. 24. № 4. P. 97–103.
56. Benhar M. // Free Rad. Biol. Med. 2018. V. 127. P. 160–164.
57. Panasenko O.M., Gorudko I.V., Sokolov A.V. // Advances in biological chemistry. 2013. V. 53. P. 195–244.
58. Kagan V.E., Tyurin V.A., Jiang J., Tyurina Y.Y., Ritov V.B., Amoscato A.A., Osipov A.N., Belikova N.A., Kapralov A.A., Kini V.V., et al. // Nat. Chem. Biol. 2005. V. 1. P. 223–232.
59. Chen G., Guo G., Zhou X., Chen H. // Oncol. Lett. 2020. V. 19. № 1. P. 579–587.
60. Lei G., Zhang Y., Koppula P., Liu X., Zhang J., Lin S.H., Ajani J.A., Xiao Q., Liao Z., Wang H., et al. // Cell Res. 2020. V. 30. P. 146–162.
61. Dixon S.J., Lemberg K.M., Lamprecht M.R., Skouta R., Zaitsev E.M., Gleason C.E., Patel D.N., Bauer A.J., Cantley A.M., Yang W.S., et al. // Cell. 2012. V. 149. № 5. P. 1060–1072.
62. Dyomin E.M., Proskurnina E.V., Vladimirov Yu.A. // Moscow University Bulletin. Series 2: Chemistry. 2008. V. 49. № 5. P. 354–360.
63. Capdevila D.A., Oviedo Rouco S., Tomasina F., Tortora V., Demicheli V., Radi R., Murgida D.H. // Biochemistry. 2015. V. 54. № 51. P. 7491–7504.
64. Kobayashi H., Nagao S., Hirota S. // Angew. Chem. Int. Ed. Engl. 2016. V. 55. № 45. P. 14019–14022.
65. Singh H., Pritchard E.T. // Can. J. Biochem. Physiol. 1962. V. 40. P. 317–318.
66. Ruottinen M., Kuosmanen V., Saimanen I., Kaaronen V., Rahkola D., Holopainen A., Selander T., Kokki H., Kokki M., Eskelinen M. // Anticancer Res. 2020. V. 40. № 1. P. 253–259.
67. Bel'skaya L.V., Kosenok V.K., Massard Z.H., Zav'yalov A.A. // Annals of the Russian academy of medical sciences. 2016. V. 71(4). P. 313–322.
68. Login C.C., Baldea I., Tiperciuc B., Benedec D., Vodnar D.C., Decea N., Suciu S. // Oxidative Med. Cell. Long. 2019. V. 2019. P. 1607903.
69. Tarasov S.S., Koryakin A.S. // Bulletin of Perm University. Biology. 2016. V. 3. P. 292–296.
70. Shaw S., Rubin K.P., Lieber C.S. // Digestive Dis. Sci. 1983. V. 28. № 7. P. 585–589.
71. Men'shchikova E.B., Zenkov N.K., Lankin V.Z. Oxidative stress. Pathological conditions and diseases. Novosibirsk: ARTA, 2008. 284 p.
72. Cole T., Heller C., Mcconnell H.M. // Proc. Natl. Acad. Sci.

USA. 1959. V. 45. № 4. P. 525–528.
73. Hole E.O., Sagstuen E., Nelson W.H., Close D.M. // Radiation Res. 2000. V. 153. № 6. P. 823–834.
74. Chiesa M., Giamello E., Livraghi S., Paganini M.C., Polliotto V., Salvadori E. // J. Physics. Condensed Matter: an Institute of Physics journal. 2019. V. 31. № 44. P. 444001.
75. Sapezhinskij I.I., Emanuel' N.M. // Reports of the USSR Academy of Sciences. 1965. V. 165. №4. P. 845–847.
76. Osipov A.N., Savov V.M., YAh"yaev A.V., Zubarev V.E., Azizova O.A., Kagan V.E., Vladimirov Yu.A. // Biophysics. 1984. № 29(4). P. 533–536.
77. Azizova O.A., Osipov A.N., Savov V.M., YAh"yaev A.V., Zubarev V.E., Kagan V.E., Vladimirov Yu.A. // Biophysics. 1985. № 30(1). P. 36–39.
78.Gazarian I.G., Lagrimini L.M., Mellon F.A., Naldrett M.J., Ashby G.A., Thorneley R.N. // Biochem. J. 1998. V. 333(Pt 1). P. 223–232.
79.Shliapintokh V.J., Vasil´Ev R.F., Karpukhine O.N., Postnikov L.M., Kibalko L.A. // J. Chim. Phys. 1960. V. 57. P. 1113–1122.
80. Vassil'ev R.F. // Progress Reaction Kinetics. 1967. V. 4. P. 305–352.
81. Vladimirov Yu.A. Superweak fluorescence during biochemical reactions. M.: Science, 1966. 126 p.
82. Margulis G.V. // Superweak luminescence in biology / Edited by A.I. Zhuravlev. – M.: Science. 1972. P. 72–75.
83.Proneth B., Conrad M. // Cell Death Differ. 2019. V. 26. № 1. P. 14–24.
84. Aspee A., Lissi E.A. // J. Protein Chem. 2001. V. 20. № 6. P. 479–485.
85. Aspee A., Lissi E.A. // Luminescence: J. Biol. Chem. Luminescence. 2000. V. 15. № 5. P. 273–282.
86. Lissi E.A., Caceres T., Videla L.A. // Free Rad. Biol. Med. 1988. V. 4. № 2. P. 93–97.
87. Novikov V.V., Ponomapev V.O., Novikov G.V., Kuvichkin V.V., Yablokova E.V., Fecenk E.E. // Biophysics. 2010. V. 55. № 4. P. 631–639.
88. Tekuckaya E.E., Baryshev M.G., Il'chenko G.P. // Biophysics. 2015. V. 60. №6. P. 1099–1103.
89. Gnaim S., Shabat D. // J. Am. Chem. Soc. 2017. V. 139. № 29. P. 10002–10008.
90.Belyakov V.A., Vassil'ev R.F. // Photochem. Photobiol. 1967. V. 6. № 1. P. 35–40.
91. Melville H.W., Richards S. // J. Chem. Soc. 1954. P. 944–952.
92. Vikulina A.S., Alekseev A.V., Proskurnina E.V., Vladimirov Yu.A. // Biochemistry (Moscow). 2015. V. 80. № 10. P. 1298–1302.
93. Yang W.S., Stockwell B.R. // Trends Cell Biol. 2016. V. 26. № 3. P. 165–176.
94. Vladimirov Y.A., Olenev V.I., Suslova T.B., Cheremisina Z.P. // Adv. Lipid Res. 1980. V. 17. P. 173–249.
95. Semyonov N.N. // Russian Chemical Reviews. 1976. V. 36. № 1. P. 3–33.
96. Semyonov N.N. // Soviet Physics Uspekhi. 1931. V. 11. № 2. P. 250–275.
97. Pringsheim P. Fluorescence and Phosphorescence. New York and London: Intersci. Publ., 1949. 794 p.
98. Konev S.V. Electronically excited states of biopolymers. Minsk: Science and Technology, 1965. 186 p.
99. De Oliveira S., De Souza G.A., Eckert C.R., Silva T.A., Sobral E.S., Fávero O.A., Ferreira M.J.P., Romoff P., Baader W.J. // Química Nova. 2014. V. 37. № 3. P. 497–503.
100. Bastos E.L., Romoff P., Eckert C.R., Baader W.J. // J. Agricult. Food Chem. 2003. V. 51. № 25. P. 7481–7488.
101. Russell G.A. // J. Am. Chem. Soc. 1957. V. 79(14). P. 3871–3877.
102. Dole M. // J. Phys. Chem. 1987. V. 91. № 12. P. 3117–3119.
103. Timmins G.S., Dos Santos R.E., Whitwood A.C., Catalani L.H., Di Mascio P., Gilbert B.C., Bechara E.J. // Chem. Res. Toxicol. 1997. V. 10. № 10. P. 1090–1096.
104. Niu Q., Mendenhall G.D. // J. Am. Chem. Soc. 1990. V. 112. № 4. P. 1656–1657.
105. Cadenas E. // Annu. Rev. Biochem. 1989. V. 58. P. 79–110.
106. Cilento G., Adam W. // Free Rad. Biol. Med. 1995. V. 19. № 1. P. 103–114.
107. Vasil'ev R.F., Trofimov A.V. // Kinetics Catalysis. 2009. V. 50. № 4. P. 540–542.
108. Sharov V.S., Driomina E.S., Vladimirov Y.A. // J. Biolum. Chemilum. 1996. V. 11. № 2. P. 91–98.
109. Vladimirov Yu.A., Suslova T.B., Olenev V.I. // Biophysics. 1969. V. 14. № 5. P. 836–845.
110. Vladimirov Yu.A., Gutenev P.I., Kuznecov P.I. // Biophysics. 1973. V. 18. № 6. P. 1024–1029.
111. Vasil'ev R.F., Veprincev T.L., Dolmatova L.S., Naumov V.V., Trofimov A.V., Caplev Yu.B. // Kinetics and Catalysis. 2014. V. 55. №2. P. 157–162.
112. Vasil'ev R.F., K"ncheva V.D., Fedorova G.F., B"tovska D.I., Trofimov A.V. // Kinetics and Catalysis. 2010. V. 51. №4. P. 533–541.
113. Fedorova G.F., Menshov V.A., Trofimov A.V., Vasil'ev R.F. // The Analyst. 2009. V. 134. № 10. P. 2128–2134.
114. Slavova-Kazakova A.K., Angelova S.E., Veprintsev T.L., Denev P., Fabbri D., Dettori M.A., Kratchanova M., Naumov V.V., Trofimov A.V., Vasil'ev R.F., et al. // Beilstein J. Organic Chem. 2015. V. 11. P. 1398–1411.
115. Fedorova G.F., Menshov V.A., Trofimov A.V., Tsaplev Y.B., Vasil'ev R.F., Yablonskaya O.I. // Photochem. Photobiol. 2017. V. 93. № 2. P. 579–589.
116. Fedorova G.F., Lapina V.A., Menshov V.A., Naumov V.V., Trofimov A.V., Tsaplev Y.B., Vasil'ev R.F., Yablonskaya O.I. // Photochem. Photobiol. 2019. V. 95. № 3. P. 780–786.
117. Vladimirov Yu.A., Sergeev P.V., Sejfulla R.D., Rudnev Yu.N. // Molecular Biology. 1973. V. 7. № 2. P. 247–253.
118. Li H.I., Vladimirov Yu.A., Deev A.I. // Biophysics. 1990. V. 35. № 1. P. 82–85.
119. Rubene D.Ya., Sharov V.S., Olenev V.I., Tirzit G.D., Dubur G.Ya., Vladimirov Yu.A. //
Russian Journal of Physical Chemistry. 1981. V. 55 №2. P. 511–512.
120. Tsukagoshi K., Taniguchi T., Nakajima R. // Anal. Chim. Acta. 2007. V. 589. № 1. P. 66–70.
121. Saleh L., Plieth C. // Nat. Protocols. 2010. V. 5. № 10. P. 1627–1634.
122. Mcdermott G.P., Conlan X.A., Noonan L.K., Costin J.W., Mnatsakanyan M., Shalliker R.A., Barnett N.W., Francis P.S. // Anal. Chim. Acta. 2011. V. 684. № 1–2. P. 134–141.
123. Ginsburg I., Kohen R., Shalish M., Varon D., Shai E., Koren E. // PLoS One. 2013. V. 8. № 5. P. e63062.
124. Xie G.Y., Zhu Y., Shu P., Qin X.Y., Wu G., Wang Q., Qin M.J. // J. Pharmaceut. Biomed. Analysis. 2014. V. 98. P. 40–51.
125. Malejko J., Nalewajko-Sieliwoniuk E., Szabunko J., Nazaruk J. // Phytochem. Analysis: PCA. 2016. V. 27. № 5. P. 277–283.
126. Sun S., Xu S., Xu Y., Guo L., Liu H., Yang L., Wang Z. // Anal. Chim. Acta. 2019. V. 1046. P. 148–153.
127. Kishikawa N., El-Maghrabey M., Nagamune Y., Nagai K., Ohyama K., Kuroda N. // Anal. Chem. 2020. V. 92. № 10. P. 6984–6992.

128. Volkova P.O., Alekseev A.V., Dzhatdoeva A.A., Proskurnina E.V., Vladimirov Yu.A. // MSU Bulletin, Series 2: Chemistry. 2016. V. 57. № 1. P. 41–52.
129.Vladimirov Yu.A., Proskurnina E.V., Izmajlov D.Yu. // Bull. Exp. Biol. Med. 2007. V. 144. № 3. P. 390–396.
130. Barnard M.L., Robertson B., Watts B.P., Turrens J.F. // Am. J. Physiol. 1997. V. 272. № 2. Pt 1. P. L262–L267.
131. Pollet E., Martinez J.A., Metha B., Watts B.P., Jr., Turrens J.F. // Arch. Biochem. Biophys. 1998. V. 349. № 1. P. 74–80.
132. Watts B.P., Jr., Barnard M., Turrens J.F. // Arch. Biochem. Biophys. 1995. V. 317. № 2. P. 324–330.
133. Vladimirov Yu.A., Ribarov S.R., Bochev P.G., Benov L.C., Klebanov G.I. // Gen. Physiol. Biophys. 1990. V. 9. № 1. P. 45–54.
134. Vikulina A.S., Dzhatdoeva A.A., Lobichenko E.N., Proskurnina E.V., Vladimirov Yu.A. // Journal of Analytical Chemistry. 2017. V. 72. № 7. P. 639–644.

Inactivating Gene Expression with Antisense Modified Oligonucleotides

Sidney Altman[1*], Carlos Angele-Martinez[2]
[1]Yale University New Haven CT USA, Arizona State University, Tempe AZUSA
[2]Yale University New Haven CT USA
*E-mail: sidney.altman@yale.edu
Received March 11, 2021; in final form, September 21, 2021
DOI: 10.32607/actanaturae.11522

ABSTRACT **Modified nucleotides, including phosphoramidates and mesyl nucleotides, are very effective in inactivating gene expression in bacteria.** ***Gyr A*** **is the target gene in several organisms, including** *Plasmodium falciparum*. **Antisense reactions with bacteria infecting citrus plants are promising but incomplete. Human tissue culture cells assayed with a different target are also susceptible to the presence of mesyl oligonucleotides.**
KEYWORDS **modified nucleotides, gene expression, bacteria,** *Plasmodium falciparum*, **citrus plants.**

INTRODUCTION

Over several years, the research focused on RNase P has been relying on standard oligonucleotides A, C, U, G in RNA (*Fig. 1*). That was sufficient to probe both the function and structure of the enzyme in bacteria [1–5]. However, once the focus switched to the study of the suppression of the activity of various genes, the advent of phosphoramidates (PMs; [6, 7]; see *Fig. 2*) and 2'OMe nucleotides, which have the advantage of being characterized by a higher membrane permeability and nuclease resistance compared to those of standard oligonucleotides, has led to a spate of attempts using modified oligonucleotides (MOs) as antisense oligonucleotides to turn gene expression off.

Various permutations of MOs (i.e., using different modified oligos at various positions in the antisense molecules) proved unsuccessful in gene inactivation studies. Fully modified MOs were nonspecifically lethal in living cells. When using modified oligonucleotides, the application of RNase P and a particular MO to target gene expression has the potential to kill the bacteria being studied (*gyr A*, the ultimate target; [8]) in lethal gene suppression studies. In the present report, critical metabolism functions were not extensively studied.

The target chosen was the essential gene *gyr A* [8], the aspecific target gene sequence in the gene being almost invariant in several bacteria (*Table 1*). An MO with a 5' peptide attached (*Fig. 2*) was used to test most of the bacteria with the gyr A target. This oligonucleotide facilitated the import of MOs in bacteria.

RNase P will cleave any oligonucleotide containing the 3'CCA sequence and at least one extra nucleotide

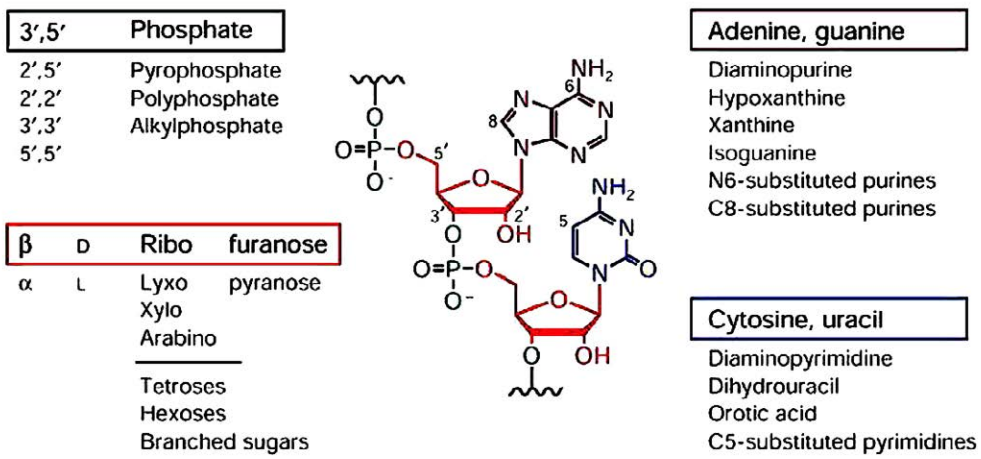

Fig. 1. Schematic portrayal of the standard ribonucleotides with substitutes in different positions

Table 1. The sequences of parts of the *gyr A* gene that are complementary to the *E. coli gyr A* gene listed above. Note the mismatches in Watson–Crick (W-C) base pairing. The mismatches are shown in red. Gyr 313-14 is simply the name of one of the preparations

Alignment of GyrA 313 bacterial sequences

Gyr 313-14:	ACCCTGACCGACCA
Escherichia coli	CGGTCAGGGT
Acinetobacter ADP1	CGGTCAGGGC
Acinetobacter baumannii	TGGTCAGGGT
Bacillus subtilis	CGGTCACGGA
Clostridium difficile	TGGTCATGGT
Enterobacter cloacae	TGGCCAGGGT
Enterococcus faecalis	CGGCCACGGA
Klebsiella pneumonia	CGGCCAGGGT
Mycobacterium marinarum	CGGTCAGGGC
Mycobacterium smegmatis	CGGCCAGGGC
Pseudomonas aeruginosa	CGGCCAGGGC
Pseudomonas syringae	CGGTCAGGGC
Salmonella enterica ssp. typhimurium	TGGTCAGGGT
Staphylococcus aureus	TGGCCAAGGT
Streptococcus pneumoniae	TGGTCATGGG
Listeria monocytogenes	TGGACATGGT
Xylella fastidiosa	GGGTCAAGGT
Candidatus Liberibacter asiaticus	AGGACAAGGA

at its 5' end adjacent to the double-stranded region (For details please refer to *Fig. 3*) [9]. The initial experiments to suppress the activity of the genes that provide drug resistance (penicillin, chloramphenicol) used the known properties of RNase P (*Table 2*, [10–12]). The success of the new methodology is apparent: under the conditions used by us, *Streptococcus* and *Staphylococcus* were inhibited only to a level of 10^{-2} after 6 h of incubation at 37°C. Two major pathogens, *Yersinia pestis* and *Francisellatularensis*, assayed using MOs in a slightly different way, were also inhibited to

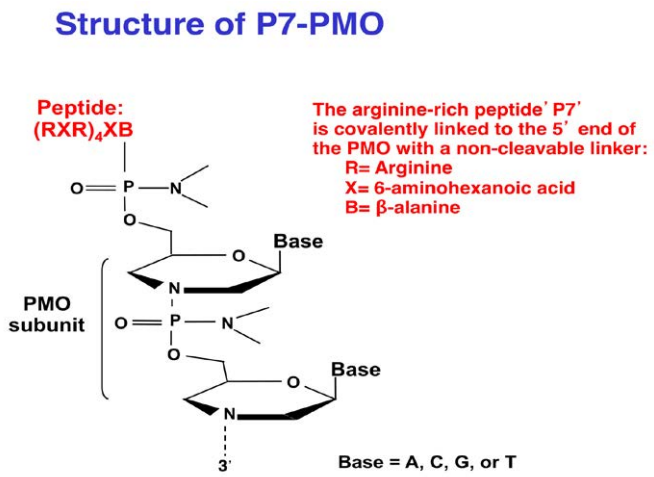

Fig. 2. The portrayal of a phosphoramidate with a basic peptide attached to the 5′ end. Courtesy of Sarepta

a level of 40–50% [13, 14], but *gyr A* was not the target in the two cases, and these experiments were never pursued. The new methodology and the gyr A target can be employed to ensure a much lower survival rate under the conditions used.

Table 1 lists several sequences in bacteria that are complements to the *E. coli gyr A* sequence as a target. It is noteworthy that there are several W-C mismatches in some bacteria, but at the most three proved successful in the experiments that were performed. The viability of bacteria infected with an appropriate MO decreased from 3 to 6 orders of magnitude after the incubation with the MO at 37°C for 6 h (*Table 2; Figs. 2 and 4*). Several bacteria responsible for acute human infections (*Streptococcus* and *Staphylococcus*) can be inactivated in the way noted above. A MO with an attached peptide facilitated the penetration of MO into bacteria, as

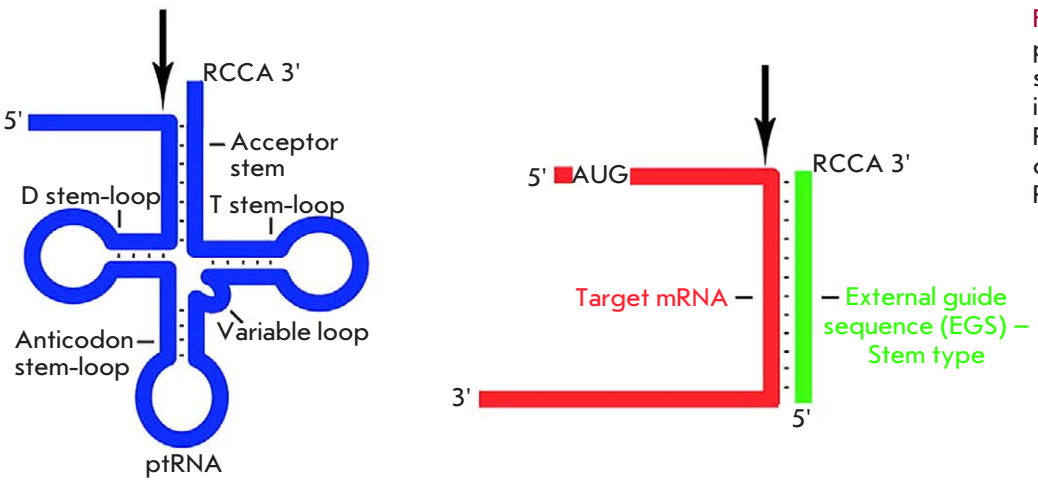

Fig. 3. (Left) Schematic portrayal of a tRNA precursor with the arrow indicating the site of cleavage by RNase P (Right). Portrayal of a minimal substrate for RNase P

Table 2. Inactivation of various genes using the antisense technology*

Inhibition of gene expression by appropriate conjugate	
Gene	**Organism**
gyrA	Gram negative and Gram positive bacteria
bla(ampicillin)	*E. coli*
Cm (chloramphenicol)	"
gyrA	*P. falciparum*
DXR	"
Chloroquine resist.	"
Artemisinin clear.	"

*Bacteria and *P. falciparum* were exposed to an antisense molecule (~ 5 ug/ml) at 37°C for 6 hrs. Please see the text for the details.

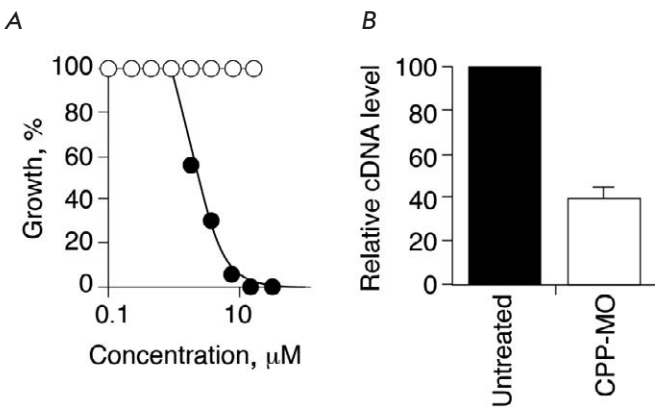

Fig. 4. Survival of *P. falciparum* in red blood cells after treatment with an antisense oligonucleotide

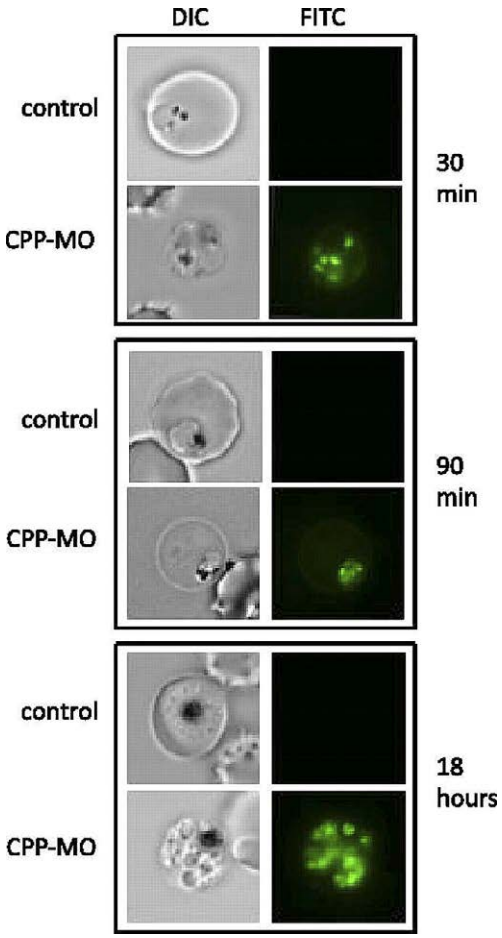

Fig. 5. Development of *P. falciparum* in red blood cells after treatment with an antisense oligonucleotide. Fluorescence microscopy images are shown on the right-hand side of the figure. No lysis of red blood cells by the fluorescent dye occurred

shown in *Table 2* [15, 16] and *Fig. 4*. Subsequently, the *in vitro* inactivation of *P. falciparum* in red blood cells was tested again, with targeting of the *gyr A* gene of this organism [17, 18]. These experiments have been successful (*Figs. 5 and 6*). Note that the development of the *P. falciparum* is clearly inhibited (50%) at a MO concentration of 0.5 μg/ml (*Fig. 6*). The MO used was effective against *P. falciparum* cells, being resistant to different drugs (arteminisin, etc.), as well as against the normal parasite. The prospect of using the MO as an anti-malarial therapy remains to be explored.

The general method failed to work in one experiment in mice where the amount of MO was inadequate and no lipofectamine was used to aid cell penetration of the MO and additionally there was no taking into consideration the cost of MO synthesis and the enzymatic subunit of *Escherichia coli*, RNase P. Research then subsequently shifted to bacterial infection in plants (e.g., inactivation of citrus plants by infecting bacteria).

The citrus industry in the U.S. has suffered devastating losses from infection by the insect *Diaphorinacitri* carrying a bacteria that renders saplings and trees unable to produce fruit [19]. *Table 1* shows the sequence of the complement of the *Wolbachia gyrA* gene. Several *Wolbachia* species can infect citrus saplings. RNase P can be isolated from *D. melanogaster* S2 cells *in vitro* to indicate the ability of similar flies to produce the enzyme. It would cleave tRNA precursors and M1 RNA in separate experiments. To show cleavage of the *gyr A* sequence, the *Wolbachia* sequence (*Table 1*), the MO, and the *gyr* RNA were exposed to M1 RNA, as well as to the purified *E. coli* RNase P. Preliminary analysis of the M1 RNA MO reactions with *gyrA* RNA, with low levels of radioactivity, indicated that some successful

Fig. 6. Schematic portrayal of an oligonucleotide with substitutions indicated, including the mesyl group

Structure of PO-ODNs, PS-ODNs, and μ-ODNs used in the study.

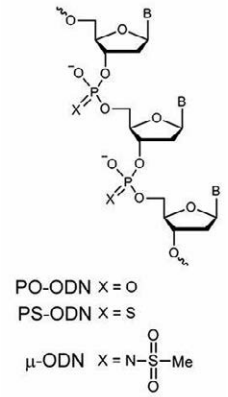

cleavage took place. These experiments must be repeated, along with the reactions with the *Wolbachia gyr A* sequence, which has only three mismatches with *E. coli gyr A*. If these reactions succeed, confirming the lethality of *Wolbachia in vitro*, a method of administration to hundreds or thousands of saplings must still be developed.

The *C. liberibacterasiaticus*, another factor in infecting saplings, has four mismatches in its *gyr A* gene compared to the one in *E. coli* (*Table 1*), an indication that complementarity would not be a valid counterpart in our experiments using MOs (*Table 1*).

Stetsenko et al. have recently synthesized a new modified oligonucleotide named mesyl MO (*Fig. 6* [20]) that is DNA-based and is more effective in inactivating gene expression. Its lethality characteristics are increased in comparison with previously designed modified oligos. RNase H attacks the DNA-miR21 hybrid. This new MO is much less successful in aiding cells separated by a scratch test to migrate during wound healing than cells transfected with other MO oligos (*Fig. 7*). This method of synthesizing mMO should be tested for inactivating the expression of the various genes mentioned in this paper. The new mesyl oligo is much more resistant to nonspecific nuclease degradation than other oligos and is 22 nts long, making it unique in human cells. A lipofectamine-driven encapsulation provides entry of this oligonucleotide into the cells in tissue culture. The targets listed in *Fig. 7* include miR21, specific to the new MO, and other non-specific targets. At zero time, all the samples showed intact colonies.

During the past few years, antisense oligonucleotides have been used to inhibit the function of various molecules in tissue culture cells. The prospect for designing new antibiotics has not been quite as bright as was promised by the industry, but some results have been achieved with derivatives of aminoglycosides and a few other molecules. Derivatives of hammerhead ri-

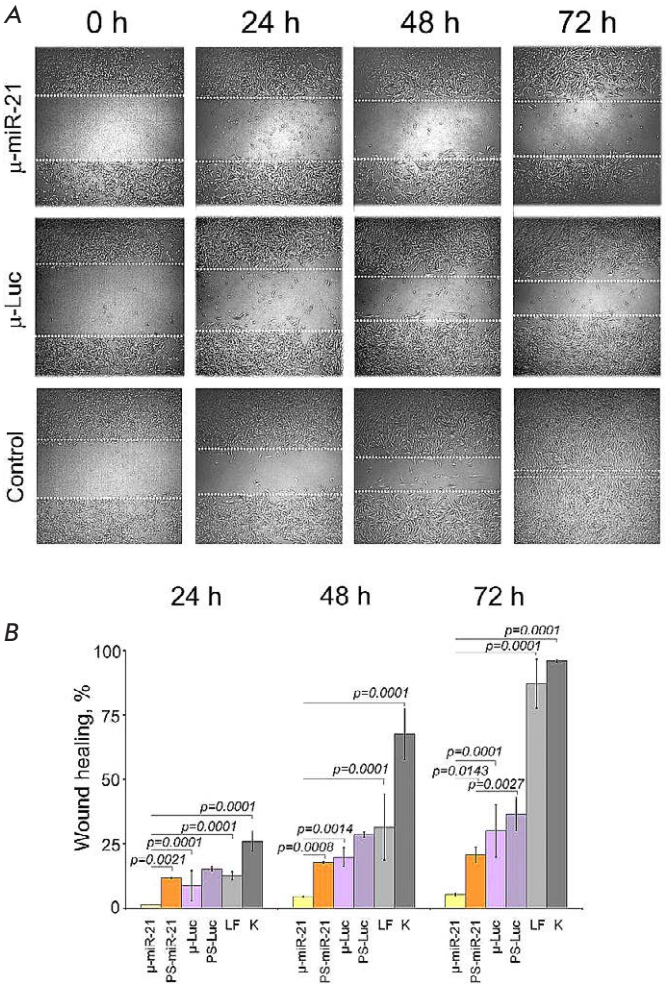

Fig. 7. The kinetics of wound healing with different mesyloligonculeotides. Zero time points were identical or corresponded to whole colonies. *A*. The image of the colonies at different time points. *B*. The kinetics of wound healing. K is the control. Other non-specific targets are also indicated

bozymes are still being studied as potential mechanisms of gene inactivation. The design of small pieces of RNA with distinct three-dimensional structures as gene inactivation inhibitors is in progress. Antisense has also been used to alter splicing reactions. In one case, antisense molecules have been productively used as therapy in cases of Duchenne muscular dystrophy [6]. The future of antisense molecules, modified or otherwise, appears bright. ●

We thank Professors A. Gabibov and A. Belogurov Jr. for their encouragement, Prof. A. Forster for comments, and our esteemed colleagues at Yale for their valuable advice and work.

REFERENCES

1. Stark B.C., Kole R., Bowman E.J., Altman S. // Proc. Natl. Acad. Sci. USA. 1978. V. 75. P. 3717–3721.
2. Guerrier-Takada C., Gardiner K., Marsh T., Pace N., Altman S. // Cell. 1983. V. 35. P. 849–857.
3. Lan P., Tan M., Zhang Y., Niu S., Chen J., Shi S., Qui S., Wang X., Peng X., Cai G., et al. // Science. 2018. V. 362. № 6415. P. eaat6678.
4. Wu J., Niu S., Tan M., Huang C., Li M., Song Y., Wang Q., Chen J., Shi S., Lan P., et al. // Cell. 2018. V. 175. P. 1393–1404.
5. Wan F., Wang Q., Tan J., Tan M., Chen J., Shi S., Lan P., Wu J., Lei M. // Nat. Comm. 2019. V. 10. P. 2617.
6. Kole R., Krainer A.R., Altman S. // Nature Drug Discovery. 2012. V. 11. P. 125–140.
7. Gait M.J., Arzumanov A.A., McClorey G., Godfrey C., Betts C., Hammond S., Wood M.J.A. //Nucl. Acid Ther. 2019. V. 29. P. 1–12.
8. Swanberg S.L, Wang J.C. // J. Mol. Biol. 1987. V. 197. P. 729–736.
9. Thomas B.C., Li X., Gegenheimer P. //RNA. 2000. V. 6. № 4. P. 545–553.
10. Panchal R.G., Geller B.L., Mellbye B., Lane D., Iversen P.L., Bavari S. // Nucl. Acid Ther. 2012. V. 22. № 5. P. 316–322.
11. Altman S. Ribonuclease P. New York: Springer Science, 2010. 280 p.
12. Wesolowski D., Tae H.S., Gandotra N., Llopis P., Shen N., Altman S. // Proc. Natl. Acad. Sci. USA. 2011. V. 108. P. 16582–16587.
13. Ko J.-H., Izadjoo M., Altman S. //RNA. 2008. V. 14. P. 1656–1662.
14. Xiao G., Lundblad E.W., Izadjoo M., Altman S. // PLoS One. 2008. V. 3. P. e3719–3725.
15. Shen N., Ko J.-H., Xiao G., Wesolowski D., Shan G., Geller B., Izadjoo M., Altman S. // Proc. Natl. Acad. Sci. USA. 2009. V. 106. P. 8163–8168.
16. Wesolowski D., Alonso D., Altman S. // Proc. Natl. Acad. Sci. USA. 2013. V. 110. P. 8686–8689.
17. Augagneur Y., Wesolowski D., Tae H.-S., Altman S., Ben Mamoun C. //Proc. Natl. Acad. Sci. USA. 2012. V. 109. P. 6235–6240.
18. Garg A., Wesolowski D., Alonso D., Deitsch K.W., Ben Mamoun C., Altman S. // Proc. Natl. Acad. Sci. USA. 2015. V. 112. P. 11935–11940.
19. Ren S.-L., Li Y.-H., Ou D., Guo Y.-J., Qureshi J.A., Stansly P.A., Qiu B.L. // Microbiologyopen. 2018. V. 7. P. e00561.
20. Miroshnichenko S.K., Patutina O.A., Burakova E.A., Chelobanov B.P., Fokina A.A., Vlassov V.V., Altman S., Zenkova M.A., Stetsenko D.A. //Proc. Natl. Acad. Sci. USA. 2019. V. 116. P. 1229–1234.

A Monoiodotyrosine Challenge Test in a Parkinson's Disease Model

A. R. Kim*, E. N. Pavlova, V. E. Blokhin, V. V. Bogdanov, M. V. Ugrumov
Koltzov Institute of Developmental Biology of Russian Academy of Sciences, Moscow, 119334 Russia
*E-mail: alexandrrkim@gmail.com
Received April 09, 2021; in final form, June 03, 2021
DOI: 10.32607/actanaturae.11399

ABSTRACT **Early (preclinical) diagnosis of Parkinson's disease (PD) is a major challenge in modern neuroscience. The objective of this study was to experimentally evaluate a diagnostic challenge test with monoiodotyrosine (MIT), an endogenous inhibitor of tyrosine hydroxylase. Striatal dopamine was shown to decrease by 34% 2 h after subcutaneous injection of 100 mg/kg MIT to intact mice, with the effect not being amplified by a further increase in the MIT dose. The selected MIT dose caused motor impairment in a neurotoxic mouse model of preclinical PD, but not in the controls. This was because MIT reduced striatal dopamine to the threshold of motor symptoms manifestation only in PD mice. Therefore, using the experimental mouse model of preclinical PD, we have shown that a MIT challenge test may be used to detect latent nigrostriatal dysfunction.**
KEYWORDS **Parkinson's disease, early diagnosis, challenge test, monoiodotyrosine, MPTP.**
ABBREVIATIONS **DHBA – 3,4-dihydroxybenzylamine; HPLC-ED – high-performance liquid chromatography with electrochemical detection; MIT – monoiodotyrosine; MPTP – 1-methyl-4-phenyl-1,2,3,6-tetrahydropyridine; PD – Parkinson's disease; TH – tyrosine hydroxylase.**

INTRODUCTION

The pathogenesis of Parkinson's disease (PD), a frequent neurodegenerative disorder, is based on the degradation of the brain's dopaminergic nigrostriatal system that regulates motor function [1]. PD is characterized by a prolonged asymptomatic preclinical stage during which there is activation of the mechanisms that compensate the insufficiency of the nigrostriatal system [2]. Only 20–30 years after the disease onset, when the dopaminergic neuronal loss in the substantia nigra (SN) has reached more than 50%, and the striatal dopamine level has decreased below its threshold value (20–30% of the control level), does the patient develop specific motor symptoms that enable the diagnosis to be made [3].

In this context, of great importance is the development of a method for detecting latent neurodegeneration in the nigrostriatal system to diagnose PD long before the disease transits to its irreversible clinical stage. One of the most promising approaches is a challenge test involving short-term and reversible inhibition of tyrosine hydroxylase (TH), the key enzyme of dopamine synthesis [4]. The use of such an inhibitor at a dose that lowers the striatal dopamine level by 30–40% relative to its control values will not cause motor disorders in healthy people. In turn, the striatal dopamine level at the preclinical PD stage is initially reduced and its further decrease by an inhibitor will lead to hitting the threshold of motor symptoms manifestation, which enables the diagnosis to be made [5].

As a challenge agent, we used monoiodotyrosine (MIT), a reversible TH inhibitor that is present in the body as an intermediate in the synthesis of thyroid hormones [6]. Unlike synthetic inhibitors, such as α-methyl-*p*-tyrosine, MIT is of endogenous origin and undergoes rapid metabolism, which minimizes the duration of dopamine synthesis inhibition and reduces the risk of side effects [7].

The purpose of this study was to experimentally develop a MIT challenge test for the detection of latent neurodegeneration in a preclinical mouse model of PD. As a model, we used a neurotoxic preclinical PD model, developed earlier in our laboratory, based on dosed systemic administration of 1-methyl-4-phenyl-1,2,3,6-tetrahydropyridine (MPTP), a precursor of the dopaminergic neuron neurotoxin [8], to mice.

EXPERIMENTAL

We used 80 male C57BL/6 mice aged 2–2.5 months with a weight of 22–26 g (Stolbovaya nursery), which were kept under standard vivarium conditions with free access to food and water. Animal experiments

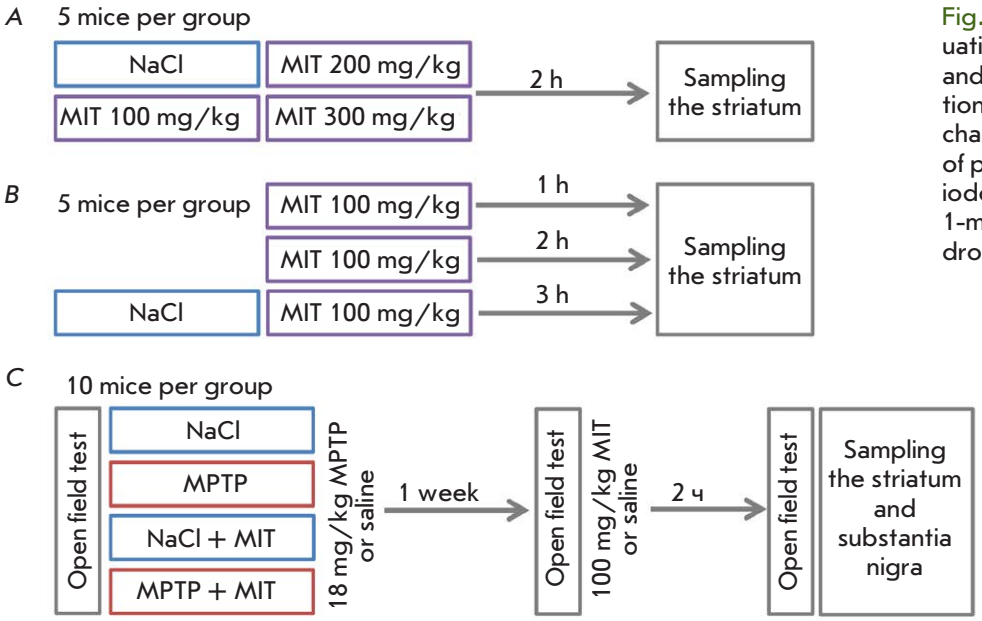

Fig. 1. Experimental schemes: evaluation of the optimal dose of MIT (*A*) and time interval after its administration (*B*) to normal mice, and the MIT challenge test in the MPTP model of preclinical PD (*C*). MIT – monoiodotyrosine, NaCl – saline, MPTP – 1-methyl-4-phenyl-1,2,3,6-tetrahydropyridine

were approved by the Ethics Committee of the Koltsov Institute of Developmental Biology of the Russian Academy of Sciences (Protocol No. 43 of November 19, 2020).

During the study, three experiments were performed (*Fig. 1*). In the first experiment, the effect of various MIT doses on the striatal dopamine level in intact mice was assessed and the optimal dose was selected for further analysis (*Fig. 1A*). In the second experiment, the selected MIT dose (100 mg/kg) was used to assess the pharmacodynamics and determine the optimal time interval for a maximum decrease in the striatal dopamine level in intact mice after administration (*Fig. 1B*). The third experiment was devoted to the development of a MIT challenge test in the neurotoxic MPTP mouse model of preclinical PD (*Fig. 1C*).

MIT (hereinafter, all reagents are from Sigma-Aldrich, USA) was dissolved in a physiological solution (0.9% NaCl) containing 5% ascorbic acid and 0.5% dimethyl sulfoxide and administered subcutaneously to animals at the indicated doses. The control groups received a similar solution without MIT. To simulate PD at the preclinical stage, mice were once subcutaneously injected with MPTP at a dose of 18 mg/kg [8]. The control groups received physiological saline.

The locomotor activity of the mice was assessed based on measures of the distance traveled and the number of rearings in an open-field behavior test. For adaptation, mice were transferred to a behavior testing room 2 h before the start of the test. The open-field test was performed using a PhenoMaster automated system (TSE Systems, Germany) for 6 min. The parameters were calculated using the supplied software.

To collect the nigrostriatal system structures, isoflurane anesthetized mice were decapitated and the dorsal striatum and SN were isolated from the brain according to the previously described procedure [8]. Samples of the brain structures were weighed, frozen in liquid nitrogen, and stored at −70°C. The dopamine concentration in the samples was measured by high-performance liquid chromatography with electrochemical detection according to [9].

Data are presented as a mean (a percentage of the control values) ± standard error of the mean. Data normality was examined using the Shapiro–Wilk test. Statistical analysis of the results was performed with the one-way ANOVA method, parametric Student's *t*-test, or nonparametric Mann–Whitney test using the GraphPad Prism 6.0 software package (GraphPad Software, USA). $P \leq 0.05$ was used as the statistical significance.

RESULTS AND DISCUSSION

Selection of the effective dose of MIT and the time after its administration

During selection of the MIT dose, 100 mg/kg MIT was found to provide the maximum decrease in the striatal dopamine concentration in normal mice (34% of the control level) (*Fig. 2A*). However, a further increase in the MIT dose, up to 200 and 300 mg/kg, did not lead to a further decrease in the dopamine level (*Fig. 2A*),

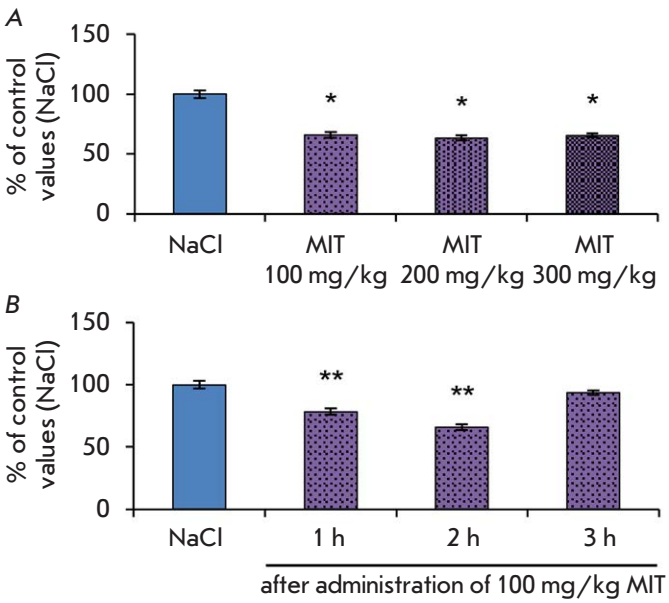

Fig. 2. Striatal dopamine in mice 2 h after administration of various MIT doses (*A*) and 1, 2, or 3 h after administration of 100 mg/kg MIT (*B*). *$p < 0.05$ compared to controls (NaCl); **$p < 0.05$ compared to controls and all other groups. MIT – monoiodotyrosine

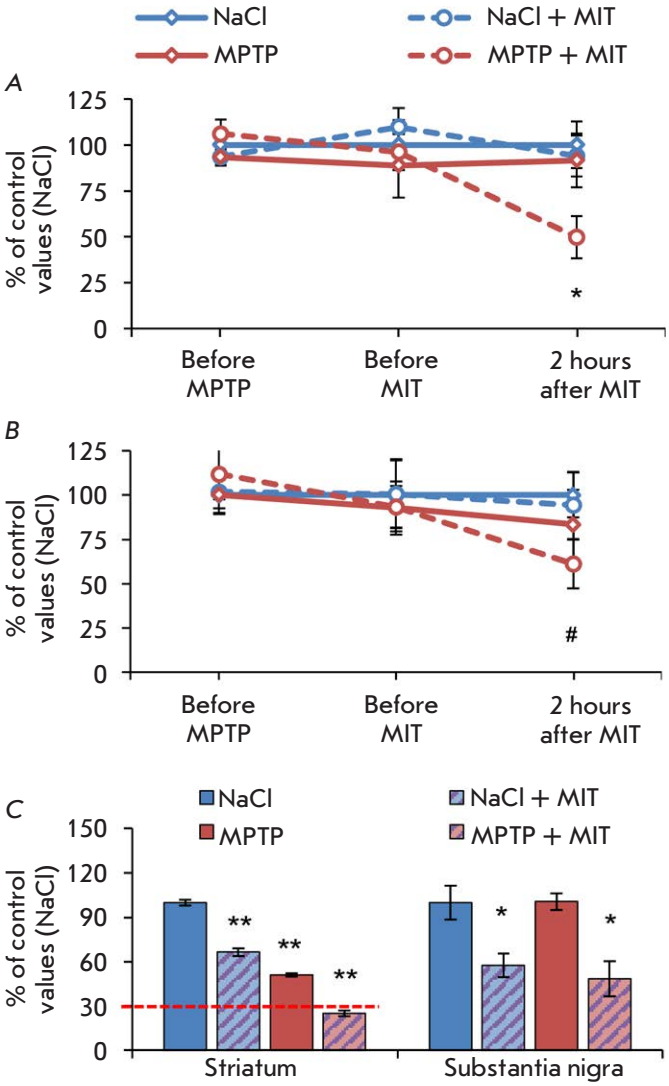

Fig. 3. Total distance (*A*) and number of rearings (*B*) in the open-field test and the dopamine level in the striatum and substantia nigra (*C*) of MPTP-treated or saline-treated (NaCl) mice 2 h after administration of 100 mg/kg MIT. *$p < 0.05$ compared to controls (NaCl); **$p < 0.05$ compared to controls and all other groups; $^{\#}p < 0.15$ compared to controls

which indicates TH saturation with the inhibitor and the absence of a linear MIT dose-dependency in this range. Therefore, 100 mg/kg was chosen as the effective MIT dose for further experiments.

An analysis of time intervals revealed that the striatal dopamine concentration decreased by 22% compared to that in the controls 1 h after MIT administration and by 35% after 2 h; after 3 h, the dopamine level was completely restored to its control values (*Fig. 2B*). These results confirm the short duration and reversibility of the MIT inhibitory effect on TH in the striatum. Therefore, a time interval of 2 h after inhibitor administration was chosen for the development of the MIT challenge test.

Interestingly, the same dose (100 mg/kg) of α-methyl-*p*-tyrosine was previously shown to reduce the striatal dopamine level more efficiently, by 40.2%, 4 h after its administration [5]. In this case, according to *in vitro* estimates, MIT is a more effective TH inhibitor in comparison with α-methyl-p-tyrosine [10]. Apparently, faster metabolism of MIT under *in vivo* conditions limits its inhibitory effect on TH.

Challenge test in an experimental preclinical PD model

An important factor in modeling PD is a precisely identified threshold of neurodegeneration at which motor symptoms appear. This is a loss of 50–60% of dopaminergic neuronal bodies in the SN and a decrease in the number of their axons and the striatal dopamine concentration by 70–80% compared to those in the controls [8]. Therefore, we chose an unchanged motor activity of animals in the open-field test, unchanged nigral dopamine content, and a decrease in the striatal dopamine level by less than 70% as the key parameters of a preclinical PD model.

The traveled distance and the number of rearings in the open-field test in mice that received 18 mg/kg MPTP before MIT administration (i.e. 1 week after MPTP administration) did not differ from those in the controls (*Fig. 3A,B*). In addition, administration of MPTP did not affect the dopamine level in the SN but decreased its level in the striatum by 49% (*Fig. 3C*), which is less than the indicated threshold of 70%. Thus, the key parameters of the experimental model corresponded to the characteristics of the preclinical PD stage.

Two hours after a subcutaneous injection of 100 mg/kg MIT, the mice modeling the preclinical PD stage developed motor symptoms: the distance traveled in the open-field test decreased by 50% relative to that in the control group (*Fig. 3A*), and the number of rearings reduced by 39% (*Fig. 3B*). In this case, there were no similar changes in the motor activity of either healthy mice receiving MIT or MPTP mice receiving physiological saline.

Apparently, this was because MIT caused a decrease in the dopamine concentration by 75% of the control level (i.e. below the threshold of motor symptom appearance) only in the striatum of mice in the preclinical PD model (*Fig. 3C*). Therefore, administration of MIT at the selected dose provoked motor symptoms in the preclinical PD model; i.e. in mice with latent insufficiency of the nigrostriatal system.

It is important to note that systemic TH inhibitors are relatively safe and have long been used in clinical practice. Another TH inhibitor, α-methyl-*p*-tyrosine, is used in the treatment of pheochromocytoma, a benign adrenal tumor [4, 5]. The drug doses used in this case lead to the inhibition of dopamine synthesis by 35–80%, and the duration of the daily intake varies from several weeks to several years [11], which indicates the absence of serious side effects even upon prolonged TH inhibition. However, there is evidence of potential neurotoxicity for MIT [12] and further research should pay particular attention to the analysis of the short-term and long-term effects of its action on the brain and peripheral organs.

Therefore, the experimental preclinical mouse model of PD was a successful demonstration of the effectiveness of the MIT challenge test in the detection of a latent insufficiency in the dopaminergic nigrostriatal system. In this study, the optimal dose of MIT and the time after its administration were determined. The next stage in the development of a method for early PD diagnosis based on the MIT challenge test involves preclinical studies of pharmacokinetics, the toxicological properties, and long-term effects of MIT exposure. ●

This study was supported by the Russian Science Foundation (grant No. 20-75-00034).

REFERENCES

1. Bernheimer H., Birkmayer W., Hornykiewicz O., Jellinger K., Seitelberger F. // J. Neurol. Sci. 1973. V. 20. P. 415–455.
2. Bezard E., Gross C. // Prog. Neurobiol. 1998. V. 55. P. 93–116.
3. Agid Y. // Lancet. 1991. V. 337. P. 1321–1324
4. Ugrumov M. // CNS Neurosci. Ther. 2020. V. 26. P. 997–1009.
5. Khakimova G.R., Kozina E.A., Kucheryanu V.G., Ugrumov M.V. // Mol. Neurobiol. 2017. V. 54. P. 3618–3632.
6. Citterio C.E., Targovnik H.M., Arvan P. // Nat. Rev. Endocrinol. 2019. V. 15. P. 323–338.
7. Tan S.A., Lewis J.E., Berk L.S., Wilcox R.B. // Clin. Physiol. Biochem. 1990. V. 8. P. 109–115.
8. Ugrumov M.V., Khaindrava V.G., Kozina E.A., Kucheryanu V.G., Bocharov E.V., Kryzhanovsky G.N., Kudrin V.S., Narkevich V.B., Klodt P.M., Rayevsky K.S., Pronina T.S. // Neuroscience. 2011. V. 181. P. 175–188.
9. Kim A.R., Nodel M.R., Pavlenko T.A., Chesnokova N.B., Yakhno N.N., Ugrumov M.V. // Acta Naturae. 2019. V. 11. № 4 (43). P. 99–103.
10. Udenfriend S., Zaltzman-Nirenberg P., Nagatsu T. // Biochem. Pharmacol. 1965. V. 14. P. 837–845.
11. Wachtel H., Kennedy E.H., Zaheer S., Bartlett E.K., Fishbein L., Roses R.E., Fraker D.L., Cohen D.L. // Ann. Surg. Oncol. 2015. V. 22. Suppl. 3. P. S646–654.
12. Fernández-Espejo E., Bis-Humbert C. // Neurotoxicology. 2018. V. 67. P. 178–189.

A Mouse Model of Nigrostriatal Dopaminergic Axonal Degeneration As a Tool for Testing Neuroprotectors

A. A. Kolacheva*, M. V. Ugrumov
Koltzov Institute of Developmental Biology of Russian Academy of Sciences, Moscow, 119334 Russia
*E-mail: annakolacheva@gmail.com
Received April 20, 2021; in final form, July 14, 2021
DOI: 10.32607/actanaturae.11433

ABSTRACT **Degeneration of nigrostriatal dopaminergic neurons in Parkinson's disease begins from the axonal terminals in the striatum and, then, in retrograde fashion, progresses to the cell bodies in the substantia nigra. Investigation of the dynamics of axonal terminal degeneration may help in the identification of new targets for neuroprotective treatment and be used as a tool for testing potential drugs. We have shown that the degeneration rate of dopaminergic axonal terminals changes over time, and that the striatal dopamine concentration is the most sensitive parameter to the action of 1-methyl-4-phenyl-1,2,3,6-tetrahydropyridine (MPTP). This model was validated using neuroprotectors with well-known mechanisms of action: the dopamine transporter inhibitor nomifensine and SEMAX peptide that stimulates the secretion of endogenous neurotrophic factors or acts as an antioxidant. Nomifensine was shown to almost completely protect dopaminergic fibers from the toxic effect of MPTP and maintain the striatal dopamine concentration at the control level. However, SEMAX, slightly but reliably, increased striatal dopamine when administered before MPTP treatment, which indicates that it is more effective as an inductor of endogenous neurotrophic factor secretion rather than as an antioxidant.**
KEYWORDS **Parkinson's disease, axonal terminal, model, test system, neuroprotector.**
ABBREVIATIONS **DA – dopamine; DA-ergic neuron – dopaminergic neuron; DAT – dopamine transporter; HPLC-ED – high performance liquid chromatography with electrochemical detection; IHC – immunohistochemistry; MPP+ – 1-methyl-4-phenylpyridinium; MPTP – 1-methyl-4-phenyl-1,2,3,6-tetrahydropyridine; PD – Parkinson's disease; TH – tyrosine hydroxylase; VMAT2 – vesicular monoamine transporter 2.**

INTRODUCTION

Investigation of the molecular mechanisms of neurodegeneration and neuroplasticity is the key to understanding the mechanisms underlying normal aging, accompanied by a constant relatively slow loss of neurons (4.5% over 10 years) and the pathogenesis of congenital and chronic nervous system diseases associated with an accelerated loss of neurons [1]. One of the most common neurodegenerative diseases, Parkinson's disease (PD), is characterized by impaired motor function due to the loss of the dopaminergic (DA-ergic) neurons of the nigrostriatal system. Currently, only symptomatic treatment with dopamine (DA) agonists is used in PD, which does not stop neuronal loss, leading to rapid disability in patients. Attempts to additionally use neuroprotective therapy have not yet been successful. Indeed, drugs with neuroprotective properties, which have shown high efficiency in animal models of Parkinsonism, have not passed clinical trials [2, 3]. This is associated with a critical decrease in the number of DA-ergic neurons by the time of treatment initiation [4]. On the other hand, primary screening of neuroprotective agents in PD models does not consider the dynamics of neuronal degeneration when the test agent is administered either before induced death of DA-ergic neurons or after, stimulating compensatory brain reserves.

Previously, using 1-methyl-4-phenyl-1,2,3,6-tetrahydropyridine (MPTP), we developed a mouse model of the early clinical PD stage, which was used to study the late period of DA-ergic neuronal death and the period of development of compensatory processes. However, the initial period of neurodegeneration development was not investigated. Therefore, the purpose of this study was to develop a model of degeneration of DA-ergic neuronal terminals in the striatum and test potential neuroprotective agents. A comprehensive study of the morphological and functional parameters of axonal terminals in the initial period after MPTP

administration identified the parameters most sensitive to the action of neurotoxin.

At the next stage, the developed test system was used to test two known neuroprotectors with different mechanisms of action: nomifensine, an inhibitor of the DA membrane transporter involved in the penetration of specific toxins (MPP+, 6-HDA) into DA-ergic neurons, followed by oxidative stress and subsequent neuronal death; and SEMAX, a fragment of the adrenocorticotropic hormone, a Met-Glu-His-Phe-Pro-Gly-Pro peptide that can act either as an inducer of the synthesis of endogenous neurotrophic factors or an antioxidant, depending on the way of its administration [5, 6].

EXPERIMENTAL

We used male C57BL/6 mice (2–2.5 months of age). The mice were kept in standard vivarium conditions (free access to food and water and a 12 h day/night cycle). Animal manipulations were performed according to the protocol that was approved by the Bioethics Committee of the Koltsov Institute of Developmental Biology of the Russian Academy of Sciences and was consistent with national and international requirements.

The morphological and functional state of DA-ergic axonal terminals in the initial period of their degeneration in the striatum was assessed 2 h after two injections of MPTP (Sigma Aldrich, USA) at a single dose of 12 mg/kg with an interval of 2 h. Control animals were injected with 0.9% NaCl according to a similar scheme (*Fig. 1A*). Tyrosine hydroxylase (TH) (n = 3–4) in striatal slices was detected by immunohistochemistry (IHC), followed by the counting of axonal terminals in four areas of the dorsal striatum as described previously [7]. Also, the striatal DA concentration was determined by high-performance liquid chromatography with electrochemical detection (HPLC-ED) (n = 5–7) (*Fig. 1A*).

R/S-nomifensine, 1,2,3,4-tetrahydro-2-methyl-4-phenyl-8-isoquinolinamine (Sigma, USA), was administered subcutaneously at a single dose of 10 mg/kg 30 min before each of four subcutaneous MPTP injections at a dose of 12 mg/kg with an interval of 2 h (n = 8–9) (*Fig. 1B*). A Met-Glu-His-Phe-Pro-Gly-Pro peptide (SEMAX) was administered intranasally at a dose of 50 μg/kg, according to two schemes (the agent was provided by the National Research Center "Kurchatov Institute"). The synthesis of endogenous neurotrophic factors was induced by a SEMAX injection 12 h before the first of the four MPTP injections at a dose of 12 mg/kg with an interval of 2 h (*Fig. 1C*); as an antioxidant, SEMAX was administered 1 h after the last of the four MPTP injections at a dose of 12 mg/kg

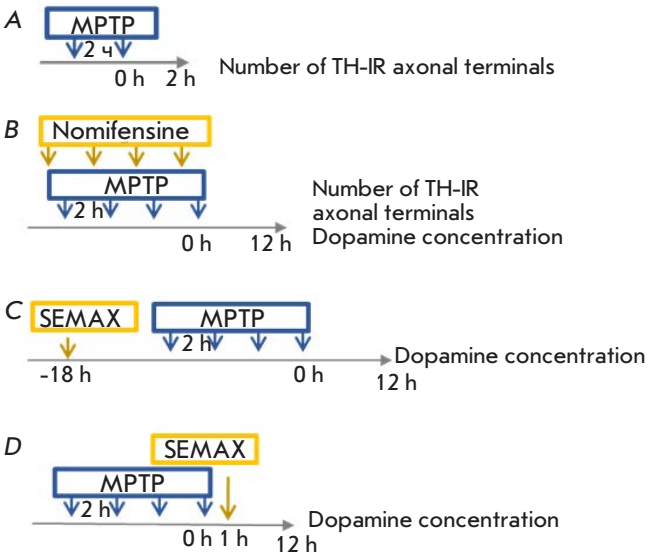

Fig. 1. Experiment design. (*A*) The number of TH-immunoreactive axonal terminals in striatal slices and the striatal DA concentration (HPLC-ED) 2 h after two MPTP injections (subcutaneously (s.c.) 12 mg/kg with an interval of 2 h). (*B*) Nomifensine (s.c. 10 mg/kg) was administered 30 min before each of 4 MPTP injections (s.c. 12 mg/kg with an interval of 2 h). Twelve hours after the last MPTP injection, the striatal DA concentration was determined by HPLC-ED and the number of TH-immunoreactive axonal terminals was assessed immunohistochemically in striatal slices. SEMAX (intranasally (i.n.) 50 μg/kg) was administered once either 12 h before the first MPTP injection (*C*) or 1 h after the last MPTP injection (*D*). The striatal DA concentration was determined by HPLC-ED 12 h after the last MPTP injection

with an interval of 2 h (*Fig. 1D*) (n = 5–10). Material (striatum) for all neuroprotectors was collected 12 h after the last MPTP injection, and the DA concentration in the tissue was determined by HPLC-ED. Also, the nomifensine experiment included a quantification of TH-immunoreactive axonal terminals in the striatum. Details of the procedures for immunohistochemical detection of TH, counting of axonal terminals, and measuring of the striatal DA concentration are described elsewhere [7].

The statistical significance of the collected data was assessed using the parametric Student's t-test and nonparametric Mann–Whitney U-test. Differences were considered statistically significant at $p < 0.05$; $p < 0.1$ was considered as a trend towards change. Data are presented as a mean ± standard error of the mean and expressed as a percentage of the controls taken as 100%.

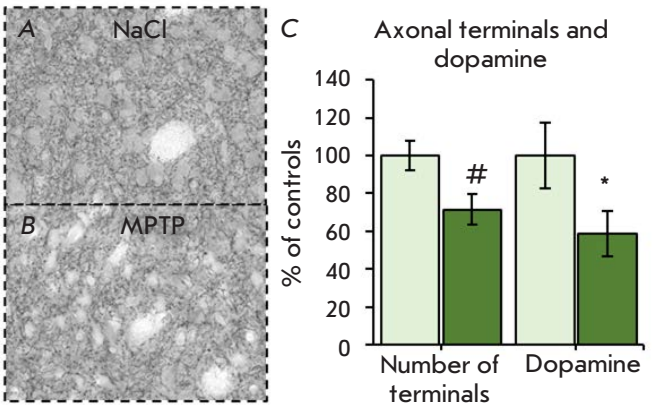

Fig. 2. TH-immunoreactive axonal terminals (*A*, *B*), their number, and the DA concentration (*C*) in the striatum 2 h after two MPTP injections (12 mg/kg with an interval of 2 h). * $p < 0.05$, # $p < 0.1$

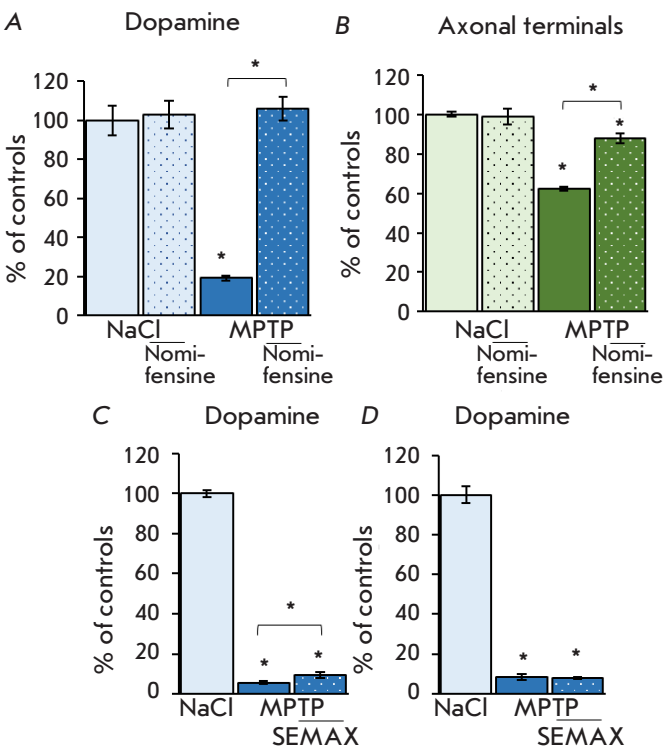

Fig. 3. The DA concentration (*A*) and the number of TH-immunoreactive axonal terminals (*B*) in the striatum 12 h after four MPTP injections (12 mg/kg) and a nomifensine injection (10 mg/kg) 30 min before each MPTP injection. The striatal DA concentration 12 h after four MPTP injections (12 mg/kg) and a SEMAX injection (50 μg/kg) 12 h before the first MPTP injection (*B*) or 1 h after the last MPTP injection (D). * $p < 0.05$

RESULTS AND DISCUSSION

Degeneration of nigrostriatal DA-ergic neurons in PD begins from the axonal terminals (varicosities) in the striatum and progresses retrogradely to the neuronal bodies [4]. It should be noted that there are few studies that have explored the period of nigrostriatal system degeneration at the striatum level in the early stages after administration of MPTP. Almost all of these studies determined only the optical density per unit area using a semiquantitative immunohistochemical analysis of TH in striatal slices [8, 9], which was interpreted as the degree of axonal degeneration. However, this is not entirely correct because the axonal TH content in PD and disease models changes [10].

Previously, we demonstrated that degeneration of DA-ergic axonal terminals in the striatum stops 6 h after four MPTP injections, after which compensatory processes begin to develop (e.g., an increase in the TH activity) [7]. The number of axonal terminals after 3 and 6 h was 67 and 55% of the control value, respectively [7]. In this period, the rate of axonal terminal degeneration within the first hour was 4%. However, this is an indication that the number of terminals at the time of the first MPTP injection should have been about 120%. Therefore, to clarify the rate of nigrostriatal system degeneration within the initial period, we selected a point 2 h after two MPTP injections and found that the number of varicosities was 72% of the control value (*Fig. 2A–C*). Comparing these data, it appears reasonable to conclude that the rate of loss of axonal terminals is not linear: it is about 7%/h within the first 4 h after the first MPTP injection and 1%/h during the next 5 h.

The nonlinear pattern of axonal terminal degeneration may be associated with the metabolism of MPP+ (a toxin formed from MPTP in glial cells) that is absorbed by DA-ergic neurons using DAT and induces oxidative stress. Once inside a neuron, MPP+ competes with DA for loading into vesicles via the vesicular monoamine transporter 2 (VMAT2), which is a mechanism that protects neurons from death.

The high rate of axonal terminal degeneration up to 2 h after the second MPTP injection is probably associated with the initiation of oxidative stress by MPP+ and the inability to neutralize it by accumulation in DA-filled vesicles. The neurotransmitter is gradually released and degraded, and the striatal DA concentration amounts to 59% 2 h after two MPTP injections (*Fig. 2B*). At the next stage, the rate of axonal terminal degeneration abruptly decreases due to an established balance between the uptake of MPP+ into vesicles and the ongoing release of DA with its degradation.

Therefore, a model of DA-ergic axonal terminal degeneration for testing potential neuroprotectors should primarily focus on the striatal DA concentration as the indicator most sensitive to the action of MPTP. However, given the nonlinear pattern of DA-ergic axonal terminal degeneration, the actual period of neuroprotective action is limited to 6 h after induction of nigrostriatal system neurodegeneration.

At the next stage, we evaluated the possibility of using the dynamics of axonal terminal degeneration as a test system for drugs with neuroprotective properties. For this purpose, we used two neuroprotective agents possessing the "direct" (selective) and "indirect" effects. The direct effect is inhibition of neurotoxin uptake through DAT. Indeed, along with MPTP, there are other neurotoxins that can selectively enter DA-ergic neurons and cause oxidative stress: e.g., salsolinol that forms from DA and can be captured by DAT [11].

Administration of nomifensine was shown to maintain the striatal DA concentration at the control level upon MPTP treatment and significantly protect axonal terminals (*Fig. 3A,B*). Furthermore, given that uptake of MPP+ occurs through DAT, its inhibition by nomifensine is also the "reference" for the action of potential neuroprotectors.

SEMAX can stimulate the production of endogenous neurotrophic factors and act as an antioxidant [5, 6]. To separate these two effects, we used two experiment designs. In the first case, SEMAX was administered 12 h before MPTP to increase the expression of endogenous neurotrophic factors, or 1 h after the last MPTP injection. An increase in DA was observed only in the group receiving SEMAX 12 h before MPTP (*Fig. 3C,D*). Also, this group showed a significant decrease in DA turnover (DOPAC/DA) compared to the group receiving MPTP alone (data not shown). Given that SEMAX does not affect the striatal DA level [12], the obtained data indicate a neuroprotective effect of SEMAX on DA-ergic neurons; however, to enhance this effect, the experiment design should be altered; e.g., through use of multiple injections of the agent.

CONCLUSION

Thus, we may conclude that the most sensitive indicator of the effectiveness of the neuroprotector action is the striatal DA concentration, which reflects biochemical changes. In the case of a positive effect on the neurotransmitter level, it is necessary to focus on organic changes in the striatum by counting the DA-ergic axonal terminals. Also, the dynamics of DA-ergic neuronal terminal degeneration may be used as a test system for assessing the effectiveness of neuroprotectors. ●

This study was supported by the Russian Science Foundation (grant No. 20-75-00110).

REFERENCES

1. Fearnley J.M., Lees A.J. // Brain. 1991. V. 114. P. 2283–2301.
2. DATATOP: a multicenter controlled clinical trial in early Parkinson's disease. Parkinson Study Group // Arch. Neurol. 1989. V. 46. № 10. P. 1052–1060.
3. Schirinzi T., Martella G., Imbriani P., Di Lazzaro G., Franco D., Colona V.L., Alwardat M., Sinibaldi Salimei P., Mercuri N.B., Pierantozzi M., et al. // Front. Neurol. 2019. V. 10. P. 148.
4. Kordower J.H., Olanow C.W., Dodiya H.B., Chu Y., Beach T.G., Adler C.H., Halliday G.M., Bartus R.T. // Brain. 2013. V. 136. P. 2419–2431.
5. Dolotov O.V., Seredenina T.S., Levitskaya N.G., Kamensky A.A., Andreeva L.A., Alfeeva L.Yu., Nagaev I.Yu., Zolotarev Yu.A., Grivennikov I.A., Engele Yu., et al. // Dokl Biol Sci. 2003. V. 391. № 1. P. 292–295.
6. Levitskaya N.G., Sebentsova E.A., Andreeva L.A., Alfeeva L.Y., Kamenskii A.A., Myasoedov N.F. // Neurosci. Behav. Physiol. 2004. V. 34. № 4. P. 399–405.
7. Kolacheva A.A., Kozina E.A., Volina E.V., Ugryumov M.V. // Neurochem. 2014. V. 8. № 3. P. 184–192
8. Kurosaki R., Muramatsu Y., Kato H., Araki T. // Pharmacol. Biochem. Behav. 2004. V. 78. № 1. P. 143–153.
9. Jakowec M.W., Nixon K., Hogg E., McNeill T., Petzinger G.M. // J. Neurosci. Res. 2004. V. 76. № 4. P. 539–550.
10. Kozina E.A., Khakimova G.R., Khaindrava V.G., Kucheryanu V.G., Vorobyeva N.E., Krasnov A.N., Georgieva S.G., Kerkerian-Le Goff L., Ugrumov M.V. // J. Neurol. Sci. 2014. V. 340. № 1–2. P. 198–207.
11. Matsubara K., Senda T., Uezono T., Fukushima S., Ohta S., Igarashi K., Naoi M., Yamashita Y., Ohtaki K., Hayase N., et al. // Eur. J. Pharmacol. 1998. V. 348. № 1. P. 77–84.
12. Eremin K.O., Kudrin V.S., Grivennikov I.A., Miasoedov N.F., Rayevsky K.S. // Dokl Biol Sci. 2004. V. 394. P. 1–3.

Targeting Extracellular Vesicles to Dendritic Cells and Macrophages

L. A. Ovchinnikova[1], I. N. Filimonova[1], M. Y. Zakharova[1,2], D. S. Balabashin[1], T. K. Aliev[1,3], Y. A. Lomakin[1*], A. G. Gabibov[1,3]

[1]Shemyakin-Ovchinnikov Institute of Bioorganic Chemistry RAS, Moscow, 117997 Russia
[2]Pirogov Russian National Research Medical University, Moscow,117997 Russia
[3]Lomonosov Moscow State University, Moscow,119991 Russia
*E-mail: yasha.l@bk.ru

Received April 13, 2021; in final form, May 12, 2021
DOI: 10.32607/actanaturae.11478

ABSTRACT **Targeting protein therapeutics to specific cells and tissues is a major challenge in modern medicine. Improving the specificity of protein therapeutic delivery will significantly enhance efficiency in drug development. One of the promising tools for protein delivery is extracellular vesicles (EVs) that are enveloped by a complex lipid bilayer. EVs are secreted by almost all cell types and possess significant advantages: biocompatibility, stability, and the ability to penetrate the blood–brain barrier. Overexpression of the vesicular stomatitis virus protein G (VSV-G) was shown to promote EV formation by the producer cell. We have developed an EV-based system for targeted delivery of protein cargoes to antigen-presenting cells (APCs). In this study, we show that attachment of a recombinant llama nanobody α-CD206 to the N-terminus of a truncated VSV-G increases the selectivity of EV cargo delivery mainly to APCs. These results highlight the outstanding technological and biomedical potential of EV-based delivery systems for correcting the immune response in patients with autoimmune, viral, and oncological diseases.**

KEYWORDS **extracellular vesicles, nanocages, APC, targeted delivery, nanobody, CD206, VSV-G.**

ABBREVIATIONS **APC – antigen-presenting cell; EV – extracellular vesicle; DC – dendritic cell; MP – macrophage; MNC – mononuclear cell; MBP – myelin basic protein; MS – multiple sclerosis; GM-CSF – granulocyte-macrophage colony-stimulating factor; IL – interleukin; VSV-G – vesicular stomatitis virus glycoprotein.**

INTRODUCTION

The current rapid progress in modern biomedicine is based on the development of therapeutic drugs with high selectivity and low toxicity. The design of these drugs is associated with the development of highly active therapeutic components and also with their effective delivery to certain organs, tissues, and target cells [1, 2]. The current significant progress in targeted drug delivery has been achieved using antibody targeted therapy, darpins, and nanoparticles [3–6]. The use of extracellular vesicles (EVs) as carriers of protein molecules has a number of advantages: (1) natural biocompatibility of the cell membrane and EV membranes; (2) the ability of EVs to penetrate the blood–brain barrier; and (3) the possibility of changing the protein composition of the EV membrane [7]. Modification of the protein profile of EV membranes enables a targeted delivery of therapeutic EV cargoes into the desired cells [8, 9].

The precursors of EVs in the targeted delivery of therapeutic drugs and the most extensively studied carriers are liposomes. Many liposome-based drugs have successfully passed clinical trials and been introduced into clinical practice [10–12]. One of the promising liposome-based agents for the treatment of multiple sclerosis (MS) is Xemys [13–15]. This agent consists of mannosylated liposomes loaded with immunodominant peptides of the myelin basic protein (MBP). Therapeutic peptides are delivered directly to antigen-presenting cells (APCs) – dendritic cells (DCs) and macrophages (MPs) – by means of the mannose residues on the liposome surface. The presumptive mechanism of action is hyperpresentation of the delivered MBP fragments by the class II major histocompatibility complex on the APC surface, which causes immunosuppression and suppression of autoimmune inflammation. This agent has successfully passed preclinical trials and phase II clinical trials. Phase III clinical trials are expected to be carried out prior to approval for use in the Russian Federation. However, the treatment of MS requires a regular, lifelong administration of these liposomes to

the patient, which is associated with economic costs and inconvenience for patients. EVs may be more convenient carriers of MBP fragments for the long-term therapy of MS patients. The existing methods for EV production [16] enable the development of genetically encoded EVs loaded with MBP peptides. The use of autologous human cells as producer cells will provide a transition towards personalized medicine and avoid the need for regular injections that reduce the quality of life [17].

This paper describes a system for the targeted delivery of the EV content to APCs. A DC and MP surface marker, CD206 (mannose receptor), was chosen [18], by analogy with Xemys. This receptor binds glycoconjugates terminated in mannose, fucose, or N-acetyl-d-glucosamine residues, which are abundantly present on the surface of pathogenic microorganisms [19]. Conformational changes in the receptor, which are induced by interaction with a mannose residue, lead to the internalization of the bound pathogen and its transport to lysosomes [20], which explains the high expression level of this receptor on DCs and MPs—classical APCs of the human immune system. We have developed a system for the production of EVs with a surface-displayed llama nanobody specific to human and mouse CD206. These vesicles are about 100–140 nm in size and carry exosomal markers [7]. We have shown the possibility of delivering a cargo protein to the desired cells, including human DC and MP, using targeted vesicles. The obtained data will enable the use of the strategy of targeting genetically encoded vesicles to APCs for the development of agents to correct the immune response in patients with autoimmune, viral, and oncological diseases.

EXPERIMENTAL

Plasmids

To produce the pCMV-NanoLuc-Jun construct (Addgene ID: 167308), the gene encoding NanoLuc luciferase was amplified from the For_NanoLuc and Rev_NanoLuc primers (*Table*) and ligated into the pCMV-Jun vector at the *HindIII/KpnI* restriction sites. The sequence encoding a truncated VSV-G (pCMV-VSV-G_truncated) (amino acid sequence: EHPHIQDAASQLPDDESLFFGDTGLSKNPIELVEGWFSSWKSSIASFFFIIGLIIGLFLVLRVGIHLCIKLKHTKKRQIYTDIEMNRLGK) was amplified from the full-length VSV-G (AddgeneID: 138479) from the For_VSVG_trunc and Rev_VSVG_trunc primers (*Table*) and cloned into the pCMV vector at the *BstBI/ClaI* sites.

The gene encoding the llama nanobody α-CD206 (clone 3.49) [21] was synthesized and cloned at the 5'-end of the truncated VSV-G into the pCMV-VSV-G_truncated construct for eukaryotic expression and into the pET22 vector for prokaryotic expression. For the production of the recombinant llama antibody α-CD206 in a prokaryotic expression system, a histidine tag for affinity purification and a 3xFLAG epitope for detection with secondary antibodies were added to the protein C-terminus.

Cell lines

HEK293T cells were cultured in a complete DMEM medium supplemented with 10% fetal bovine serum (Gibco, USA); Jurkat and DC2.4 cell lines were cultured in a complete RPMI medium supplemented with 10% fetal bovine serum (Gibco, USA).

To produce stimulated DC and MP populations, mononuclear cells (MNCs) were isolated from human peripheral blood by centrifugation in a Ficoll gradient. The resulting cells were incubated in a complete RPMI medium supplemented with 10% fetal bovine serum until the DC and MP precursors adhered to the plastic. Thereafter, non-adherent cells were removed and IL-4 (50 ng/mL) and GM-CSF (100 ng/mL) were added to the adherent cells. Differentiation of MNCs into dendritic cells was performed for 6 days with a change of medium containing a fresh portion of cytokines every 2 days.

Primers used to generate the constructs

Primer	Sequence
For_CD206	5'-TGGGGTGAATTGCTTCGGAAGTCAGGTTCAACTGCAGGAGTC-3'
Rev_CD206	5'-GAATGTGAGGATGTTCGAAGCTGCCTCCTCCTGAGC-3'
For_NanoLuc	5'-TCTGGTACCATGGTCTTCACACTCGAA-3'
Rev_NanoLuc	5'-GGGTGGTGGTGGTGGCAAGCTT-3'
For_VSVG_trunc	5'-GGGGTGAATTGCTTCGAACATCCTCACATTCAAG-3'
Rev_VSVG_trunc	5'-AGAGATGAACCGACTTGGAAAGGGCTCC-3'

All cell lines were maintained at 37°C and 8% CO_2.

Production of the llama antibody α-CD206-FLAG in a prokaryotic expression system

The recombinant llama antibody α-CD206 was produced in a prokaryotic expression system, *E. coli* BL21 (DE3) cells. An overnight cell culture was inoculated into a 2xYT medium at a 1:100 ratio and grown to OD_{600} = 0.6. Expression was induced by the addition of 1 mM isopropyl-β-D-1-thiogalactopyranoside. The culture was incubated under high aeration at 28°C for 16 h. Then, it was centrifuged at 3,500g and 4°C for 10 min. The resulting pellet was resuspended in lysis buffer (50 mM Tris-HCl pH 8.0; 150 mM NaCl; 1 mM PMSF) and added with lysozyme to a final concentration of 0.2 mg/mL. Cells were incubated at room temperature until the solution became viscous. The cell mass was disintegrated ultrasonically. The resulting solution was centrifuged at 20,000 g and 4°C for 10 min. The supernatant was filtered through a 0.45 μm filter and loaded onto a Ni-NTA column (Qiagen). Impurity proteins were removed by washing the column with the loading buffer (50 mM Tris-HCl pH 8.0; 150 mM NaCl) and wash buffer with imidazole (50 mM Tris-HCl pH 8.0; 150 mM NaCl; 20 mM imidazole). The antibody was eluted by buffer (50 mM Tris-HCl pH 8.0; 150 mM NaCl; 350 mM imidazole).

Staining of DCs and MPs with the recombinant llama antibody α-CD206

The possibility of using the recombinant llama antibody α-CD206 for the targeted delivery of protein therapeutics to APCs was verified in DCs and MPs from human peripheral blood. For this purpose, 500,000 cells were washed twice in PBS buffer, re-suspended in 100 μL of a solution containing 15–300 μg/mL of the recombinant llama antibody α-CD206-FLAG, and incubated at 4°C and constant gentle stirring for 1 h. After incubation, the cells were washed twice with PBS and stained with an anti-FLAG epitope secondary antibody conjugated with a fluorescent PE label according to the manufacturer's protocol (BioLegend, USA). For control staining, a PE anti-human CD206 antibody (BioLegend, USA) was used. As a negative control, HEK293T cells and non-stimulated MNCs were stained.

Production and purification of extracellular vesicles

EVs were produced in HEK293T cells. For this purpose, the cells were concomitantly transfected with 3 constructs: pCMV-VSV-G (or pCMV-VSV-G_truncated, or pCMV-α-CD206_VSV-G_truncated), pCMV-EPN, and pCMV-NanoLuc after reaching 90% confluence. The EV-containing cell medium was harvested after 48 h and subjected to differential centrifugation (300 g for 10 min and 1,000 g for 20 min). The supernatant was filtered through a 0.4 μm membrane and concentrated using Amicon Ultra-0.5 mL 10 kDa centrifugal filters (Millipore, Ireland). The concentrate was washed several times with PBS to remove off-target proteins. The EV concentration was determined using a CBQCA Protein Quantitation Kit (Invitrogen, USA).

Incubation of extracellular vesicles with cells

EVs carrying the reporter protein luciferase were aligned according to the protein concentration in the sample, added to 300,000 cells (Jurkat and DC2.4), and incubated at 37°C and 8% CO_2 for 2 h. Soluble NanoLuc-Jun luciferase, not loaded into EVs, was used as a control. After incubation, the cells were washed with PBS at 300 g for 10 min and incubated in buffer with proteinase K (Invitrogen, USA) to a final concentration of 0.1 mg/mL at 37°C for 15 min. After incubation, the cells were washed twice in PBS. The NanoGlo Luciferase Assay System (Promega, USA) was used to analyze the luciferase content in the cells. For the assay, 30,000 cells were resuspended in 15 μL of PBS and added to 15 μL of the lysis buffer containing a luciferase substrate. The signal was detected on a Varioskan plate reader (Thermo Scientific, USA) at 460 nm.

Targeted delivery of NanoLuc to DCs and MPs using targeted EVs

A heterogeneous population of stimulated DCs and MPs from human peripheral blood was added with targeted EVs (carrying the truncated VSV-G variant fused with the α-CD206 antibody on their surface) at a concentration of 5–20 μg/mL and incubated at 37°C and 8% CO_2 for 2 h. The cells were then gently washed according to the above-described procedure, re-suspended in the complete DMEM medium, and incubated in a vesicle-free medium for 16 h. After 16 h, the cells were stained with a PE anti-human α-CD206 antibody (Biolegend, USA). The cells were sorted on a Sony SH800 cell sorter (Germany). Two cell subsets, $CD206^+$ and $CD206^-$, were sorted. For the luciferase assay, 30,000 cells were taken from each subset.

RESULTS AND DISCUSSION

Production of a recombinant antibody specific to the surface marker of dendritic cells and macrophages

For the targeted delivery of EVs cargoes to APCs, we chose the DC and MP (M2) surface marker CD206 (macrophage mannose receptor) [18]. We selected the cross-reactive llama nanobody Nb3.49 interacting with the human and mouse mannose receptor [21]. This cross-reactivity is extremely useful in preclinical studies of targeted extracellular vesicles in mouse models,

while this antibody can be also used in clinical trials. To test the functionality and specificity of this antibody, we created the recombinant nanobody α-CD206-FLAG in a prokaryotic expression system, based on the pET22 vector. A histidine tag was used for detection and affinity purification; additionally, a 3xFLAG epitope was fused to the N-terminus of the protein to increase the detection sensitivity.

The specificity of the produced nanobody was verified in a subset of human DCs. For this purpose, mononuclear cells (MNCs) from human peripheral blood were cultured in a complete culture medium in the presence of IL-4 and GM-CSF for a week, with partial replacement of the medium every two days. Under these conditions, the differentiation of DC and MP is stimulated in the culture of human lymphocytes [22]. The purified recombinant nanobody α-CD206-FLAG was added to the resulting DC culture, and, then, after incubation and washing, the anti-FLAG epitope secondary antibody conjugated with a fluorescent PE label was added for the detection (*Fig. 1*). Staining of stimulated human MNCs using the recombinant nanobody α-CD206-FLAG enabled clear detection of a DC subset comparable with a subset isolated by staining with the commercially available fluorescent antibody α-CD206-PE. Thus, we had confirmed the functionality and specificity of α-CD206-FLAG in the llama nanobody format. This allows further EVs utilization for targeted protein delivery to APCs.

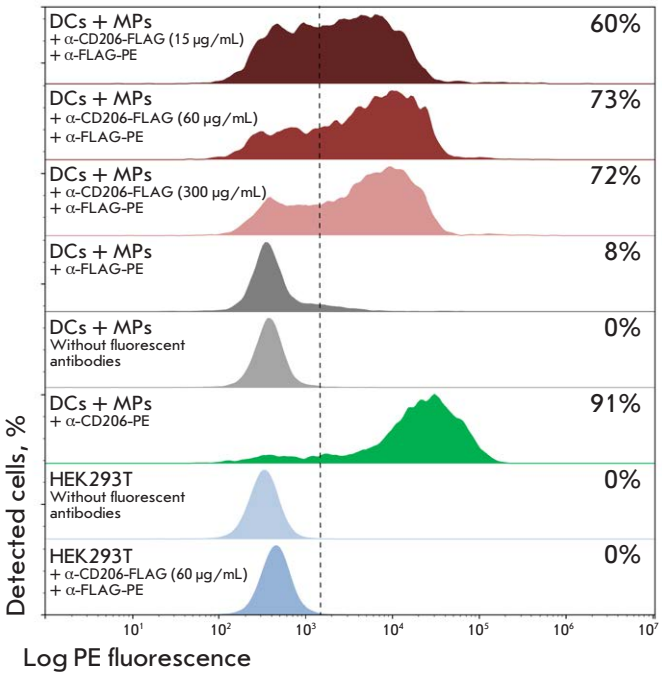

Fig 1. FACS analysis of DC and MP staining with the recombinant α-CD206 nanobody. DC and MP differentiation from human peripheral blood MNCs was stimulated by using IL-4 and GM-CSF for 7 days. Cell binding with the recombinant nanobody α-CD206-FLAG was visualized with a fluorescent secondary antibody, α-FLAG-PE (dark red, red, pink), or a commercially available antibody, α-CD206-PE (green). Unstained cells and cells stained with secondary antibodies alone (α-FLAG-PE) are shown in grey. The lower panel shows control binding of the recombinant nanobody α-CD206-FLAG with HEK293T cells (blue). The X axis shows the fluorescence signal intensity, and the Y axis shows the number of positive events. Each histogram shows the percentage of cells bound to the analyzed antibodies

Extracellular vesicle content delivery into cells

Evaluating the effectiveness of a specific delivery of a therapeutic agent into target cells is an essential stage in the development of protein drug carriers. The most convenient way of undertaking this evaluation is to use fluorescent proteins or luciferase as the agent to be delivered. A significant disadvantage of the use of fluorescent proteins for these purposes is their high molecular weights and the need to use highly sensitive detection methods. For this reason, we used NanoLuc luciferase as the agent to be delivered. This luciferase has good spectral characteristics and a small size of 19 kDa.

The surface of target cells is covered with a large amount of membrane proteins. These proteins are able to mediate a nonspecific interaction of soluble proteins with target cells *in vitro*, distorting the visualization of the real distribution of delivered EVs' cargoes among cells. In our experiments, we minimized the level of the nonspecific signal mediated by the adhesion of soluble (not encapsulated in vesicles) luciferase by additional incubation of cells with proteinase K. Extracellular vesicles loaded with luciferase and soluble NanoLuc were added to the target cells. After incubation for 2 h, the cells were washed free of the vesicles and soluble NanoLuc with phosphate-buffered saline alone or with further incubation with proteinase K. As can be seen from *Fig. 2*, the incubation of cells with proteinase K reduces the non-specific signal level compared to that in cells incubated in buffer without proteinase K. In this case, the signal from cells incubated with EVs is more than an order of magnitude higher than that from cells incubated with soluble NanoLuc. The use of proteinase K in the washing steps confirms that the luciferase is delivered into the cells and does not adhere to the membrane. Therefore, we were able to ensure delivery of luciferase into cells using extracellular vesicles and to optimize the conditions for the detection of this signal.

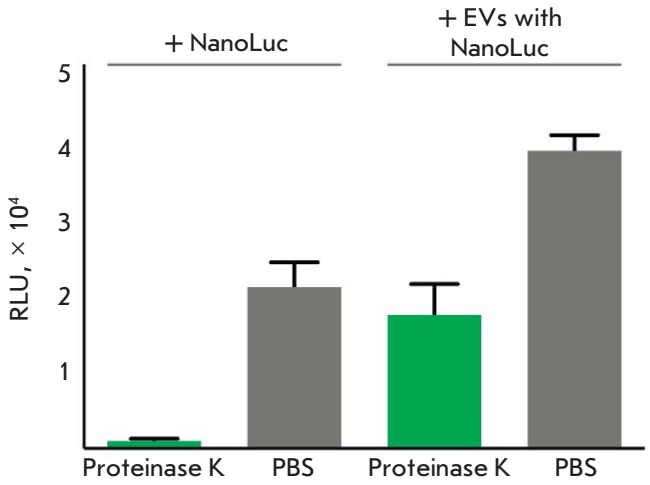

Fig 2. Detection of NanoLuc delivered to target cells via EVs. An additional step of incubation with proteinase K (green bars) enables detection of the luciferase delivered into the cells without a nonspecific signal from NanoLuc adhered to the cell membrane. Cells washed with PBS alone are shown as grey bars. A luciferase assay was used to detect NanoLuc delivered inside the cells

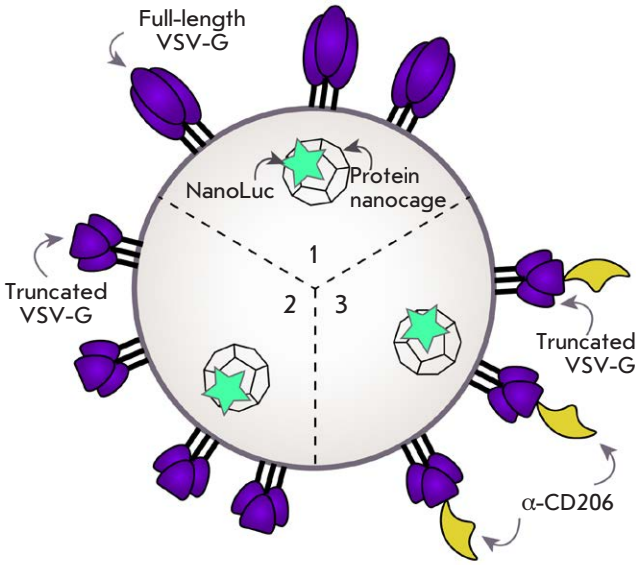

Fig 3. Schematic of an EV with different VSV-G molecules. 1 – full-length VSV-G, 2 – truncated VSV-G, 3 – truncated VSV-G fused with the α-CD206 nanobody

The main component underlying the ability of extracellular vesicles to penetrate into the target cell is the viral glycoprotein VSV-G. This glycoprotein binds to the low-density lipoprotein receptor abundantly present on the surface of mammalian cells [23]. Therefore, using the full-length VSV-G for vesicle content delivery into target cells cannot provide a high specificity of targeted delivery. In our study, we enhanced the specificity of targeted delivery by using a truncated VSV-G. This VSV-G variant comprises only the core part of the protein [24], which is responsible for the budding of extracellular vesicles from the producer cell and the release of the vesicle contents inside the target cell. In this case, it is possible to use a truncated VSV-G sequence combined with a recombinant nanobody capable of highly specific interaction with the target cell, without losing the functionality of the resulting extracellular vesicles. To test the efficiency of agent delivery into the cells, we used EVs loaded with NanoLuc luciferase and carrying various VSV-G variants on their surface: (1) full-size VSV-G, (2) truncated VSV-G, and (3) truncated VSV-G with a surface-exposed nanobody that specifically recognizes the dendritic cell and macrophage marker CD206 (*Fig. 3*).

To test the functioning of vesicles carrying various variants of the VSV-G glycoprotein, we used the DC2.4 mouse dendritic cell line and Jurkat cell line (immortalized human T cells). The cells were incubated with various vesicle variants or a solution of free luciferase and washed in the presence of proteinase K. RLU values obtained in the luciferase assay are shown in *Fig. 4*. In this experiment, the values obtained during the incubation of cells with vesicles carrying the full-length VSV-G were taken as 100%, because, in this case, there was maximum interaction between the vesicles and target cells. The use of a truncated VSV-G reduces the efficiency of luciferase delivery to target cells 5- to 10-fold. This is associated with impaired recognition by the low-density lipoprotein receptor. Fusion of the α-CD206 nanobody with the truncated VSV-G significantly increased the targeted protein delivery to the target cells. In this case, the use of the α-CD206 antibody provided a more efficient delivery of the protein to DC2.4 dendritic cells than to Jurkat cells.

In the future, extracellular vesicles are planned to be used for the targeted delivery of therapeutic agents in the human body. However, the use of immortalized cell lines does not allow for a reliable reconstruction of the actual APC distribution and marker expression level on the cell surface. To prove the functionality of the developed targeted extracellular vesicles loaded with a truncated VSV-G in a heterogeneous cell population,

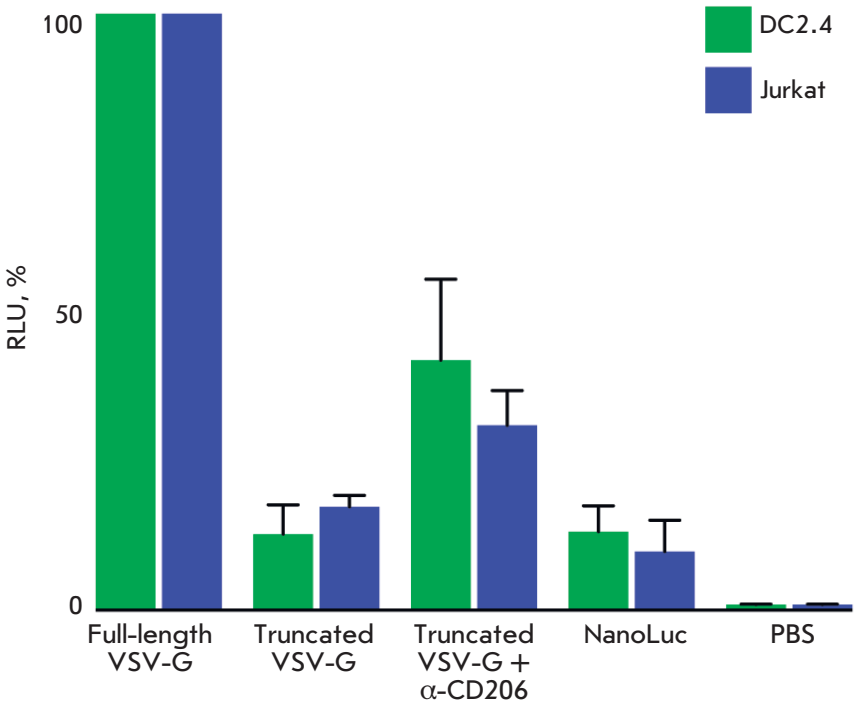

Fig 4. Comparison of protein delivery into target cells using EVs exposing different VSV-G molecules. Delivery analysis was performed in DC2.4 (green bars) and Jurkat (blue bars) cell lines. The delivery efficiency with the full-length VSV-G was taken as 100% for each cell line. Soluble luciferase NanoLuc without vesicles (sample NanoLuc) was used as a control

we used human peripheral blood MNCs subjected to stimulated DC and MP differentiation. Targeted extracellular vesicles loaded with luciferase were incubated with a heterogeneous population of $CD206^+$ and $CD206^-$ cells. Next, the analyzed cells were washed, stained with the fluorescent antibody α-CD206-PE, and sorted into two subsets of $CD206^+$ and $CD206^-$ cells using flow cytometry. The content of luciferase delivered into the target cells was detected separately in the $CD206^+$ and $CD206^-$ cell subsets. We were able to achieve a high specificity of luciferase delivery mainly to $CD206^+$ cells (*Fig. 5*).

CONCLUSION

Currently, one of the priorities in drug development is enhancing the selectivity of delivery. In this study, we proposed an improved method for the targeted delivery of protein therapeutics encapsulated in EVs. The high biocompatibility and biodegradability of EVs confers them a huge advantage over artificial nanoparticles. Attachment of the recombinant llama antibody α-CD206 to the N-terminus of a truncated VSV-G increases the selectivity of EV delivery predominantly to $CD206^+$ cells without a significant decrease in the production of these EVs. The functionality of the developed constructs was confirmed in immortalized mouse DC2.4 dendritic cells and hetero-

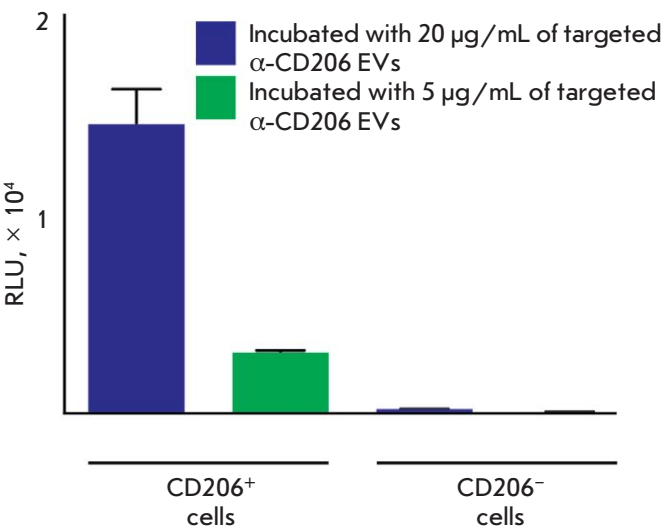

Fig 5. Targeted protein delivery to $CD206^+$ cells using EVs. Targeted α-CD206 EVs loaded with NanoLuc were incubated with stimulated DCs and MPs from human peripheral blood. After sorting of the $CD206^+$ and $CD206^-$ subsets, the NanoLuc protein was shown to be delivered predominantly inside $CD206^+$ cells. The same quantity of $CD206^+$ and $CD206^-$ cells was analyzed in the luciferase assay

geneous subsets of stimulated DCs and MPs from human peripheral blood. On the basis of our findings, the strategy of targeting genetically encoded extracellular vesicles to APCs may be used in the development of drugs for the correction of the immune response in patients with autoimmune, viral, and oncological diseases. Vesicles can deliver not only target proteins, but also lipids, nucleic acids, and transcription factors to cells [1]. In the future, EV-based targeted drug delivery could be used in gene therapy. Currently, many studies focus on the development of EV-based delivery systems. These vesicles are specifically loaded with proteins [25], peptides [26], and RNAs [27, 28]. In this case, there is a serious problem having to do with the transfer of various off-target ballast molecules by the produced EVs. Delivery of undesirable components into the target cell can seriously affect the biocompatibility of the drug and lead to unpredictable side effects. One of the ways to solve this problem is to use autologous cells for the production of vesicles [29]. The safety of these EVs has been confirmed by clinical trials [30–32]. However, the long-term effect of natural EV content delivery into cells should also be carefully evaluated during the development of potential drugs. ●

This study was supported by the Russian Science Foundation (grant No. 18-74-10079 "Self-assembled genetically encoded nanocages as a tool for the treatment of multiple sclerosis").

REFERENCES

1. Sokolov A.V., Kostin N.N., Ovchinnikova L.A., Lomakin Y.A., Kudriaeva A.A. // Acta Naturae. 2019. V. 11. P. 28–41. https://doi.org/10.32607/20758251-2019-11-2-28-41.
2. Stepanov A.V., Belogurov A.A., Ponomarenko N.A., Stremovskiy O.A., Kozlov L.V., Bichucher A.M., Dmitriev S.E., Smirnov I.V., Shamborant O.G., Balabashin D.S., et al. // PLoS One. 2011. V. 6. P. e20991. https://doi.org/10.1371/journal.pone.0020991.
3. Mirkasymov A.B., Zelepukin I.V., Nikitin P.I., Nikitin M.P., Deyev S.M. // J. Control Release. 2021. V. 330. P. 111–118. https://doi.org/10.1016/j.jconrel.2020.12.004.
4. Shilova O.N., Deyev S.M. // Acta Naturae. 2019. V. 11. P. 42–53. https://doi.org/10.32607/20758251-2019-11-4-42-53.
5. Belogurov A., Kozyr A., Ponomarenko N., Gabibov A. // BioEssays. 2009. V. 31. P. 1161–1171. https://doi.org/10.1002/bies.200900020.
6. Durova O.M., Vorobiev I.I., Smirnov I.V., Reshetnyak A.V., Telegin G.B., Shamborant O.G., Orlova N.A., Genkin D.D., Bacon A., Ponomarenko N.A., et al. // Mol. Immunol. 2009. V. 47. P. 87–95. https://doi.org/10.1016/j.molimm.2008.12.020.
7. Ovchinnikova L.A., Terekhov S.S., Ziganshin R.H., Bagrov D.V., Filimonova I.N., Zalevsky A.O., Lomakin Y.L. // Pharmaceutics. 2021. V. 13. P. 768. https://doi.org/10.3390/pharmaceutics13060768.
8. Buschmann D., Mussack V., Byrd J.B. // Adv. Drug Deliv. Rev. 2021. V. 174. P. 348–368. https://doi.org/10.1016/j.addr.2021.04.027.
9. Ukrainskaya V.M., Rubtsov Y.P., Knorre V.D., Maschan M.A., Gabibov A.G., Stepanov A.V. // Acta Naturae 2019. V. 11. P. 33–41. https://doi.org/10.32607/20758251-2019-11-4-33-41.
10. Beltrán-Gracia E., López-Camacho A., Higuera-Ciapara I., Velázquez-Fernández J.B., Vallejo-Cardona A.A. // Cancer Nanotechnol. 2019. V. 10. P. 11. https://doi.org/10.1186/s12645-019-0055-y.
11. Lamichhane N., Udayakumar T.S., D'Souza W.D., Simone C.B., Raghavan S.R., Polf J., Mahmood J. // Molecules. 2018. V. 23. P. 288. https://doi.org/10.3390/molecules23020288.
12. Bulbake U., Doppalapudi S., Kommineni N., Khan W. // Pharmaceutics. 2017. V. 9. P. 9. https://doi.org/10.3390/pharmaceutics9020012.
13. Belogurov A.A., Stepanov A.V., Smirnov I.V., Melamed D., Bacon A., Mamedov A.E., Boitsov V.M., Sashchenko L.P., Ponomarenko N.A., Sharanova S.N., et al. // FASEB J. 2013. V. 27. P. 222–231. https://doi.org/10.1096/fj.12-213975.
14. Belogurov A., Zakharov K., Lomakin Y., Surkov K., Avtushenko S., Kruglyakov P., Smirnov I., Makshakov G., Lockshin C., Gregoriadis G., et al. // Neurotherapeutics. 2016. V. 13. P. 895–904. https://doi.org/10.1007/s13311-016-0448-0.
15. Ivanova V.V., Khaiboullina S.F., Gomzikova M.O., Martynova E.V., Ferreira A.M., Garanina E.E., Sakhapov D.I., Lomakin Y.A., Khaibullin T.I., Granatov E.V., et al. // Front. Immunol. 2017. V. 8. P. 1335. https://doi.org/10.3389/fimmu.2017.01335.
16. Votteler J., Ogohara C., Yi S., Hsia Y., Nattermann U., Belnap D.M., King N.P., Sundquist W.I. // Nature. 2016. V. 540. P. 292–309. https://doi.org/10.1038/nature20607.
17. Menzin J., Caon C., Nichols C., White L.A., Friedman M., Pill M.W. // J. Manag. Care Pharm. 2016. V. 19. P. https://doi.org/10.18553/jmcp.2013.19.s1.s24.
18. Wollenberg A., Mommaas M., Oppel T., Schottdorf E.M., Günther S., Moderer M. // J. Invest. Dermatol. 2002. V. 118. P. 327–334. https://doi.org/10.1046/j.0022-202x.2001.01665.x.
19. Fiani M.L., Barreca V., Sargiacomo M., Ferrantelli F., Manfredi F., Federico M. // Int. J. Mol. Sci. 2020. V. 21. P. 6318. https://doi.org/10.3390/ijms21176318.
20. Szolnoky G., Bata-Csörgö Z., Kenderessy A.S., Kiss M., Pivarcsi A., Novák Z., Newman K.N., Michel G., Ruzicka T., Maródi L., et al.// J. Invest. Dermatol. 2001. V. 117. P. 205–213. https://doi.org/10.1046/j.1523-1747.2001.14071.x.
21. Blykers A., Schoonooghe S., Xavier C., D'Hoe K., Laoui D., D'Huyvetter M., Vaneycken I., Cleeren F., Bormans G., Heemskerk J., et al. // J. Nucl. Med. 2015. V. 56. P. 1265–1271. https://doi.org/10.2967/jnumed.115.156828.
22. Ahn J.S., Agrawal B. // Int. Immunol. 2005. V. 17. P. 1337–1346. https://doi.org/10.1093/intimm/dxh312.
23. Finkelshtein D., Werman A., Novick D., Barak S., Rubinstein M. // Proc. Natl. Acad. Sci. USA. 2013. V. 110. P. 7306–7311. https://doi.org/10.1073/pnas.1214441110.
24. Kolangath S.M., Basagoudanavar S.H., Hosamani M., Saravanan P., Tamil Selvan R.P. // VirusDisease. 2014. V. 25. P. 441–446. https://doi.org/10.1007/s13337-014-0229-5.
25. Yim N., Ryu S.-W., Choi K., Lee K.R., Lee S., Choi H., Kim

J., Shaker M., Sun W., Park J., et al. // Nat Commun. 2016. V. 7. P. 12277. https://doi.org/10.1038/ncomms12277.
26. Nakase I., Noguchi K., Aoki A., Takatani-Nakase T., Fujii I., Futaki S. // Sci Rep. 2017. V. 7. P. 1991. https://doi.org/10.1038/s41598-017-02014-6.
27. Lamichhane T.N., Jeyaram A., Patel D.B., Parajuli B., Livingston N.K., Arumugasaamy N., Schardt J.S., Jay S.M. // Cell Mol. Bioeng. 2016. V. 9. P. 315–324. https://doi.org/10.1007/s12195-016-0457-4.
28. O'Loughlin A.J., Mäger I., de Jong O.G., Varela M.A., Schiffelers R.M., El Andaloussi S., Wood M.J.A., Vader P. // Mol. Ther. 2017. V. 25. P. 1580–1587. https://doi.org/10.1016/j.ymthe.2017.03.021.
29. Somiya M. // J. Cell Commun. Signal. 2020. V. 14. P. 135–146. https://doi.org/10.1007/S12079-020-00552-9.
30. Dai S., Wei D., Wu Z., Zhou X., Wei X., Huang H., Li G. // Mol. Ther. 2008. V. 16. P. 782–790. https://doi.org/10.1038/mt.2008.1.
31. Morse M.A., Garst J., Osada T., Khan S., Hobeika A., Clay T.M., Valente N., Shreeniwas R., Sutton M.A., Delcayre A., et al. // J. Transl. Med. 2005. V. 3. P. 9. https://doi.org/10.1186/1479-5876-3-9.
32. Escudier B., Dorval T., Chaput N., André F., Caby M.-P., Novault S., Flament C., Leboulaire C., Borg C., Amigorena S., et al. // J. Transl. Med. 2005. V. 3. P. 10. https://doi.org/10.1186/1479-5876-3-10.

A Method for Assessing the Efficiency of the Nucleotide Excision Repair System *Ex Vivo*

A. A. Popov[1], K. E. Orishchenko[2,3], K. N. Naumenko[1], A. N. Evdokimov[1], I. O. Petruseva[1], O. I. Lavrik[1,3*]

[1]Institute of Chemical Biology and Fundamental Medicine SB RAS, Novosibirsk, 630090 Russia
[2]Institute of Cytology and Genetics SB RAS, Novosibirsk, 630090 Russia
[3]Novosibirsk National Research State University, Novosibirsk, 630090 Russia
*E-mail: lavrik@niboch.nsc.ru

Received February 06, 2021; in final form, April 23, 2021
DOI: 10.32607/actanaturae.11430

ABSTRACT **The nucleotide excision repair (NER) is one of the main repair systems present in the cells of living organisms. It is responsible for the removal of a wide range of bulky DNA lesions. We succeeded in developing a method for assessing the efficiency of NER in the cell (*ex vivo*), which is a method based on the recovery of TagRFP fluorescent protein production through repair of the damage that blocks the expression of the appropriate gene. Our constructed plasmids containing bulky nFlu or nAnt lesions near the *tagrfp* gene promoter were shown to undergo repair in eukaryotic cells (HEK 293T) and that they can be used to analyze the efficiency of NER *ex vivo*. A comparative analysis of the time dependence of fluorescent cells accumulation after transfection with nFlu- and nAnt-DNA revealed that there are differences in how efficient their repair by the NER system of HEK 293T cells can be. The method can be used to assess the cell repair status and the repair efficiency of different structural damages.**

KEYWORDS **nucleotide excision repair, *ex vivo* methods, DNA damages.**

ABBREVIATIONS **NER – nucleotide excision repair; ODN – oligodeoxyribonucleotide; ATP – adenosine triphosphate; nFlu – N-[6-(5(6)-fluoresceinylcarbamoyl)hexanoyl]-3-amino-1,2-propandiol; nAnt – N-[6-(9-antracenylcarbamoyl)hexanoyl]-3-amino-1,2-propandiol; MCS – multiple cloning site; kbp – kilo base pairs.**

INTRODUCTION

The nucleotide excision repair (NER) system removes the bulky DNA lesions resulting from exposure to various factors: chemically active compounds, UV, and X-ray. There are two types of NER. Global genome NER is responsible for the search and removal of bulky lesions in the entire genome, regardless of its functional state, using XPC factor complexes for primary recognition of the damage site [1]. Transcription-coupled NER is activated by stalling of the RNA polymerase II transcription complex by a bulky lesion in the transcribed DNA strand [2]. About 30 protein factors and enzymes, identical in both NER types, then form a number of complexes on DNA which perform lesion removal, repair synthesis, and ligation.

The use of approaches that focus on exploring the structure and functions of the proteins involved in NER has the potential to help elucidate the process mechanism and to identify the main stages affecting its efficiency, as well as the composition and structure of the multiprotein complexes that appear and act at different NER stages [1, 3]. In most studies, the activity of the eukaryotic NER system *in vitro* is assessed using extended DNA containing natural bulky lesions at a given position or their synthetic analogs, as well as fractionated cell extracts containing a set of NER proteins (NER-competent extracts) [4, 5]. Nevertheless, the development of approaches that can help investigate and compare efficiency in bulky lesion repair in living cells (*ex vivo*) remains topical in both fundamental and applied research.

This paper describes a method for such assessments using model plasmids with a bulky lesion near the promoter region of the gene encoding the TagRFP fluorescent protein. The schematic for creating model plasmids with a bulky lesion and assessing the efficiency of NER *ex vivo* through monitoring of the recovery of reporter fluorescent protein expression, which happened to be impaired by a bulky DNA lesion, by the repair machinery of eukaryotic cells is shown in *Fig. 1.*

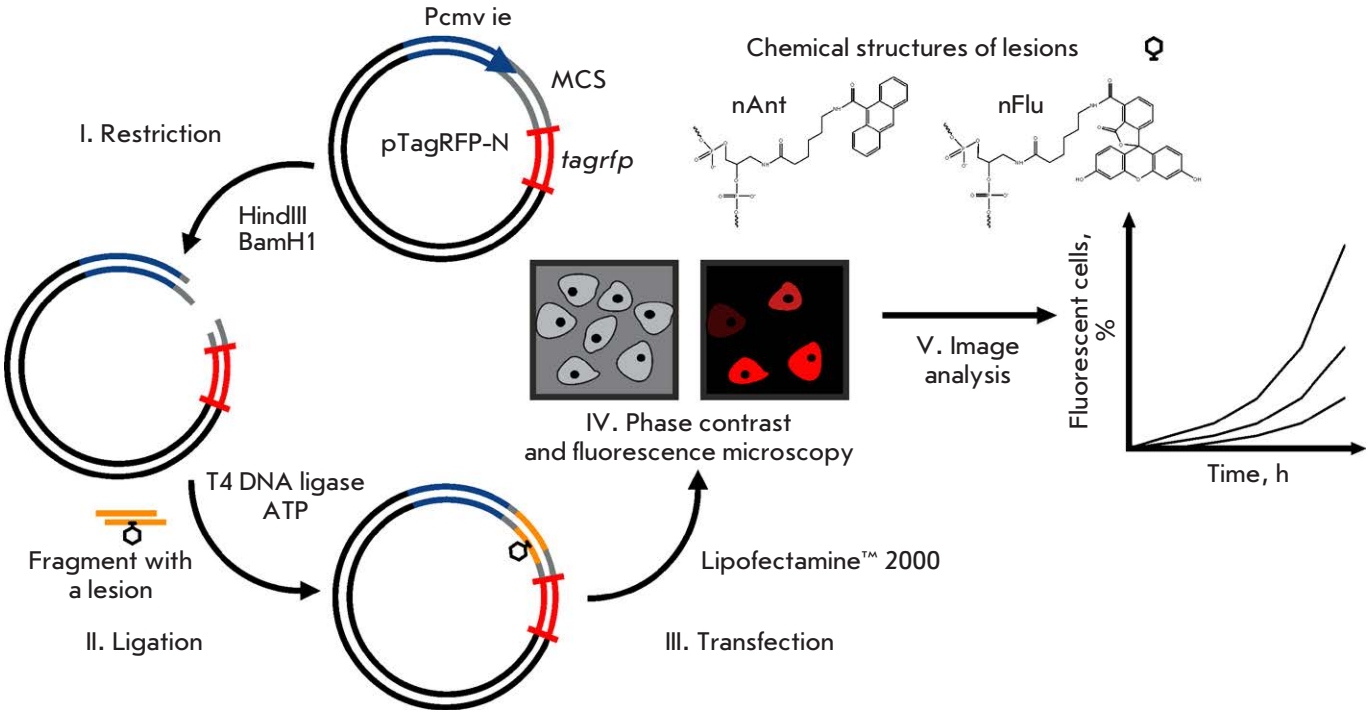

Fig. 1. Schematic of a method for assessing the NER system efficiency *ex vivo*

EXPERIMENTAL

HEK 293T cells were cultured in a IMDM medium (Gibco) supplemented with 10% FBS (Gibco), 1% GlutaMAX™ Supplement (Gibco), 10^5 U/L penicillin, 100 mg/L streptomycin, and 2.5 mg/L amphotericin β at 37°C and 5% CO_2.

ODNs for creating inserts were synthesized in the Laboratory of Biomedical Chemistry (Institute of Chemical Biology and Fundamental Medicine SB RAS) according to the procedure described in [5]. The ODN sequences are shown in the *Table*.

A 38-bp segment (622–660 bp, MCS) was excised from the pTagRFP-N plasmid using the restriction endonucleases HindIII and BamHI (SibEnzyme) by incubation of 1 μg of the plasmid with 1 U HindIII and 1 U BamHI in a W buffer (SibEnzyme) at 37°C for 1 h. After enzyme inactivation (70°C, 20 min) and DNA precipitation according to the standard procedure [6], the linearized plasmid was dissolved in water and a 40-fold molar excess of the DNA insert, 2 U T4 DNA ligase (SibEnzyme) in a SE buffer, and 5 mM ATP were added. The plasmid was ligated at 12°C for 16 h. Then, the reaction mixture was warmed up (65°C, 20 min) and the DNA from the reaction mixture after ligation was separated in 0.8% agarose gel. The circular plasmid with inserts was eluted from the agarose gel using a DNA elution kit (diaGene), according to the manufacturer's protocol.

Table. ODN sequences

No.	ODN
1	5'-P-agctgctgctcatctcgagatctgagtacattggattgccat-tctccgagtgtattaccgtgacg-3'
2	5'-P-gatccgtcacggtaatacactcggagaatggcaatcca-at**M1**tactcagatctcgagatgagcagc-3', where **M1** is nFlu
3	5'-P-gatccgtcacggtaatacactcggagaatggcaatcca-at**M2**tactcagatctcgagatgagcagc-3', where **M2** is nAnt

Transfection of cells with the plasmid was performed using Lipofectamine™ 2000 (Invitrogen), according to the manufacturer's protocol. The cells were seeded onto a 24-well plate at an amount of 2.5×10^4 cells per well in 500 μL of a culture medium containing no antibiotics. Upon reaching 50–70% confluence, the medium was removed and the cells were added with a complex of the plasmid (150 ng) and the Lipofectamine™ 2000 reagent in a serum-free medium. Fluorescence was detected using the Cell-IQ MLF system (Chip-Man Technologies, Finland) for long-term intravital monitoring of the cells at the Common Use Center of the Institute of Cytology and Genetics, SB RAS. The cells were pictured at 10-min intervals

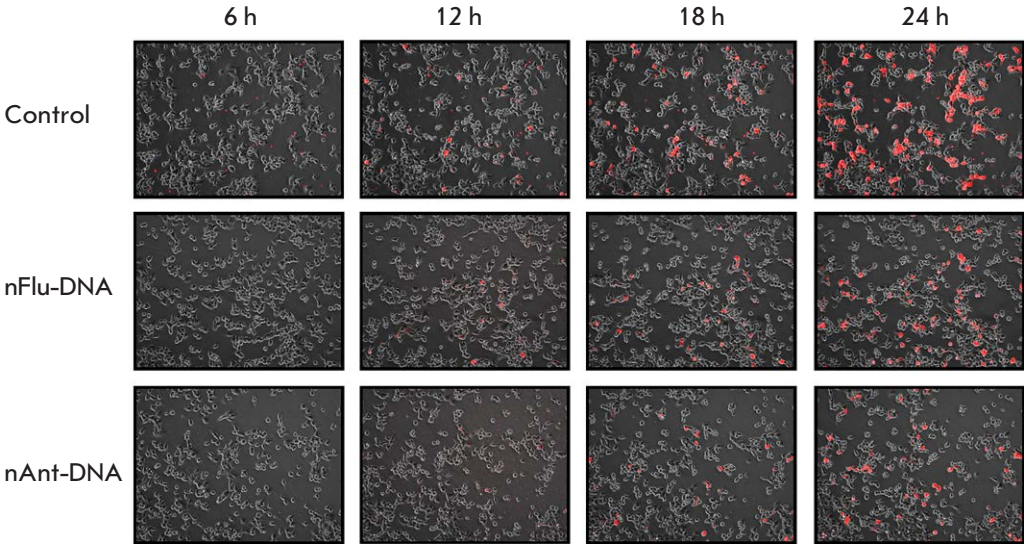

Fig. 2. TagRFP expression in HEK 293T cells transfected with plasmid DNAs. The images were created by overlay of fluorescence and phase-contrast images in ImageJ. Plasmid DNA substrates are shown on *left*; time after cell transfection is shown on *top*

in the phase contrast and fluorescence modes using a Nikon CFI Plan Fluorescence DL ×10 objective. The resulting images were analyzed using the ImageJ and Cell-IQ Analyzer software.

The statistical analysis was performed using the Statistica10 software. All experiments were performed at least in triplicate, and the statistical significance was determined using the Student's *t*-test.

RESULTS AND DISCUSSION

The approach based on the reactivation of the fluorescent protein expression after removal of a DNA lesion that blocks the expression has been successfully used in NER studies [7, 8]. We decided to modify this approach in order to detect the fluorescence signal in living cells using the Cell-IQ MLF device for intravital examination, which combines a microscope with phase contrast and fluorescence imaging modes, as well as a system for supplying CO_2 and maintaining temperature, ensuring optimal conditions for the cells during a prolonged imaging process. The software supplied with the device enables one to analyze images and extract information on the total number and the number of cells expressing fluorescent proteins, the fluorescent signal intensity, cell motility, and other parameters.

To create DNA with bulky lesions, we used the pTagRFP-N vector (4.7 kbp) containing the *tagrfp* gene encoding the monomeric fluorescent protein RFP from the sea anemone *Entacmaea quadricolor* [9]. The advantages of using TagRFP include the generated bright fluorescent signal, the stability of the protein at high pHs, rapid maturation, and the absence of toxic effects on the cells. The *tagrfp* gene is driven by the early promoter of cytomegalovirus (Pcmv ie), which is adjacent to a multiple-cloning site (MCS) with recognition sites for various restriction endonucleases, which enables cloning of the required DNA insert into this region.

Recombinant plasmids containing bulky nFlu and nAnt lesions (hereinafter referred to as nFlu and nAnt DNA, respectively) were synthesized. The pronounced substrate properties of these lesions, which were revealed in a specific excision reaction catalyzed by NER proteins from various cell extracts *in vitro* [5, 10], were taken into account when using nFlu and nAnt to create model plasmids.

The efficiency in NER of nFlu- and nAnt-DNA in HEK 293T human embryonic kidney cells was analyzed. We assessed the time of emergence of cells whose fluorescence indicated recovery of the TagRFP protein expression (*Fig. 2*). A plasmid with a DNA insert without a bulky lesion was used as a control. An evaluation of the number of fluorescent cells in the total cell population using the Cell-IQ Analyzer and ImageJ revealed differences in efficiency between the nAnt- and nFlu-DNA repair systems. In nAnt-DNA-transfected cells, the first fluorescent cells were detected 10 h after transfection, while in nFlu-DNA-transfected cells, the first fluorescent cells were observed after 8 h (*Fig.3A*). The number of fluorescent cells 12 h after transfection was 1.56 ± 0.39% in the case of nAnt-DNA-transfected cells and 4.59 ± 0.76% in the case of nFlu-DNA-transfected cells (*Fig. 3B*). To achieve a similar number of fluorescent cells transfected with nAnt-DNA, it took another 2 h, and the number was 4.27 ± 0.67% after 14 h.

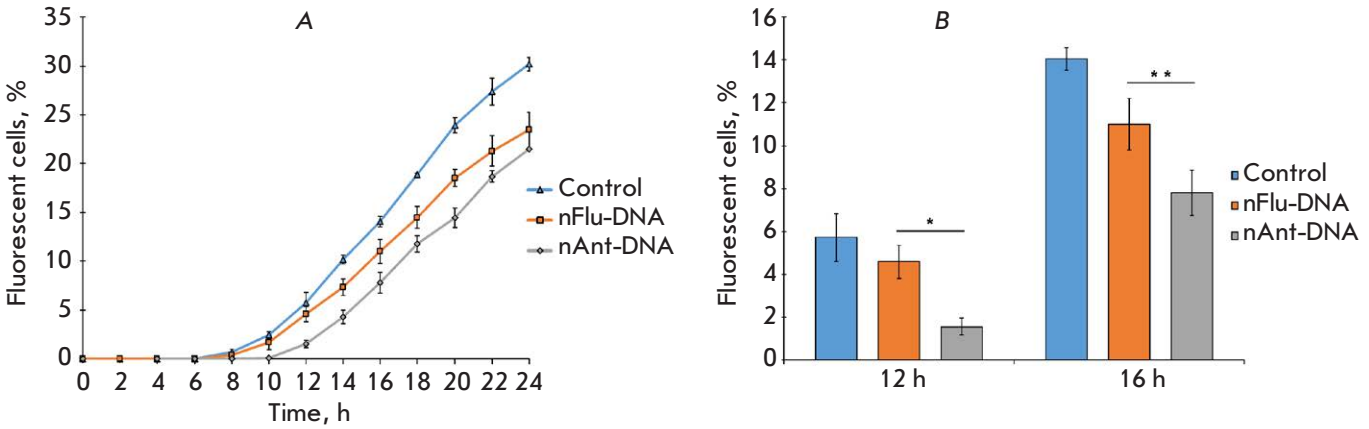

Fig. 3. Analysis of the NER efficiency of plasmid DNAs *ex vivo* in HEK 293T cells.
(*A*) – the number of fluorescent cells (%) over time after transfection with plasmid DNAs; (*B*) – a representative diagram demonstrating the differences in the quantities of fluorescent cells transfected with nFlu- or nAnt-DNA 12 h and 16 h after transfection. The confidence levels are $^{*}p < 0.01$ and $^{**}p < 0.05$

The repair of nFlu-DNA proceeds faster than the repair of nAnt-DNA, which is consistent with the results observed for the repair of the nAnt- and nFlu-DNA duplexes *in vitro* in the presence of proteins of NER-competent extracts from various cancer cell lines (HeLa, SiHa, C33A) [5].

Many factors underlie the difference in the efficiency of bulky lesion repair when using the NER system. These may be the structural damage differences that determine the nature of the primary recognition of the damaged site and the efficiency of the subsequent verification of the damage by the proteins of the TFIIH complex [11], as well as the rate and efficiency of a NER system response in various cells to the damaging effect. Further investigation of NER using a combination of *in vitro* and *ex vivo* approaches may enduce significant progress in our understanding of this process in eukaryotic cells.

CONCLUSION

Therefore, the proposed method enables one to assess efficiency in the removal of bulky nAnt and nFlu lesions from model plasmids by the NER system of HEK 293T cells. The method is a promising tool for studying NER; it enables one to compare both the repair status of various cells and efficiency in the repair of various structural lesions. ●

This study was supported by the Russian Science Foundation (project No. 19-74-10056); acquisition and analysis of images were partially supported by the budget project No. 0259-2021-0011.

REFERENCES

1. Schärer O.D. // Cold Spring Harb. Perspect. Biol. 2013. V. 5. № 10. P. 1–20.
2. Svejstrup J.Q. // Nat. Rev. Mol. Cell Biol. 2002. V. 3. № 1. P. 21–29.
3. Luijsterburg M.S., von Bornstaedt G., Gourdin A.M., Politi A.Z., Moné M.J., Warmerdam D.O., Goedhart J., Vermeulen W., van Driel R., Höfer T. // J. Cell Biol. 2010. V. 189. № 3. P. 445–463.
4. Reardon J.T., Sancar A. // Methods Enzymol. 2006. V. 408. P. 189–213.
5. Evdokimov A., Petruseva I., Tsidulko A., Koroleva L., Serpokrylova I., Silnikov V., Lavrik O. // Nucl. Acids Res. 2013. V. 41. № 12. P. 1–10.
6. Maniatis T., Fritsch E.F., Sambrook J. Molecular Cloning: A Laboratory Manual. Cold Spring Harbor, Cold Spring Harbor University Press, 2001. 2231 p.
7. Kitsera N., Gasteiger K., Lühnsdorf B., Allgayer J., Epe B., Carell T., Khobta A. // PLoS One. 2014. V. 9. № 4. P. 1–6.
8. Kitsera N., Rodriguez-Alvarez M., Emmert S., Carell T., Khobta A. // Nucl. Acids Res. 2019. V. 47. № 16. P. 8537–8547.
9. Merzlyak E., Goedhart J., Shcherbo D., Bulina M., Shcheglov A., Fradkov A., Gaintzeva A., Lukyanov K., Lukyanov S., Gadella T.W.J., et al. // Nat. Methods. 2007. V. 4. № 7. P. 555–557.
10. Lukyanchikova N., Petruseva I., Evdokimov A., Silnikov V., Lavrik O. // Biochem. 2016. V. 81. № 3. P. 263–274.
11. Batty D.P., Wood R.D. // Gene. 2000. V. 241. № 2. P. 193–204.

GENERAL RULES

Acta Naturae publishes experimental articles and reviews, as well as articles on topical issues, short reviews, and reports on the subjects of basic and applied life sciences and biotechnology.

The journal *Acta Naturae* is on the list of the leading periodicals of the Higher Attestation Commission of the Russian Ministry of Education and Science. The journal Acta Naturae is indexed in PubMed, Web of Science, Scopus and RCSI databases.

The editors of *Acta Naturae* ask of the authors that they follow certain guidelines listed below. Articles which fail to conform to these guidelines will be rejected without review. The editors will not consider articles whose results have already been published or are being considered by other publications.

The maximum length of a review, together with tables and references, cannot exceed 50,000 characters with spaces (approximately 30 pages, A4 format, 1.5 spacing, Times New Roman font, size 12) and cannot contain more than 16 figures.

Experimental articles should not exceed 30,000 symbols (approximately 15 pages in A4 format, including tables and references). They should contain no more than ten figures.

A short report must include the study's rationale, experimental material, and conclusions. A short report should not exceed 12,000 symbols (5–6 pages in A4 format including no more than 12 references). It should contain no more than three figures.

The manuscript and all necessary files should be uploaded to www.actanaturae.ru:

1) text in Word 2003 for Windows format;
2) the figures in TIFF format;
3) the text of the article and figures in one pdf file;
4) the article's title, the names and initials of the authors, the full name of the organizations, the abstract, keywords, abbreviations, figure captions, and Russian references should be translated to English;
5) the cover letter stating that the submitted manuscript has not been published elsewhere and is not under consideration for publication;
6) the license agreement (the agreement form can be downloaded from the website www.actanaturae.ru).

MANUSCRIPT FORMATTING

The manuscript should be formatted in the following manner:

- Article title. Bold font. The title should not be too long or too short and must be informative. The title should not exceed 100 characters. It should reflect the major result, the essence, and uniqueness of the work, names and initials of the authors.
- The corresponding author, who will also be working with the proofs, should be marked with a footnote *.
- Full name of the scientific organization and its departmental affiliation. If there are two or more scientific organizations involved, they should be linked by digital superscripts with the authors' names. Abstract. The structure of the abstract should be very clear and must reflect the following: it should introduce the reader to the main issue and describe the experimental approach, the possibility of practical use, and the possibility of further research in the field. The average length of an abstract is 20 lines (1,500 characters).
- Keywords (3 – 6). These should include the field of research, methods, experimental subject, and the specifics of the work. List of abbreviations.
- INTRODUCTION
- EXPERIMENTAL PROCEDURES
- RESULTS AND DISCUSSION
- CONCLUSION

  The organizations that funded the work should be listed at the end of this section with grant numbers in parenthesis.
- REFERENCES

  The in-text references should be in brackets, such as [1].

RECOMMENDATIONS ON THE TYPING AND FORMATTING OF THE TEXT

- We recommend the use of Microsoft Word 2003 for Windows text editing software.
- The Times New Roman font should be used. Standard font size is 12.
- The space between the lines is 1.5.
- Using more than one whole space between words is not recommended.
- We do not accept articles with automatic referencing; automatic word hyphenation; or automatic prohibition of hyphenation, listing, automatic indentation, etc.
- We recommend that tables be created using Word software options (Table → Insert Table) or MS Excel. Tables that were created manually (using lots of spaces without boxes) cannot be accepted.
- Initials and last names should always be separated by a whole space; for example, A. A. Ivanov.
- Throughout the text, all dates should appear in the "day.month.year" format, for example 02.05.1991, 26.12.1874, etc.
- There should be no periods after the title of the article, the authors' names, headings and subheadings, figure captions, units (s – second, g – gram, min – minute, h – hour, d – day, deg – degree).
- Periods should be used after footnotes (including those in tables), table comments, abstracts, and abbreviations (mon. – months, y. – years, m. temp. – melting temperature); however, they should not be used in subscripted indexes (T_m – melting temperature; $T_{p.t}$ – temperature of phase transition). One exception is mln – million, which should be used without a period.
- Decimal numbers should always contain a period and not a comma (0.25 and not 0,25).
- The hyphen ("-") is surrounded by two whole spaces, while the "minus," "interval," or "chemical bond" symbols do not require a space.
- The only symbol used for multiplication is "×"; the "×" symbol can only be used if it has a number to its

right. The "·" symbol is used for denoting complex compounds in chemical formulas and also noncovalent complexes (such as DNA·RNA, etc.).
- Formulas must use the letter of the Latin and Greek alphabets.
- Latin genera and species' names should be in italics, while the taxa of higher orders should be in regular font.
- Gene names (except for yeast genes) should be italicized, while names of proteins should be in regular font.
- Names of nucleotides (A, T, G, C, U), amino acids (Arg, Ile, Val, etc.), and phosphonucleotides (ATP, AMP, etc.) should be written with Latin letters in regular font.
- Numeration of bases in nucleic acids and amino acid residues should not be hyphenated (T34, Ala89).
- When choosing units of measurement, SI units are to be used.
- Molecular mass should be in Daltons (Da, KDa, MDa).
- The number of nucleotide pairs should be abbreviated (bp, kbp).
- The number of amino acids should be abbreviated to aa.
- Biochemical terms, such as the names of enzymes, should conform to IUPAC standards.
- The number of term and name abbreviations in the text should be kept to a minimum.
- Repeating the same data in the text, tables, and graphs is not allowed.

GUIDENESS FOR ILLUSTRATIONS

- Figures should be supplied in separate files. Only TIFF is accepted.
- Figures should have a resolution of no less than 300 dpi for color and half-tone images and no less than 600 dpi.
- Files should not have any additional layers.

REVIEW AND PREPARATION OF THE MANUSCRIPT FOR PRINT AND PUBLICATION

Articles are published on a first-come, first-served basis. The members of the editorial board have the right to recommend the expedited publishing of articles which are deemed to be a priority and have received good reviews.

Articles which have been received by the editorial board are assessed by the board members and then sent for external review, if needed. The choice of reviewers is up to the editorial board. The manuscript is sent on to reviewers who are experts in this field of research, and the editorial board makes its decisions based on the reviews of these experts. The article may be accepted as is, sent back for improvements, or rejected.

The editorial board can decide to reject an article if it does not conform to the guidelines set above.

The return of an article to the authors for improvement does not mean that the article has been accepted for publication. After the revised text has been received, a decision is made by the editorial board. The author must return the improved text, together with the responses to all comments. The date of acceptance is the day on which the final version of the article was received by the publisher.

A revised manuscript must be sent back to the publisher a week after the authors have received the comments; if not, the article is considered a resubmission.

E-mail is used at all the stages of communication between the author, editors, publishers, and reviewers, so it is of vital importance that the authors monitor the address that they list in the article and inform the publisher of any changes in due time.

After the layout for the relevant issue of the journal is ready, the publisher sends out PDF files to the authors for a final review.

Changes other than simple corrections in the text, figures, or tables are not allowed at the final review stage. If this is necessary, the issue is resolved by the editorial board.

FORMAT OF REFERENCES

The journal uses a numeric reference system, which means that references are denoted as numbers in the text (in brackets) which refer to the number in the reference list.

For books: the last name and initials of the author, full title of the book, location of publisher, publisher, year in which the work was published, and the volume or issue and the number of pages in the book.

For periodicals: the last name and initials of the author, title of the journal, year in which the work was published, volume, issue, first and last page of the article. Must specify the name of the first 10 authors. Ross M.T., Grafham D.V., Coffey A.J., Scherer S., McLay K., Muzny D., Platzer M., Howell G.R., Burrows C., Bird C.P., et al. // Nature. 2005. V. 434. № 7031. P. 325–337.

References to books which have Russian translations should be accompanied with references to the original material listing the required data.

References to doctoral thesis abstracts must include the last name and initials of the author, the title of the thesis, the location in which the work was performed, and the year of completion.

References to patents must include the last names and initials of the authors, the type of the patent document (the author's rights or patent), the patent number, the name of the country that issued the document, the international invention classification index, and the year of patent issue.

The list of references should be on a separate page. The tables should be on a separate page, and figure captions should also be on a separate page.

The following e-mail addresses can be used to contact the editorial staff: actanaturae@gmail.com, tel.: (495) 727-38-60.